

**Experimental and Numerical Investigation of Fatigue behavior for
Marine Clays and Offshore Monopile-Clay System**

Bayan Fakhri Abu Safieh

A Thesis
In the Department of
Building, Civil, and Environmental Engineering

Presented in Partial Fulfillment of the Requirements
For the Degree of
Doctor of Philosophy (Civil Engineering)

at Concordia University
Montreal, Quebec, Canada

March 2022

© Bayan Abu Safieh, 2022

**CONCORDIA UNIVERSITY
SCHOOL OF GRADUATE STUDIES**

This is to certify that the thesis prepared

By: Bayan Fakhri Abu Safieh

Entitled: Experimental and Numerical Investigation of Fatigue behavior for Marine Clays
and Offshore Monopile-Clay System

and submitted in partial fulfillment of the requirements for the degree of
Doctor of Philosophy (Civil Engineering)

Complies with the regulations of the University and meets the accepted standards with respect to originality
and quality.

Signed by the final examining committee:

_____ Dr. Alex De Visscher	Chair
_____ Dr. Adel Hanna	Thesis Supervisor
_____ Dr. Biao Li	Examiner
_____ Dr. Ahmed Soliman	Examiner
_____ Dr. Mojtaba Kheiri	Examiner
_____ Dr. Sai Vanapalli	External Examiner

Approved by:

Dr. Mazdak Nik-Bakht, Graduate Program Director

2022

Dr. Mourad Debbabi, Dean

ABSTRACT

Experimental and Numerical Investigation of Fatigue behavior for Marine Clays and Offshore Monopile-Clay System

Bayan Fakhri Abu Safieh, Ph.D.

Concordia University, 2022

The design of foundations supporting offshore structures and subjected to excessive cyclic loading episodes become challenged when embedded in soft marine clays. A deterioration in the undrained shear strength of marine clays with the generation of excess pore water pressure under cyclic loading significantly affects the offshore infrastructure's stability. It leads to large lateral deformations that might be failing both superstructure and infrastructural systems. Monopiles are extensively used in supporting offshore structures due to their high resistance to extensive lateral cyclic loading. The response of the Monopile-Clay system to lateral cyclic loading drew the attention of researchers over the years; they conducted experimental, field, and numerical studies to examine the suitability of the methods adopted in the design codes, which is still a controversial issue. This research aims to study the cyclic performance of marine clays and the monopile-clay system and measure the marine clay fatigue life and how it interferes with the system's failure. A parametric sensitivity analysis using the Artificial Intelligence technique was proposed to highlight the complicated behavior of marine clays and to allocate the clay parameter(s) that primarily affect its behavior when subjected to cyclic loading. Datasets collected from the literature were used to measure the threshold cyclic stress ratio (*CSR*) for a wide range of marine clays worldwide. Moreover, a modified safe zone concept was proposed to predict the clay's response, whether it fails or maintains equilibrium. The most significant clay parameters that impact its response were detected, and a predictive ANN model was proposed. The model successfully predicts the marine clay response to cyclic loading. The fatigue life estimation of marine clays was measured by performing a series of strain-controlled tests under different strain amplitudes. Three major turning points in the marine clay's fatigue life were defined: (1) the crack initiation, (2) the crack propagation fatigue life, and (3) the transition point where the plastic strains become dominant and control the clay's behavior. Furthermore, a new correlation of the degradation parameter (*t*) was proposed based on cycling the marine clays until failure. A 2D numerical investigation was performed under the same tested parameters of the strain-controlled tests to measure the monopile-clays system fatigue life. The system was analyzed under displacement-controlled loading amplitude to measure the actual clay's response and deterioration over the embedded depth of the monopile and by increasing the number of cycling. The detected *P – N* profiles can be an efficient tool to develop new design criteria that fulfill the fatigue limit state (FLS) requirements.

*To the Purest Hearts in the World
The Symbol of Tender and Devotion*

Mom & Dad

To my strength

My Sister, Brothers, and their families

To all Those Whom I Concern and Love

MY SPECIAL DEDICATION

ACKNOWLEDGEMENT

After completing my thesis on the virtue and blessing of God, I want to express my honest gratitude to my supervisor, *Dr. Adel Hanna*, for his support, patience and help throughout working on the research and preparing this thesis. Moreover, for his helpful directions and valuable comments throughout my studying journey. Being a student of Dr. Hanna is a great honor for me; his immense knowledge and motivation give me the power to excel in my research. Also, I would like to thank the thesis committee for their time in reading and evaluating this research.

A special thanks to the *Middle East University-Jordan* for granting me a scholarship to receive a doctorate from Concordia University. Also, I want to thank my colleagues, *Dr. Altayeb Qasem*, *Sohail Akhtar*, and those who helped and supported me. My sincere thanks to *Dr. Michel Kuntz* from WSP, *Dr. Riad Diab* and *Malika Ladjel* from SNC-Lavalin, *Dr. Torsten Witchtmann* from KIT-Germany, and *Dr. T. Hong* from China for their contribution and collaboration by providing testing samples and raw data. A special thanks to the lab coordinator and technicians in the BCEE department, *Riccardo Gioia*, *Roberto Avila Pirez*, and *Alexis Gosselin*, for the tremendous efforts and support they provide throughout my experimental work. They were always there to help, even during the unprecedented conditions of the pandemic.

My wakeless respect and thanks to my parents, *Dr. Fakhri Abu Safieh* and *Dr. Nawal Saif*, for their endless love and support throughout my hard days in the foreignness years. Despite the distances, they always gave me strength and encouraged me throughout my study. I took my passion for learning from them and that a day is wasted if we do not learn something new in it.

TABLE OF CONTENTS

LIST OF FIGURES	vii
LIST OF TABLES	xi
LIST OF ABBREVIATIONS	xii
CHAPTER 1: INTRODUCTION	1
1.1 Problem Statement	2
1.2 Research Objectives	5
1.3 Implications of the Research	5
1.4 Thesis Framework	6
CHAPTER 2: CRITICAL REVIEW	7
2.1 Marine Clay Cyclic Response	7
2.1.1 Cyclic Stress-Controlled Tests	7
2.1.2 Cyclic Strain-Controlled Tests	15
2.2 Marine Clay-Monopile Cyclic Response	17
2.3 Research Gaps	23
2.4 research Significance	24
CHAPTER 3: PARAMETRIC ANALYSIS FOR MARINE CLAYS PROPERTIES: MACHINE LEARNING TECHNIQUES	25
3.1 Marine Clay Static Response	26
3.2 Stress-Controlled Cyclic Response	28
3.3 Marine Clays Cyclic Response Assessment	30
3.3.1 Threshold Cyclic Stress Ratio	30
3.3.2 Modified Safe Zone Concept	35
3.4 Parametric Analysis and Feature Selection	39
3.4.1 Data Pre-processing	39
3.4.2 Feature Selection	40
3.4.3 Parametric Sensitivity Analysis (ANN-Model)	47
3.4.4 Cyclic Strain Development	51

CHAPTER 4: STRAIN-CONTROLLED FATIGUE BEHAVIOR OF MARINE CLAYS	56
4.1 Incentive Overview	56
4.2 Experimental Test Plan	61
4.2.1 Marine Clay Collection and Preparation	61
4.2.2 Triaxial Machine Setup	63
4.2.3 Experimental Program and Testing Procedure	64
4.3 Analysis of Strain-Controlled Tests Results	66
4.3.1 Nomenclatures	66
4.3.2 Effect of Confining Pressure	68
4.3.3 Effect of Amplitude	71
4.3.4 Effect of Frequency	74
4.4 Marine Clays Fatigue Life Estimation	77
4.4.1 Strain-Controlled Tests Analysis	78
4.4.2 Fatigue Initiation and Propagation Life	86
4.4.3 Degradation Index of Marine Clays	96
CHAPTER 5: MONOPILE-MARINE CLAY CYCLIC FATIGUE RESPONSE	101
5.1 Monopile-Marine Clay Cyclic Response Assessment	101
5.2 Monopile-Marine Clay Cyclic Fatigue Behavior	105
5.3 2D FEM Displacement-controlled Models	105
5.3.1 Model Geometry and Boundary Conditions	105
5.3.2 FEM Model Meshing and Loading Procedure	107
5.4 Analysis of the 2D FEM Models	108
5.4.1 $P - N$ Profiles	108
5.4.2 $\delta - N$ Profiles	114
5.4.3 Strain Development	115
5.4.4 Stiffness Profiles	119
CHAPTER 6: CONCLUSIONS AND FUTURE WORK	121
6.1 Concluded Remarks	121
6.2 Research Limitations	124
6.3 Future Work	125
REFERENCES	126
APPENDIX A: MACHINE LEARNING PYTHON SAMPLE CODES AND RESULTS	131
APPENDIX B: STRAIN-CONTROLLED CYCLIC CHECK TEST RESULTS	137

LIST OF FIGURES

Figure 1.1:	Monopile-Clay system response to lateral cyclic loading	2
Figure 1.2:	Monopile stiffness degradation and response to marine clay deterioration when subjected to lateral cyclic loading	3
Figure 1.3:	Winkler springs model and p-y curves	4
Figure 1.4:	General form for the criteria of predicting p-y curves, After (Matlock, 1970)	4
Figure 2.1:	Effect of frequency (f) on marine clays' cyclic strength (q_{cyc} vs ε_a)	9
Figure 2.2:	Effect of frequency (f) on marine clays' pore water pressure (u vs ε_a)	9
Figure 2.3:	q_{cyc} vs N for different marine clays under cyclic loading	10
Figure 2.4:	u vs N for different marine clays under cyclic loading	10
Figure 2.5:	Sensitivity effect, u vs N for different marine clays	11
Figure 2.6:	Safe zone concept based on the combined effect of physical and mechanical parameters of Marine Clays as proposed by (Hanna & Javed, 2014)	12
Figure 2.7:	Failed and survived samples, CSR vs N for different marine clays	13
Figure 2.8:	Undisturbed and remolded clay behavior, q_{cyc} vs ε_a [After Hanna & Javed, 2014]	14
Figure 2.9:	Undisturbed and remolded clay behavior, CSR vs N [After Hanna & Javed, 2014]	14
Figure 2.10:	Undisturbed and remolded clay behavior, u vs N [After Hanna & Javed, 2014]	15
Figure 2.11:	Field tests results of (Jeong, Kim, Kim, & Shin, 2007) and (Zhu, Zhu, Li, Liu, & Liu, 2017) studies	18
Figure 2.12:	Reduction in shear strength due to cyclic loading	21
Figure 2.13:	Procedure of obtaining $p - y$ curve from the clay stress-strain behavior, After (Bouazid, Bhattacharya, & Dash, 2013)	22
Figure 2.14:	Soil reaction components applied to a monopile, After (Byrne, et al., 2015)..	22
Figure 2.15:	Proposed research methodology	24
Figure 3.1:	Marine clays behavior under monotonic loading	27
Figure 3.2:	Saint-Hyacinthe marine clays behavior under static loading and different effective confining pressure	27
Figure 3.3:	Different failure modes for Marine clay samples under monotonic loading	28
Figure 3.4:	Cyclic response of marine clays, q_{cyc} vs ε_a for sample No. 15, (Wichtmann, Anderson, Sjursen, & Berre, 2013)	29
Figure 3.5:	Pore water pressure generation during cyclic loading, u vs ε_a for sample No. 15, (Wichtmann, Anderson, Sjursen, & Berre, 2013)	30

Figure 3.6:	<i>CSR vs N</i> for different marine clays: Hyudo et al. (1992) theory application	32
Figure 3.7:	Application of demarcation line (<i>CSR vs N</i>) proposed by (Hanna & Javed, 2014) for different marine clays	32
Figure 3.8:	Failed and survived samples, <i>CSR vs N</i> for different marine clays	33
Figure 3.9:	Polynomial regression model for the threshold <i>CSR</i> of the collected dataset	34
Figure 3.10:	Proposed demarcation line for the collected marine clays' dataset	34
Figure 3.11:	Models' performance and confidence zones	36
Figure 3.12:	Error rate curve to select the <i>K-Neighbor Number</i> and Confusion Matrix	37
Figure 3.13:	Testing dataset predicted using the <i>K – NN</i> classification model with $k = 4$	38
Figure 3.14:	Modified safe zone concept with different confidence scores	38
Figure 3.15:	Data Preprocessing in ML	41
Figure 3.16:	Clay Properties correlation matrix	42
Figure 3.17:	The ExtraTrees Classifier, after (Chakrabarty & Biswas, 2020)	43
Figure 3.18:	Features importance using the ExtraTreesClassifier	43
Figure 3.19:	(a) GradientBoostingClassifier technique, after (Baturynska & Martinsen, 2021), and (b) Features' importance indices	44
Figure 3.20:	Features importance using the Backward Elimination Technique	45
Figure 3.21:	Biological Neural Network (Negnevitsky, 2002)	47
Figure 3.22:	Artificial Neural Network Technique [After (Shahin, Jaksa, & Maier, 2008)]	48
Figure 3.23:	The proposed <i>ANN</i> model	49
Figure 3.24:	The measured Falses and sensitivity indices of the <i>ANN – model</i> to input parameters	50
Figure 3.25:	The axial strain correlations with the cyclic test's parameters	52
Figure 3.26:	Proposed cyclic strain development curves (Zhang, Sun, & Cao, 2020)	53
Figure 3.27:	<i>ANN</i> models to predict the cyclic strain (ϵ_a)	54
Figure 4.1:	Hysteresis loops for different cycles q_{cyc} vs ϵ_a	57
Figure 4.2:	Stress/Strain-Time history profile during cycling until complete failure at $N = 413$	57
Figure 4.3:	(a) Stress/Strain amplitude profile during cycling until failure at $N = 413$, and (b) The marine clay sample after testing	58
Figure 4.4:	Abitibi marine clay sample's test results with $\sigma'_3 = 50$ kPa and $\pm\Delta\epsilon_a = 5\%$	59
Figure 4.5:	Secant moduli for the first and last cycles	61
Figure 4.6:	Degradation indices variation with number of cycles for Saint-Hyacinthe sample, $N_f = 413$, and Abitibi clay sample, $N = 10000$	61
Figure 4.7:	Marine clay samples' preparation: extraction from Shelby tubes, segmentation, wax-coating, and labeling	62

Figure 4.8:	The fully automated Triaxial Machine setup used in the study	63
Figure 4.9:	The initial and stopping conditions for the saturation schedule in the performed tests	64
Figure 4.10:	A sample of the consolidation and Shearing configuration in monotonic tests	65
Figure 4.11:	Sample of strain-controlled tests loading configuration	65
Figure 4.12:	Sinusoidal wave properties	66
Figure 4.13:	Stress-time profile during the strain-controlled cyclic test	67
Figure 4.14:	Cyclic $\sigma - \varepsilon$ curve properties	67
Figure 4.15:	Hysteresis loops during the test (q_{cyc} vs ε_a) for different confining pressures	69
Figure 4.16:	Strain-Time history profile for different confining pressures	69
Figure 4.17:	Stress-Time history profile and samples after testing for different confining pressures	70
Figure 4.18:	Pore water pressure generation for different confining pressures tests	70
Figure 4.19:	Hysteresis loops during the test (q_{cyc} vs ε_a) for different amplitudes	72
Figure 4.20:	Strain-Time history profile for different amplitudes	72
Figure 4.21:	Stress-Time history profile and samples after testing for different amplitudes	73
Figure 4.22:	Pore water pressure generation during the tests for different amplitudes	74
Figure 4.23:	Hysteresis loops during the test (q_{cyc} vs ε_a) for different frequencies	75
Figure 4.24:	Strain-Time history profile for different frequencies	76
Figure 4.25:	Stress-Time history profile for different frequencies	76
Figure 4.26:	Microscopy surface investigation for 5.00mm amplitude strain-controlled test	78
Figure 4.27:	Strain-time profiles for all tests	79
Figure 4.28:	Stress-time profiles and hysteresis loops at different stages	80
Figure 4.29:	Mean stress and strain	81
Figure 4.30:	Microscopy investigation for surface fatigue cracks filled with cemented clay paste for different samples	84
Figure 4.31:	Microscopy investigation for surface fatigue notches in the form of intrusions and extrusions	84
Figure 4.32:	(a) Microscopy investigation for surface crack slip bands, and (b) Crack propagation in a half-cut sample	85
Figure 4.33:	Microscopy investigation for surface crack cementation and surface notches after 24 hours air drying	85
Figure 4.34:	Pore water pressure generated during the performed strain-controlled tests	86
Figure 4.35:	Hysteresis loops of the performed strain-controlled tests	87
Figure 4.36:	The changes in stress amplitude ($\Delta\sigma$) and volume change (ΔV) for $\Delta\varepsilon = 5.00\%$	88

Figure 4.37: The changes in stress amplitude ($\Delta\sigma$) and volume change (ΔV) for $\Delta\varepsilon = 2.50\%$	90
Figure 4.38: The changes in stress amplitude ($\Delta\sigma$) and volume change (ΔV) for $\Delta\varepsilon = 1.25\%$	91
Figure 4.39: The changes in stress amplitude ($\Delta\sigma$) and volume change (ΔV) for $\Delta\varepsilon = 0.75\%$	92
Figure 4.40: Total strain amplitude and Elastic/Plastic strain components for $\Delta\varepsilon = 5.00\%$	94
Figure 4.41: $\Delta\varepsilon - N$ curves for Abitibi marine clays' Fatigue life estimation	95
Figure 4.42: Marine clay samples after testing and air drying for days	96
Figure 4.43: Actual $\Delta\varepsilon - N$ and strain components' curves for Abitibi marine clays	96
Figure 4.44: Degradation index and parameter for the tested samples	98
Figure 4.45: Degradation parameter for this study and studies in the literature	99
Figure 4.46: Degradation index for this study and (Idriss, Dobri, & Singh, 1978)	100
Figure 5.1: Polynomial regression model for the threshold <i>CSR</i> of the collected dataset ...	103
Figure 5.2: Proposed demarcation line for the collected dataset of monopile-clay system	103
Figure 5.3: Pile head deformation with loading levels for different studies	104
Figure 5.4: 2D FEM Model Geometry and material properties	106
Figure 5.5: 2D FEM model boundary conditions, gravity, and applied loads	107
Figure 5.6: 2D FEM model domain discretization and constitutive model parameters	108
Figure 5.7: 2D FEM model ($y = 0.12m$) peak load profile: right-side	109
Figure 5.8: 2D FEM model ($y = 0.12m$) peak load profile: left-side	110
Figure 5.9: 2D FEM model ($y = 0.12m$): (a) pore water pressure distribution and (b) Displacement in x	111
Figure 5.10: 2D FEM model ($y = 0.35m$): (a) pore water pressure distribution and (b) Displacement in x	112
Figure 5.11: 2D FEM model ($y = 0.35 m$) peak load profile: (a) Mudline level and (b) At the pile tip	113
Figure 5.12: 2D FEM model ($y = 0.12 m$) peak displacement profile: (a) Mudline level and (b) At the pile tip.....	114
Figure 5.13: 2D FEM model ($y = 0.35 m$) peak displacement profile: (a) Mudline level and (b) At the pile tip	115
Figure 5.14: 2D FEM model ($y = 0.35 m$): (a) Strain development and (b) Pore water pressure generation	116
Figure 5.15: 2D FEM model ($y = 0.12 m$): (a) Strain development and (b) Pore water pressure generation	117
Figure 5.16: 2D FEM models strain profiles: (a) $y = 0.35 m$ and (b) $y = 0.12 m$	118
Figure 5.17: Secant stiffness profiles for the 2D FEM analysis at different depths	120

LIST OF TABLES

Table 2.1:	List of collected data from the literature	7
Table 2.2:	Summary for strain-controlled studies in the literature	16
Table 2.3:	Summary of existing studies - Experimental and field studies on Clay-Monopile system lateral cyclic response	17
Table 2.4:	Field tests characteristics for two selected studies	18
Table 2.5:	Summary of Existing studies - Numerical modeling studies on Clay-Monopile system lateral cyclic response	20
Table 3.1:	Some marine clay's physical properties from different locations	26
Table 3.2:	List of collected data from the literature	31
Table 3.3:	Accuracies of different classifiers in predicting the clays' response	35
Table 3.4:	List of collected data from the literature	40
Table 3.5:	Summary of the relative importance and the selected features	46
Table 3.6:	Proposed ANN models and Data Proportions	49
Table 3.7:	Sensitivity of the ANN model to the input parameters	50
Table 4.1:	Marine clays' locations and physical properties (Average values)	62
Table 4.2:	Experimental program of strain-controlled cyclic tests	66
Table 4.3:	Number of cycles required to reach failure for the strain-controlled tests	77
Table 4.4:	Life estimation for Abitibi marine clays	93
Table 4.5:	Summary for the degradation index correlation in the literature (Strain-controlled)	97
Table 4.6:	Summary for the degradation index correlations in this study	98
Table 5.1:	List of collected data from the literature	102

LIST OF ABBREVIATIONS

<i>N</i>	<i>Number of cycles</i>
<i>SLS</i>	<i>Serviceability Limit State</i>
<i>P</i>	<i>Soil reaction force</i>
<i>y</i>	<i>Pile lateral deflection response</i>
ϵ_{50}	<i>Strains at 50% of ultimate soil resistance load</i>
$w\%$	<i>In-situ water content</i>
$w_L\%$	<i>Liquid limit</i>
$w_p\%$	<i>Plastic limit</i>
$I_p\%$	<i>Plasticity index</i>
$I_L\%$	<i>Liquidity index</i>
e_o	<i>Initial void ratio</i>
γ_o	<i>In-situ unit weight</i>
$S\%$	<i>Degree of saturation</i>
S_t	<i>Clays' sensitivity</i>
<i>OC</i>	<i>Organic content</i>
<i>OCR</i>	<i>Overconsolidation ratio</i>
<i>q</i>	<i>Deviatoric stress</i>
q_s	<i>Static shear strength</i>
q_{cyc}	<i>Cyclic shear strength</i>
Δu	<i>Excess pore water pressure</i>
$\sigma - \epsilon$	<i>Stress-strain diagram</i>
$\pm \Delta \sigma_d$	<i>Total stress amplitude</i>
$\pm \Delta \epsilon_a$	<i>Total strain amplitude</i>
$\Delta \epsilon_{Elastic}$	<i>Elastic strain component</i>
$\Delta \epsilon_{plastic}$	<i>Plastic strain component</i>
<i>CSR</i>	<i>Cyclic stress ratio</i>
<i>f</i>	<i>Frequency</i>
σ_3	<i>Confining pressure</i>
σ_p	<i>Preconsolidation pressure</i>
ϵ_a	<i>Axial strain</i>
S_u	<i>Undrained shear strength</i>
<i>MLT</i>	<i>Machine learning techniques</i>

<i>F/E</i>	<i>Failed/Maintained equilibrium</i>
<i>SL</i>	<i>Significance level</i>
<i>E_s</i>	<i>Secant stiffness modulus</i>
<i>δ</i>	<i>Degradation index</i>
<i>t</i>	<i>Degradation parameter: stiffness degradation rate</i>
<i>CH</i>	<i>High plastic clay</i>
<i>CU</i>	<i>Consolidated-Undrained Triaxial test</i>
<i>B</i>	<i>Skempton's pore water pressure parameter</i>
<i>ΔV</i>	<i>Change in volume</i>
<i>N_f</i>	<i>Number of cycles at failure</i>
<i>N_i</i>	<i>Crack initiation life</i>
<i>N_t</i>	<i>Number of cycles at the transition point (elastic-plastic)</i>
<i>γ_c</i>	<i>Shear strain amplitude</i>

CHAPTER 1

INTRODUCTION

The design of foundations supporting offshore structures becomes challenging when embedded in soft marine clays due to the excessive deformations generated under cyclic loading episodes from winds, waves, flow-induced vibration, and earthquakes. Offshore structures are usually designed for an average lifespan of 25 years and subjected to severe irregular episodes of lateral cyclic loading with an extremely high number of cycles N that may exceed 10^7 cycles as reported by the researchers. One of the challenges associated with designing offshore structures is the infrastructure system conditions: the marine clay properties and the proper foundations to support these structures.

Marine clays are high plastic soft clays and are the most common seabed soils of different offshore areas worldwide. Predominantly, marine clays are thick layers with varying properties and mineralogy appertaining to their origin and location. However, when subjected to excessive cyclic loading, the marine clay strength deteriorates with pore water pressure generation, significantly affecting the infrastructure stability. As a result of the strength deterioration, the marine clay softens, and a new clay zone with different properties is created in parallel with fatigue cracks initiation. Accordingly, the monopiles tolerate large lateral deformations, leading to failure.

Large diameter pile foundations (monopiles) are extensively used in supporting offshore structures due to their high resistance to extensive axial and lateral cyclic loading. In the meantime, increasing monopile size to improve the marine clay-monopile system stability becomes one of the leading industrial areas concerns. The increase in size may be referred to the fact that the offshore construction is going deeper and deeper from the coastal shore, where the decrease of embedment length is a must. Consequently, the applied cyclic loads from winds and surface waves and clay's strength deterioration will highly impact the monopile response. Accordingly, the response of the monopile and marine clay systems to lateral cyclic loading drew the attention of researchers over the years, and different studies were conducted to understand the system failure. Moreover, many researchers expand their investigations to understand marine clay's cyclic behavior as a key to understanding the monopile-clay system response to cyclic loading.

1.1 PROBLEM STATEMENT

The monopile-clay system, shown in **Figure 1.1a**, has a mutually time-dependent response to cyclic loading from surface waves and wind loading. Loads applied to monopiles will transfer to clay and causes a direct loss of shear strength and remolding/softening behavior; the soft marine clays behave as a nonlinear and non-homogeneous material (**Figure 1.1b**). The clay strength deteriorates over time with increasing the applied cyclic loading represented by the number of cycles (N), causing fatigue cracks and remolding of clays behind the monopile near the mudline. As a result, the monopile accumulates large lateral deformations near the mudline and at the tip depending on the pile stiffness, as reported by (**Hong, et al., 2017**) and shown in **Figures 1.1c** and **1.2**.

Over the design life span of offshore structures, the Monopile-Clay system's failure may occur after a certain number of lateral loading cycles. Therefore, much caution and design considerations are required to maintain these structures' serviceability and function ability. The monopile-marine clay system undergoes large deformations during its life span as it is subjected to lateral cyclic loading over time. Therefore, the design of the monopile-clay system has different criteria as summarized by (**Arany, Bhattacharya, Macdonald, & Hogan, 2017**); the serviceability limits state criterion (*SLS*) concerns the allowed lateral pile head deformation after long-term loading to avoid failure. The pile geometry and the soil stiffness are essential parameters in predicting the pile head movement. Moreover, the fatigue limit state criterion (*FLS*) concerns the fatigue life of the system, which can be defined by the number of cycles required to reach failure.

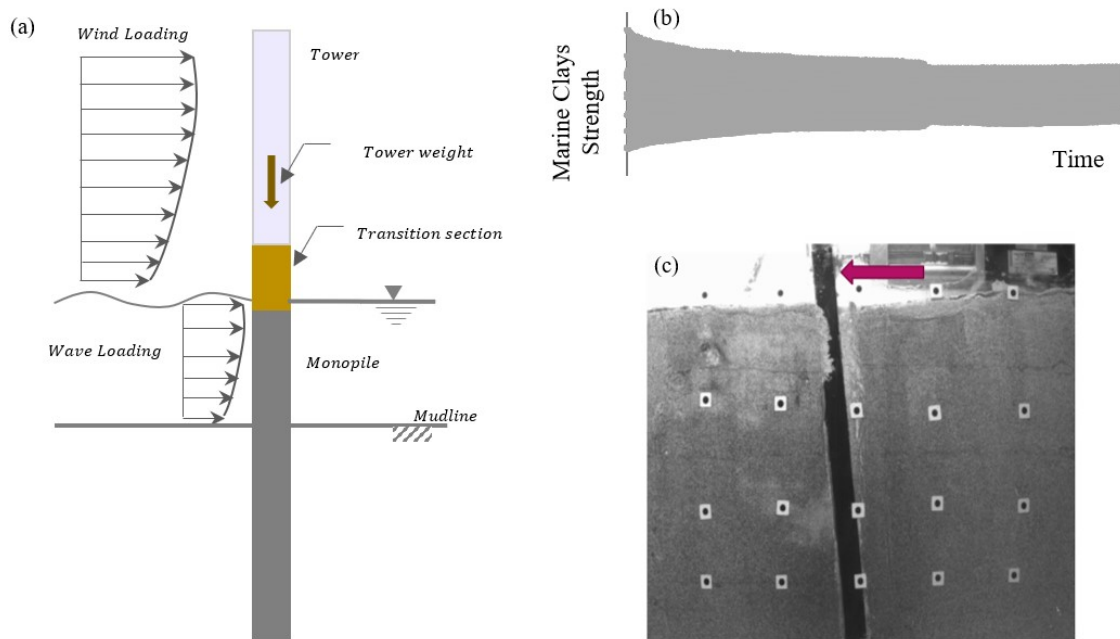


Figure 1.1: Monopile-Clay system response to lateral cyclic loading (a) Field loading exerted on the system, after (Lombardi, Bhattacharya, & Wood, 2013), (b) Undrained strength deterioration with time for marine clays (The present study), and (c) Accumulation of lateral deformation and gap opening under lateral loading (Hong, et al., 2017).

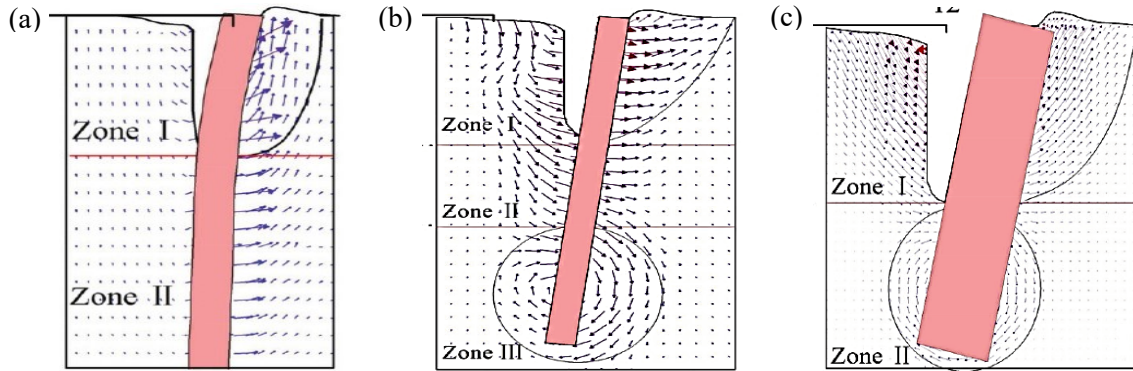


Figure 1.2: Monopile stiffness degradation and response to marine clay deterioration when subjected to lateral cyclic loading: (a) Flexible pile, (b) Semi-rigid pile, and (c) rigid pile (Hong, et al., 2017).

The American Petroleum Institute code (API) highlighted the importance of studying the soil behavior to characterize the soil response to loading (API, 2005). Many studies in the literature performed laboratory tests to investigate the effect of marine clay properties on its strength deterioration when subjected to cyclic loading. The most common test is the triaxial stress-controlled cyclic test that measures the clay stiffness deterioration by applying a constant stress amplitude. It was agreed in the literature that marine clay properties significantly affect its response to cyclic loading, but which of these properties is mainly affecting its behavior is still a debate.

Most of the studies in the literature were performed on a specific marine clay, and the proposed correlations and theories have limited applicability as the properties of marine clays change per their locations. In addition, the varying of the marine clay's mechanical and physical properties make it hard to study more than two or three parameters correlations at once, which raises the possibility of applying Machine Learning and Artificial Intelligence techniques.

On the other hand, predicting the fatigue life of marine clays can provide the offshore structures' designers with beneficial parameters to enhance the design criteria. The strain-controlled cyclic tests are considered an efficient tool for predicting fatigue life as they provide the actual stress and strain response during cycling. The most controversial issue in studying the fatigue life of marine clays is the definition of failure. Very few studies in the literature were performed on a strain-controlled basis, and a maximum number of cycles performed was $N \leq 1000$, which do not simulate the field conditions.

The failure mechanism of the Clay-Monopile system and its response to lateral cyclic loading is also a concern, and many researchers performed studies to model it. Winkler springs are the most widely used method in which the pile is modeled as a beam-column attached to a series of nonlinear springs that represent the soil layer surrounding the pile, as shown in **Figure 1.3**. Based on this model, load-transfer ($p - y$) curves were constructed and proposed by several researchers to define the relationship between the pile lateral deflection response (y) and soil reaction force (P). It is of importance to mention here that two predefined values from the clay stress-strain diagram are required to construct these curves; the ultimate soil resistance P_u and strains at 50% of ultimate soil resistance load (ϵ_{50}).

Some researchers' concern was accurately predicting the load-deflection behavior of laterally loaded piles by conducting experimental tests on small-scale or full-scale flexible or rigid piles embedded in soft clays. Others conducted field tests to study pile-soil response to lateral cyclic loading were reported in the literature. However, few field studies are available in the literature, which is likely due to the high cost of conducting such studies and the difficulties associated with the field tests. Numerical modeling is an efficient tool to model large-scale soil problems such as pile-soil system response to lateral cyclic loading. However, it requires precision in selecting the problem domain, interface elements, and a representative clay model to simulate soils' actual behavior, which is assumed to be challenging for researchers.

1.2 RESEARCH OBJECTIVES

The influence of physical and mechanical properties on the cyclic response of marine clays is a crucial factor that helps to understand the complicated behavior of the Clay-Monopile system when subjected to lateral cyclic loading. Also, understanding the fatigue life of marine clays can help predict the infrastructure system's response over the life span of an offshore structure.

This research aims to:

1. Allocate the clay parameter(s) that mainly affect marine clay response to cyclic loading and predict the marine clay response to cyclic loading by performing parametric sensitivity analysis and using Artificial Intelligence techniques.
2. Study the fatigue life of marine clay by performing cyclic strain-controlled tests and define the crack initiation and propagation life.
3. Perform a numerical model to measure the Clay-Monopile system response to cyclic loading and correlate the system's fatigue life to the marine clay fatigue life.

1.3 IMPLICATIONS OF THE RESEARCH

Phase I concern highlights the complicated behavior of the marine clays when subjected to cyclic loading and allocating the clay parameters that mainly affect its behavior, which will be an asset in future design considerations. In addition, machine learning techniques can efficiently understand the intercorrelation between marine clay's parameters and predict its response to cyclic loading, whether it will fail or maintain equilibrium, concerning the clay's physical and mechanical properties.

The fatigue life of marine clays is a crucial factor in maintaining a safe design over the life span of offshore structures. Performing strain-controlled tests on natural marine clays and applying cyclic loading till the failure occurs can efficiently provide comprehensive information about the fatigue life of marine clays. Therefore, the fatigue life estimation is considered the last step in designing offshore foundations without predictive criteria. Defining the main components of marine clay's fatigue life: crack initiation, plastic transition, and failure will enhance the design process and replace the existed design criteria with a damage tolerance design criterion.

The degradation parameter is another critical design factor; in the literature, this parameter was measured based on short-term cyclic loading following (**Matlock, 1970**) assumption that the load

degradation profile will stabilize within the first 100 *cycles*. Consequently, measuring the degradation parameter over the fatigue life of marine clays under cyclic loading will be more practical and enhance the design process.

Numerical modeling is an essential tool in modeling the response of the Clay-Monopile system on a large scale, which better represents and simulates the actual behavior of a clay particle subjected to long-term cyclic loading. In addition, Monopiles can be modeled in their actual size to understand better the marine clay's response, where the size effect is one of the crucial parameters that affect the behavior. The marine clays' response to the loads transferred through large-scaled monopile better describes the load profile over the embedded length, opening a new window to modify the existing load-deformation transfer curves adopted in the design codes. Moreover, studying the fatigue behavior of the system by applying a large number of cycles supports the fact that clays' strength degradation will not reach zero and that clays went through periods of softening and hardening through their fatigue life.

1.4 THESIS FRAMEWORK

The thesis consisted of six chapters. **Chapter 1** is a brief introduction to introduce the problem statement and research objectives, followed by a critical review in **Chapter 2** that comprehensively discusses the available studies in the literature related to the problem statement. **Chapter 3** covers the marine clay response to cyclic loading under stress-controlled tests. Also, the chapter covers different techniques to assess the clay response, taking advantage of the available data in the literature, including regression analysis, classification algorithms, and deep learning techniques. **Chapter 4** is an experimental investigation to estimate the fatigue life of marine clay by assessing the actual behavior under strain-controlled Triaxial testing. Moreover, the degradation index and degradation parameters are studied based on long-term cyclic loading. **Chapter 5** covers the monopile-marine clay system response to displacement-controlled cyclic loading; actual load-transfer curves were detected under different amplitudes and long-term cyclic loading. Finally, **Chapter 6** provides the concluded remarks, research limitations, and future research.

CHAPTER 2

CRITICAL REVIEW

2.1 MARINE CLAY CYCLIC RESPONSE

2.1.1 Cyclic Stress-Controlled Tests

Several studies performed stress-controlled cyclic tests were selected in this research to discuss the marine clay response to cyclic loading. These studies describe the behavior of marine clays under cyclic loadings considering different clay parameters and having different physical and mechanical properties, depending on the origin and site conditions, as listed in **Table 2.1**. All studies performed tests on undisturbed samples under undrained conditions to simulate the field conditions. Except for **(Hanna & Javed, 2014)**, they tested undisturbed and remolded samples. The cyclic deviator stress (q_{cyc}), axial strain (ϵ_a) and pore water pressure (u) determined based on the value where the sample fails or maintains equilibrium. It is essential to mention that all the marine clays in the collected data set were firm to very soft and medium to extra sensitive clays based on the CFEM (2006 Errata) classifications (**Canadian Geotechnical Society, 2006**).

Table 2.1: List of collected data from the literature.

Study	No. of Collected Data	Location	Depth	Parameters	
				Physical	Mechanical
(Hanna & Javed, 2014)	85	Canada	4-5		
(Li, Dan, & Wang, 2011)	18	China	11		
(Moses & Rao, 2007)	13	India	1.5	$w\%, w_L, w_p$	$\sigma_3, q_s, u, \epsilon_a,$
(Rao & Moses, 2003)	8	India	1.5	$I_L, I_p,$	q_{cyc}, N, f, S_u
(Wichtmann, Anderson, Sjursen, & Berre, 2013)	33	Norway	6-12	$S\%$	CSR, OCR
(Wang, Guo, Cai, Xu, & Gu, 2013)	4	China	3		

Figure 2.1 shows the reported cyclic strength of marine clays with cyclic strains, and the datasets were classified based on two categories: high and low frequencies. Generally, it is found that clay samples with lower frequencies showed higher cyclic shear stress (q_{cyc}). However, the data set collected from **(Wang, Guo, Cai, Xu, & Gu, 2013)** with a loading frequency of 1 Hz produces higher values of q_{cyc} if compared with other data sets with the same loading frequencies, knowing that this study applied 50 000 cycles on the tested samples with no failure. Also, **(Wichtmann, Anderson, Sjursen, & Berre, 2013)** Performed their tests under low frequencies of 0.001 – 0.01 Hz but gives almost the lowest values of q_{cyc} as shown in the figure, and all samples failed under higher cyclic strain compared with other studies.

The pore water pressure variation with the cyclic strain is shown in **Figure 2.2**. it can be seen that the frequency does not significantly affect the pore water pressure generation except for a lower frequency of $f < 0.003$ Hz, where higher pore water pressure values were recorded. The higher recorded values from **(Hanna & Javed, 2014)** can be due to the higher period of each cycle, which allows the clay to generate pore water pressure slowly during the applied cycles. In addition, this may be referred to the high clay sensitivity, higher liquidity index (I_L), higher over consolidation ratios (OCR) and lower initial water content reported in this study.

Most of the studies agreed that the clay's cyclic shear strength and the generation of pore water pressure would increase by the increasing number of cycles N during the tests. However, samples from the same clay origin will not necessarily fail under the same number of cycles N or generate the same pore water pressure as well; this can be concluded from the scattered pattern in **Figure 2.3** and **Figure 2.4**. In other words, one or more marine clays' physical and mechanical properties control the clay response to cyclic loading. In addition, a smaller number of cycles were required for most samples with low frequencies to fail or maintain equilibrium (**Figure 2.3**).

The generation of pore water pressure with the number of cycles and the variation of clay sensitivity is shown in **Figure 2.5**. It is found that most of the extra-sensitive clays generated much higher pwp values if compared with medium and sensitive clays. However, the behavior of the sensitive clays was more complicated where some sensitive clays generated high pwp , while some generated low values as per the medium sensitive clays. It can be seen that the marine clay's physical and mechanical properties highly influence the behavior of the marine clay under cyclic loading. For example, sensitive clays that generated low pwp values have a higher plasticity index and lower liquidity index than that developed higher pwp . The sensitivity classification was based on the Canadian Foundation Engineering Manual (**Canadian Geotechnical Society, 2006**).

(Wang, Guo, Cai, Xu, & Gu, 2013) reported that during the early stages of the loading, the pore water pressure continued to increase rapidly and then tended to stabilize after a lower strain rate increase reported after a large number of cycles. The researchers highlighted the effect of the stress level on the development of cyclic strain and pore water pressure. They reported a critical CSR of 0.3 for tests under different confining pressures.

Also, **(Ren, Xu, Xu, Teng, & Lv, 2018)** studied the pore water pressure development of marine clays under long-term cyclic loading. They proposed a new hyperbolic correlation to predict the pore water pressure in low frequencies. Furthermore, they concluded that the effect of frequency depends on other cyclic test parameters, including the cyclic stress ratio, the number of cycles, and the duration of cyclic loading, which can be ignored when studying the long-term behavior of marine clay.

E

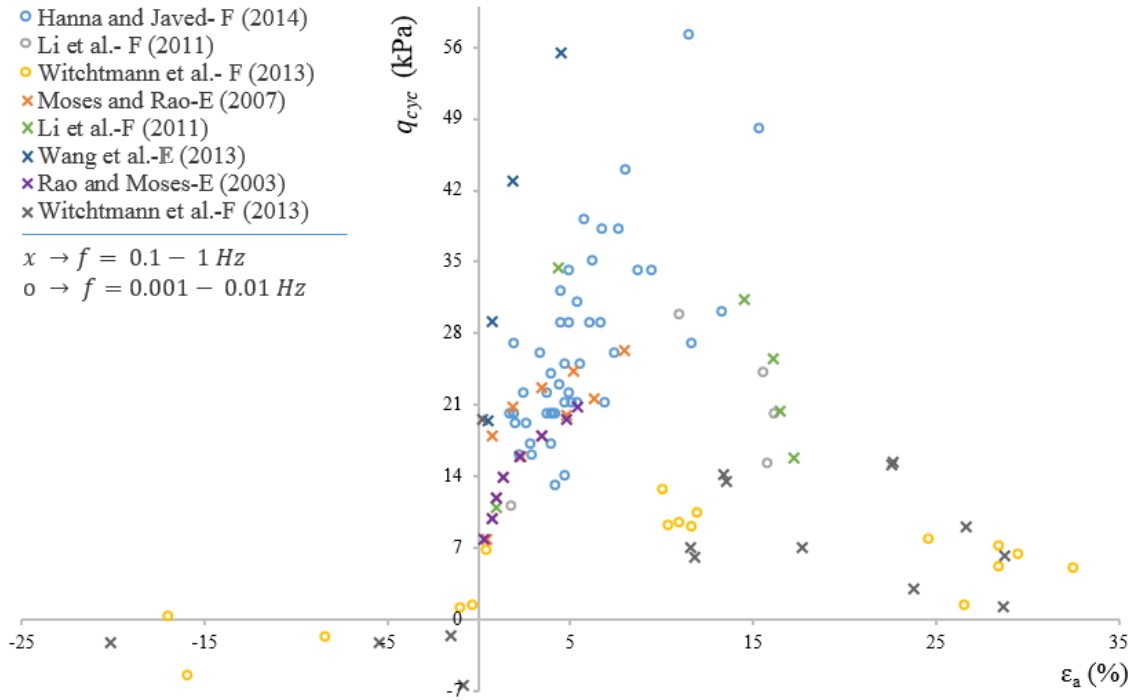


Figure 2.1: Effect of frequency (f) on marine clays' cyclic strength (q_{cyc} vs ϵ_a).

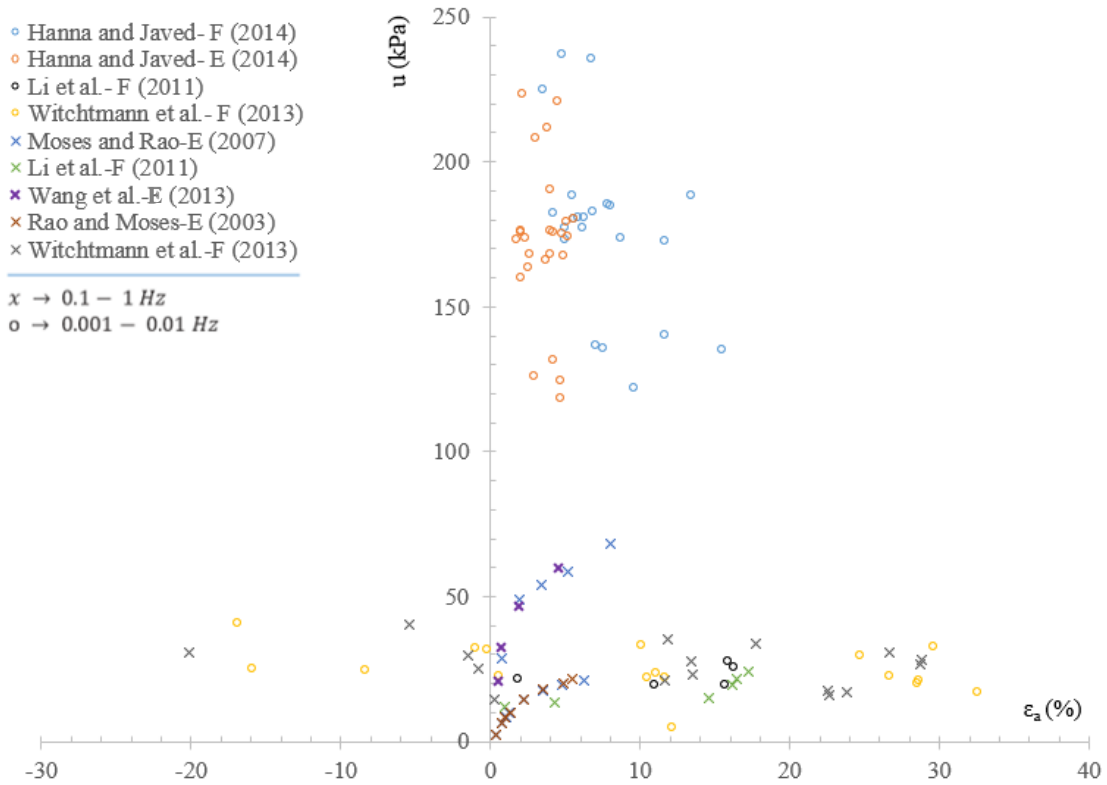


Figure 2.2: Effect of frequency (f) on marine clays' pore water pressure (u vs ϵ_a).

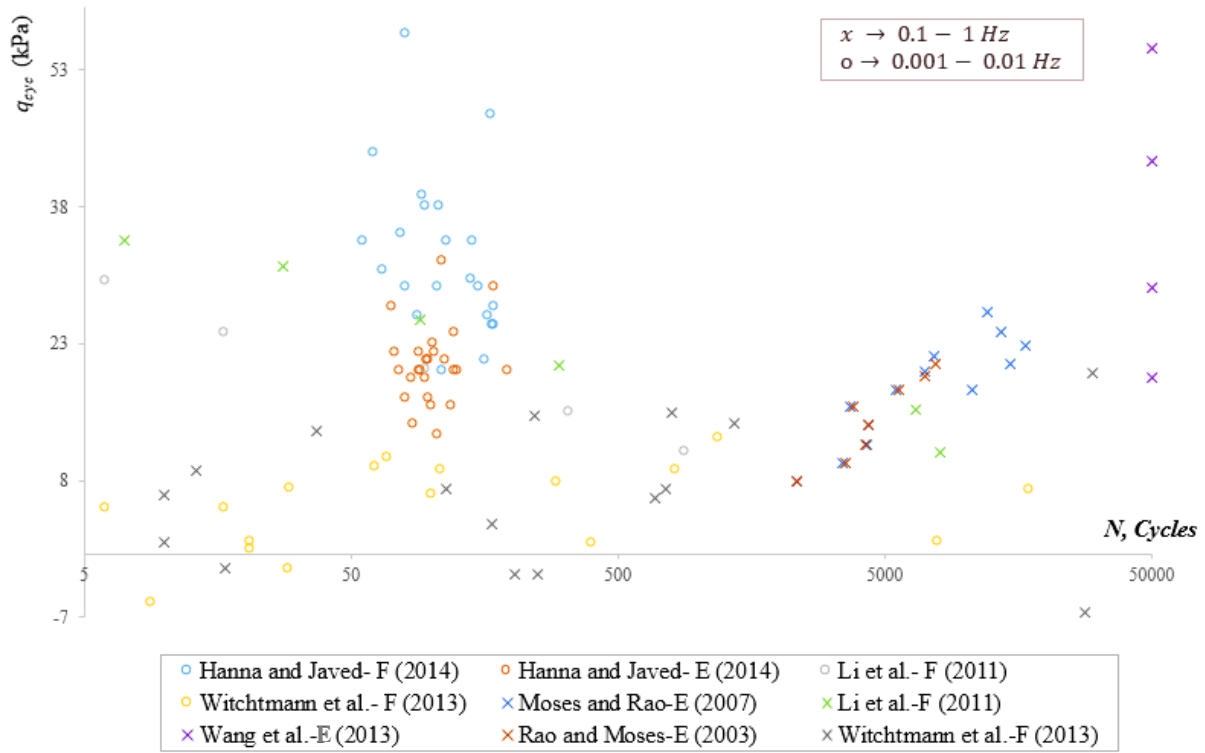


Figure 2.3: q_{cyc} vs N for different marine clays under cyclic loading.

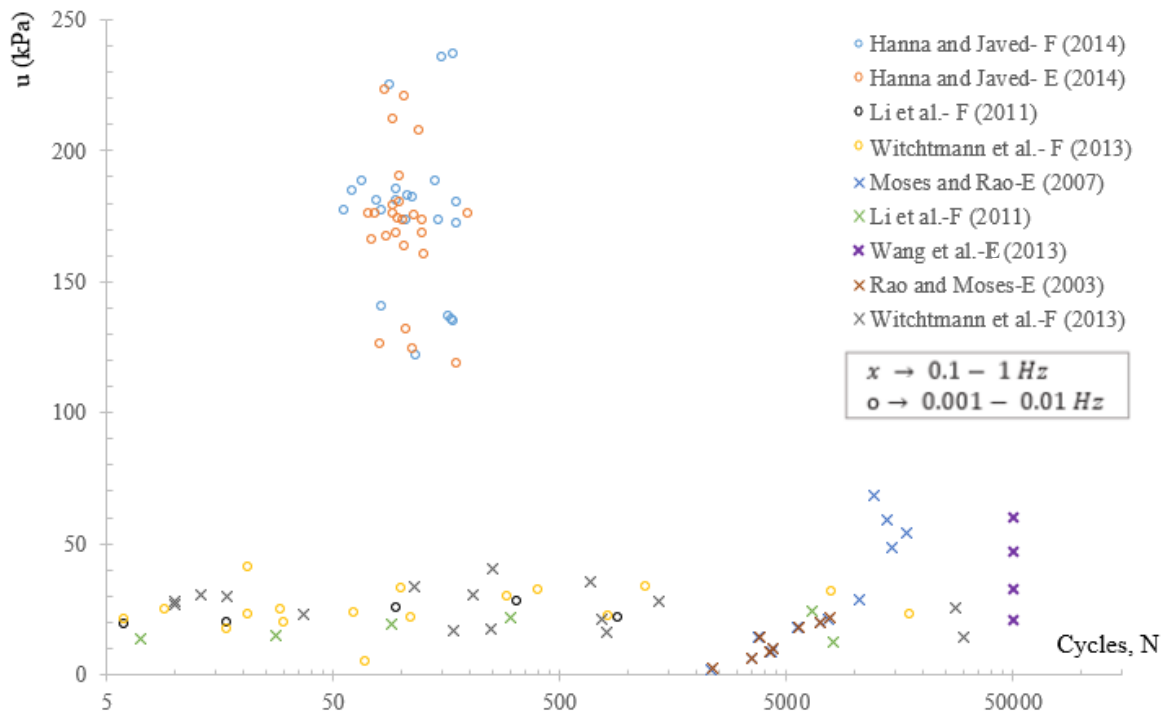


Figure 2.4: u vs N for different marine clays under cyclic loading.

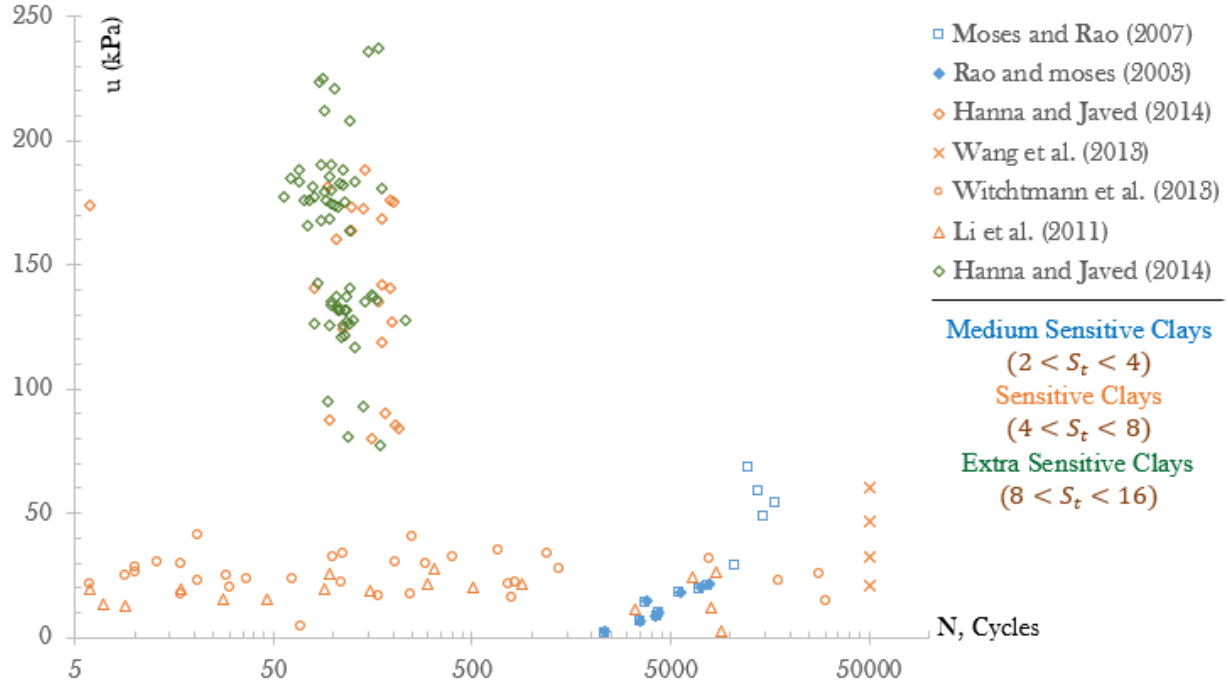


Figure 2.5: Sensitivity effect, u vs N for different marine clays.

The cyclic stress ratio and the number of cycles were the main two cyclic tests parameters studied in the literature. All studies performed different stress-controlled tests by varying the stress level to measure its effect on the marine clay cyclic behavior. **(Hanna & Javed, 2014)** Conducted experimental analysis on sensitive Champlain clay obtained from Quebec to examine the influence of the physical and mechanical properties which govern the shear strength of clays subjected to cyclic loading. An extensive triaxial tests on undisturbed (UD) and remoulded (RM) samples were conducted using different confining pressure N , loading frequency, cyclic stress ratio, and overconsolidation ratios.

The test datasets are scattered, reflecting the combined effect of the physical and mechanical parameters that govern this complex behavior. The pore-water pressure was a critical parameter that moves the effective stress path toward the failure envelope, which explains the role of the mechanical parameters governing this complex behavior. They found that sensitive marine clays subjected to cyclic loading will remain in equilibrium or a quasi-elastic resilient state if the magnitude of cyclic deviator stress remains below the stress threshold level for a given degree of saturation and stress conditions. A safe zone was established based on the critical/minimum values of the cyclic stress ratio corresponding to N (**Figure 2.6**) to incorporate the combined effects of the physical and mechanical parameters that govern the clay behavior. The proposed concept successfully classified the failed and maintained equilibrium datasets and can predict the threshold cyclic stress ratio CSR at which the sample will fail if subjected to a higher stress ratio. Still, the applicability of this concept to other marine clays in different locations and higher numbers of cycles is a controversial issue. The proposed demarcation line is given by **Equation 2.1**.

$$(CSR)_f = -14.23 \ln(N_f) + 107.1 \dots \dots \dots \mathbf{2.1}$$

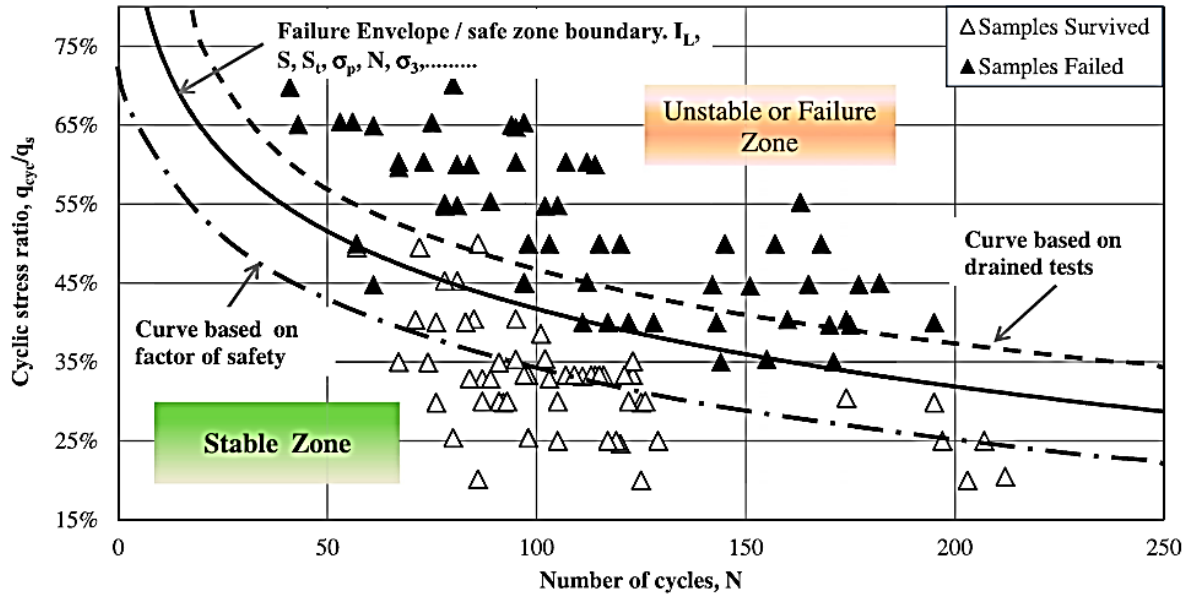


Figure 2.6: Safe zone concept based on the combined effect of physical and mechanical parameters of Marine Clays as proposed by (Hanna & Javed, 2014).

(Rao & Moses, 2003), (Moses & Rao, 2007) performed stress-controlled tests to measure the cyclic stress ratio just before failure for clays' samples. They reported that the threshold *CSR* is dependent on the stress level and frequencies applied during testing. Most of the studies in the literature agreed on the importance of the stress level (*CSR*) as a key parameter of the cyclic parameters in the stress-controlled tests. However, few studies proposed measuring the threshold or critical cyclic stress ratio. (Hyodo, Yasuhara, & Hirao, 1992) performed a series of stress-controlled tests on Ariake clay in Japan and proposed steps predict the time-dependent behavior of marine clays in undrained conditions. Two parameters were defined, the possibility of cyclic failure $RR(N)$ and the relative effective stress ratio (η^*) between the initial and failure points in the $p' - q$ space. The parameter (η^*) is a function of $RR(N)$ in which the latter can be calculated using **Equation 2.1** (the subscript f is denoting the failure), which represents a power relationship for the *CSR* and the number of cycles at 5% double amplitude strain (Log scale). The researchers proposed two correlations to predict the pore water pressure (u_p) and strain (ϵ_{DA}) response during cyclic loading.

$$(CSR)_f = 0.624N_f^{-0.071} \dots \dots \dots \mathbf{2.2}$$

The cyclic stress ratio distribution with the increasing number of cycles is shown in **Figure 2.7**. The datasets collected from the literature for different marine clays and locations listed in **Table 2.1** are used to understand the correlations of the *CSR* and number of cycles and their effect on the marine clay response. In addition, more datasets were collected from four studies and added to understand the correlations better(i.e. (Hyde, Yasuhara, & Hirao, 1993), (Hyodo, Yasuhara, & Hirao, 1992), (Guo, et al., 2013), and (Lei, Xu, Jiang, & Jiang, 2020)). The scattered data in **Figure 2.7** show an inflection behavior at a certain number of cycles, where the datasets can be divided into short and long-term behavior. The clays tend to fail at higher cyclic stress ratios in the

short term and maintain equilibrium at lower values. While in the long-term lives, the clays tend to stabilize at different cyclic stress ratios, except for some cases where the samples failed under low CSR and a high number of cycles. It can be concluded that the proposed methods in the literature do not apply to other marine clays as each of these methods were performed on a specific type of marine clays, and this led to the importance of proposing a new model that can help in understanding the intercorrelations between the marine clays' physical and mechanical properties and their response to long-term cyclic loading.

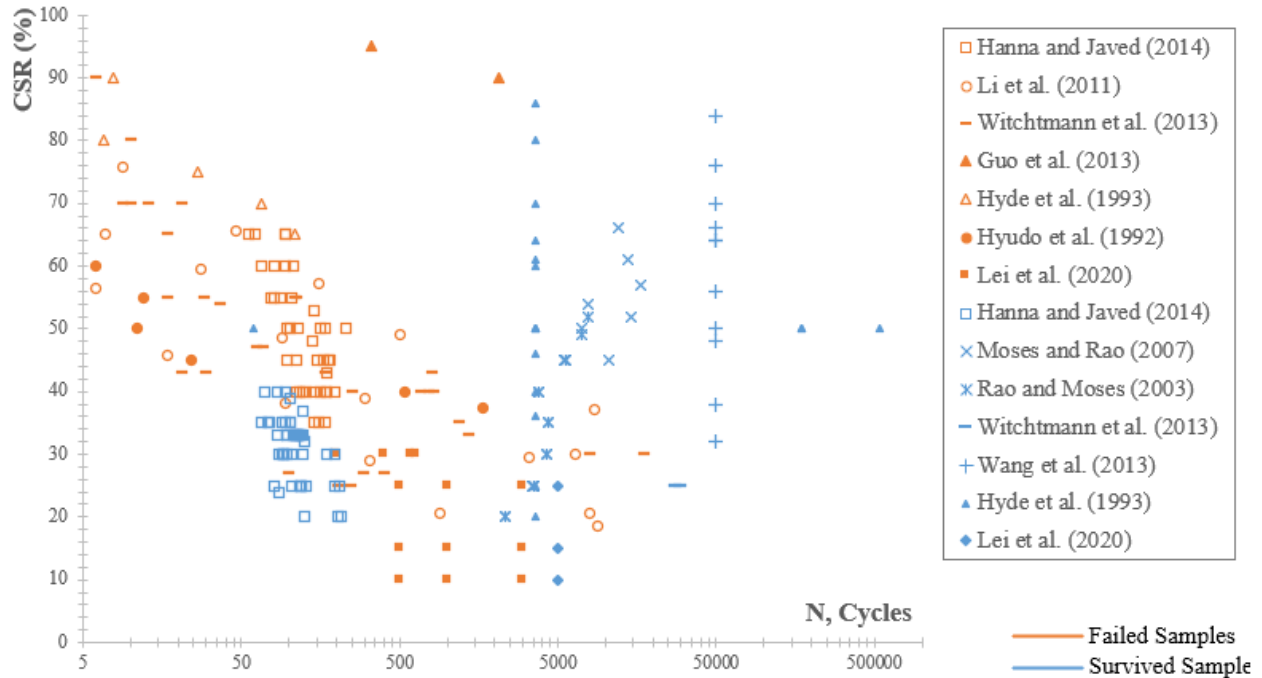


Figure 2.7: Failed and survived samples, CSR vs N for different marine clays.

(Hanna & Javed, 2014) studied the effect of remolding the marine clay on its cyclic response. The remolded samples have lower cyclic strength and tend to fail or maintain equilibrium under lower cyclic strain, as seen in **Figure 2.8**. However, the undisturbed samples maintained equilibrium at low cyclic strains. And a cyclic threshold strength of $q_{cyc} \cong 13 \text{ kPa}$ can be defined. **Figure 2.9** show the variation of the stress level with the number of cycles for the remolded and undisturbed samples, in which the remolded samples failed under low-stress levels of $CSR \leq 0.12$. Still, the remolded clays failed or maintained equilibrium under a wide range of cycles, which means that the remolded clay can withstand cyclic loading for a long time as much as the undisturbed clay does but under lower stress levels.

Figure 2.10 shows that the clay condition does not affect the pore water pressure development during cyclic tests. However, the researchers reported that the test results of clays having the largest liquidity index (I_L) showed that the pore pressure rose faster at lower strain for RM -samples, causing an early failure than the UD -samples.

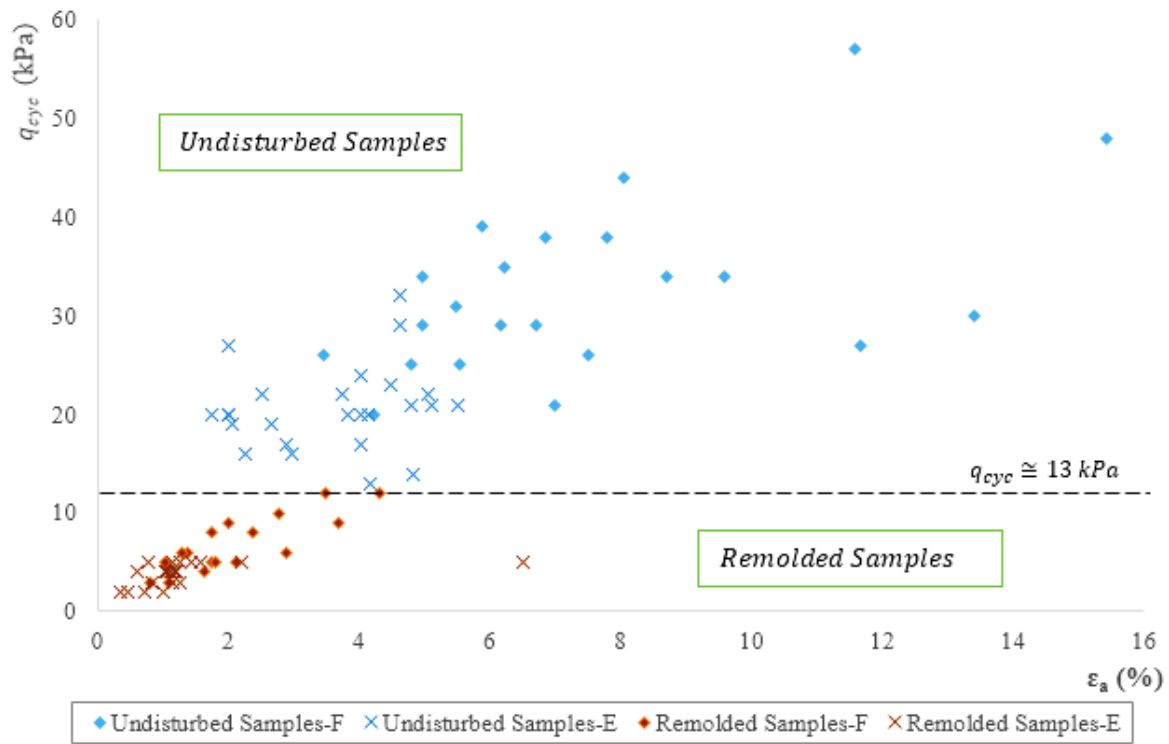


Figure 2.8: Undisturbed and remolded clay behavior, q_{cyc} vs ϵ_a [After Hanna & Javed, 2014].

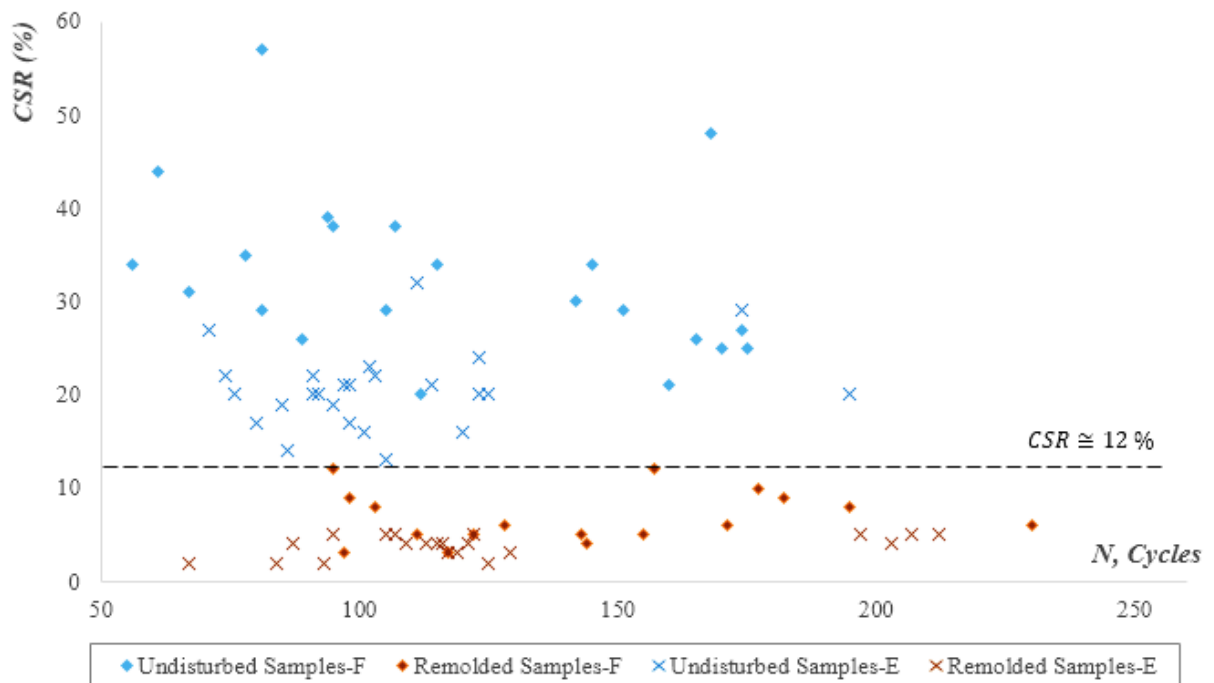


Figure 2.9: Undisturbed and remolded clay behavior, CSR vs N [After Hanna & Javed, 2014].

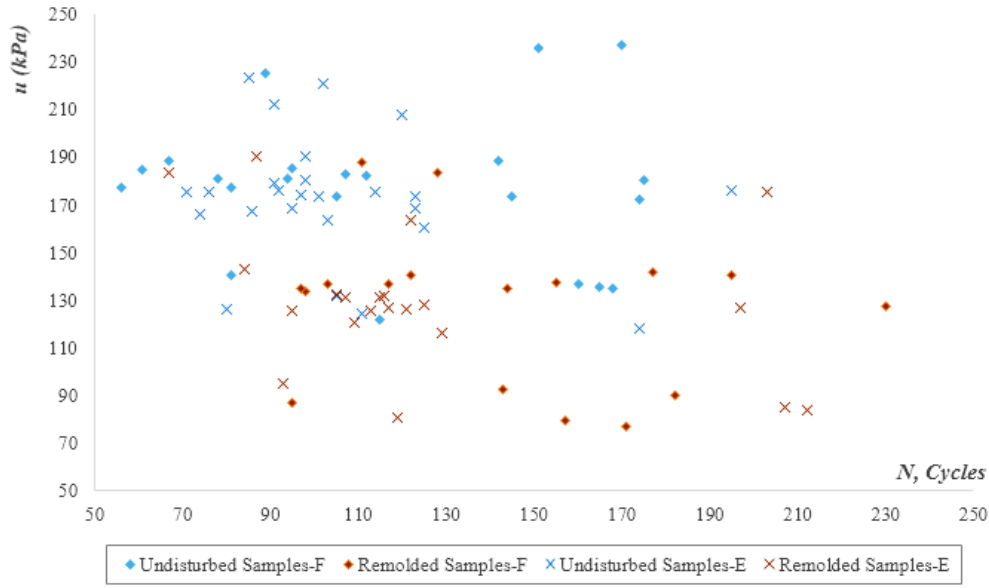


Figure 2.10: Undisturbed and remolded clay behavior, u vs N [After **Hanna & Javed, 2014**].

2.1.2 Cyclic Strain-Controlled Tests

The cyclic strain-controlled tests are widely used in testing the fatigue of structural elements such as steel and other metals, which provides more information about the long-term response to cyclic loading. The actual strength degradation is recorded when a constant strain amplitude is applied to the testing material until failure occurs. In the geotechnical field, remarkably few researchers performed such tests to study the marine clay response to cyclic loading. However, marine clays tolerate long-term stiffness deterioration when a foundation transfers cyclic loads over offshore structures' life span.

(**Idriss, Dobry, Doyle, & Singh, 1976**) performed strain-controlled tests to model the marine clay degradation in the free field when subjected to earthquake loading. They developed an equation to predict the backbone curve of marine clays as a function of shear strength and shear modulus. The degradation index (δ) and the degradation parameter (t) are two parameters introduced by (**Idriss, Dobry, & Singh, 1978**) to depict the performance of marine clay under cyclic loading. The researchers performed undrained cyclic Triaxial strain-controlled tests on samples collected from the San Francisco Bay Mud-US. They recorded the decrease in deviatoric stress at the tips of different loops at different cycles and defined the degradation index using the secant modulus of each loop using **Equation 4.1**. The degree of degradation (δ) was measured on the assumption that the strain amplitude ϵ_c Remains constant during the test, and that δ decreases linearly with increasing the number of cycles for any strain amplitude creating the degradation parameter (t). The degradation parameter is defined as the slope of the $\log \delta - \log N$ plot. It is essential to mention that the parameters were measured for a number of cycles that did not exceed 100 cycles.

$$\delta = \frac{(E_s)_N}{(E_s)_1} = \frac{(\sigma_d)_N / \epsilon_c}{(\sigma_d)_1 / \epsilon_c} = \frac{(\sigma_d)_N}{(\sigma_d)_1} \dots \dots \dots \mathbf{2.3}$$

Following (Idriss, Dobry, & Singh, 1978), researchers performed strain-controlled tests and modified several correlations for the degradation index and parameters listed in **Table 2.2**. Researchers' main concern was developing and proposing a new correlation for the degradation parameter as an essential design parameter representing the rate of marine clay degradation when subjected to time-dependent cyclic loading. However, the maximum applied cycles were 100 *cycles* which do not simulate the field conditions and lead to the question of whether these correlations represent the degradation rate of marine clays over the life span of offshore structures? Offshore structures in marine clays tolerate a high number of cycles that exceed 100 *cycles*, which leads to the fact that more cycles should be applied to measure the fatigue behavior of marine clays under cyclic loading.

(Hu, Ding, & Liu, 2010) performed cyclic simple shear tests on natural marine clays and measured the degradation index for 1000 *cycles*. They reported that most of the marine clay degradation occurred during the early stages of loading, in which the degradation index reaches a value of $\cong 0.3$. In addition, they highlighted the significant effect of cyclic strain amplitude on the degradation. At higher amplitudes $\geq 5\%$, the degradation occurs in the first 100 *cycles* of the cyclic loading showing more degradation. In comparison, at lower amplitudes $\leq 0.5\%$, the marine clay has a 0.05 degradation for a large number of cycles showing minor degradation.

Table 2.2: Summary for strain-controlled studies in the literature.

<i>Study</i>	Tested Parameters	Test Performed	Applied N	Max. amplitude
(Idriss, Dobri, & Singh, 1978)	δ, t	<i>Cyclic Triaxial</i>	100	4
(Idriss, Moriwaki, Wright, Doyle, & Ladd, 1980)	δ, t	<i>Cyclic Shear Test</i>	100	$\gamma_c = 0.5$
(Vucetic & Dobry, 1988)	δ, t, OCR	<i>Triaxial and Shear</i>	98	5
(Lee & Sheu, 2007)	δ, t	<i>Cyclic Triaxial</i>	100	4.2
(Hu, Ding, & Liu, 2010)	δ, t	<i>Cyclic Shear Test</i>	1000	$\gamma_c = 0.5$
(Mortezaie & Vucetic, 2013)	δ, t	<i>Cyclic Triaxial</i>	20	$\gamma_c = 0.5$
(Xiaoa, Guib, & Xuc, 2018)	δ, t, OC	<i>Cyclic Triaxial</i>	100	$\gamma_c = 1$

(Vucetic & Dobry, 1988) studied the effect of the overconsolidation ratio on the degradation parameter of marine clays and found that it decreases with increasing *OCR*. They also proposed an equation to translate the relationship between the degradation parameter *t* and cyclic strain to another loading condition: from $t_{Triaxial}$ vs ε_c to t_{Shear} vs γ_c by using **Equation 2.4**.

$$\varepsilon_c = \frac{\gamma_c}{\sqrt{3}} \quad \dots \dots \dots \quad \mathbf{2.4}$$

(Xiao, Guib, & Xu, 2018) studied the effect of the organic content on the degradation parameter of marine clays by performing a series of cyclic triaxial tests on natural marine clays. They applied several tests by varying the organic content and frequencies and reported decreased degradation index by increasing the organic content. Also, they found that the degradation index increases with increasing frequency.

2.2 MARINE CLAY-MONOPILE CYCLIC RESPONSE

Some researchers' concern was accurately predicting the load-deflection behavior of laterally loaded piles; they conducted experimental tests using different parameters and techniques on piles embedded in soft clays with different scale and stiffness conditions (**Table 2.3**). Most of the researchers approved that the pile stiffness and L/D ratio highly affected the response piles under lateral cyclic loading, on the other hand; the clay indices (*i. e.*, I_L, I_C) also have a marked effect on the system response. The soil flow mechanisms around rigid, flexible, and semi-rigid piles subjected to lateral cyclic loading were tested by (**Hong, et al., 2017**), who propose different soil flow mechanisms and pile behavior.

One of the remarkable limitations of the experimental studies is the number of loading cycles applied during the test, in which a maximum number of cycles $N \cong 500$ was reported in the literature. This number of cycles does not represent the cycles in the field loading, except for (**Lombardi, Bhattacharya, & Wood, 2013**), who studied the long-term performance of a scaled model of wind turbine supported by a monopile.

Table 2.3: Summary of existing studies - Experimental and field studies on Clay-Monopile system lateral cyclic response.

Study	Objectives and Setup	Tested Parameters	Pile Stiffness	Clays	Cyclic Loading
1 Experimental Tests					
Rao et al. 1992 Rao & Rao, 1993 Prasad & Rao, 1994	<ul style="list-style-type: none"> ▪ $P - y$ behavior ▪ Uplift behavior ▪ Pneumatic control loading system 	$e, K_{rc}, I_L, N, D, I_c, L/D$	Flexible Rigid Helical	Marine clay	One-way (up to $N = 500$)
Khemakhem, et al., 2010	<ul style="list-style-type: none"> ▪ $P - y$ behavior ▪ Centrifuge Test (50g) 	Stiffness	Rigid	Specwhite Kaolin	One-way "N = 50 sinusoidal"
Zhang, et al., 2011		Stiffness Reconsolidation	Flexible	Specwhite Kaolin	One-way/ Two-way "up to $N = 40$ "
Hong et al., 2017		Soil-flow mechanisms	Flexible, Rigid, Semi-rigid	Specwhite Kaolin	One-way "up to $N = 100$ "
Lombardi et al., 2013	<ul style="list-style-type: none"> ▪ Long-term behavior of OWT. ▪ Scaled model 	$f, \zeta, N, P/GD^2, D$	Model Pile	Specwhite Kaolin	1P 172,000 Cycles
2 Field Tests					
Jeong, et al., 2007	<ul style="list-style-type: none"> ▪ $P - y$ behavior 	f , Plastic hinge	Small, Full scale	Marine clay	One-way Two-way
Sa'don et al., 2014	<ul style="list-style-type: none"> ▪ Analytical model ▪ Field tests 	Stiffness	Long elastic	Residual clay	Excitation Frequencies
Byrne, et al., 2015	<ul style="list-style-type: none"> ▪ Field data to validate the numerical model. ▪ PISA Project 	M/HD L/D	Monopile	Quaternary clay	One-way
Zhu et al., 2017	<ul style="list-style-type: none"> ▪ The behavior of driven large-diameter piles. 	f, α, t	Large diameter	Soft clay	One-way $N = 20/6\text{min.}$ "

It is vital to notice the use of Specwhite Kaolin to model the marine clay, which is questionable since it may not represent the actual behavior of marine clay. Furthermore, the experimental studies were mainly conducted using small-scale hollow aluminum piles that did not represent the field conditions.

Minimal field studies reported in the literature are likely due to the high cost and challenges of conducting such studies. The pile stiffness and load frequencies were the main tested parameters of different pile sizes, as shown in **Table 2.3**. However, the number of cycles N applied to these field tests was generally low and did not represent the field conditions. In addition, the field studies agreed on the occurrence of the plastic hinge at a shallower depth ($3D - 4D$) compared to the reported values in the experimental studies ($6D - 7D$), which may affect the design considerations.

A comparison made with the field test results reported by (Jeong, Kim, Kim, & Shin, 2007) and (Zhu, Zhu, Li, Liu, & Liu, 2017) for 340 kN load to compare the results of field studies, **Figure 2.11** shows the horizontal displacement and bending moments. The tests characteristics for both studies are listed in **Table 2.4**. Both field tests agreed that the plastic hinge, at which the bending moment reached its maximum value, occurred at a shallower depth of about $3D-4D$ compared with the reported values in the literature ($6D$ or $7D$) for soft clays. However, Zhu et al. (2017) reported a max horizontal lateral displacement much higher than Jeong et al. (2007) due to the pile stiffness variation in the two methods.

Table 2.4: Field tests characteristics for two selected studies
[(Jeong, Kim, Kim, & Shin, 2007), (Zhu, Zhu, Li, Liu, & Liu, 2017)].

Study	Pile	Pile ϕ , m	Embedded L, m	Clay Layer, m	Cyclic Loading	$p - y$ Curves
Jeong, et al., 2007	Drilled-Shaft	2.4	45 ($L/D = 18.75$)	19	Incremental loading (ASTM D-3966) 10 min intervals Target Load: 850 kN	O'Neill (1984)
Zhu, et. al., 2017	Open-ended/Steel	2.2	57.4 ($L/D = 26.1$)	24.5	20 6 min each cycle Target Load: 300 kN	Zhu et al. (2012)

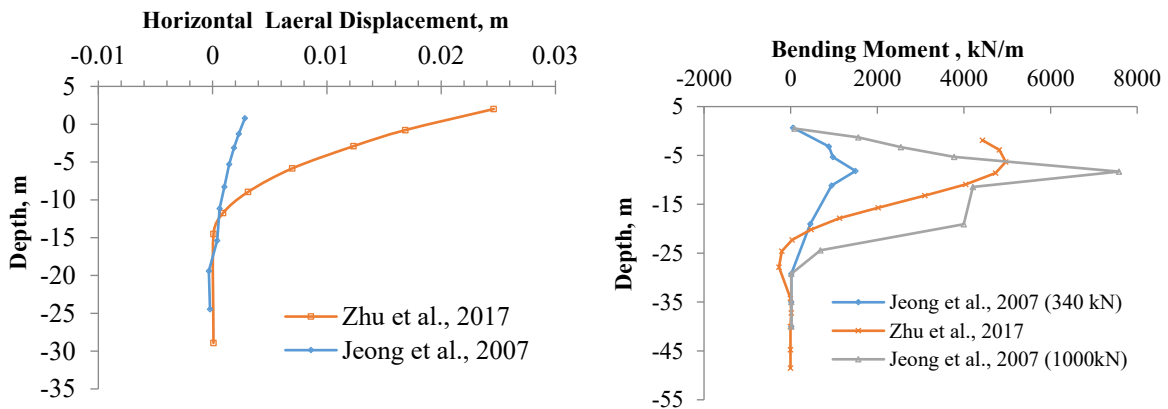


Figure 2.11: Field tests results of (Jeong, Kim, Kim, & Shin, 2007) and (Zhu, Zhu, Li, Liu, & Liu, 2017) studies: (a) Lateral Displacement; (b) Bending moment.

Most experimental and field studies applied one-way cyclic loading to the Clay-Monopile system, referring to the most critical loading since the two-way loading may improve the system response. In addition, most of the studies showed that the adopted criteria of the **API code** are relatively conservative. As a result, it overestimates or underestimates the load-deformation behavior of the Clay-Monopile system.

As mentioned previously, many difficulties are associated with the field tests to measure the response of the pile-soil system subjected to lateral cyclic loading and the high cost required to conduct such studies. On the other hand, there are still concerns about the size effect in the conducted experimental tests due to the small-size piles used, which may not reflect the actual behavior of the large-diameter piles in the field. Therefore, numerical studies are assumed to be an effective tool in simulating large-scale problems. Furthermore, these methods are usually validated using field or experimental tests results conducted in parallel with the numerical analysis or the available test results in the literature.

The numerical techniques become an effective tool for simulating large-scale problems, i.e., Clay-Monopile system response to lateral cyclic loading, owing to the previously mentioned limitations of experimental and field tests. Therefore, numerical studies reported in the literature were conducted using different constitutive models and numerical techniques, as shown in **Table 2.5**. In addition, some researchers proposed new methods to construct $p - y$ curves such as (**Rajashree & Sundaravadivelu, 1996**) and (**Dewaikar, Padmavathi, & Salimath, 2008**).

(**Hong, et al., 2017**) Studied the plastic hinge formation and the accumulation of lateral deformation behind the laterally loaded piles that may reflect the design considerations. The results agreed with that reported by the field tests and numerical studies (**Byrne, et al., 2015**) and (**Zdravković, et al., 2015**). The latter presented the concept of the rotational flow mechanism or what they call "kick-back" at lower depths of short piles and proposed a new design method as discussed in the previous sections.

Most of the reported studies in the literature were concerning conducting laboratory, field, and numerical studies to overcome the nonconservative estimation of the available design codes; the researchers considered different parameters in their studies that significantly affect the Clay-Monopile system response. However, a few studies in the literature propose new methods to construct the load-deformation curves or new design approaches, as listed in **Table 2.5**. (**Bouزيد, Bhattacharya, & Dash, 2013**) modified a technique to construct continuous $p - y$ curves taking the advantage of the whole stress-strain curve of a representative clay, they developed a semi-analytical FE approach to defining the scaling factors M_c and N_c used in transferring the stress-strain diagram to the load-deformation curve. (**Byrne, et al., 2015**) Proposed a new design consideration for large piles under laterally cyclic loadings. Their method, as mentioned before, agreed with what (**Hong, et al., 2017**) proposed.

As discussed before, the clay indices and parameters control the behavior and response of marine clays to cyclic loading. Although there is no clear evidence for which one of these parameters controls the behavior, a maximum of two or three parameters can be studied and compared. Studies in the literature focused on the general behavior of marine clays without considering the clay parameter variation; the pore water pressure generation also was one of the crucial parameters studied and reported in the literature. Very few studies raise the importance and influence of clay sensitivity on the cyclic behavior of marine clays. However, the **CFEM** reported that the clay

response becomes a hazard for sensitive clays when subjected to lateral distortion (**Canadian Geotechnical Society, 2006**).

Table 2.5: Summary of Existing studies - Numerical modelling studies on Clay-Monopile system lateral cyclic response.

Study	Objectives and Tools	Proposed Model (Numerical/ Analytical)
1 Numerical Modelling Tests		
Rajashree & Sundaravadivelu (1996)	<ul style="list-style-type: none"> ▪ The response of laterally loaded pile in soft clay ▪ Written nonlinear FE code 	<ul style="list-style-type: none"> ▪ Clays: 20 elastoplastic sub-element Springs ▪ Piles: beam element ▪ No gap formation ▪ Validated with Rao et al. (1992)
Budkowska & Priyanto (2003a,b)	<ul style="list-style-type: none"> ▪ The sensitivity of maximum deformations due to changes of design variables ▪ Nonlinear FD program Com624P 	<ul style="list-style-type: none"> ▪ Virtual work principle ▪ Detect which part of the surrounding soil is nonlinearly elastic, linear softening, or plastic flow.
Fakharian et al. (2008)	<ul style="list-style-type: none"> ▪ To model the monotonically and cyclically lateral loaded piles ▪ ANSYS and Flac-3D 	<ul style="list-style-type: none"> ▪ FEM and FDM ▪ Clays: strain-softening law for cyclic loading and Von Mises law for monotonic loading ▪ Validated with Matlock (1970)
Dewaikar et al. (2008)	<ul style="list-style-type: none"> ▪ To compute the ultimate lateral resistance of a long, flexible pile ▪ New method to construct $p - y$ curves 	<ul style="list-style-type: none"> ▪ Iterative analysis ▪ Tested variables: pile diameter, eccentricity, and N ▪ Validated with Matlock (1970)
Haiderali, et al. (2015)	<ul style="list-style-type: none"> ▪ To investigate the cyclic lateral loading of monopile in London clay ▪ One-way and two-way loading ▪ Abaqus 2012 ▪ Clays inside pile included 	<ul style="list-style-type: none"> ▪ 3D soil-pore fluid FE analysis ▪ Clays: t_{ij} constitutive model (consider σ_2)/ 8-noded brick elements (C3D8P) ▪ Interface: small sliding surface-to-surface ▪ Pile: 8-noded shell elements (SC8R) ▪ Validated with centrifuge test
Zdravković et al. (2015)	<ul style="list-style-type: none"> ▪ To model the response of large diameter pile to lateral cyclic loading ▪ FE code ICFEP 	<ul style="list-style-type: none"> ▪ 3D- FE Analysis ▪ Clays: 20-noded hexahedral elements/ Tresca ▪ Piles: 8-noded shell elements/ elastic ▪ Interface: 16-noded zero-thickness elements/ Tresca
Hong et al. (2017)	<ul style="list-style-type: none"> ▪ To reveal 3D soil flow mechanisms ▪ The influence of pile diameter on soil flow and lateral soil resistance 	<ul style="list-style-type: none"> ▪ Clays: C3D8P element/ and hypoplastic clay model ▪ Pile: S4 shell elements ▪ Interface: zero-thickness slip elements (Coulomb friction law) ▪ Validated by centrifuge tests
2 Design approaches		
Bouzid et al. (2013)	<ul style="list-style-type: none"> ▪ Propose a new method to construct continuous p-y curves 	<ul style="list-style-type: none"> ▪ Mobilized Strength Design (MSD) concept ▪ M_c and N_c based on semi-analytical FE analysis ▪ Pile: series of discs ▪ Interface: 6-noded elements ▪ Validated with FE software (COMSOL 2009)
Byrne, et al. (2015)	<ul style="list-style-type: none"> ▪ To develop a new design method for large diameter monopiles under lateral loading ▪ Field test and numerical modeling 	<ul style="list-style-type: none"> ▪ A kick-back concept proposed ▪ Extension of $p - y$ approach in which additional soil reaction terms are included ▪ Recommended to include more advanced geotechnical effects

The behavior of an undisturbed sample clay in undrained conditions and subjected to both static and cyclic loading (Javed, 2011) is shown in Figure 2.12. The significant shear strength loss reported due to cyclic loading with relatively low $CSR = 0.33$ is a worthwhile if compared with the results reported by other researchers such as (Rao & Rao, 1993), where they found that no significant loss of shear strength will occur with $CSR < 0.65$.

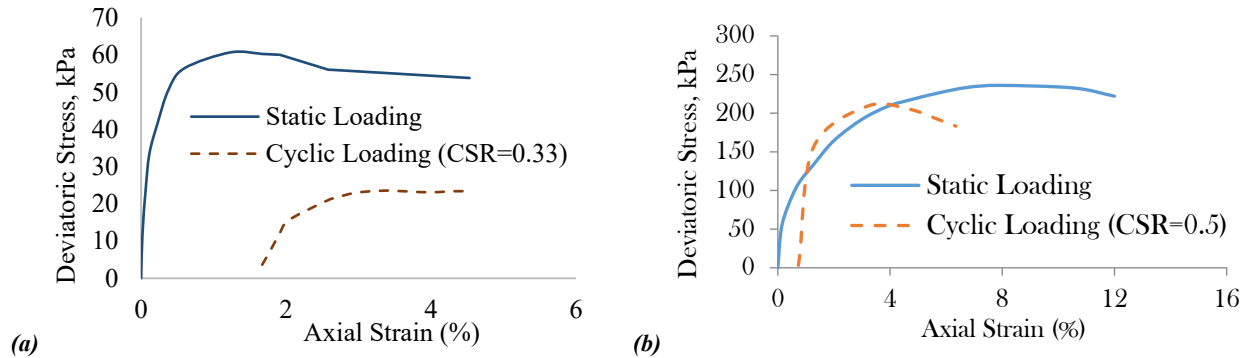


Figure 2.12: Reduction in shear strength due to cyclic loading: (a) After (Javed, 2011), (b) After (Rao & Rao, 1993).

Most of the previously discussed papers were concerning conducting laboratory, field, and numerical studies to overcome the nonconservative estimation of the available design codes by considering different parameters that significantly affect the pile-clay system response. In addition, a minimal number of studies proposed a new design or load distribution approaches found in the literature; these studies and a study of marine clay behavior under cyclic loading will be discussed in this section.

(Bouziid, Bhattacharya, & Dash, 2013) Uses the principle of mobilized strength design to conduct a semi-analytical linear-elastic FE analysis and construct continuous $p - y$ curves. Most of stress-strain features were retained by using two scaled coefficients N_c (for stress) and M_c (for strain) to construct the continuous $p - y$ curve as shown in Figure 2.13. They use a cylindrical coordinate system to model the pile-soil behavior. The pile was modelled using a series of embedded discs subjected to horizontal loading and six-nodded interface elements. Normal and shear stresses exist as they are not materials used to model the soil-pile interface. The method was validated by applying the same problem in FE software (COMSOL 2009). They reported that the API curve underestimated the pile head response at initial loading and overestimated the pile capacity at higher loads. Also, it found that the API had a similar ultimate capacity to the proposed method using the reduced N_c and M_c .

(Byrne, et al., 2015) Based on the previously mentioned field tests and numerical modeling conducted by (Byrne, et al., 2015) and (Zdravković, et al., 2015), the researchers proposed a new design method for large diameter piles subjected to lateral monotonic loading. They suggested that it is essential to include the fatigue design and assessment of the dynamic performance of the pile-soil system. The design approach extends the $p - y$ approach in which additional soil reaction terms are included as shown in Figure 2.14. The $p - y$ curves in the proposed method will be

established on a site-specific basis instead of the local conditions as in the conventional methods. This approach will depend on extracting the stresses induced on the soil-pile interface in a finite element analysis on model piles and using these stresses to establish site-specific soil reaction curves, which could be used to conduct the detailed design. They found that the API method underpredicts the stiffness and ultimate capacity of the pile in clays for both short and long piles. Also, it found that the distributed load curves alone are insufficient to compute the pile response accurately. Each load component offers approximately equal contributions to the computed lateral load H . The researchers recommended including advanced geotechnical effects: multidirectional loading, damping, densification, age hardening, installation methods, and creeps in future studies.

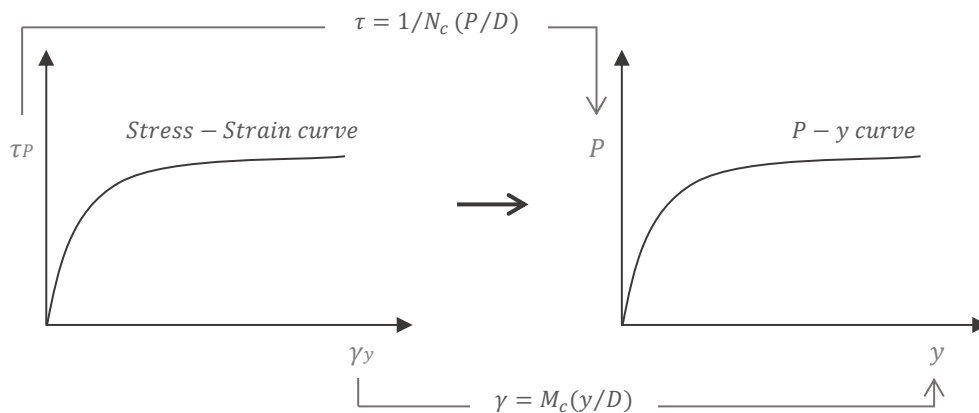


Figure 2.13: Procedure of obtaining $p - y$ curve from the clay stress-strain behavior, After (Bouزيد, Bhattacharya, & Dash, 2013).

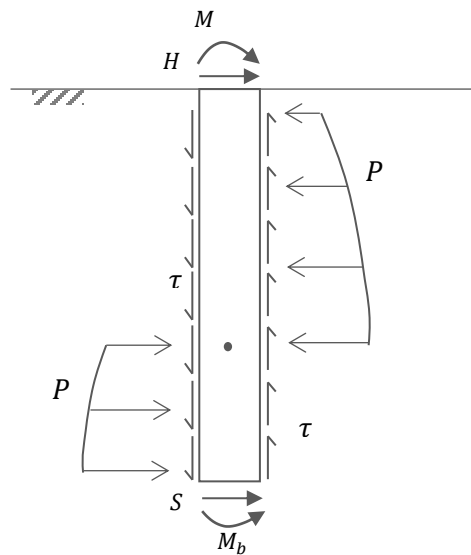


Figure 2.14: Soil reaction components applied to a monopile, After (Byrne, et al., 2015).

2.3 RESEARCH GAPS

The most crucial failure of the monopile-marine clay system is the serviceability failure. The failure is time-dependent, where the monopile accumulates lateral deformations responding to marine clay stiffness degradation. Accordingly, understanding the fatigue behavior of marine clays is essential. Most of the studies performed in the literature are stress-controlled tests, in which a constant stress amplitude is applied and the strain development measured.

Most of the stress-controlled tests were performed to study the effect of marine clay's physical and mechanical properties on its response to cyclic loading. However, one or two of these parameters were varied and discussed due to the complexity of the marine clays' properties. In addition, the results obtained cannot be generalized to all marine clays worldwide as they have different mineralogy and physical properties. Some researchers were concerned with predicting the marine clay threshold stress level, where the soil will fail if loaded more. Still, these proposed methods cannot be applied to all marine clays. One of the limitations of the stress-controlled studies available in the literature is that most of these studies can describe the short-term response to cyclic loading. Few studies applied a large number of cycles with limiting the studied parameters, which does not simulate the field conditions.

The strain-controlled tests count for the actual stress-strain response to cyclic loading, where the time-dependent response to cyclic loading can be observed. Unfortunately, few studies in the literature performed strain-controlled tests, and a maximum of 1000 *cycles* were applied. Moreover, the absence of measuring the fatigue life of marine clays by applying cycles until failure is a significant limitation for this type of testing.

The widely used p - y transfer load method proposed by (Matlock, 1970) and adopted by several design codes is still controversial for the monopile-marine clay system response. It is calibrated to simulate certain field conditions. From the previously discussed studies in the literature, it can observe that most of the proposed models were corrected and calibrated to match the tested site condition. The available empirical theories extracted from these studies may not be applicable for other site conditions or the recent offshore structures, as the offshore construction is growing with time and going deeper.

There are some concerns about the scale effect of using small-scale piles to model the Clay-Monopile response to lateral cyclic loading in the experimental studies. It may not represent the field behavior of large-diameter piles. Therefore, an improving analysis method is required for large diameter piles in future studies to replace the existing methods. Numerical modelling was an efficient tool to model large-scale soil problems such as the Clay-Monopile system response to lateral cyclic loading. Using numerical models can help perform a fatigue-life estimation for the monopile-clay system by applying a constant strain amplitude and measuring the system response.

Most laboratory tests modelled the clay using the Specwhite Kaolin clays due to the difficulty of collecting representative clay samples from the field. As reported by (Rossato, Ninis, & Jardine, 1992), Kaolin has lower drained and undrained shear strength and stiffness than natural marine clays; this may affect the test results and its suitability to model the clay behavior. The researchers emphasized the importance of studying clay strength and its deformation behavior as a critical design factor significantly affects pile behavior and response to lateral cyclic loadings.

2.4 RESEARCH SIGNIFICANCE

This research correlates the marine clay fatigue response to cyclic loading and the monopile-marine clay system fatigue response. The fatigue life of marine clays will be estimated by performing strain-controlled cyclic Triaxial tests and cycling the samples until failure. Numerical modeling effectively solves large-scale geotechnical problems like the monopile-clay system fatigue response to cyclic loading. In addition, the clay parameters that mainly affect the marine clay to cyclic loading can be reported using Machine Learning Techniques and the available data in the literature for the stress-controlled cyclic tests. The proposed research hierarchy is shown in **Figure 2.15**.

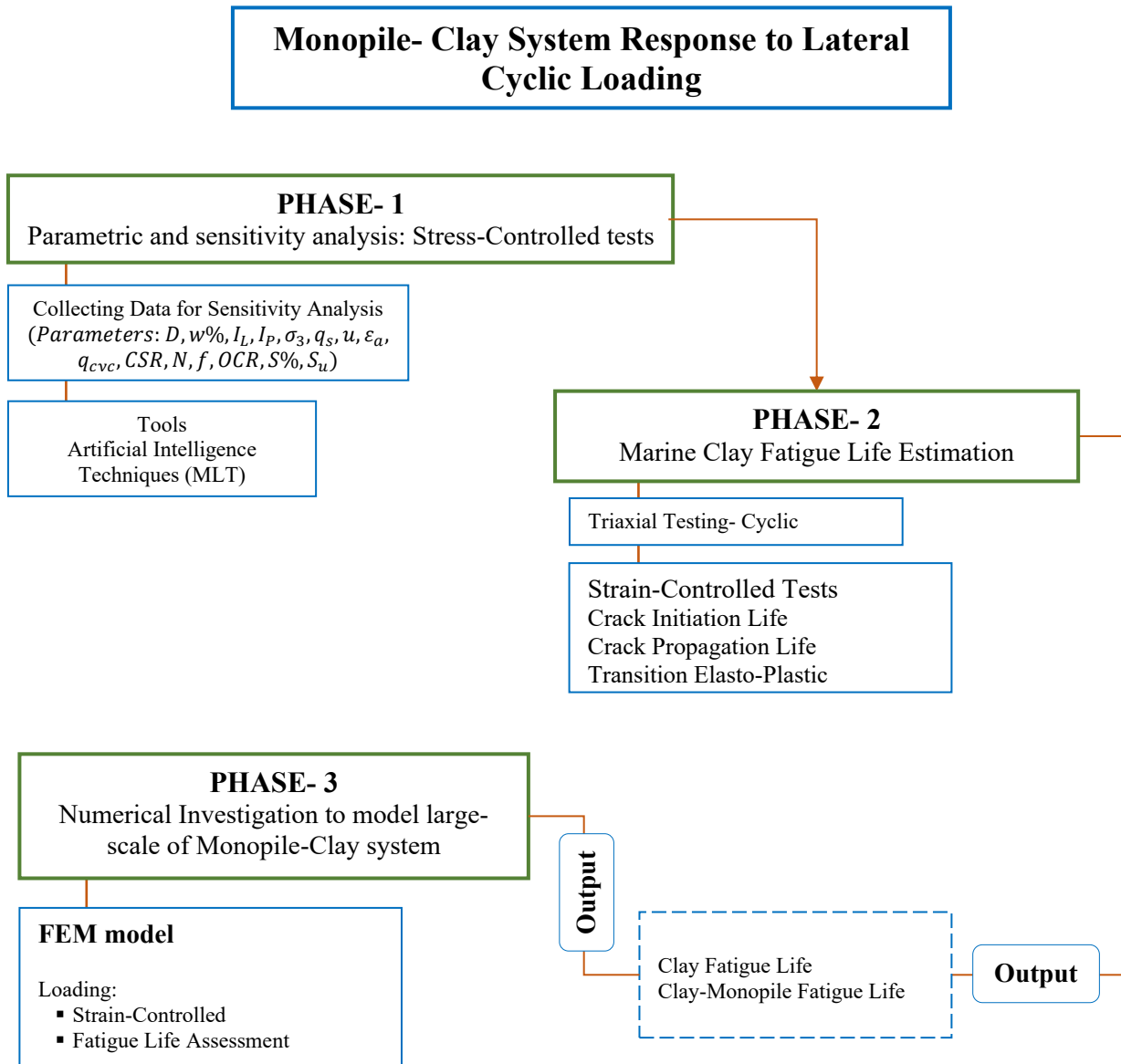


Figure 2.15: Proposed research methodology.

CHAPTER 3

PARAMETRIC ANALYSIS FOR MARINE CLAYS PROPERTIES: MACHINE LEARNING TECHNIQUES

"A profile of relevant soil properties at a site is required to characterize the soil resistance for extreme event analysis. Soil strength data are particularly important in characterizing soil resistance. In some cases, other model parameters (such as initial soil stiffness and damping) are correlated with strength values and thus can be estimated from the strength profile or other rules of thumb" (API, 2000).

When an offshore infrastructure system is subjected to severe cycles of winds and surface waves through the life span of these structures, an accumulation of deformations and strength deterioration in marine clays are one of the significant failure causes of the system. Therefore, the marine clay response to cyclic loading is controversial in geotechnical research; the complexity of the marine clay structures, non-homogeneity, and mineralogy makes it hard to emulate its response when subjected to cyclic loading.

The physical and mechanical properties control the marine clay response to cycling; many studies in the literature performed laboratory tests to investigate the effect of marine clay properties on its strength deterioration when subjected to cyclic loading. The most common test is the triaxial stress-controlled cyclic test that measures the clay stiffness deterioration by applying a constant stress amplitude. It was agreed in the literature that marine clay properties significantly affect its response to cyclic loading, but which of these properties is mainly affecting its behavior is still a debate. The main objective of this chapter is to define which of the marine clay parameters are significantly affect stiffness deterioration by performing a parametric analysis and using machine learning techniques. Correlations and failure assessment will also be presented in this chapter after highlighting the marine clay response under monotonic and stress-controlled cyclic tests.

3.1 MARINE CLAYS STATIC RESPONSE

Marine clays are soft clays usually saturated to fully saturated, with physical properties that differ depending on their location and origin. Marine clays have a relatively high plasticity index, in situ water content, and liquidity index. Experimental or field tests can be conducted to figure out the mechanical properties of marine clays. Data for tested marine clays collected from the literature will be used to understand better the 'marine clays' behavior when subjected to static and cyclic loading. **Table 3.1** shows some marine clay's physical properties for these clays collected from different locations worldwide.

The stress-strain diagram for clay samples collected from Saint-Hyacinthe in Quebec, Canada, and other studies from the literature are shown in **Figure 3.1a**. The marine clays under monotonic loading behave as nonlinear and non-homogeneous material. This behavior can be clearly defined by the stress-strain curve in which the strength nonlinearly increases until it reaches an ultimate value and continues deforming at a slow rate. Alternatively, some clays show peak strength and then continue deforming dramatically until failure. All selected clays were tested under 40 – 50 *kPa* confining pressure. The clays' response variance shown in the figure indicates how the clays' properties influence the static behavior. For example, clays from Saint-Hyacinthe show a weak response to loading; the very high sensitivity of this clay may explain the low shear strength response and quick failure of this clay. Other clays' properties may affect the behavior, which can be studied separately, but only two or three parameters can be included in a graph.

The pore water pressure generation under static loading is also affected by the clay history and properties. **Figure 3.1b** illustrates the increase of pore water pressure under monotonic loading. The pore water pressure increases at a high rate during the beginning of the test and then tends to stabilize or continue to increase until the end of the test. It is essential to mention that the softer the clay is, the higher pore water generated during a monotonic test. Moreover, the lower the water pressure generated, the higher the clay's strength is. However, for (Wang, Guo, Cai, Xu, & Gu, 2013), the clay generated higher pore water pressure but lower strength than (Wichtmann, Anderson, Sjursen, & Berre, 2013). Which again highlighted the effect of the clay properties on its response to loading.

The confining pressure (σ_3) is one of the clay's mechanical properties that significantly affect its static behavior. The effect of the confining pressure is shown in **Figure 3.2** for samples collected from Saint-Hyacinth in Quebec. The figure shows that the clay strength response increases with increasing the confining pressure; however, the samples tested under 50 *and* 100 *kPa* deteriorate at a higher rate (20% loss of strength occurred before reaching 5% strain values). Studies in the literature agreed with this behavior.

Table 3.1: Some marine clay's physical properties from different locations.

<i>Location</i>	<i>w</i> %	<i>w_L</i> %	<i>I_p</i> %	<i>I_L</i> %	<i>e₀</i>	<i>γ₀</i>	<i>S</i> %	<i>S_t</i>
This Study- Saint-Hyacinthe- /Canada	75.5	77.1	45.87	0.90	1.863	14.96	100	19.80
Moses and Rao (2007)- India	80	88	60	0.87	2.13	14.48	100	3.00
Wang et al (2013)- China	67.5	63.4	35.8	1	1.896	15.51	100	5.15
Wichtmann et al (2017)- Norway	64	63	33.7	1.03	1.73	16.18	100	5.3

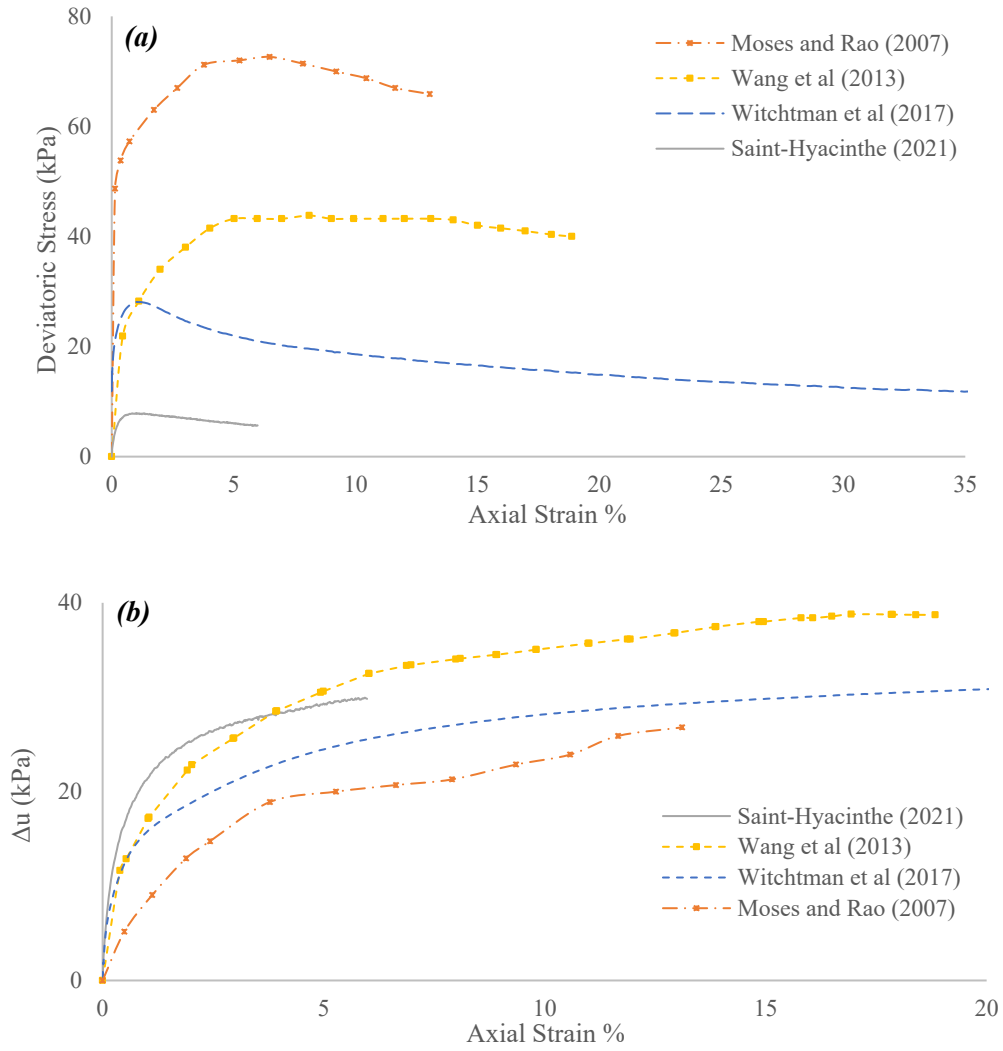


Figure 3.1: Marine clays behavior under monotonic loading (a) Stress-Strain diagram, (b) Change in pore water pressure.

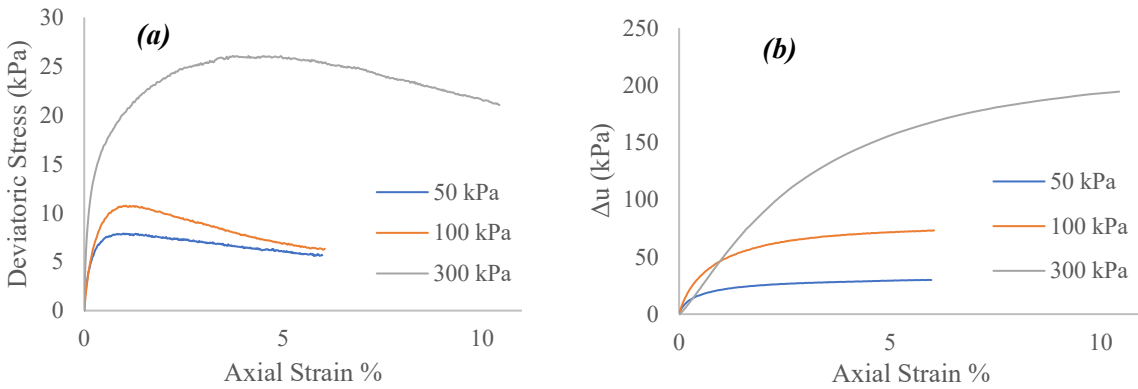


Figure 3.2: Saint-Hyacinthe marine clays behavior under static loading and different effective confining pressure: (a) Stress-Strain diagram, (b) Change in pore water pressure.

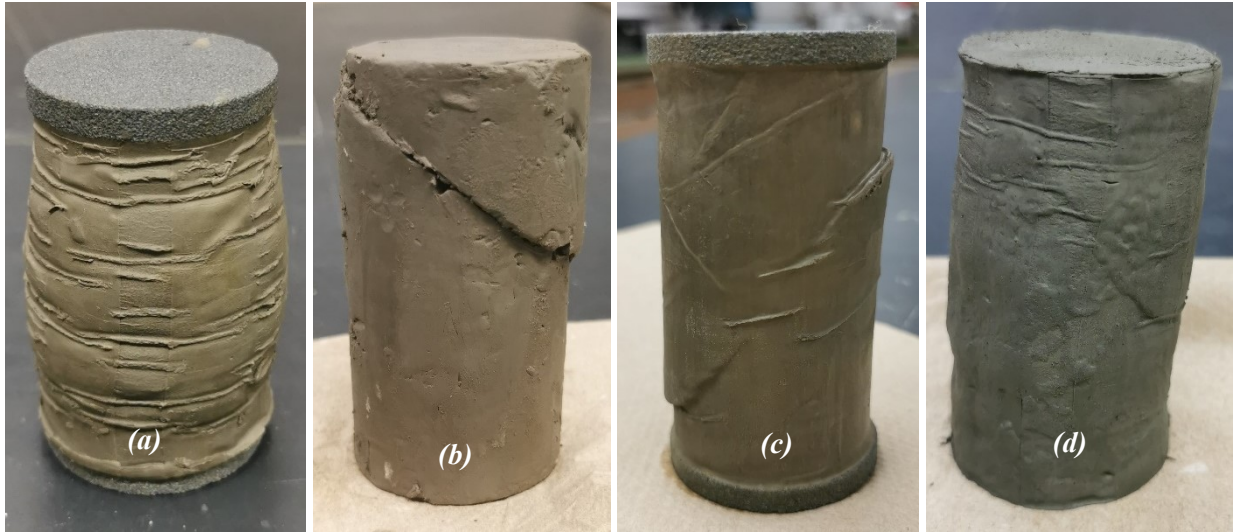


Figure 3.3: Different failure modes for Marine clay samples under monotonic loading: (a) and (b) Southshore marine clays, (c) Saint-Hyacinthe marine clays, and (d) Saint-Amble marine clays.

Different failure modes for marine clays tested under monotonic loading were detected, as shown in **Figure 3.3**. Most samples have a shear failure mode, while some had a shear failure mode associated with a bulging and significant drop in the sample height. The mode of failure is an indicator of the response of the marine clay, where the clays' origin and properties highly affect this response.

3.2 STRESS-CONTROLLED CYCLIC RESPONSE

When subjected to cyclic loading, marine clays undergo a remolding and softening behavior that reduces strength and may lead to cyclic failure after several cycles. Simultaneously, if no failure occurs after cyclic loading, the clays will suffer a residual shear strain and permanent pore water pressure (Li, Dan, & Wang, 2011). Consequently, it is essential to study the marine clay strength and its deformation behavior as a critical design factor that significantly affects the infrastructure system's behavior and response to lateral cyclic loadings.

The most common test type is the *stress – controlled* triaxial test. The clay sample is firstly saturated and consolidated under certain effective confining pressure; then cyclic vertical stress can be applied with an amplitude of $\pm\Delta\sigma_d$. The accumulative cyclic strain and pore water pressure are recorded in which a significant increase of cyclic strain and a continuous increase in pore water pressure is expected.

To discuss the response of marine clays to cyclic loading (*Stress – Controlled test*), taking advantage of the available raw data from (Wichtmann, Anderson, Sjørnsen, & Berre, 2013), sample No. 15 is selected to represent the typical stress-strain behavior of marine clays. The sample loaded cyclically up to failure with a total test duration of 225.35 min. The sample failed after 1362 cycles. **Figure 3.4** shows that the sample deflected under cyclic loading and reaches a peak value representing its maximum resistance and then deteriorate until it fails. Furthermore, to highlight the clay behavior and response just before failure, the $\sigma - \varepsilon$ diagram for the last two cycles is also

included in the figure. Compared with the response at one cycle before failure (Cycle No. 1361), the sample showed unstable behavior at failure (Cycle No.1362, duration: 7.032s) when responding to cyclic loading, demonstrated in the intensive turbulence of the $\sigma - \varepsilon$ diagram. **Figure 3.5** shows pore water pressure generation during cycling; it increases and ratchets at a high rate until reaching a peak value, then tends to stabilize.

The behavior and response of marine clays to cyclic loading are similar to those recorded by other researchers. However, the number of cycles required to reach failure, if the sample will fail or maintain equilibrium, and at which rate the clays' strength deteriorate, all these measurements vary with the loading conditions and the clays' physical and mechanical properties previously discussed in the preceding chapter. Furthermore, it was concluded that the marine clay properties highly affected its response to cyclic loading.

All studies were agreed that the loading conditions, represented by the cyclic stress ratio CSR , is mainly affected the clays' response. However, some researchers stated that higher CSR would result in clays' failure for the same clay; others performed long-term cyclic tests and found that some clays will fail at lower CSR and maintain equilibrium at higher values. Indeed, each of these studies performed tests on specific marine clays, and it is hard to emulate the behavior of marine clays worldwide. Nevertheless, a threshold CSR can be predicted using the available data in the literature, which will be discussed in the subsequent sections.

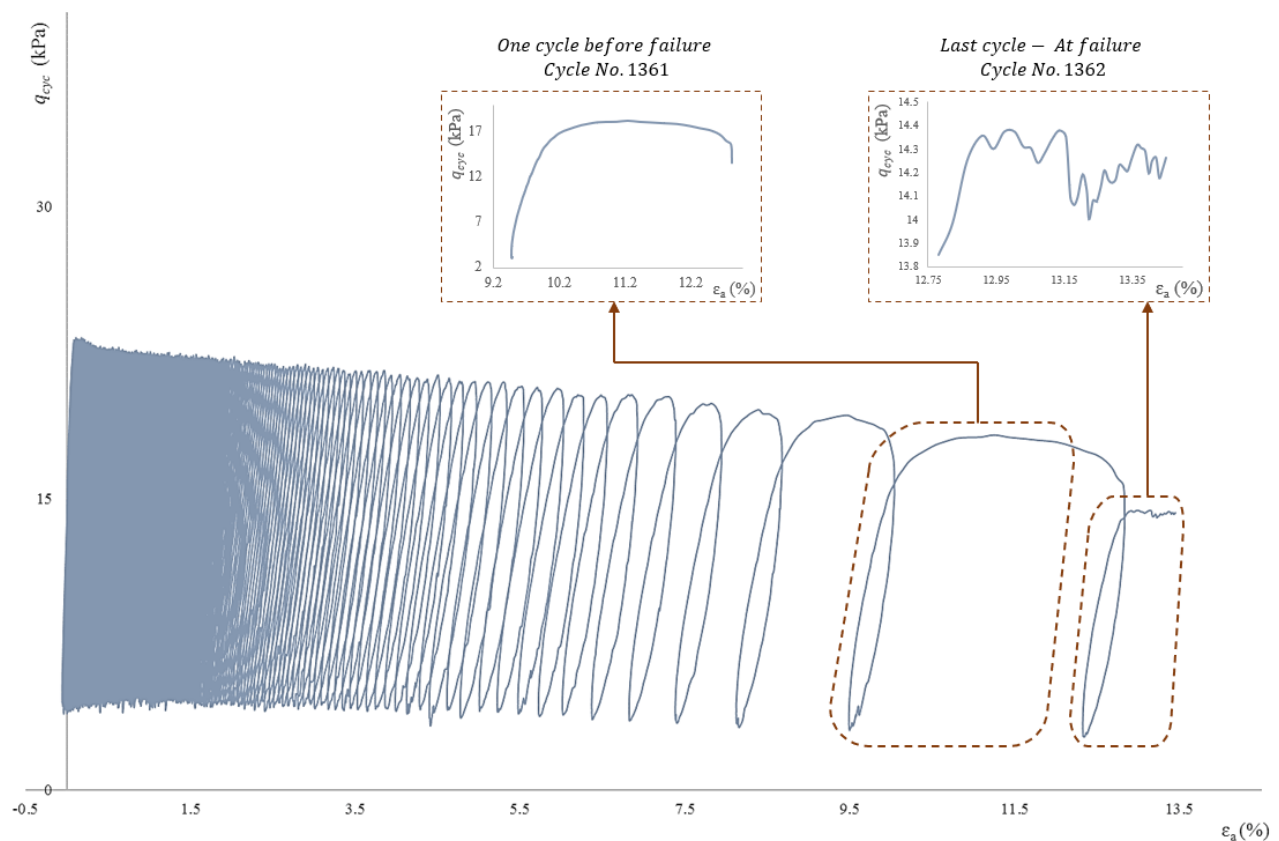


Figure 3.4: Cyclic response of marine clays, q_{cyc} vs ε_a for sample No. 15, (Wichtmann, Anderson, Sjursen, & Berre, 2013).

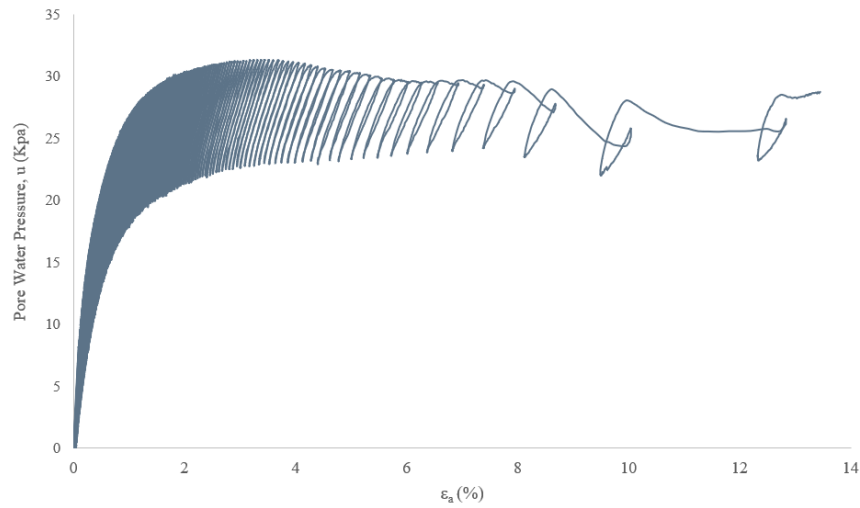


Figure 3.5: Pore water pressure generation during cyclic loading, u vs ε_a for sample No. 15, (Wichtmann, Anderson, Sjørusen, & Berre, 2013).

3.3 MARINE CLAYS CYCLIC RESPONSE ASSESSMENT

3.3.1 Threshold Cyclic Stress Ratio

Different studies were performed in the literature to highlight marine clays' history, physical, chemical, and mechanical properties effect on marine clay behavior under cyclic loading. Studies in the literature focused on the general conduct of specific marine clays without considering the clay parameters variation concerning the location. Therefore, proposed theories are not applicable for all types of marine clays. However, the marine clays' parameter(s) controlling the behavior is still ground, and a maximum of two or three parameters can be studied and compared. The pore water pressure generation also was one of the crucial parameters studied and reported in the literature. An investigation will be performed to determine the marine clays' parameter(s) that most influence their behavior under cycling loading (*stress – controlled*) in the subsequent sections.

Many researchers highlighted the marine clay degradation and failure potential with increasing or decreasing the cyclic stress ratio (*CSR*) and the number of cycles (N) (i.e., **Zhou and Gong (2001)**, **Matasovic and Vucetic (1995)**, **Li et al. (2017)**, **Hyudo et al. (1988)**, and others). Therefore, the cyclic stress ratio and the number of cycles is considered the most influential parameters controlling the marine clay behavior under undrained cyclic loading.

(**Hyodo, Yasuhara, & Hirao, 1992**) performed a series of stress-controlled tests on Ariake clay in Japan and proposed steps predict the time-dependent behavior of marine clays in undrained conditions. Two parameters were defined, the possibility of cyclic failure $RR(N)$ and the relative effective stress ratio (η^*) between the initial and failure points in the $p' - q$ space. The parameter (η^*) is a function of $RR(N)$ in which the latter can be calculated using **Equation 3.1** (the subscript f is denoting the failure), which represents a power relationship for the *CSR* and the number of cycles at 5% double amplitude strain (Log scale). The researchers proposed two correlations to predict the pore water pressure (u_p) and strain (ε_{DA}) response during cyclic loading.

$$(CSR)_f = 0.624N_f^{-0.071} \dots \dots \dots \mathbf{3.1}$$

(Hanna & Javed, 2014) proposed a new concept to describe the failure potential of marine clays. The researchers performed a series of stress-controlled tests in which the cyclic stress ratio CSR is one of the most critical input parameters. The marine clays were tested by defining the cyclic load amplitude, confining pressure, and frequency as input parameters. All physical and mechanical properties were tested and reported. The study proposed a logarithmic relationship by defining a line of demarcation following the empirical **Equation 3.2**. It separated the failed and survived samples under cyclic loading and defined the safe zone concept to predict the clays' response to cyclic loading. It also allows the designers to choose a design value of CSR that ensures safety.

$$(CSR)_f = -14.23\ln(N_f) + 107.1 \dots \dots \dots \mathbf{3.2}$$

The previously discussed studies and empirical correlations were developed based on one type of marine clays, which leads to an argument; whether these correlations are applicable for other marine clays or not? In this chapter, a series of experimental data available in the literature are collected to check the applicability of the proposed equations to different marine clays (**Table 3.2**).

The variation of CSR to the number of cycles for all studies and the two correlations are shown in **Figure 3.6** and **Figure 3.7**. (Hyodo, Yasuhara, & Hirao, 1992) the equation did not fit the scattered dataset for the failed samples of different marine clays. It can be applicable up to a number of cycles $N < 300$ cycles. Therefore, the proposed concept cannot apply to a wide range of CSR and the number of cycles for short-term and long-term behavior. Consequently, the correlations proposed to predict the pore water pressure (u_p) and strain (ϵ_{DA}) response during cyclic loading is not applicable as well.

The equation proposed by (Hanna & Javed, 2014) can better predict the marine clays' response for a number of cycles not to exceed 1850 cycles if compared with **Equation 3.1**. Therefore, the proposed concept is valid and applicable for the short-term behavior where no more than 1850 cycles are applied. Then the line of demarcation will continue with negative values and become nonviable. Still, for a number of cycles $N \leq 50$ cycles and a $CSR \geq 40\%$, the equation couldn't well predict the clays' response as shown in **figure 3.7**.

Table 3.2: List of collected data from the literature.

Study	Location	Depth	Parameters	
			Physical	Mechanical
(Hyudo et al., 1988)	Japan	---		
(Hyde et al., 1993)	Japan	---		
(Rao & Moses, 2003)	India	1.5		
(Moses & Rao, 2007)	India	1.5		
(Li, Dan, & Wang, 2011)	China	11	$w\%, w_L, w_p$	$\sigma_3, q_s, u, \epsilon_a,$
(Wichtmann et al., 2013)	Norway	6-12	$I_L, I_P,$	q_{cyc}, N, f, S_u
(Guo et al., 2013)	China	3	$S\%$	CSR, OCR
(Wang et al., 2013)	China	3		
(Hanna & Javed, 2014)	Canada	4-5		
(Lei et al., 2020)	China	10-15		

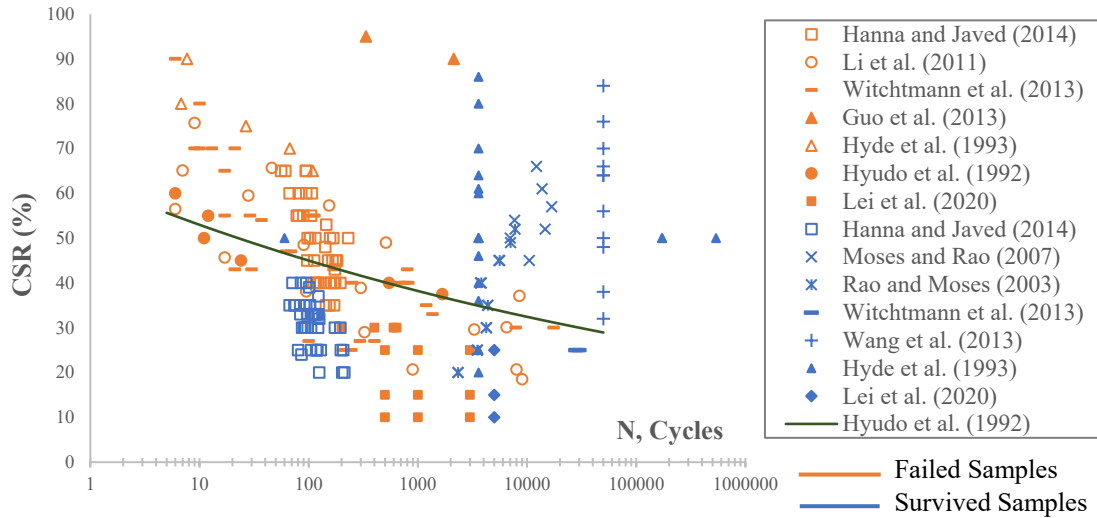


Figure 3.6: *CSR vs N* for different marine clays: **Hyudo et al. (1992)** theory application.

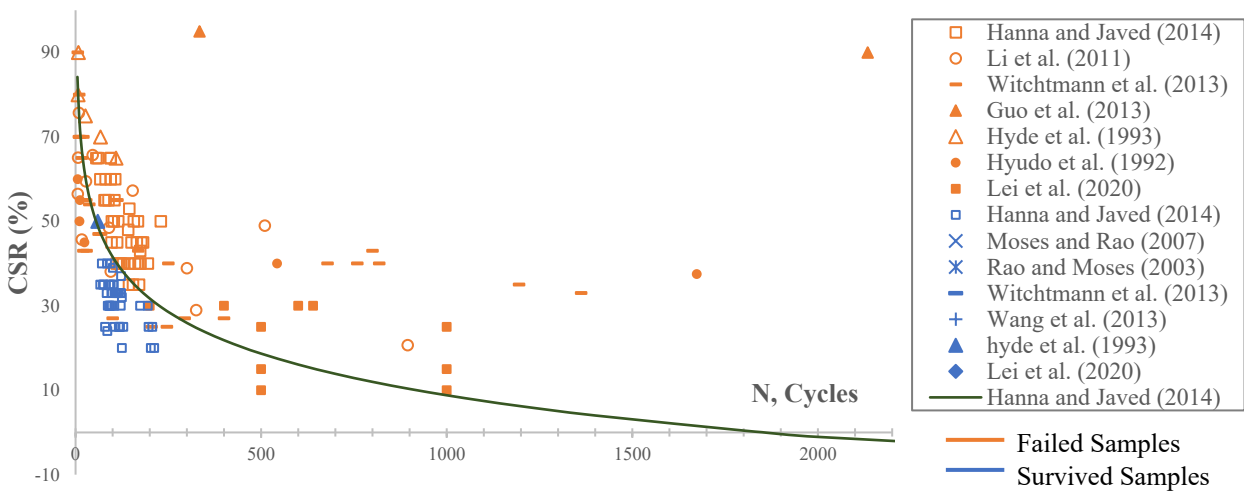


Figure 3.7: Application of demarcation line (*CSR vs N*) proposed by **(Hanna & Javed, 2014)** for different marine clays.

To better understand and classify the collected dataset, the failed and survived data series, for the cyclic stress ratio *CSR* and the number of cycles *N* needed to fail or attain equilibrium, redrawn with a semi-log scale in **Figure 3.8**. This graph will help understand the marine clays' behavior response to cyclic loading, define a threshold *CSR*, and modify the safe zone concept proposed by **(Hanna & Javed, 2014)** to become applicable for a wide range of marine clays and the number of cycles (*N*).

It can be noticed that for *N* ranges from 1 to 70 cycles, most samples tend to fail under cyclic loading of $CSR \geq 40\%$. Therefore, the demarcation line may be modified (for $N \leq 70$ cycles) to a straight line, as shown in **Figure 3.8**. In addition, below the straight line and up to $N \leq 50$ cycles, this zone may be considered an unsteady zone in which the marine clay deformed under cyclic loading and does not attain equilibrium or fail until *N* exceeds 50 cycles, or *CSR* exceeds 40%.

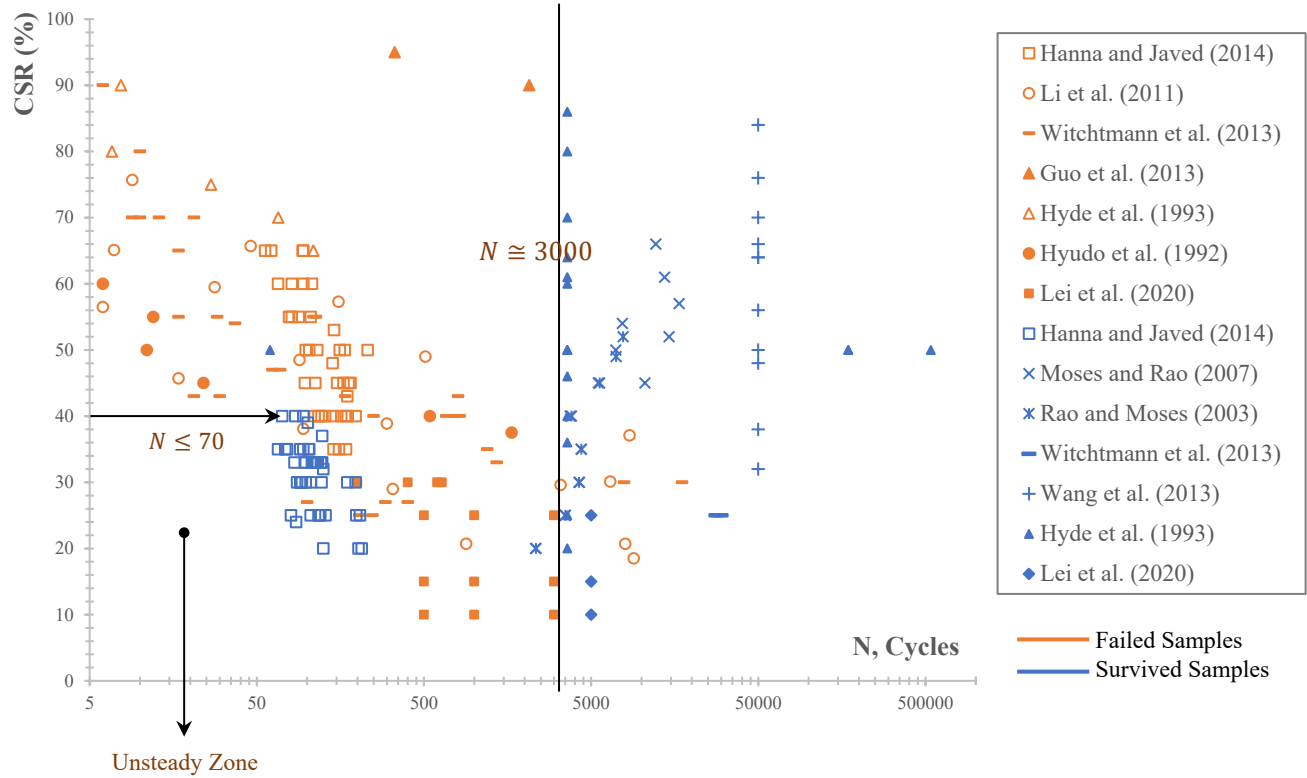


Figure 3.8: Failed and survived samples, *CSR vs N* for different marine clays.

Based on the previously discussed notes, new zones can be defined. The vertical line ($N \cong 3000$ cycles) represents the inversion behavior of both survived and failed samples where the left-hand side of this line is divided into three zones: unsteady, safe, and failure zones. A demarcation line can separate the safe/unstable and failure zones at $CSR = 40\%$ for the range $1 \leq N \leq 70$ cycles then decreases to intersect the inversion line at $N \cong 3000$ cycle. The behavior becomes more complicated and intractable on the right-hand side of the inversion line. The samples maintained equilibrium under a relatively high number of cycles, and CSR ranged between $10 - 85\%$. Simultaneously, some samples tend to fail under a high number of cycles, and $CSR \cong 20 - 40\%$. In other words, a sample may attain equilibrium under high CSR and number of cycles, whereas it may fail under the same number of cycles N and lower CSR value.

Regression analyses were performed on the threshold CSR values for the collected dataset in **Figure 3.8** to avoid data noise and overfitting. The local polynomial regression (or moving regression) best fits the data. It depends on the moving average concept to fit the data in polynomial regression bases, as shown in **Figure 3.9**. The fifth-order polynomial fitted curve with a coefficient of determination $R^2 \cong 0.92$ (relatively low variance) can define a new failure envelope.

Figure 3.10 presents the new failure envelope and demarcation lines. As previously discussed, the demarcation line will follow a straight line for N ranges from 1 to 70 cycles and $CSR \cong 40\%$. All datasets located below this line will be considered safe, and failure is not expected. If clays are loaded with the same number of cycles and higher $CSR > 40\%$, the clay will tend to fail. For N ranges from 70 to 3000 cycles and $CSR \geq 10\%$, the demarcation line will follow the polynomial

curve equation, where all datasets located above the curve will fail under cyclic loading. An inversion line at $N \cong 3000$ cycles represents the reversal behavior of marine clays. For N ranges from 3000 to ~ 42000 cycles, the demarcation line will continue to follow the polynomial curve equation, but all datasets above the curve will survive, and failure is not expected. All datasets located below the curve will tend to fail.

In conclusion, most of the collected datasets from the literature can well represent the short-term behavior of marine clays. Moreover, the failure can be predicted for clays subjected to a low number of loading cycles; cycles N not exceed 3000 cycles. In contrast, the long-term behavior of marine clays is still a controversial issue.

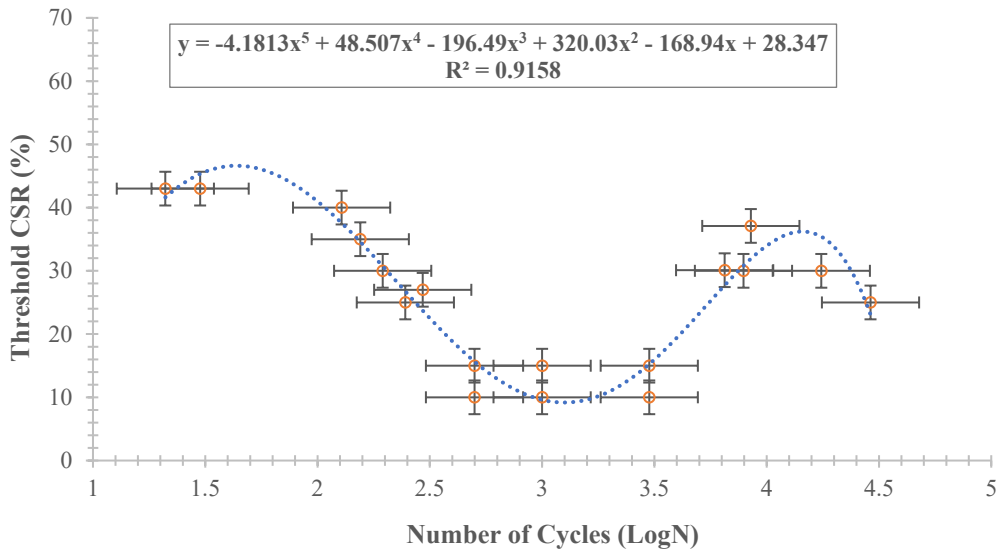


Figure 3.9: Polynomial regression model for the threshold *CSR* of the collected dataset.

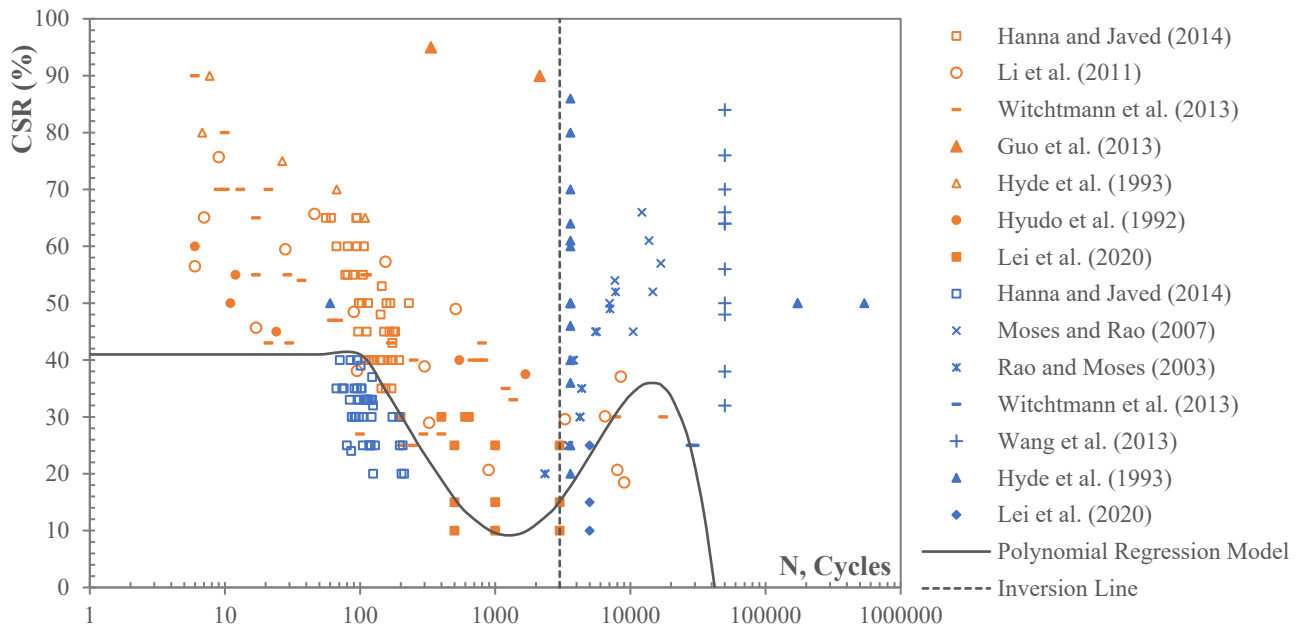


Figure 3.10: Proposed demarcation line for the collected marine clays' dataset.

3.3.2 Modified Safe Zone Concept

The machine learning classification techniques are practical tools to classify scattered data with two independent variables that correlate with a dependent variable. The CSR and N are the independent variables representing the input parameters required to predict the marine clay response (dependent variable) to cyclic loading; whether the clay will fail or attain equilibrium defined by a binary system (0 for failed and 1 for maintaining equilibrium).

Different classifiers in Machine Learning can classify a dataset into two or more categories and precisely predict a new dataset to which category belongs. A model is first trained to perceive the interrelation between the independent and dependent variables, where each classifier has a different mechanism. Then, the model tests the classifier performance and checks the accuracy in predicting the responses: the higher accuracy, the better the model performance in categorizing the datasets.

The classification machine learning techniques were used to classify the collected datasets and modify the safe zone concept proposed by (Hanna & Javed, 2014) to apply to a wide range of marine clays with different locations and properties. The datasets were split into training and testing sets, scaled, and classified by seven classifiers using a *Python* code, and the accuracy were calculated for each classifier to help in selecting the most efficient model in predicting the marine clay's response to cyclic loading giving the CSR and N as input parameters.

The *Decision Tree* and the *K – Nearest Neighbor (K – NN)* classifiers have the highest recorded accuracy as listed in **Table 3.3**. The classifiers have different predicting and classification mechanisms. When analyzing a dataset, both models define a confidence score for the dependent variable (the output). The outcome has a score of 0 for fail and 1 for maintaining equilibrium when the data points have undoubtedly single prediction and a boundary score of 0.5 that separates the two confidence zones. The models' performance for both classifiers at different criteria are shown in **Figure 3.11**; the confidence zones in the figure are rendered in two colors, gray for failed confidence zone and green for the stable confidence zone. The ($K – NN$) classifier was found to configure the scattered data and represent the modified safe zones concept better, in particular for the left-hand side of the plot (short-term behavior).

Table 3.3: Accuracies of different classifiers in predicting the clays' response.

Classifier	Accuracy
<i>Naïve Bayes</i>	67.4%
<i>Logistic Regression</i>	67.4%
<i>Support Vector Machine (SVM)</i>	71.1%
<i>Kernel SVM</i>	89.1%
<i>Random Forest Classification</i>	93.5%
<i>Decision Tree Classification</i>	95.7%
<i>K-Nearest Neighbor (K-NN)</i>	95.7%

The $K – NN$ classifier is a nonlinear model that measures the probability of a new data point failing or surviving by selecting a predefined number (K) of nearest neighbor data points in a circle with the targeted data point in the center. Then, the model assigns the new data point to the category with the most frequent neighbors inside this circle. The Euclidean distance method defines and selects the nearest neighbors, and the closer $K – number$ of neighbors are assigned to classify a

new data point. The confidence zones are rendered by defining a mesh grid; the model will rank each point on the grid with a confidence score represented by contour lines to help take the decision.

For the given dataset, the K – numbers of neighbors was selected using the elbow method by measuring the error rate for using k values ranges from 1 to 10. A higher number of neighbors may lead to distracting the model. **Figure 3.12** shows the error rate with increasing the k value; the curve shows an error rate of $\cong 0.07$ using $K = 4$ and $\cong 0.02$ using $K = 2$.

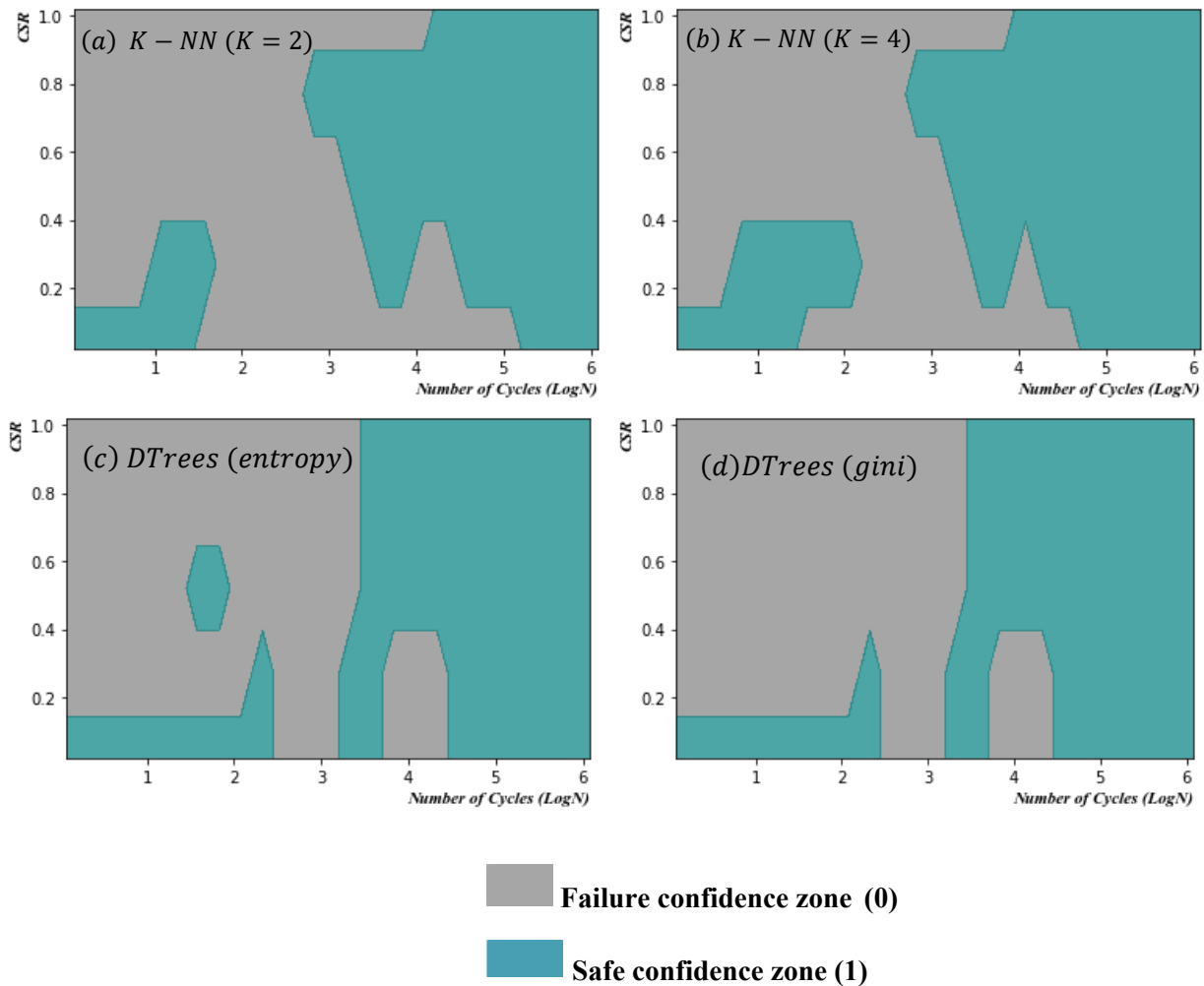


Figure 3.11: Models' performance and confidence zones: (a, b) K – Neighbor Number classifier, and (c, d) Decision Trees Classifier.

The models were trained and tested using the selected K - values; the confusion matrices shown in **Figure 3.12** were calculated as another tool used to define the accuracy. The cells highlighted in gray represent the positive and negative false (where the model failed to predict the response); it can be seen that the model with $k = 2$ and an accuracy of 97.8% erred in predicting the response for one data point out of 46 testing points. The model produces one negative false contra zero positive-false, which is a good indicator of the model accuracy as the model classified a survived sample as a failed one. The model with $k = 4$ and an accuracy of 95.7% erred in predicting the response for

two data point out of 46 testing points. The model produces one negative false contra one positive-false. The ($K - NN$) classifier with $k = 4$ will be adopted as it configures the scattered data and represents the modified safe zones concept better when compared with the regression model in **Figure 3.10**.

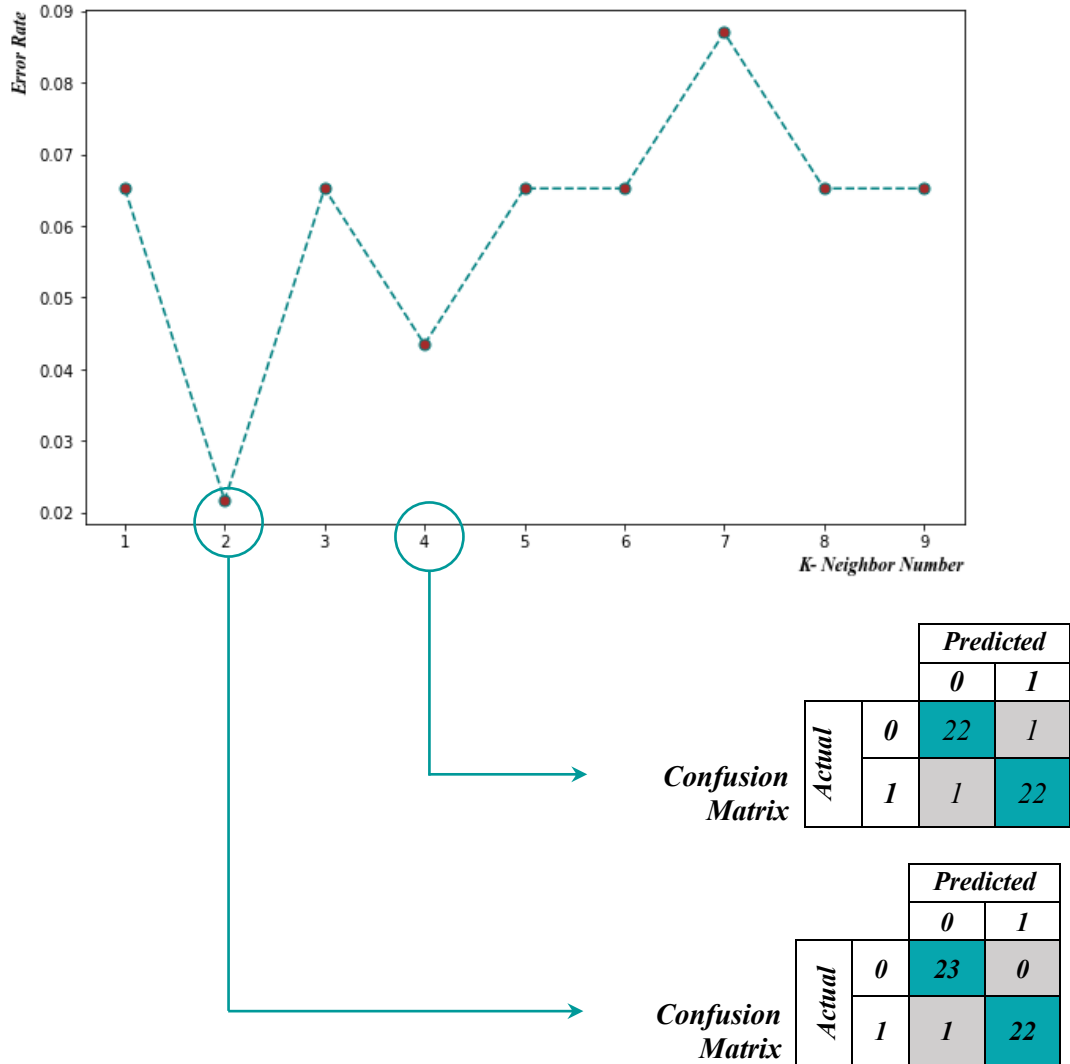


Figure 3.12: Error rate curve to select the K - Neighbor Number and Confusion Matrix.

A modified safe zone concept can be adopted after training and testing the $K - NN$ model with $k = 4$, as shown in **Figure 3.13**. To reduce the distraction during analysis, and due to the widely scattered data, $\text{Log}N$ was used as the x-ordinates. The figure shows two confidence zones where any data point in these zones is 100% failed (0 confidence score and gray zone) or survived (1 confidence score and green zone). In addition, a boundary line with a 0.5 confidence score separates the survived and failed samples for the testing datasets. The confidence score lines can be increased to predict the response better, as shown in **Figure 3.14**, where two more confidence scores of 0.25 and 0.75 were added—the scores' bar is also shown.

The confidence score lines are helpful tools for a more confident decision; for example, a data point located between the borderlines having a score of 0.25 and 0.5 can be confidently classified as failed. In the same way, if located between the borderlines 0.5-0.75, it can be confidently classified as Safe. For a data point located on the boundary of 0.5 scores, the model ranks it as failed even if it returns a negative-false. A negative-false means that the model predicts a fail behavior for a marine clay will probably maintain equilibrium; this is safer than predicting a maintaining equilibrium behavior where the clay might fail (positive-false).

The model successfully captured the variance in marine clays' behavior when subjected to different *CSR* and number of cycles. The model can predict whether a given clay will fail or maintain equilibrium when subjected to a certain number of cycles and loading amplitude. The contentious issue here is how to define the number of cycles that can be applied without failure, or in other words, the marine clays' life estimation. The clays' life estimation will be discussed in **Chapter 4**, where the *Strain – Controlled* cyclic tests are the most efficient tool for this purpose.

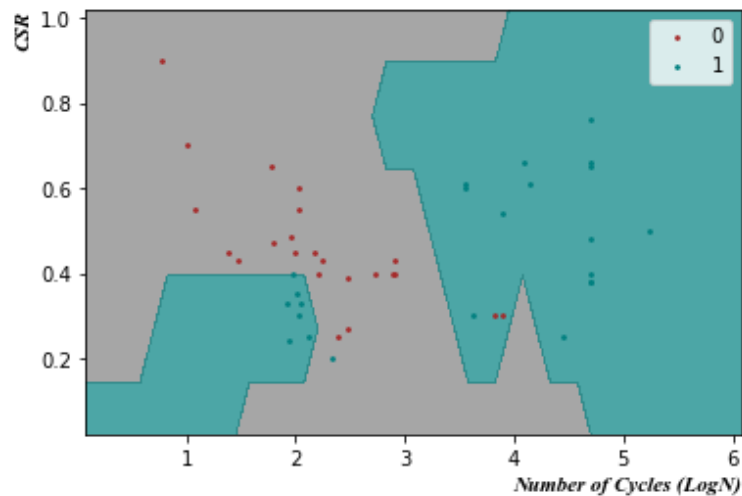


Figure 3.13: Testing dataset predicted using the $K - NN$ classification model with $k = 4$.

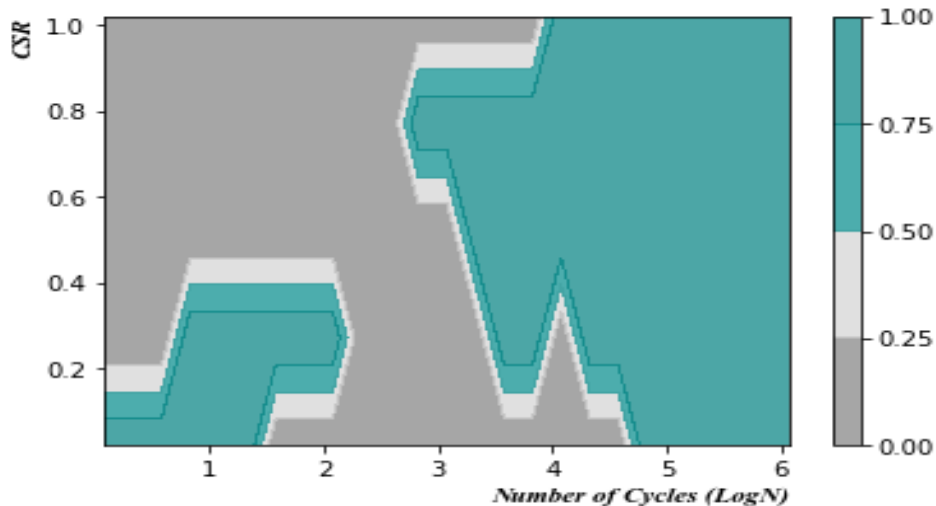


Figure 3.14: Modified safe zone concept with different confidence scores.

3.4 PARAMETRIC ANALYSIS AND FEATURE SELECTION

From the discussion on the variation of marine clays' parameters and their effect on the cyclic response, it can be deduced that the clays' indices and parameters substantially control the behavior and response of marine clays to cyclic loading. Still, no clear evidence for which one of these parameters controls the behavior where a maximum of two or three parameters can be studied and compared. Studies in the literature focused on the behavior of a specific marine clay with its own physical and mechanical properties. Nevertheless, only a few physical and mechanical parameters were studied parallel with the strain development and pore water pressure generation as the two main significant parameters. On the other hand, very few studies raise the importance and influence of clay sensitivity on the cyclic behavior of marine clays, given the fact that most of the marine clays are medium to extra sensitive soft clays. However, the Canadian Foundation Engineering Manual (*CFEM*) reported that the clay response becomes a particular hazard for sensitive clays when subjected to lateral distortion (**Canadian Geotechnical Society, 2006**).

The main objective of this chapter is to study the interrelationship between the marine clays' physical and mechanical properties and how they influence the clays' response to cyclic loading. Therefore, it is essential to understand the relationship between the shear strength and marine clays parameters to allocate the clay parameter(s) that primarily control the marine clay response to cyclic loading. The desired goal of this study will be achieved by performing a parametric analysis with the collected data set of marine clays using Machine Learning Techniques. Machine learning is an efficient predictive tool to make decisions and correlate the relationship between the independent and dependent variables for a scatter dataset.

3.4.1 Data Pre-processing

The collected dataset in this research, shown in **Table 3.4**, has 23 independent variables (Features) and one dependent variable. The independent variables represent the location, state of the sample (Remolded/Undisturbed), and the physical/mechanical properties of the marine clays. The dependent variable represents the clays' response to cyclic loading in a binary system (0 for failed and 1 for maintaining equilibrium). All analysis will be performed on Python and using the built-in libraries of the machine learning,

The first step in the machine learning analysis is data pre-processing; this step is required to convert the raw data to structured and clean data compatible with all ML-Algorithms. The dataset pre-processing in this study includes converting the categorical features into a numeric format by encoding and dataset features scaling. Two categorical features were encoded: the location where the samples came from and the state of the sample where each feature was inverted to numbers in two or more columns. For example, the state of the samples has two categories in one column (undisturbed and remolded) which will be replaced with two columns after encoding. If the sample is undisturbed, it will be converted to 1 in the first column, and thus the second column will have a 0 value and forth. **Figure 3.15** shows a sample of the data set used in the analysis before and after encoding and scaling.

Features scaling is used to narrow the wide-scale range of the features as each feature has a different scale, which can distract the algorithms during analysis. In addition, scaling was applied for specific codes where the algorithm has unique requirements. **Equation 3.3** is the formula used in standardizing the data.

$$X_{stand} = \frac{X - mean(X)}{Standard\ Deviation(X)} \dots\dots\dots 3.3$$

Where: X represents a feature or a clay parameter.

Table 3.4: List of collected data from the literature.

Study	samples	Location	Depth	Parameters	
				Physical	Mechanical
(Hyudo et al., 1988)	U	Japan	---		
(Hyde et al., 1993)	U	Japan	---		
(Rao & Moses, 2003)	U	India	1.5		
(Moses & Rao, 2007)	U	India	1.5		
(Li, Dan, & Wang, 2011)	U	China	11	$w\%, w_L,$ I_L, I_P, γ_o $S\%$	$\sigma_3, \sigma_p, \sigma_{vo}, q_s, u, \varepsilon_a,$ q_{cyc}, N, f, S_u, S_t e_o, CSR, OCR
(Wichtmann et al., 2013)	U	Norway	6-12		
(Guo et al., 2013)	U	China	3		
(Wang et al., 2013)	U	China	3		
(Hanna & Javed, 2014)	U/R	Canada	4-5		
(Lei et al., 2020)	U	China	10-15		

3.4.2 Feature Selection

It is crucial to remove the irrelevant features in a Machine learning analysis to obtain good predicting power and reduce the computational effort of the model. Therefore, in feature selection as one of the core steps in Machine Learning, the feature (or clay parameter) that least contributes to the dependent variable (Failed/Maintained Equilibrium) should be removed to obtain higher model accuracy. Hence, this analysis can be considered a primary parametric analysis for marine clays.

Before applying the feature selection analysis, it is vital to understand the relationship between the 23 selected features. The Heatmap is considered an excellent index to understand the overall relationship between the clay parameters. **Figure 3.16** shows the features correlation matrix using the Heatmap technique, where the closer the value to 1/−1 represents a high correlation between two different features. The negative index in the Heatmap legend means that an increase in one feature’s value will decrease the other feature’s value. On the other hand, the positive index indicates that an increase in one feature’s value will increase the other feature’s value. The score bar for both negative and positive values is shown in the figure.

For example, the strong relationship between the clay’s physical and mechanical properties is highly observed on the positive side of the index in the black boxes in **Figure 3.16**. Also, a strong relationship between the pre-consolidation pressure and the in situ effective stress, the cyclic and static strength, sensitivity, and degree of saturation with most of the parameters. All the correlations have direct or inverse relationships and are expected. For example, looking into the last column in the matrix that represents the dependent variable (*F/E*), it can be seen from the negative index that both cyclic stress ratio (*CSR*) and the depth have an inverse relationship with the failure probability. Clays at shallower depth tend to fail, and with increasing the *CSR*, failure is expected.

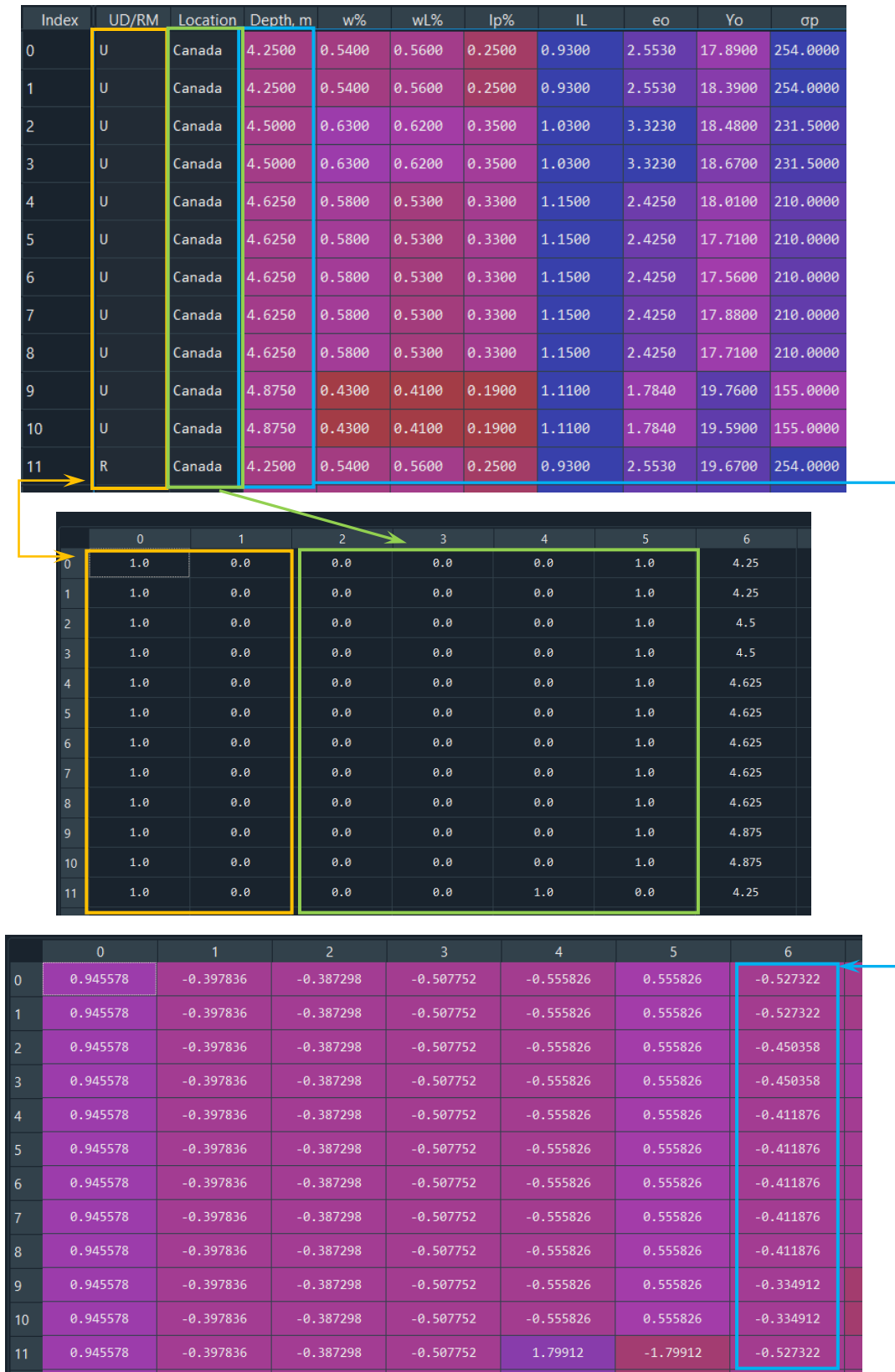


Figure 3.15: Data Preprocessing in ML: (a) dataset sample, (b) Encoding, and (c) Scaling.

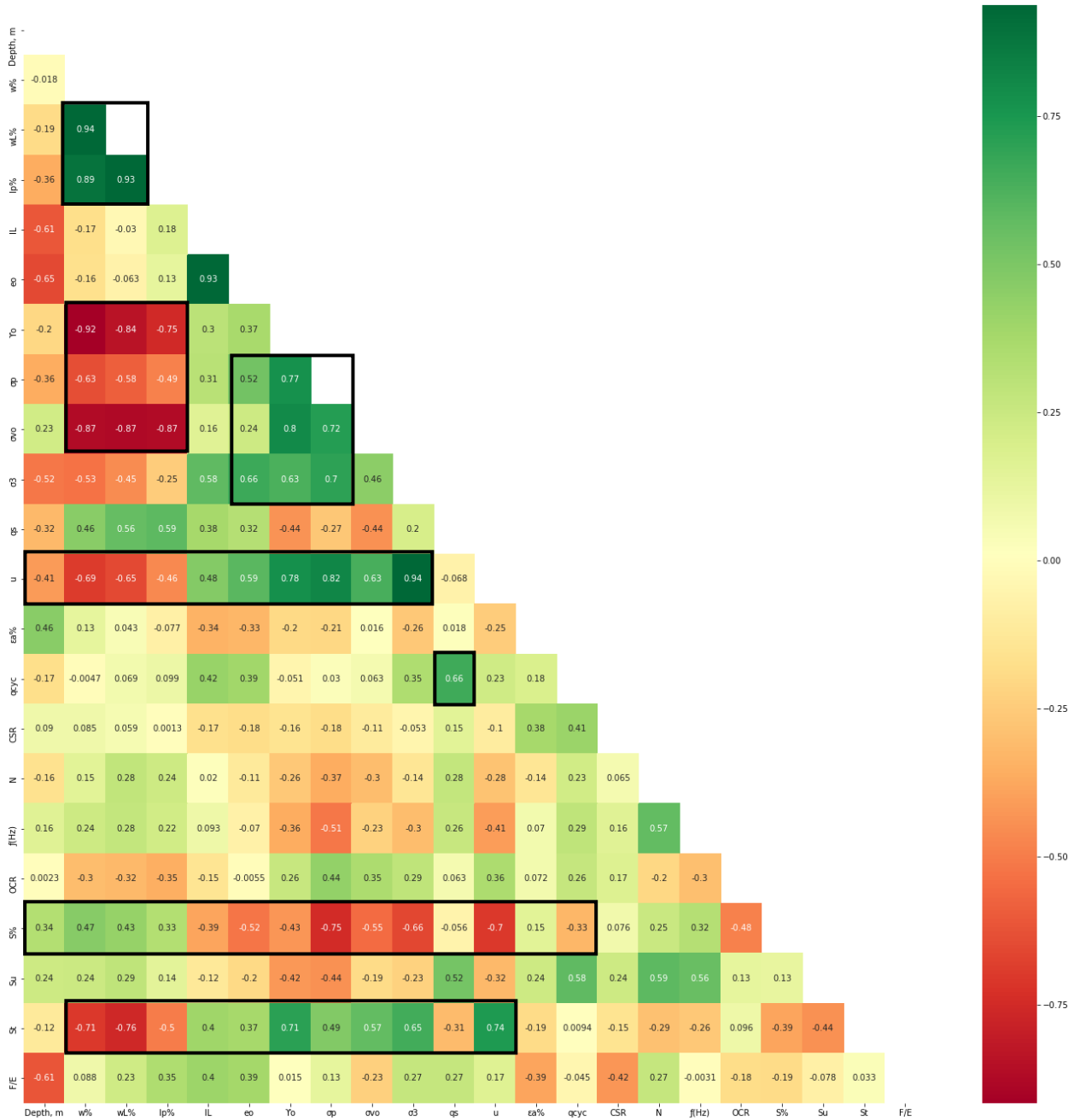


Figure 3.16: Clay Properties correlation matrix.

The correlation matrix cannot measure the feature importance; more precise tools are required to define each feature's importance and decide which feature to keep and which one to eliminate. Different techniques are available to select the features that highly contribute to the cyclic response of marine clays and to measure the importance of these features. An analysis will be performed using these techniques for comparison. The selected features will be used in an artificial neural network model to predict failure and a genetic programming model to correlate these features with the clays' strength.

The ExtraTreesClassifier is a feature selection tool that measures the correlations between the independent and dependent variables by constructing a forest of trees with nodes at which features are randomly selected to classify, as shown in **Figure 3.17**. Then, the ExtraTrees provides an importance score based on the concept of trees probability for each feature. The analysis of the features in this study and their contribution to the independent variable is shown in **Figure 3.18**.

The cyclic stress ratio is the highest in the feature’s importance indices, followed by the axial strain, number of cycles, depth, cyclic strength, in-situ unit weight, and degree of saturation. Then, the features have almost the same importance index until the static strength. The lowest importance indices were reported for the clay’s initial condition, whether remolded or undisturbed.

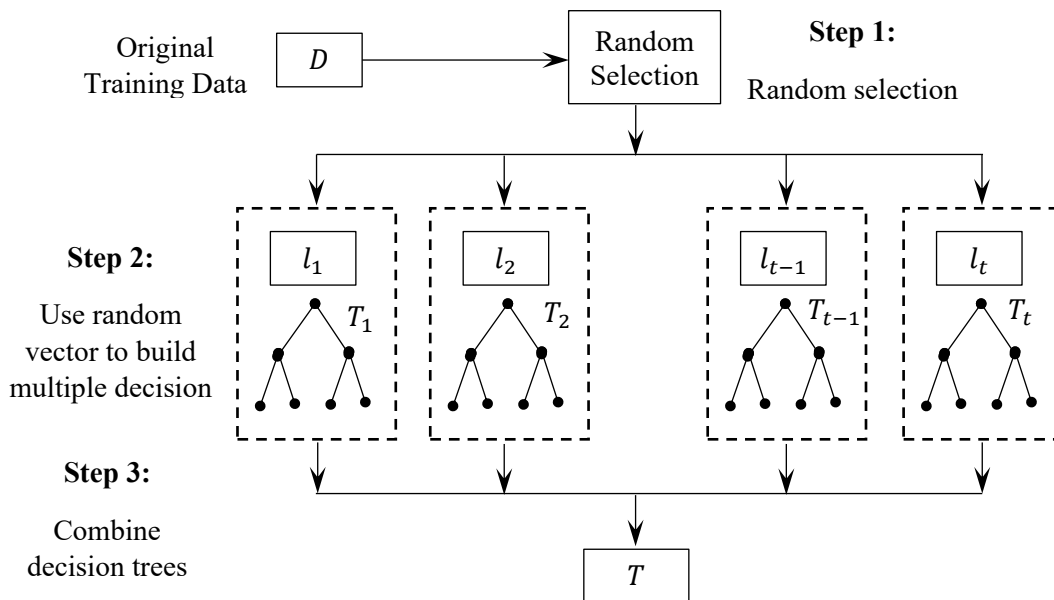


Figure 3.17: The ExtraTrees Classifier, after (Chakrabarty & Biswas, 2020).

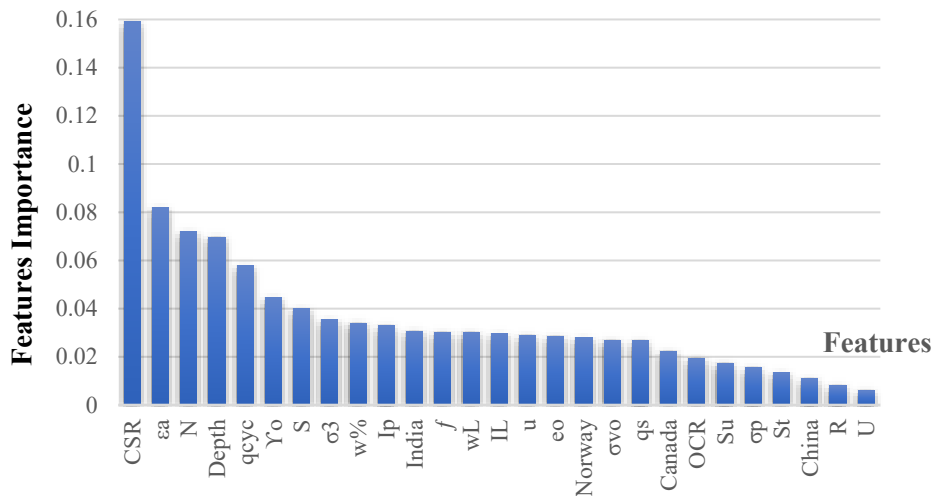


Figure 3.18: Features importance using the ExtraTreesClassifier.

The GradientBoosting classifier is one of the efficient tools in Machine Learning classification algorithms that measure the importance of the features for a complex dataset. The GradientBoosting algorithm builds a more robust classifier by adding a new learner in each iteration (**Figure 3.19a**). The dataset is first analyzed using a weak learner and calculated the residuals; then, a new learner is used to analyze the residuals until the model reaches a high predictive accuracy (Hastie, Tibshirani, & Friedman, 2017). The relative importance of each feature can be measured based on its contribution in predicting the dependent variable (Hastie, Tibshirani, & Friedman, 2017), the clay response to cyclic loading in this study (0 for failed and 1 for maintained equilibrium).

The collected dataset with the 23 features was trained using the GradientBoosting classifier to measure the relative importance of each feature. **Figure 3.19b** shows the relative importance of each clay's features after successfully training and testing the dataset with the GradientBoosting classifier. It is important to recall that the categorical data were encoded, which turns the number of features to 27 instead of 23. It can be seen from the figure that the CSR, and axial strains (ϵ_a) are still dominant and primarily affect the clay response to cyclic loading. The two classifiers measure different relative importance indices for the other features, but the same factors are still selected, showing a higher contribution to the classification accuracy.

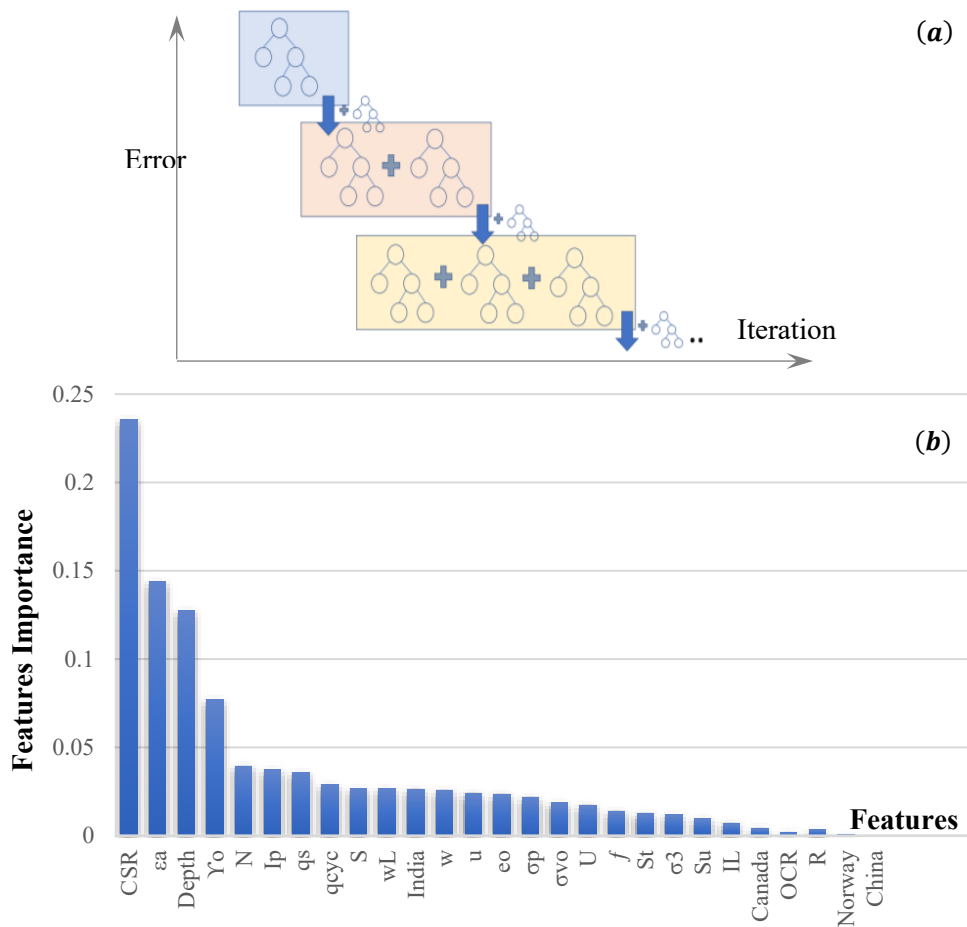


Figure 3.19: (a) GradientBoostingClassifier technique, after (Baturynska & Martinsen, 2021), and (b) Features' importance indices.

The backward elimination method for features selection uses multiple linear regression to eliminate the feature that produces the highest $P - value$; the multiple linear regression has the form given in **Equation 3.4**, where x represents the features and y represents the independent variable. The $P - value$ is a probability value with a predefined significance level used to decide whether to keep the feature (x_n) or remove it. In general, the feature that produces a $P - value$ greater than the significance level, usually defined as $SL = 0.05$ (or 5% *Probability*), has a lower contribution or is statistically insignificant and can be removed from the set of features to enhance the regression accuracy. A feature will be considered statistically significant if its $P - value < SL = 0.05$. Therefore, the multiple linear regression was first performed, including all features, then one feature with the highest $P - value$ removed in each step until all remaining features achieve $P - value < SL = 0.05$.

$$y = a_0 + a_1x_1 + a_2x_2 + \dots + a_nx_n \dots\dots\dots 3.4$$

The significance level can be between 1% and 10%; a value of $SL = 0.05$ is a standard value. However, the significance level and $P - value$ are not the only parameters used to decide whether to remove the feature or keep it. In this method, the *adjusted R^2* value is considered a crucial indicator that helps in the decision, where a model with higher *adjusted R^2* means higher performance and more accurate prediction. In a step, if removing the feature will result in decreasing the *adjusted R^2* . The analyzer can decide not to remove this feature, even if it has a $P - value > SL = 0.05$. In this case, the significance level can be considered too low and adjusted to a higher level.

Figure 3.20 shows the results of the Backward Elimination analysis performed on the collected dataset. It is essential to mention that the categorical features were removed to avoid the dummy variable trap after encoding these features. As a result, six dummy variables will be created, and there is no way to reduce these dummy variables in the multiple linear regression analysis. Consequently, only 21 features were classified using the Backward Elimination feature selection technique.

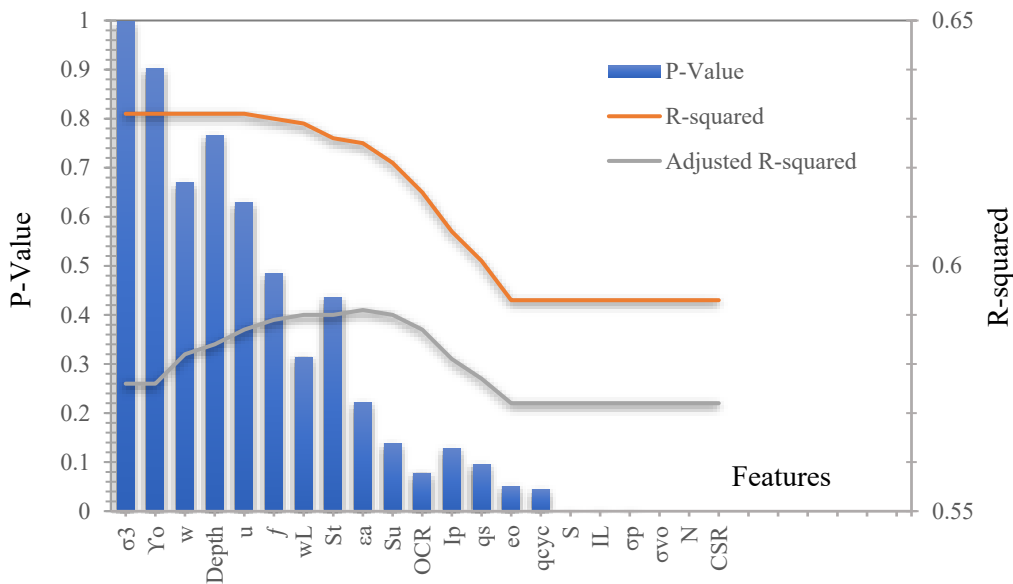


Figure 3.20: Features importance using the Backward Elimination Technique.

The column bars in **Figure 3.20** represent the $P - value$ at which a decision was made to remove the feature. In each step, the feature with the highest $P - value$ was removed, and the regressor fitted again with the remaining features until all features' $P - value$ recorded less than $SL < 0.05$. After eliminating all the statistically insignificant features, it was found that the cyclic stress ratio (CSR), the number of cycles (N), the in-situ vertical stress (σ_{vo}), the pre-consolidation pressure (σ_p), the liquidity index (I_L), degree of saturation (S), the cyclic strength (q_{cyc}) and initial void ratio (e_o) are the most statistically significant features with $SL < 0.05$.

Given the $R - squared$ and the $Adjusted R - squared$ has shown in **Figure 3.20**, it can be seen that by removing the axial strain (ε_a) feature and the following parameters, both values decreased, showing lower accuracy for the model. Consequently, it was decided not to remove the features: axial strain (ε_a), the undrained shear strength (S_u), the over-consolidation ratio (OCR), the plasticity index (I_p) and the static strength (q_s).

Table 3.5 summarizes the results of the three methods and the ten features that primarily affect the marine clay response to cyclic failure. All techniques agreed that the cyclic stress ratio (CSR) is the feature that significantly affects the marine clays' behavior. The scoring of the other features differs per the technique used, but some features were scored within the ten most significant features.

Table 3.5: Summary of the relative importance and the selected features.

Importance level	Classifiers			Selected Features
	ExtraTrees Classifier	GradientBoosting Classifier	Backward Elimination	
1	CSR	CSR	CSR	CSR
2	ε_a	ε_a	N	ε_a
3	N	$Depth$	σ_{vo}	N
4	$Depth$	γ_o	σ_p	$Depth$
5	q_{cyc}	N	I_L	γ_o
6	γ_o	I_p	$S\%$	w_L
7	$S\%$	q_s	q_{cyc}	I_p
8	σ_3	q_{cyc}	e_o	$w\%$
9	$w\%$	$S\%$	q_s	q_s
10	I_p	w_L	I_p	$S\%$
11	f	$w\%$	OCR	S_t
12	w_L	u	S_u	
13	I_L	e_o	ε_a	
14	u	σ_p	S_t	
15	e_o	σ_{vo}	w_L	
16	σ_{vo}	f	f	
17	q_s	S_t	u	
18	OCR	σ_3	$Depth$	
19	S_u	S_u	$w\%$	
20	σ_p	I_L	γ_o	
21	S_t	OCR	σ_3	

The correlation matrix in **Figure 3.16** was used to decide which feature to select and which one to remove. For example, the in-situ unit weight (γ_o) was selected by the ExtraTrees and GradientBoosting Classifiers within the first six features, while the Backward Elimination technique selected the in-situ vertical stress (σ_{vo}). In the correlation matrix, a strong correlation was detected between these two features, which match the engineering definition of the in-situ vertical stress. Consequently, selecting one of these two features will have the same effect on modeling the marine clay response; the in-situ unit weight (γ_o) was selected beside the Depth feature. Similarly, the cyclic and static strength are correlated through the cyclic stress ratio, and then the static strength was selected beside the *CSR*. Add to this, the sensitivity of the marine clays was added to the selected items, although all classifiers return a low relative importance value for this feature.

3.4.3 Parametric Sensitivity Analysis (ANN-Model)

The artificial intelligence techniques are an efficient tool to understand the complex behavior of clays and to correlate the relationship between the clay parameters and its response to loading. To allocate the clay parameter(s) that primarily control the marine clay response to cyclic loading, the selected features in the preceding section were analyzed using the Artificial Neural Network Networks (*ANN*). A predictive model was tested, and the model's sensitivity to each selected feature was predicted.

Artificial Neural Networks (*ANN*) is one of the artificial intelligence techniques that simulate the biological neural networks of the human brain. The human brain works in a nonlinear and parallel information processing system; in the learning process, the brain receives the input signals (Dendrites) and propagates them from one neuron to another by complex electrochemical reactions through the Axons (**Figure 3.21**). The connection between neurons is strengthened when the “right” answer is achieved and weakened for a “wrong” answer, which gives the neural networks the ability to learn through experience. Learning is a fundamental and essential characteristic of biological neural networks. The ease and naturalness they can learn led to attempts to emulate a biological neural network in a computer (Negnevitsky, 2002).

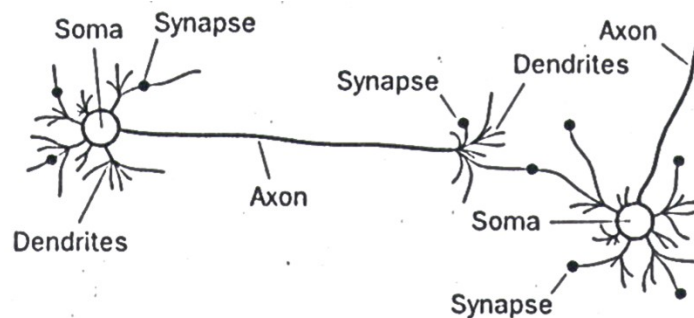


Figure 3.21: Biological Neural Network (Negnevitsky, 2002).

An artificial neural network consists of several neurons connected to weighted links passing signals from one neuron to another. Each neuron receives several input signals through its connection

while it produces a single output signal transmitted through the neuron's outgoing connection. The outgoing connection splits into many branches that transmit the same signal. The outgoing branches terminate at the incoming connections of other neurons in the network (Negnevitsky, 2002).

The multilayer neural network (Artificial Neural Network, *ANN*) used in this study consists of an input layer, two hidden layers, and an output layer. The hidden layer consists of several neurons; each neuron receives the weighted input signals (Dendrites) from the input layer. Then, neurons integrate the input signals through the built-in functions (*Sigmoid*) and normalize the output via a transfer function, as shown in **Figure 3.22**.

The back-propagation algorithm is one of the most popular supervised training algorithms for the *MLP*. The inputs generate outputs by propagating forward; since the back-propagation analysis is a supervised method and the output value is given, the algorithm calculates the error used in the back-propagation process to adjust the weights of the input value. Then, the process is repeated until the error is minimized. The training process can be approached either by pattern or epoch fashions. The epoch is defined as one complete presentation of the entire training data during the training process. In this case, the connection weights are updated after the whole data has been presented to the network.

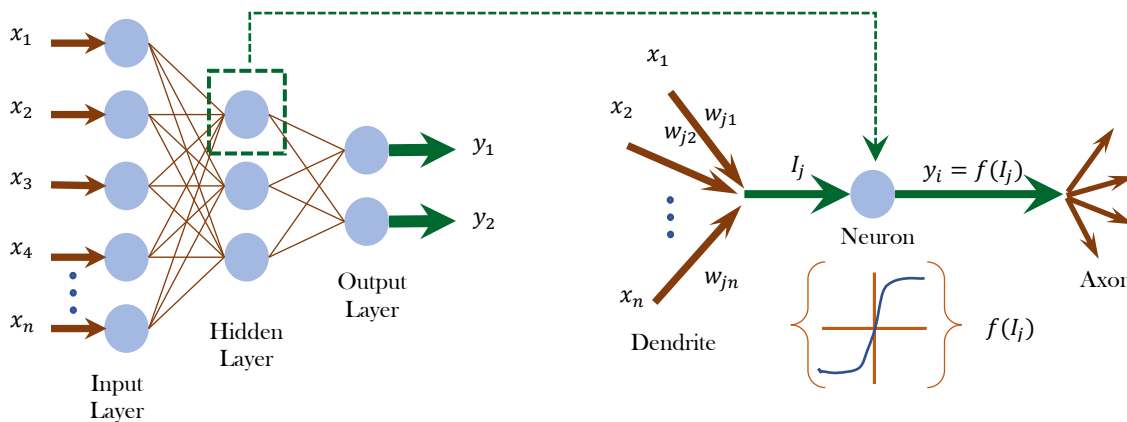


Figure 3.22: Artificial Neural Network Technique [After (Shahin, Jaksa, & Maier, 2008)].

The *ANN* model proposed in this study is a failure/maintain-equilibrium predictive model; the input layer is defined by the selected features (excluding the axial strain, ϵ_a) as listed in **Table 3.6** and two hidden layers were used. **Figure 3.23** shows the *ANN* model's structure, where a **Python** code was used to perform the *ANN* analysis. First, the input data were imported and split into training and testing sets ($X_{train}, X_{test}, y_{train}, y_{test}$) with a $test_size = 0.25$. Next, the *ANN* models are initialized using the built-in *Tensorflow, tf* module in Python libraries; two activation functions were used: *tanh* for hidden layers, and *Sigmoid* for the output layers.

Finally, the model was compiled and fitted to train the data and measure the accuracy of the training step; a maximum of 1500 *epochs* were used to enhance the training step accuracy. The selected activation functions were chosen to achieve a higher prediction accuracy after predicting the testing set (X_{test}) and measuring the prediction accuracy by the confusion matrix and accuracy scores. After training and testing the artificial neural network model, a parametric sensitivity analysis was

performed to define the model's sensitivity to each of the marine clays' selected features. The testing set (y_{test}) is repeatedly tested by setting one feature as zeros; the model accuracy is then used to define the model's sensitivity to the input parameters.

Table 3.6: Proposed ANN models and Data Proportions.

Model	Input Parameters	Hidden Layers	Output Parameters	Splitting Data set (%)		Epochs
				Training	Testing	
ANN	w^0, w_L, γ_o $I_P, S\%, Depth$ q_s, N, S_t, CSR	2 (13 Neurons each)	F/E	75	25	1500

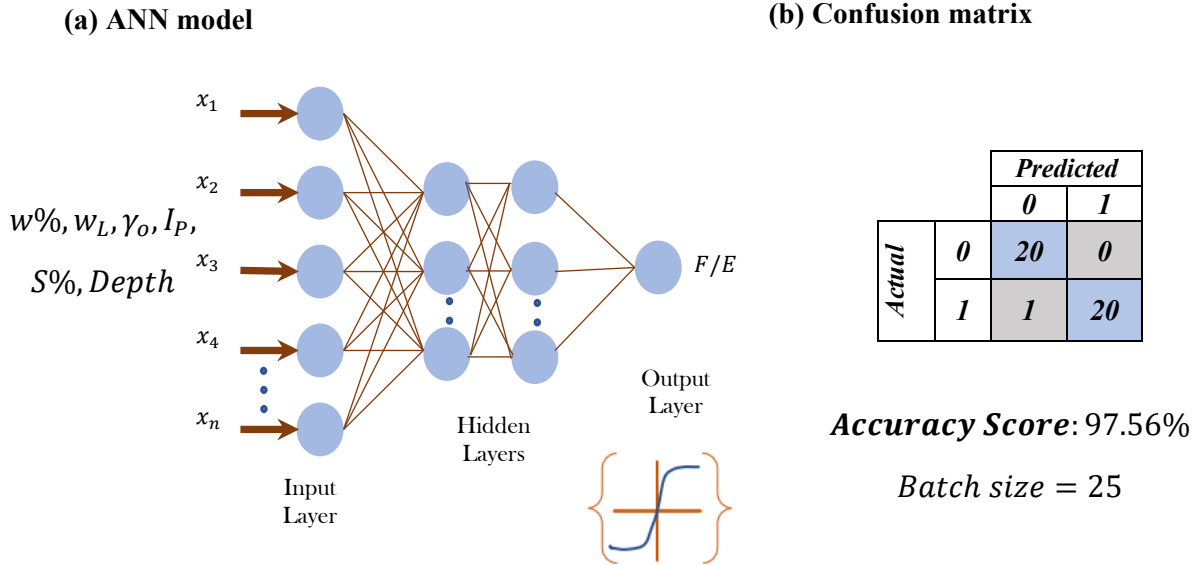


Figure 3.23: The proposed ANN model: (a) ANN model for marine clays' response to cyclic loading prediction and (b) Confusion matrix and testing data accuracy.

The input parameters for the ANN model were selected, as previously mentioned, based on the feature selection analysis. Nevertheless, the axial strain (ϵ_a) was not included in the ANN models as an input parameter. Instead, it was one of the output parameters of the ANN model with cyclic strength (q_{cyc}). The ANN confusion matrix in **Figure 3.23** shows that the model, after testing, returns one positive false with an accuracy of 97.56%. The positive-false means that the sample maintained equilibrium but was predicted as failed. It is important to recall that negative-false is more dangerous when predicting a behavior; the number of neurons in the hidden layers and epochs were selected with minimal negative-falses for the ANN model (13 neurons/layer).

By knowing the physical properties of the marine clay, the depth, the monotonic strength, and the expected number of cycles and CSR, the ANN – 1 will successfully predict the marine clays'

response to cyclic loading and whether the clay will fail or maintain equilibrium through its life. Consequently, this model is considered more particularized than the *KNN* model previously discussed as the behavior predicted concerning a particular clays' properties. Still, both models precisely predict the marine clays' response.

Table 3.7: Sensitivity of the *ANN* model to the input parameters.

Model	Input prametrns	Model accuracy ^(a)	Falses		Relative Σ Falses ^(b)	Sensitivity Index
			Positive	Negative		
ANN-1	<i>Depth</i>	78.05	1	-8	0.22	0.53
	<i>w</i> %	68.30	2	-10	0.29	0.71
	<i>w_L</i>	65.85	14	0	0.34	0.82
	<i>I_p</i>	63.41	15	0	0.37	0.88
	<i>γ_o</i>	68.30	13	0	0.32	0.76
	<i>S_t</i>	92.70	2	-1	0.07	0.18
	<i>q_s</i>	85.37	6	0	0.15	0.35
	<i>CSR</i>	58.54	0	-17	0.41	1.00
	<i>N</i>	61	14	-2	0.39	0.94
	<i>S</i> %	68.3	13	0	0.32	0.76

^(a) Measured by returning the parameter's column to *Zeros* and testing the model

^(b) Σ Falses/ Σ *y* *test* records

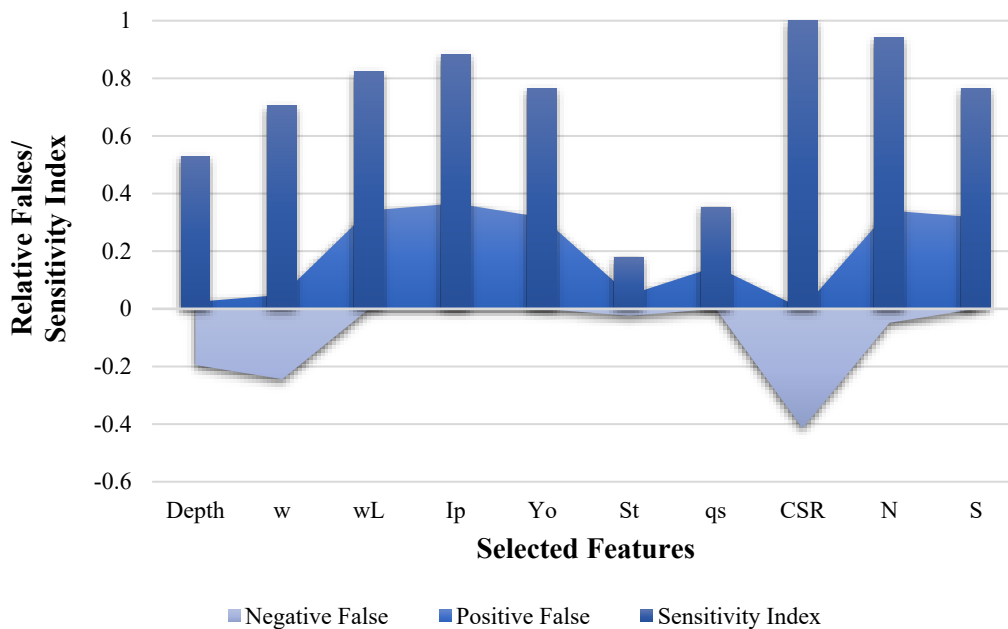


Figure 3.24: The measured Falses and sensitivity indices of the *ANN* – model to input parameters.

The sensitivity to the input parameters shown in **Table 3.7** was measured by specifying an index relative to the negative and positive falses recorded in the absence of each parameter. Therefore, the model was tested repeatedly by setting the targeted parameter to zeros to measure its impact on the model accuracy. First, both models' accuracy and confusion matrices were reported as shown in the table, and the relative error was measured. Then, an index of 1 was recorded for the highest relative error in which the model showed the highest sensitivity to the related parameter. For example, the model showed high sensitivity to the *CSR* where higher negative falses were recorded, as shown in **Figure 3.24**, followed by the number of cycles (*N*) where *two* negative falses and 14 positive falses were recorded. Finally, the sensitivity index for the number of cycles measured relative to the highest recorded value for the cyclic stress ratio (*CSR*).

Figure 3.24 shows the distribution of the negative/positive falses and the measured sensitivity index for each parameter. The lower sensitivity index was recorded for the marine clays' sensitivity (S_t) and this verifies the results obtained by the feature selection classifiers. In addition, the model generally showed high sensitivity to all parameters and lower sensitivity to the depth and static strength, which also verifies the results obtained from the feature selection classification.

3.4.4 Cyclic Strain Development

Two classifiers recorded the axial strain (ϵ_a) as the second of the highest statistically significant features, the axial strain records in the dataset are the strain values at which the marine clay sample failed or maintained equilibrium under stress-controlled cyclic tests. For the *ANN* predictive model, the input parameters were selected for those features that can be maintained without performing a cyclic test. The model successfully predicted the clays' response and showed high sensitivity to the *CSR*. Most of the studies in the literature highlighted the importance of *CSR* as a cyclic test parameter and its effect on the cyclic behavior of marine clays, and many stress-controlled tests were performed.

The relationship between the cyclic strain and the cyclic test parameters is shown in **Figure 3.25**. It can be seen that the sample can fail or maintain equilibrium at the same cyclic strain value and that there is no specific method to classify the marine clays' response. Also, in **Figure 3.25a**, all samples maintained equilibrium do not exceed a strain value of $\epsilon_a < 10\%$ and the failed samples reaches values $\epsilon_a \cong \pm 30\%$. Samples with higher cyclic strain have lower cyclic strength than those that failed with lower values. Also, the failed and maintained equilibrium samples were in the same *CSR* range, as shown in **Figure 3.25b**. Therefore, there is no clear relationship between these two parameters, which means that the cyclic strain is an independent variable as a cyclic test parameter. Similar observations were detected for the number of cycles the sample failed or maintained equilibrium (**Figure 3.25c**).

(Hyodo, Yasuhara, & Hirao, 1992) proposed a formula that correlates the *CSR* with the strain amplitude at which a sample failed; they measured the *CSR* required to reach a cyclic strain amplitude of 5%, which defined failure. **Equation 3.5** is applicable for Ariake marine clays only, although it highlighted the importance of the strain in predicting the behavior of the marine clay.

$$\epsilon_{DA} = \frac{CSR_f}{1.3 - CSR_f} \dots\dots\dots 3.5$$

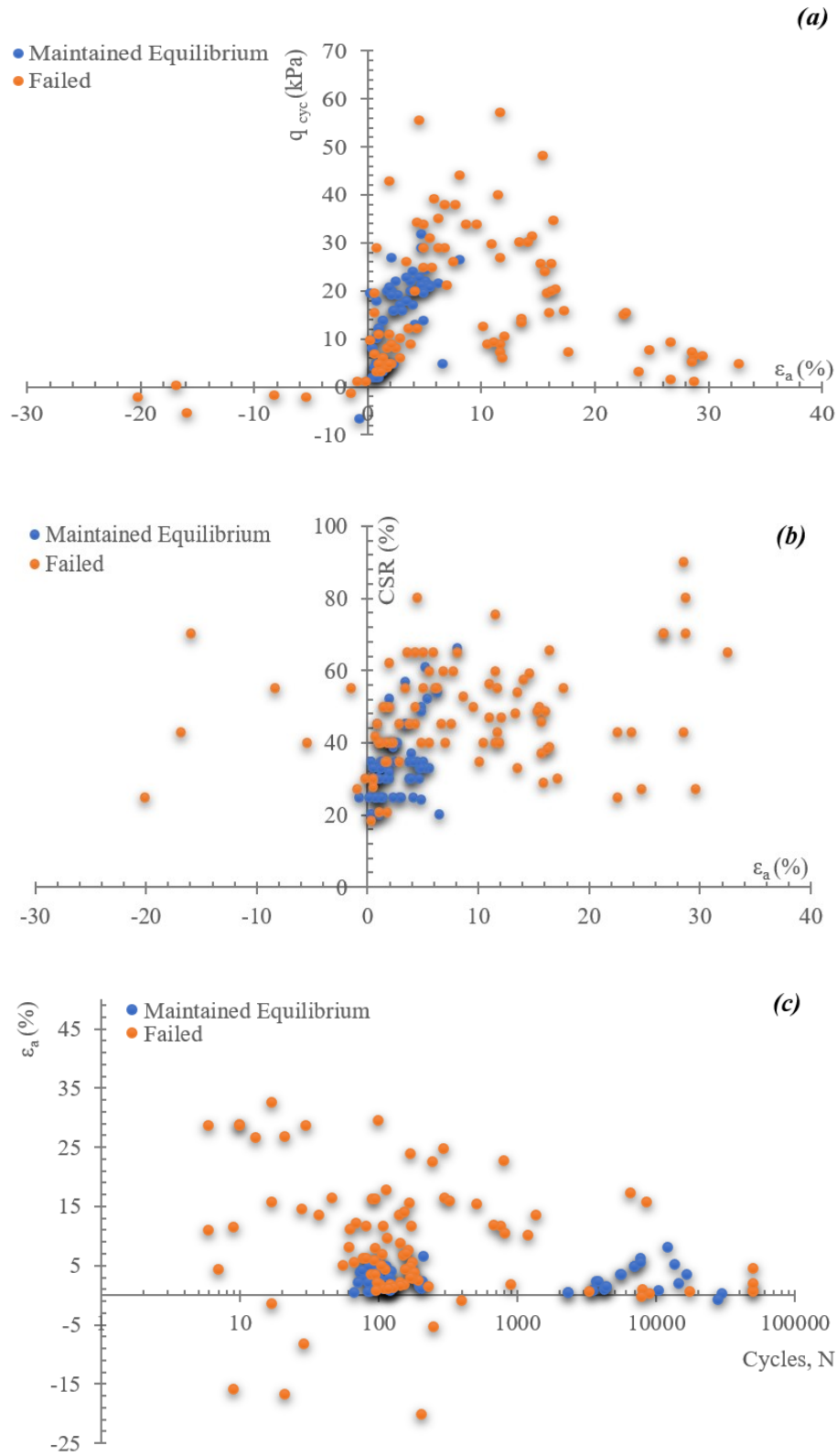


Figure 3.25: The axial strain correlations with the cyclic test's parameters: (a) q_{cyc} vs ϵ_a , (b) CSR vs ϵ_a and (c) ϵ_a vs N .

Similarly, (Hyde, Yasuhara, & Hirao, 1993) proposed an equation that measures the strain at failure as a *CSR* function. The researchers reported a rapid failure initiated at lower strains and higher cyclic stress ratio *CSR* and that the cyclic strain is a function of time. Other researchers reported the change in strain amplitude with increasing the number of cycles (*N*) (i.e. (Rao & Moses, 2003), (Moses & Rao, 2007), (DING, LIU, & HU, 2007), (Hu & Jinwei Ding, 2010), (Wang, Guo, Cai, Xu, & Gu, 2013), (Wichtmann, Anderson, Sjursen, & Berre, 2013)). A constant stress amplitude is applied for loading, and the increase in strain amplitude is recorded.

(Li, Dan, & Wang, 2011) defined a criterion for the failure of natural marine clays where the strain increased at a slow rate at the beginning of the cyclic test. An inflection was reported in which the strain rapidly increased, causing failure. Also, they found that the strain amplitude at failure is independent of the applied cyclic stress and frequencies.

Lately, another researcher defined the failure criterion of marine clays subjected to cyclic loading by the rapid strain increase at a particular stage during cycling. (Zhang, Sun, & Cao, 2020) performed stress-controlled tests on Wenchuan clays at an earthquake area under different cyclic stress ratios (*CSR*). They defined three types of cyclic strain development with increasing the number of cycles: the failure type, the transition type, and the stability type (Figure 3.26). A failure criterion was defined at the turning point, and Equation 3.6 was used to correlate the cyclic strain at turning points with the number of cycles at failure (*A* and *B* are fitting parameters). The failure type curve represents the rapid strain increase at the early cyclic loading stage and leads to failure under fewer cycles. The transition type has a slower strain increase to a particular *N*, then rapidly increased, and failure occurs. At the stability type, the increase in cyclic strain and failure occurs after a higher number of cycles applied to the clay.

$$\varepsilon_{tp} = A \times \log N_f + B \dots\dots\dots 3.6$$

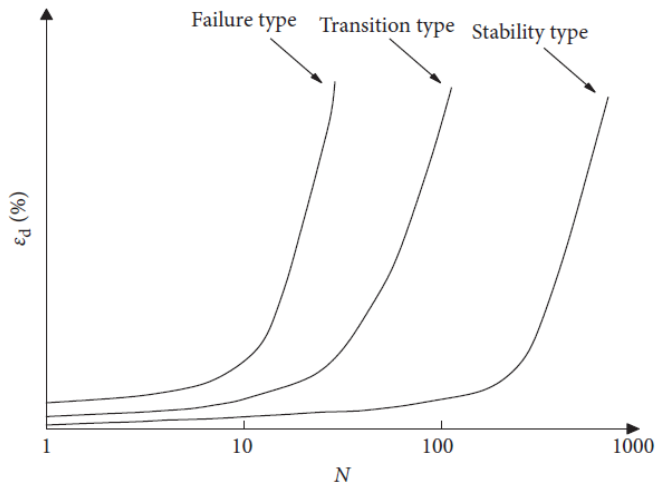


Figure 3.26: Proposed cyclic strain development curves (Zhang, Sun, & Cao, 2020).

Classification analysis was performed to model the correlation between the cyclic strain and the cyclic parameters discussed. However, all models reported low accuracy, reflecting the cyclic strain's complex correlation with other parameters. In addition, an *ANN* model was constructed to

predict the cyclic strain at failure with the selected features as input parameters, and the model also has low accuracy in predicting the axial strain. **Figure 3.27** shows the results of four ANN models executed to predict the cyclic strain (ϵ_a) by varying the number of hidden layers and other model parameters.

It was found that varying the hidden layers is inefficient in recognizing the correlations between the input and output parameters. As a result, the model returns a low accuracy for two or more hidden layers. Nevertheless, increasing the number of neurons in each hidden layer increased the accuracy, but still, the accuracy remains low. Also, the batch size at which the model recalculated the neurons' weights was changed in different ranges, avoiding overfitting, and the accuracy remains low. Performing lower epochs affect the training accuracy; at the same time, increasing the epochs to a specific limit will also reduce the training accuracy.

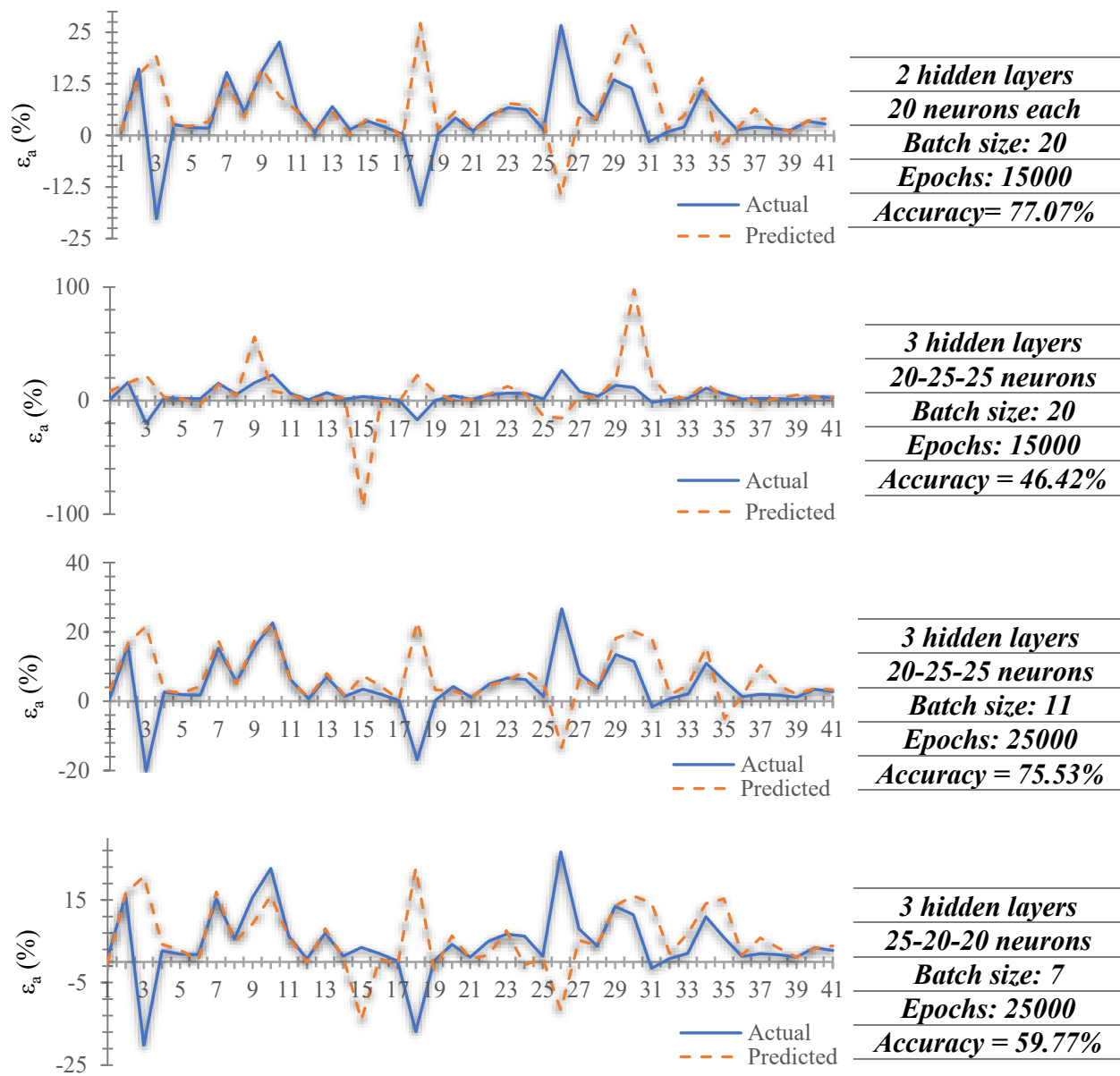


Figure 3.27: ANN models to predict the cyclic strain (ϵ_a).

The *ANN* model has one single fully connected node to predict the cyclic strain as a number; the dataset is first standardized for fitting the model and then scaled back to its original scale. The losses during training were measured by calculating the mean squared error, and the absolute percent error (*APE*) was used to calculate the model accuracy. However, the *ANN* model failed to predict the cyclic strain precisely, specifically when a marine clay failed in negative cyclic strains.

Considering the previous discussion that highlighted the importance of the strain as a cyclic test parameter and that the ML techniques failed to classify or predict the cyclic strain at failure, a different path can be followed to understand better the cyclic strain's effect on marine clay's cyclic behavior. The *strain – controlled* cyclic tests are considered an efficient tool to predict the fatigue life of the marine clays, where the clays' strength deterioration is time-dependent, as reported by many researchers. Moreover, the foundation-marine clay system tolerates a serviceability failure due to long-term deformations of the infrastructure elements under cyclic loading.

In the subsequent chapter, the long-term strength deterioration of marine clays when subjected to successive cyclic loading will be discussed at length. Furthermore, the failure criterion will be defined after testing natural marine clays under cyclic loading until failure. In *strain – controlled* tests, a constant strain amplitude is applied to the clay sample, and the strength deterioration with the increasing number of cycles is reported.

CHAPTER 4

EXPERIMENTAL INVESTIGATION OF MARINE CLAYS FATIGUE BEHAVIOR: STRAIN-CONTROLLED TRIAXIAL TESTING

4.1 INCENTIVE OVERVIEW

Most of the cyclic tests performed on marine clays and available in the literature are stress-controlled tests, where the most critical input parameter is the cyclic stress ratio (*CSR*). The clays were tested by defining the cyclic loading form (i.e., triangular, sinusoidal, rectangular) and the load amplitude. The strain-controlled tests were not commonly used in the studies performed in the literature on marine clays; however, the strain-controlled tests can better describe the fatigue behavior of clays.

In a *Strain – Controlled* test, the clay sample is subjected to a reversed constant strain amplitude of $\pm\Delta\varepsilon_a$. The degradation of shear stress and pore water pressure generation is recorded where a softening behavior of the marine clay and a continuous increase in pore water pressure is expected. The *Strain – Controlled* tests are time-dependent in which the marine clay's response to cyclic loading can be monitored; in terms of softening and hardening intervals progression. Subsequently, the relaxation or degradation modulus can be measured as an essential parameter used in the design of offshore structures.

To inspect the marine clays' response under *Strain – Controlled* cyclic test, a reversed constant strain amplitude was applied with a sinusoidal waveform to a sample collected from Saint-Hyacinthe in Montreal-Canada. Marine clay from Saint-Hyacinthe is high plastic grey clay that has an initial water content $w_n = 72\%$, a liquid limit of $w_L = 77.1\%$, a plastic limit of $w_n = 31.23\%$ and degree of saturation $S_i = 100\%$. The sample was first saturated until a *B – value of 0.95* was reached in an automated Triaxial machine, then consolidated for 24 Hrs with an effective confining pressure of $\sigma'_3 = 50 \text{ kPa}$. For the loading stage, a strain amplitude of $\pm\Delta\varepsilon_a = 5\%$ were applied with a total of 5000 cycles to estimate the number of cycles required to fail.

Figures 4.1 show the hysteresis loops for cycles at the beginning of the test, mid-life, and just before and at failure. It can be seen from the figure that the clay sample shows a softening behavior for the first few cycles where the hysteresis loops degraded, and lower tip values were recorded. After that, the sample exhibited a hardening behavior for a few subsequent cycles, and higher tip values were

recorded. Then, a continuous softening behavior manifested until failure (Cycle No. 413). The softening behavior also can be recognized in the stress-time history plot shown in **Figure 4.2**, represented by the necking in the stress profile with time during the test. The time profile also indicates a sudden increase in the strain and stress amplitudes at cycle *No.* 174. However, the marine clay's sample resumes softening until failure and complete separation. To better understand this behavior, the stress and strain amplitude profiles with increasing cycles, *N* are shown in **Figure 4.3(a)**; a semi-log scale was used. It can be seen that after a certain number of cycles (*No.* 179), an unforeseen increase in the strain amplitude causes an increase in the stress amplitude followed by a drop in the clay sample's resistance (Softening) till complete separation (*N* = 413).

The marine clay sample changes the structure during the test, softening and an apparent shear crack propagation at the end of the test, as shown in **Figure 4.3(b)**. The crack initiation and propagation can explain the unforeseen increase in the strain amplitude (at *N*= 179), leading to a fatal decrease in the clay's strength with cycling until complete failure (after 234 cycles). Also, the clay's sample moved from an elastic to plastic behavior, as shown in the stress-strain hysteresis loops in **Figure 4.1**. The loops become vast in the horizontal direction and move down, revealing a strength loss with decreasing the extrema of the compression side of loading, which the clay flow can describe.

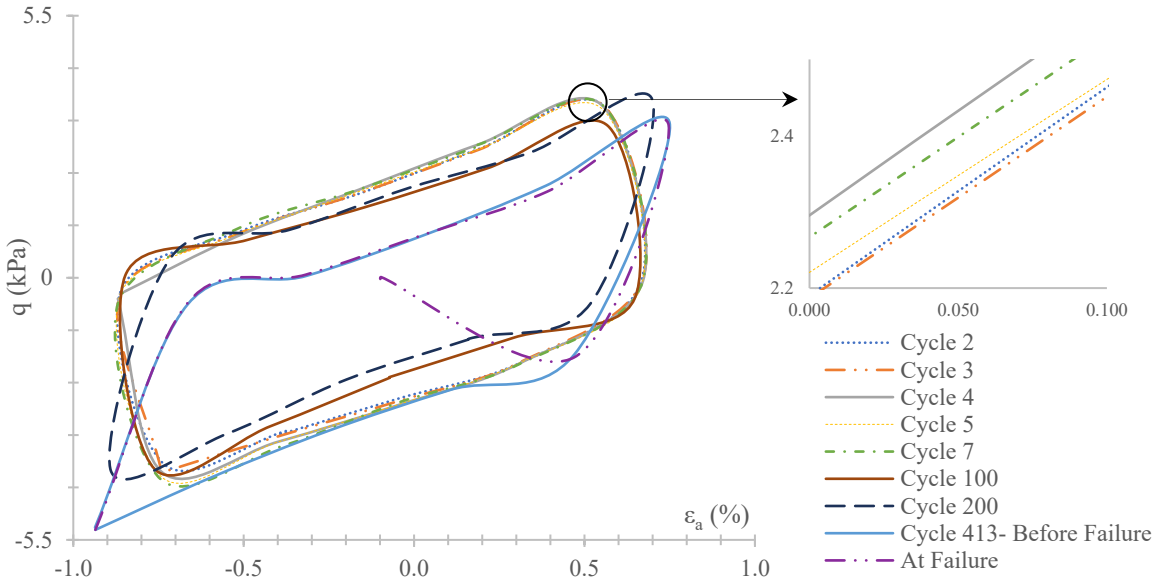


Figure 4.1: Hysteresis loops for different cycles q_{cyc} vs ϵ_a .

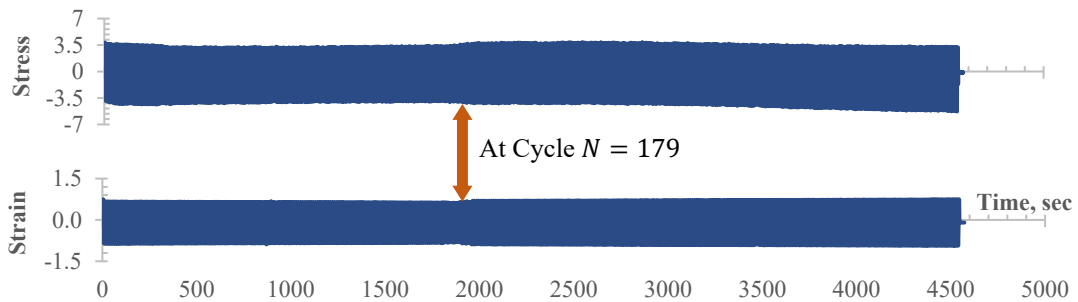


Figure 4.2: Stress/Strain-Time history profile during cycling until complete failure at, *N* = 413.

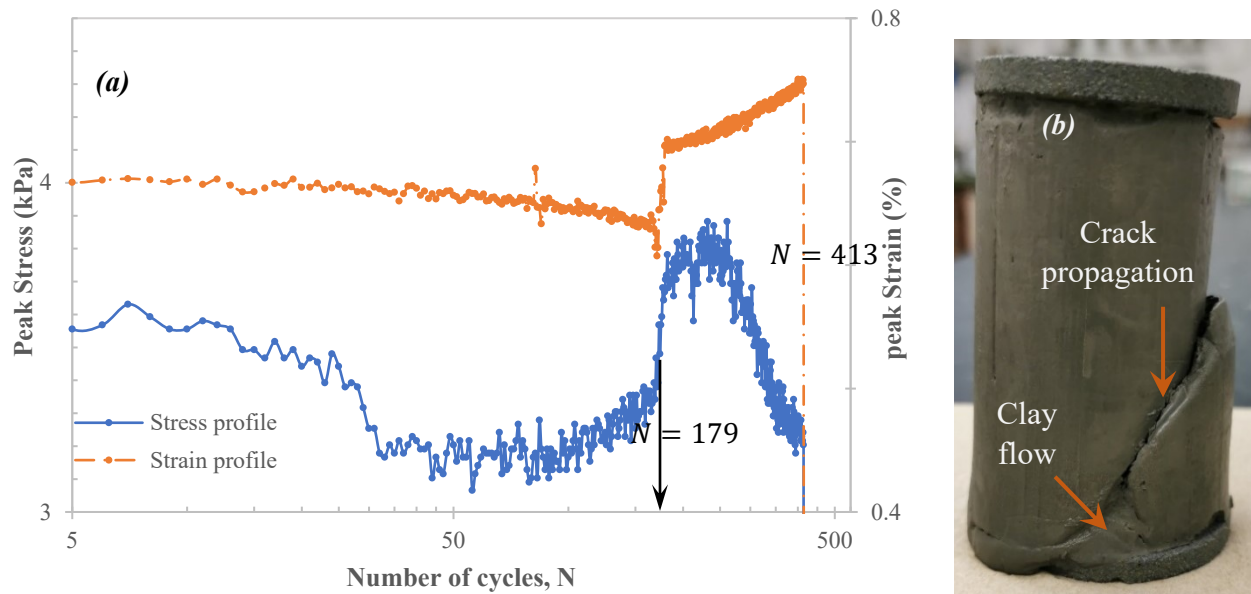


Figure 4.3: (a) Stress/Strain amplitude profile during cycling until failure at $N = 413$, and (b) The marine clay sample after testing.

Figure 4.4 shows the test results for another marine clay sample collected from the Abitibi area in Quebec-Canada and subjected to 10000 cycles. The sample is high plastic grey clay has an initial water content $w_n = 70\%$, the liquid limit of $w_L = 69.75\%$ and degree of saturation $S_i = 100\%$. The sample tested for an effective confining pressure of $\sigma'_3 = 50 \text{ kPa}$ and a strain amplitude of $\pm\Delta\varepsilon_a = 5\%$ similar to the sample from Saint-Hyacinthe. A continuous softening behavior was recorded from the beginning of the test up to a certain number of cycles. Then the behavior oscillated between hardening and softening, as shown in **Figure 4.4a**. A gradual increase in the strain amplitude occurs at cycle N16 associated with an increase in the stress amplitude; the strain amplitude continues to increase till N147 while the stress amplitude decreases at a high rate. Opposite to the sample from Saint-Hyacinthe, the strain amplitude remains constant after the slight gradual increase (N147) to the test end, as shown in **Figure 4.4b**.

The stress profile in **Figure 4.4b** shows a continuous degradation until N1755, followed by hardening and softening oscillated behavior. At N10000, a thin layer flow at the bottom side existed (**Figure 4.4c**), and cracks initiated at the middle and bottom of the sample. It could be seen that the cracks started and propagated but did not lead to complete separation. Complete separation can be reached by cycling the sample for a few more cycles. However, the clay sample can still fail between N1755 and N10000 as multiple cracks existed and propagated.

The hysteresis loops in **Figure 4.4d** can describe the same behavior as the stress tip values decrease with increasing cycles and increase during hardening cycles. Add to this, the shape of the hysteresis loops, represented by the area confined between the compression loading and unloading curves, changed during testing. For example, for cycles N2-N4, N30, N100, N500, and N1000, the loops are more pointed than the cycles N3000, N7000, and N10000, in which the latter is considered more rectangular. Thus, the hysteresis loops area is another indicator of marine clay's strength loss under cyclic loading; by decreasing the area with cycling, the clay shows an energy loss. In addition, the three cycles (N3000, N7000, and N10000) have nearly the same compression tip strength, while the tension tip strength is moving up by losing energy (area reduction).

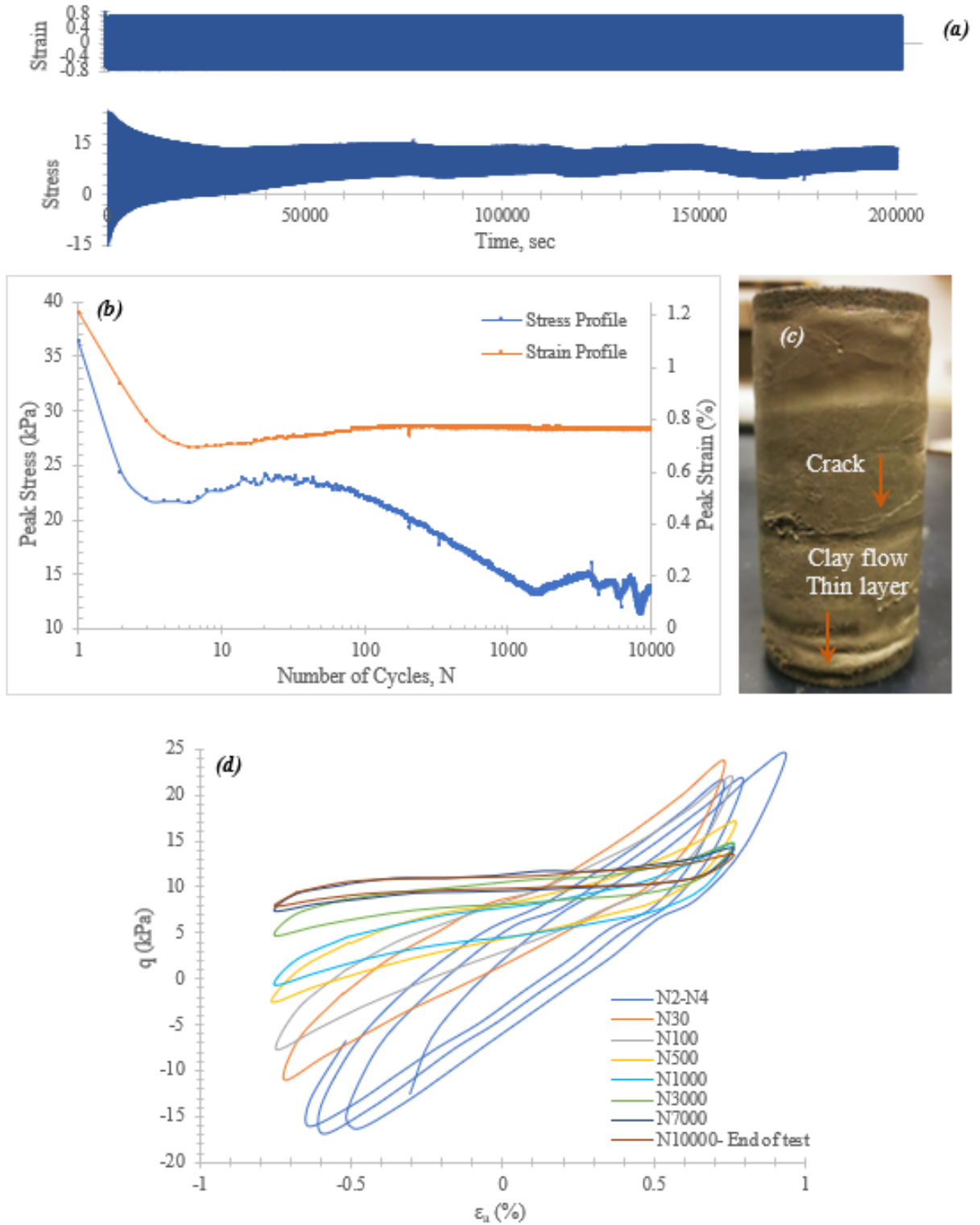


Figure 4.4: Abitibi marine clay sample's test results with $\sigma'_3 = 50 \text{ kPa}$ and $\pm\Delta\epsilon_a = 5\%$: (a) Stress/Strain-Time history profile, (b) Hysteresis loops for different cycles during the test q_{cyc} vs ϵ_a (c) Peak Stress/Strain profile (d) The marine clay sample after testing.

The degradation index (δ) and the degradation parameter (t) are two parameters introduced by (Idriss, Dobry, & Singh, 1978) to depict the performance of marine clay under cyclic loading. The researchers performed undrained cyclic Triaxial strain-controlled tests on samples collected from the San Francisco Bay Mud-US. They recorded the decrease in deviatoric stress at the tips of different loops at different cycles and defined the degradation index using the secant modulus of each loop using **Equation 4.1**. The degree of degradation (δ) was measured on the assumption that the strain amplitude ϵ_c Remains constant during the test, and that δ decreases linearly with increasing the number of cycles for any strain amplitude creating the degradation parameter (t). The degradation parameter is defined as the slope of the $\log \delta - \log N$ plot. It is essential to mention that the parameters were measured for a number of cycles that did not exceed 100 cycles.

$$\delta = \frac{(E_s)_N}{(E_s)_1} = \frac{(\sigma_d)_N / \epsilon_c}{(\sigma_d)_1 / \epsilon_c} = \frac{(\sigma_d)_N}{(\sigma_d)_1} \dots\dots\dots \mathbf{4.1}$$

Figure 4.5 indicates the first and last cycles for the previously discussed test results. Applying (Idriss, Dobri, & Singh, 1978) theory, the degradation indices for the Saint-Hyacinthe and Abitibi clay samples based on the loading side extrema (σ_d) were 0.89 and 0.37, respectively. However, both clays were loaded for more than 100 cycles with an apparent change in the strain amplitudes recorded after several cycles, making the degradation index measurement inaccurate. If the difference in strain amplitude was considered, the degradation indices should be measured based on the secant modulus of elasticity given in **Equation 4.2** to get more accurate values. The degradation indices for the Saint-Hyacinthe and Abitibi clay samples based on the Secant Modulus of Elasticity (E_s) were 0.86 and 0.11, respectively.

$$E_s = \frac{\sigma_{d \max} - \sigma_{d \min}}{\epsilon_{\max} - \epsilon_{\min}} \dots\dots\dots \mathbf{4.2}$$

It can be seen from the hysteresis loops shape of the Saint-Hyacinthe clay that the sample failed without losing much energy as the area under the curve did not change distinctly. Consequently, it had a high degradation index of $\delta = 0.86$. While for the Abitibi clay, the hysteresis loops' area diminishes with increasing the number of cycles, and the degradation index reached a value of $\delta = 0.12$ at the end of the test (N10000). Thus, the Abitibi clay loses much energy before failure, and the degradation index could indicate this failure.

The degradation index variation with the number of cycles for both clays is shown in **Figure 4.6** with a semi-log scale. Both samples were tested under the same conditions, and the degradation index decreased nonlinearly in a hyperbolic relationship at the beginning of the tests. For the saint-Hyacinthe clay, the degradation index dropped gradually until failure, and the clay failed suddenly without losing energy. On the other hand, the degradation index of the Abitibi decreases steeply with increasing the number of cycles till the end of the test. After N6000, the degradation index showed disturbance, likely indicating the failure. Thus, the degradation index (δ) can exceedingly express the response of marine clays to cyclic loading and help predict the number of cycles required to cause failure.

It can be deduced that the stress-time history profile and degradation index variation during cycling can be considered as practical tools to study the marine clays' fatigue and plastic behavior (long-term behavior). Moreover, the number of cycles required to cause failure can be predicted from the

strain-controlled triaxial tests (life estimation) by cycling the sample until failure. Therefore, a series of strain-controlled tests will be performed in the subsequent sections to study the marine clay's performance under slow cyclic loading that simulates the field conditions of offshore structures.

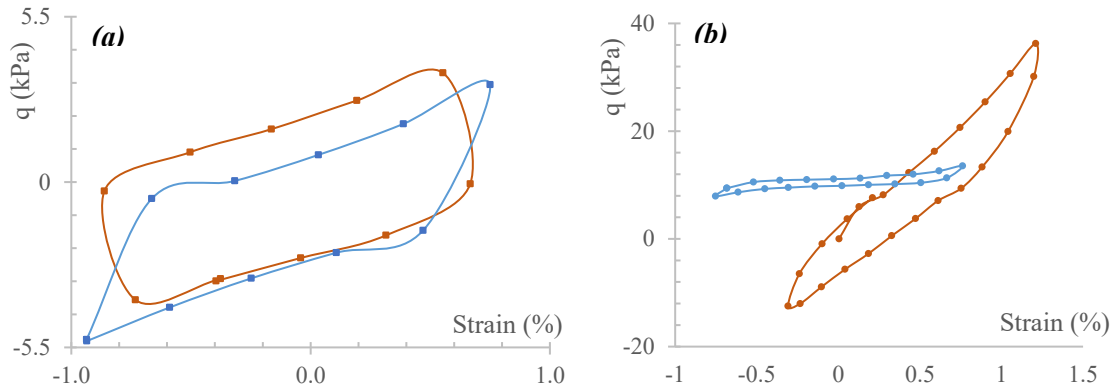


Figure 4.5: Secant moduli for the first and last cycles (a) The Saint-Hyacinthe sample, $N_f = 413$, and (b) The Abitibi clay sample, $N = 10000$.

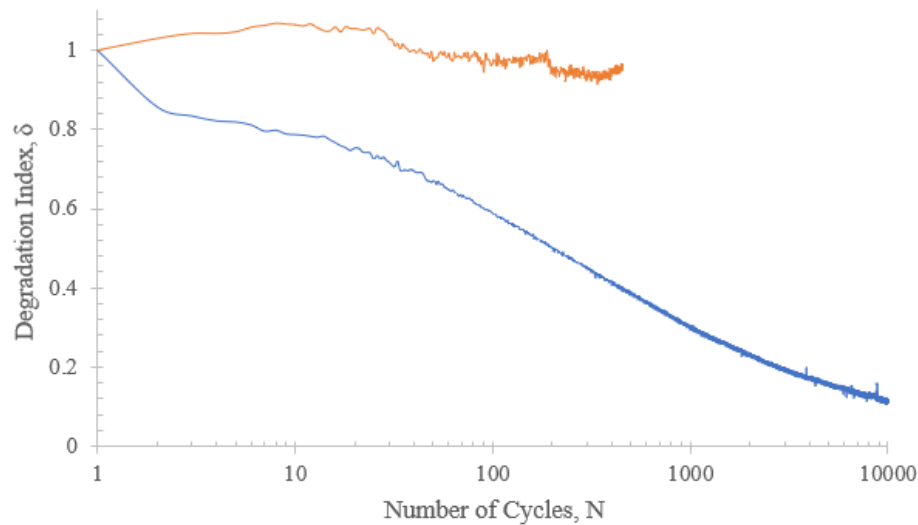


Figure 4.6: Degradation indices variation with number of cycles for Saint-Hyacinthe sample, $N_f = 413$, and Abitibi clay sample, $N = 10000$.

4.2 EXPERIMENTAL TEST PLAN

4.2.1 Marine Clays Collection and Preparation

Marine clays' samples used in this study were collected from different locations in Quebec-Canada in collaboration with two geotechnical labs, *WSP* and *SNC – Lavalin*. The clay samples obtained from *SNC-Lavalin* were collected earlier in 2017 to 2019 field projects in the Abitibi area. The specimens were extracted from Shelby tubes, wax-coated, and preserved in a humidity chamber to maintain their natural conditions. The Abitibi clays are grey and have a CH (High Plastic Clays) classification in the plasticity chart. The location and physical properties of these clays are shown in **Table 4.1**.

The clay samples obtained from WSP were collected from recent projects (2021) in 3" Shelby tubes and two different locations, Saint-Hyacinthe and Rouyn-Noranda in Quebec. All samples are grey and high plastic clay (CH) and have the physical properties shown in **Table 4.1**. The clay samples were extracted from the Shelby tubes in the Geotechnical research lab at Concordia University, then cut to several specimens and wrapped to keep the moisture. After the extraction and segmentation processes, the specimens were wax-coated using the Paraffin Wax and labeled (**Figure 4.7**).

Table 4.1: Marine clays' locations and physical properties (Average values).

<i>Location</i>	$w\%$	$w_L\%$	$I_p\%$	$I_L\%$	e_o	γ_o	$S\%$	S_t
Saint-Hyacinthe	75.5	77.1	45.87	0.90	1.863	14.96	100	19.80
Abitibi	60	69.75	30.75	0.80	1.73	16.20	100	4.84



Figure 4.7: Marine clay samples' preparation: extraction from Shelby tubes, segmentation, wax-coating, and labeling.

4.2.2 Triaxial Machine Setup

All tests in this study were performed using a fully automated Triaxial machine. The Triscan frame setup has a cross beam with a domed loading cap, an internal load cell (25 kN) with a 15.5 cm ram, a fixed top cap, and a standard cell, as shown in **Figure 4.8**. The cell has a 50mm pedestal for a specimen size of 5cm in diameter and 10cm in height with $L/D = 2$. The internal load cell is screwed to the top cap, maintaining the specimens' stability during the test. A displacement transducer attached to the loading ram with brackets is used to measure the strain and displacements input values. In addition, a pore water pressure transducer is connected to one of the standard cell valves for the pore water pressure readings. Finally, a pro dual APC unit (Automatic Pressure Controller) automatically controls the back-pressure and cell-pressure inputs during testing without manual intervention with the help of the automatic solenoid valve that controls the back pressure during the test (switch on/off).

The Clisp Studio Triaxial Advanced Software (csTriaxAdv) enables the user to perform multi-stage tests with a predefined schedule. The tests performed in this study include a consolidated undrained (CU) monotonic test with three stages: saturation (B-Check), consolidation, and static loading stages, and slow strain-controlled cyclic tests with two steps: saturation (B-Check) and cyclic loading stages. The clays were not consolidated to study the marine clays' response and life estimation under their natural conditions. The software module allows the user to define the input parameters and stop conditions for each stage, providing the flexibility of studying the clays' response and behavior under different loading conditions.

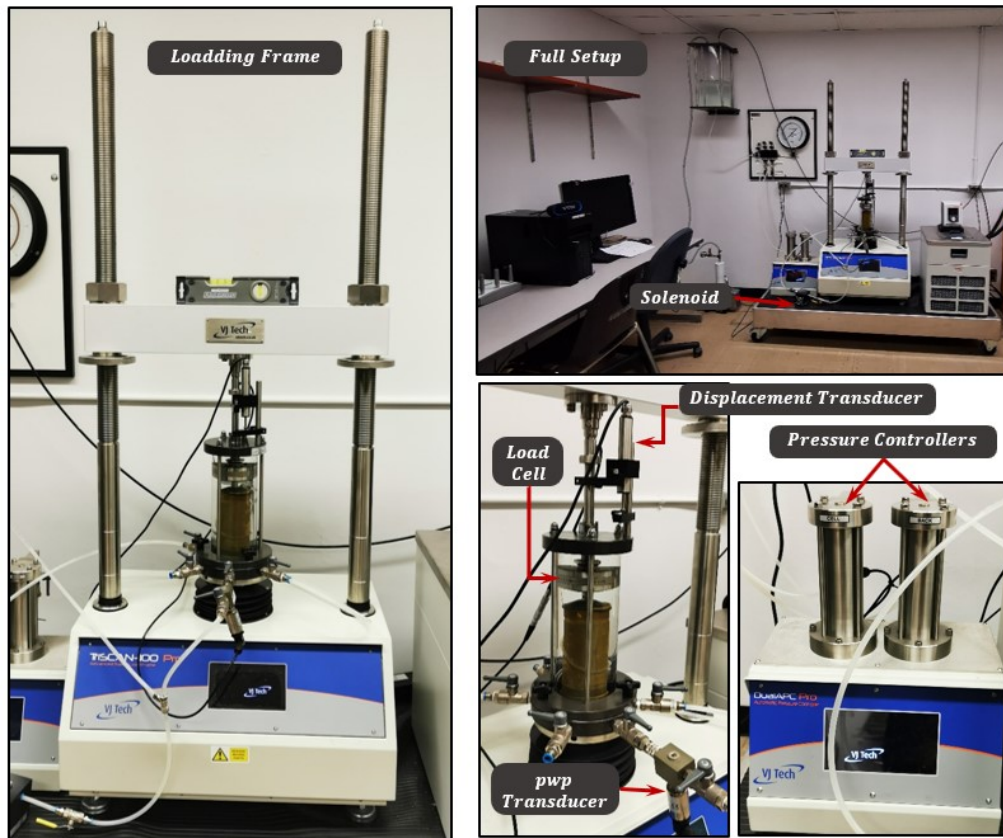


Figure 4.8: The fully automated Triaxial Machine setup used in the study.

4.2.3 Experimental Program and Testing Procedures

All specimens tested in this study have the same dimension of 5cm by 10cm and a height-to-diameter ratio of 2. After removing the wax coating, the samples were manually extracted using an extruder, installed on the pedestal, and attached to the internal loading cell through the fixed-top cap. Side drain filter papers were attached to the specimens to accelerate the consolidation process for the CU monotonic tests. No side drains were used in the slow cyclic tests.

The first stage in all tests is the saturation stage to obtain a minimum B-value of 0.95. It was reported in the literature that a marine clay sample reaches saturation after increasing the back-pressure to about 600 kPa . For that, an incremental increase of the back-pressure of $60 - 75\text{ kPa/hr}$ was applied after the first B-Check step, then a second B-check was allowed. These steps were repeated until a B-value of 0.95 or more was reached (**Figure 4.9**).

For Static triaxial tests, the saturated specimens were consolidated isotropically under specific effective confining pressures (**Table 4.2**) until a pore water pressure dissipation of 95% or a volume change of fewer than 0.002 cc^3 reported in two hours. The shearing stage was strain-controlled, where a shear rate of $1.5\%/hr$ applied to the specimens until a fall of 20% in the deviatoric stress was reported. An additional shear strain increment of 5% is allowed per the ASTM- D4767 (2020) standards. The software module enables a direct graphical presentation for the test results and permits the raw data extraction in an Excel sheet format for all these stages. **Figure 4.10** shows a sample of the loading configuration in monotonic tests.

In the strain-controlled cyclic tests, the specimens were first saturated following the previous procedures, and then cyclic loading was applied with different effective confining pressure σ'_3 , frequencies f , and strain amplitude $\pm\Delta\varepsilon_a$. All samples were subject to sinusoidal waveform cycles until failure with the properties and loading configuration shown in **Figure 4.11**. The strain-controlled tests program is listed in **Table 4.2**.

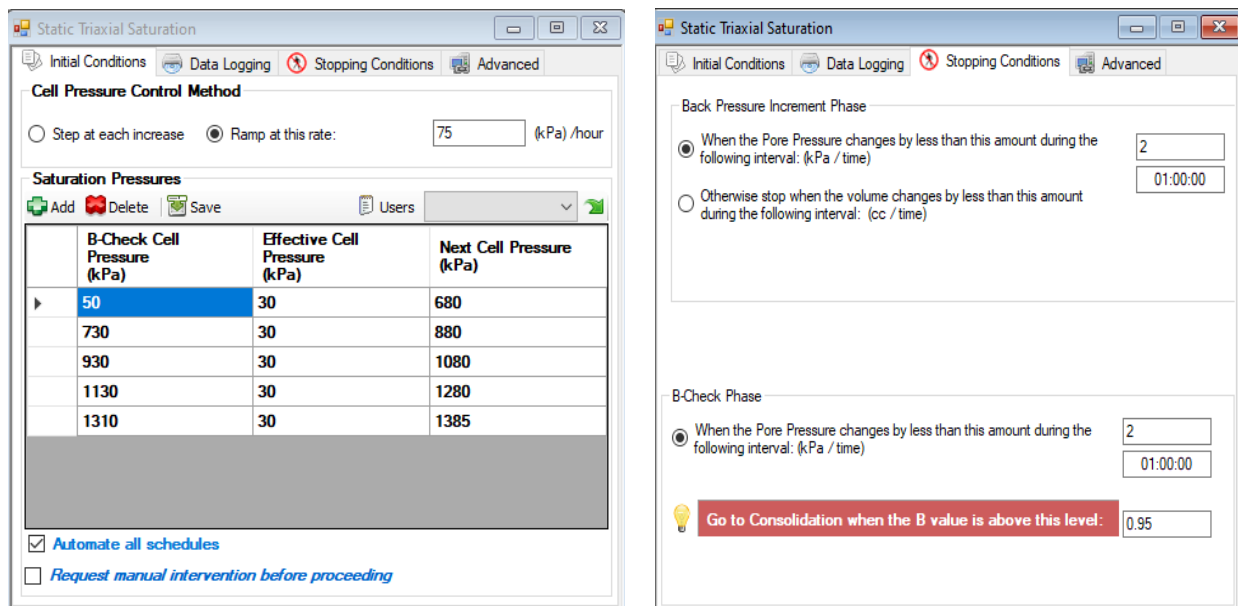


Figure 4.9: The initial and stopping conditions for the saturation schedule in the performed tests.

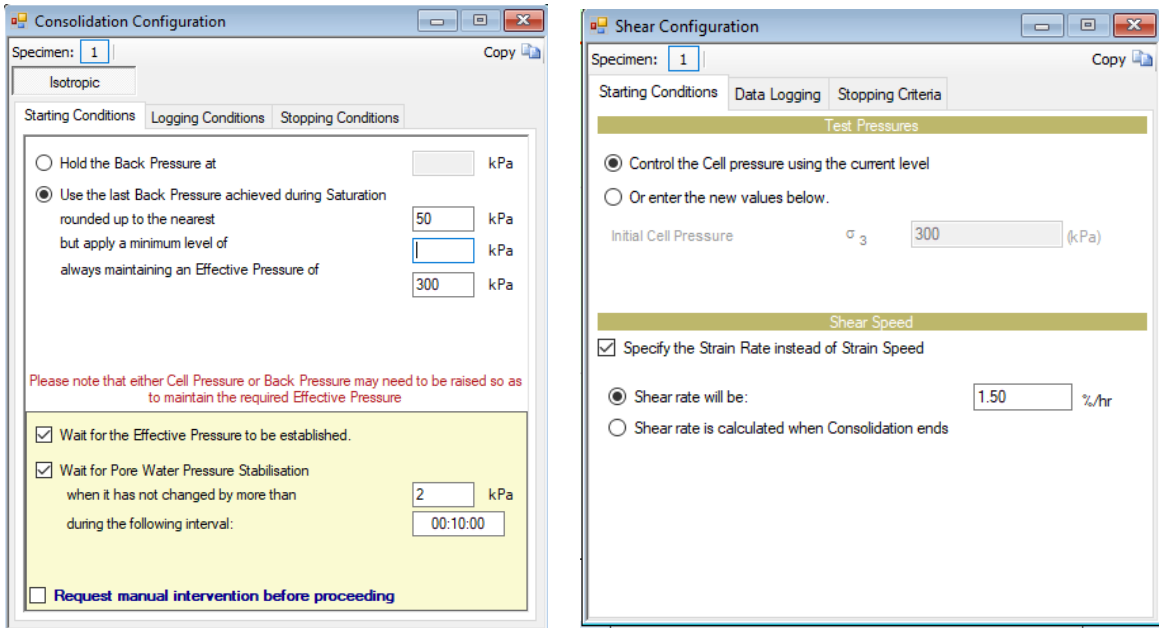


Figure 4.10: A sample of the consolidation and Shearing configuration in monotonic tests.

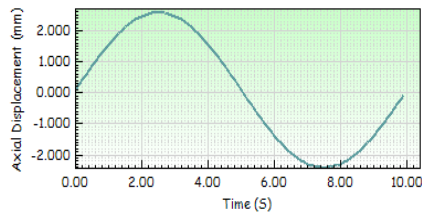
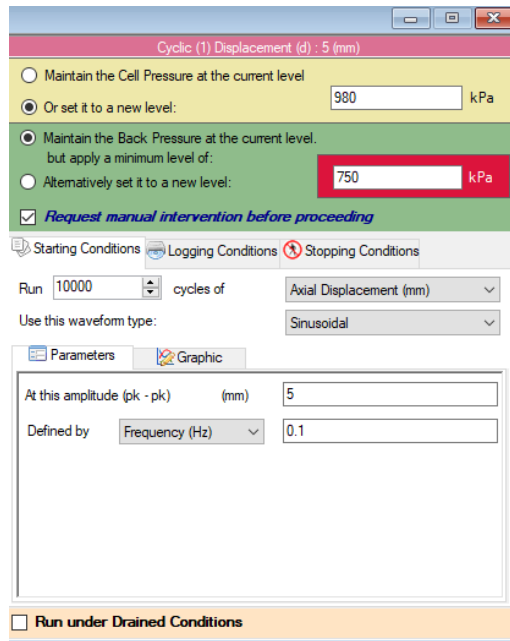


Figure 4.11: Sample of strain-controlled tests loading configuration.

Table 4.2: Experimental program of strain-controlled cyclic tests.

Confining pressure σ'_3 (kPa)	Marine clay	Target	Strain Amplitude $\pm\Delta\varepsilon_a$ (%)	Loading frequency f	Number of cycles N
Strain-Controlled Triaxial Tests					
50	Saint-Hyacinthe	Preliminary	5	0.1	5000
50	Abitibi	Study	5	0.1	10000
50	Abitibi	Effect of σ'_3	5	0.1	10000
250			5	0.1	10000
200	Abitibi	Effect of Amplitude	1.65	0.1	1000
200			1.85	0.1	5000
200			1.85	0.1	10000
200			2.5	0.1	10000
200			5	0.1	10000
200	Abitibi	Effect of Frequency	5	0.05	4500
200			5	0.01	4500
200			5	0.1	4500
200	Abitibi	Life Estimation	0.75	0.1	Until failure
200			1.25	0.1	
200			2.5	0.1	
200			5	0.1	

4.3 ANALYSIS OF STRAIN-CONTROLLED TEST RESULTS

4.3.1 Nomenclatures

Figures 4.12-14 are interpretative diagrams for the sinusoidal wave, cyclic stress response, and the hysteresis loop properties and terminologies related to the strain-controlled cyclic tests'. The terms explained in this section will be used to discuss the results of the tests.

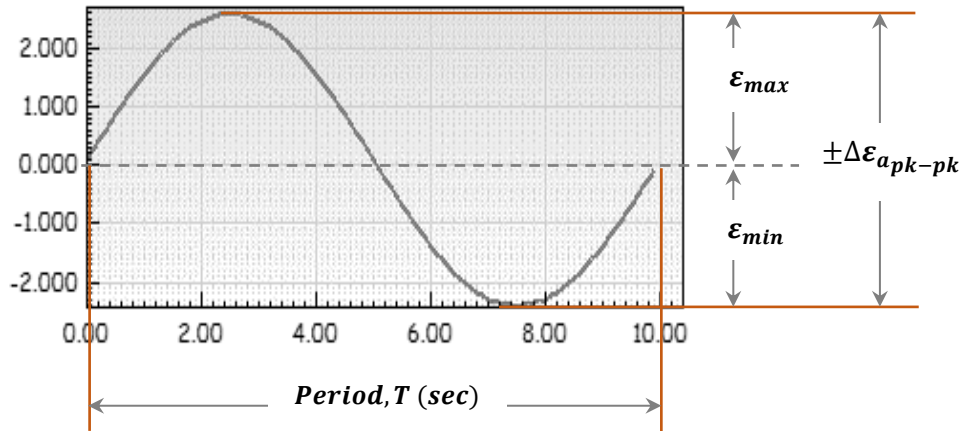


Figure 4.12: Sinusoidal wave properties.

The following terms can be defined, referring to Figure 4.12:

ϵ_{max} : Maximum strain amplitude applied during loading (+ve).

ϵ_{min} : Minimum strain amplitude applied during unloading (-ve).

$\Delta\epsilon_a$: Peak to peak strain amplitude, $\Delta\epsilon_a = \epsilon_{max} - \epsilon_{min}$

T : The period of one cycle in seconds and can be represented by the frequency, $f = 1/T$.

ϵ_{mean} : Mean strain amplitude, $\epsilon_{mean} = \frac{(\epsilon_{max} + \epsilon_{min})}{2}$, for constant strain amplitude $\epsilon_{mean} \rightarrow 0$.

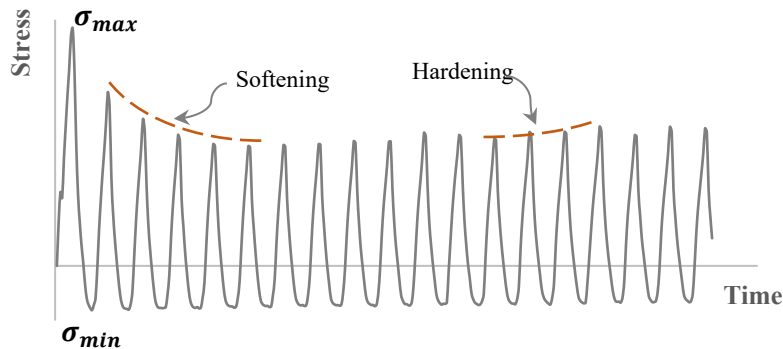


Figure 4.13: Stress-time profile during the strain-controlled cyclic test.

The following terms can be defined, referring to Figure 4.13:

σ_{max} : Maximum stress amplitude during loading (+ve).

σ_{min} : Minimum stress amplitude during unloading (-ve).

σ_{mean} : Mean strain amplitude, $\sigma_{mean} = \frac{(\sigma_{max} + \sigma_{min})}{2}$.

Softening : When the extrema (σ_{max}) of a cycle is lower than the cycle before.

Hardening : When the extrema (σ_{max}) of a cycle is higher than the cycle before.

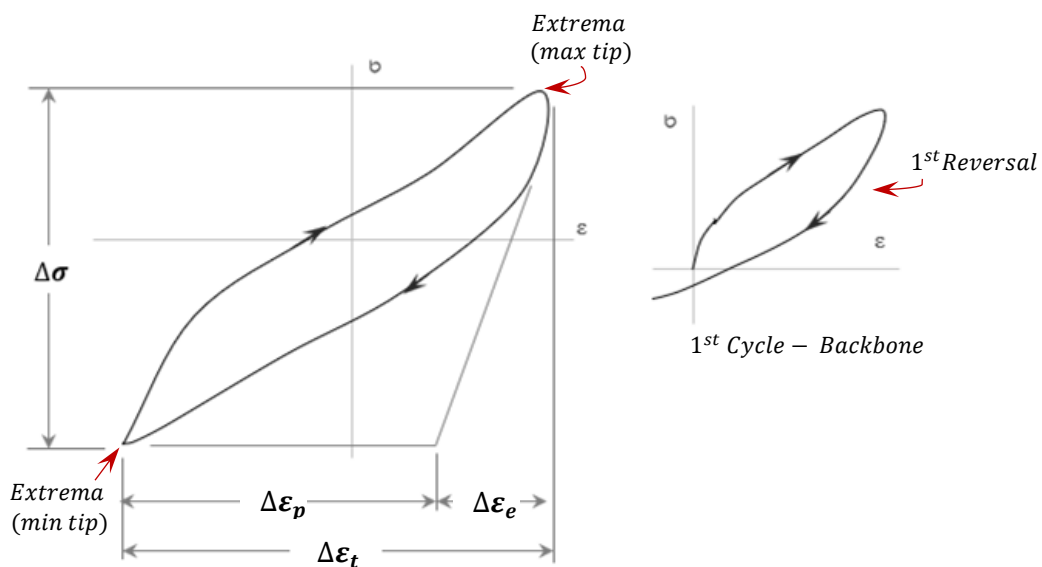


Figure 4.14: Cyclic $\sigma - \epsilon$ curve properties.

The following terms can be defined, referring to Figure 4.14:

max tip: Or the *+ve* extrema, representing $(\varepsilon_{max}, \sigma_{max})$

min tip: Or the *-ve* extrema, representing $(\varepsilon_{min}, \sigma_{min})$

$\Delta\varepsilon_e$: True elastic strain range where $\Delta\varepsilon_e = \Delta\sigma/E$.

$\Delta\varepsilon_p$: True plastic strain range.

$\Delta\varepsilon_t$: Total true strain range where $\Delta\varepsilon_t = \Delta\varepsilon_e + \Delta\varepsilon_p$.

$\Delta\sigma$: True stress range.

Reversal: Unloading curve.

Backbone: Initial loading at the beginning of the test, open loop.

4.3.2 Effect of Confining Pressure

Although researchers in the literature do not consider the confining pressure an essential factor affecting the marine clay cyclic response in strain-controlled tests, two tests were performed in this study: low and high confining pressures were selected ($\sigma'_3 = 50 \text{ kPa}$ and 250 kPa). Moreover, the clay samples from the Abitibi Clay were tested under their natural conditions (initial water content of $w\% = 58\%$). For cyclic loading, a sinusoidal waveform was performed for up to 10000 cycles, a 5mm amplitude, and 0.1 Hz frequency. Then, the stress degradation, strain profile, hysteresis loops, and pore water pressure generation with the number of cycles were reported for comparison purposes.

The hysteresis loops for the first backbone (**Figure 4.15a**), which indicates the initial loading condition, show that for lower confining pressure ($\sigma'_3 = 50 \text{ kPa}$), higher strength at the extrema, higher clay stiffness, and relatively lower absorbed energy were recorded (less hysteresis loop area). The same behavior was observed for the first cycle $N1$ (**Figure 4.15b**), except that the two samples have almost equal absorbed energy.

Both samples had nearly the same axial strain at the extrema for the first two cycles, which means that the 50 kPa sample requires more stress amplitude to cause the 1.2% and 0.9% strain. The first two cycles' reversals for both samples coincide during unloading and cross the x-axis at the same or very close axial strain values (0.33% and 0.23% for $N0$ and $N1$, respectively). These values are much lower than the extrema values, which indicates an elastic behavior and low energy loss.

Both samples show the same behavior with increasing cyclic loading and reaching the mid-life cycles (**Figure 4.15c**). However, the 50 kPa tested sample shows higher deviatoric stress at the extrema when compared with the 200 kPa tested sample, but nearly the same stiffness and energy absorbed. Simultaneously, the negative strain amplitude peak for the 200 kPa test is greater than the positive peak, while for the 50 kPa test, the peaks are almost identical. Both samples at the mid-life cycles increased the stress peak amplitudes as shown in **Figure 4.17** and had two positive stress peaks (**Figure 4.15c**).

Figure 4.15d shows the hysteresis loops at the end of the test; the two tests exhibit the same behavior as the mid-life cycles, except that the samples lose more energy as the hysteresis loop areas decrease. The reversals have a comparable axial strain value to the extrema for mid-life and end test cycles, indicating that the samples behave plastically.

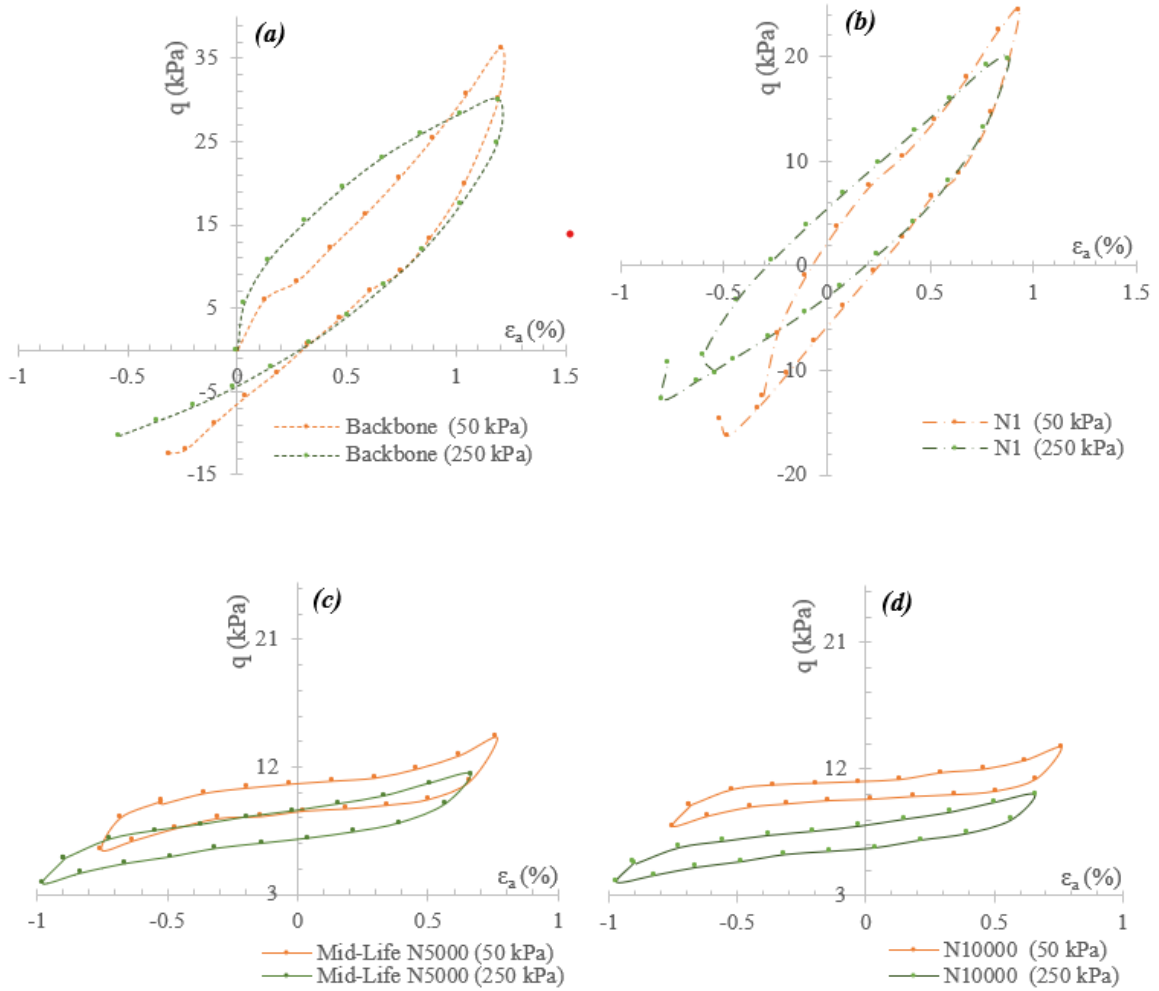


Figure 4.15: Hysteresis loops during the test (q_{cyc} vs ϵ_a) for different confining pressures: (a) First backbone, (b) first cycle, (c) At mid-life, and (d) At the end of the test.

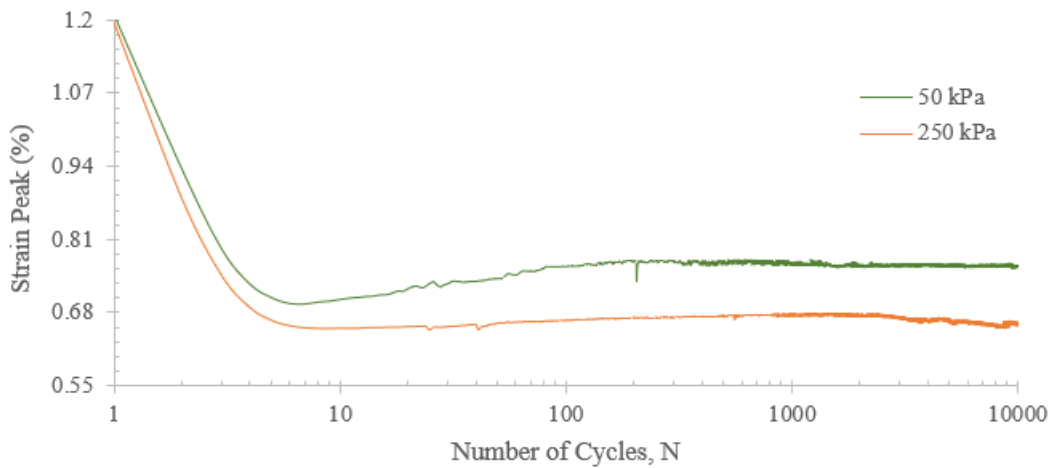


Figure 4.16: Strain-Time history profile for different confining pressures.

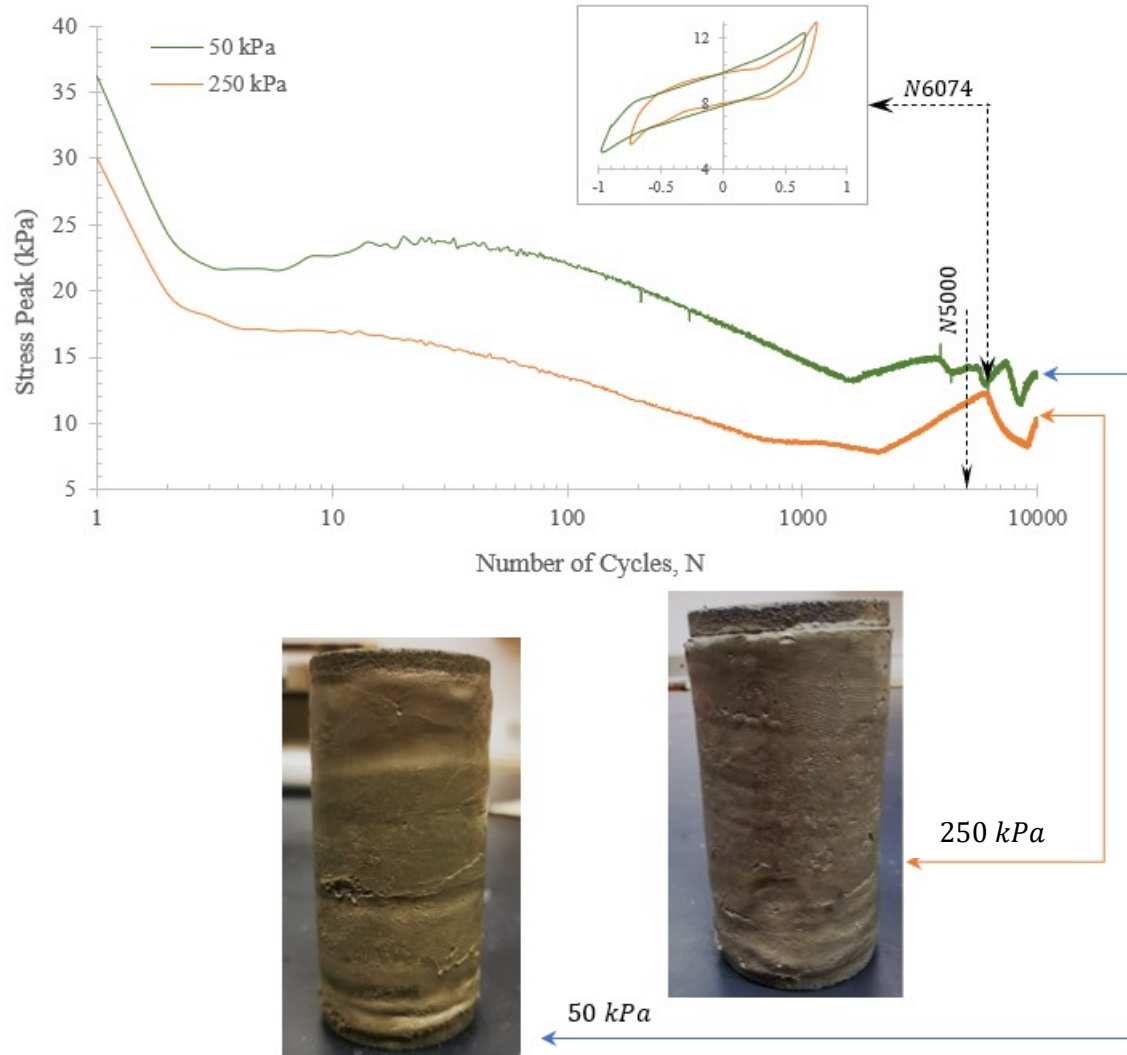


Figure 4.17: Stress-Time history profile and samples after testing for different confining pressures.

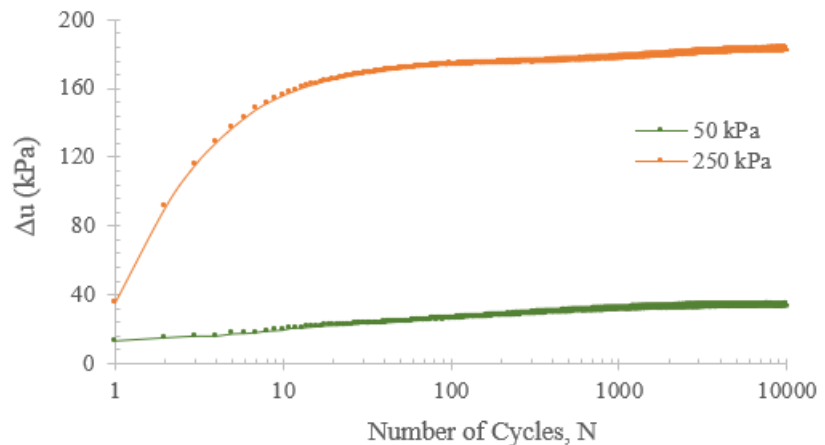


Figure 4.18: Pore water pressure generation for different confining pressures tests.

The strain-time profile in **Figure 4.16** shows that both samples followed the same form of strain amplitude progressing during the test. All turning points, increasing or decreasing strain amplitudes, were happening at almost the same number of cycles. The same behavior can be seen in the stress-time profile (**Figure 4.17**). Both samples degraded under cyclic loading linearly in the first few cycles then continued degrading in a hyperbolic relationship in the semi-log curve ($\sigma - \log N$), reaching the maximum degradation at $N > 1500$ cycles followed by oscillating cycles of hardening and softening till the test end. At $N=6074$, the samples' hysteresis loops were almost identical, as shown in **Figure 4.17**.

At the end of the test, the samples' exhibited a thick, soft layer representing clay flow at the bottom side (**Figure 4.17**). Also, both samples initiated multiple cracks at the middle and bottom sides with no complete propagation and failure. The sample tested for 50 kPa confining pressure generates relatively low pore water pressure $\cong 33$ kPa compared with the 200 kPa tested sample that generates $\cong 182$ kPa, as shown in **Figure 4.18**, which is considered normal as a higher confining pressure was applied.

It can be seen that the confining pressure does not affect the marine clay fatigue behavior under cyclic loading significantly. Consequently, an effective confining pressure of 200 kPa will be applied for the tests in this research.

4.3.3 Effect of Amplitude

Most of the literature's research studied the marine clay behavior under different strain amplitudes to measure the clays' degradation. However, limited research is available for the strain-controlled cyclic tests on marine clays, and less than 1000 cycles were applied. Therefore, in this research, and to study the effect of strain amplitude on the fatigue behavior of marine clays, 10000 cycles were applied to three samples from the Abitibi clays. The clay was tested under its natural conditions (no consolidation schedule) in cyclic Triaxial tests; a confining pressure of 200 kPa and frequency of 0.1 Hz were applied. The strain amplitudes of 1.85, 2.50, and 5.00 mm applied to the samples; the stress degradation, strain profile, hysteresis loops, and pore water pressure generation with the number of cycles were reported for comparison purposes.

The initial loading condition is shown in **Figure 4.19a**, where the maxima of the hysteresis loops increased with decreasing the applied strain amplitude. The 1.85 and 2.50 mm tested samples have relatively high stiffnesses that are much higher than the 5.00 mm stiffness. However, the reversal of the 5.00 mm tested sample indicates more elastic behavior compared with the other two samples.

The first cycle hysteresis loops (**Figure 4.19b**) show that the 1.85 and 2.50 mm tested samples lose more energy after one cycle, the hysteresis loops' areas and the stresses at the extrema notably decreased compared with the 5.00 mm tested sample. The 1.85 mm tested sample shows the highest stress degradation after the first cycle, and the 5.00 mm tested sample shows the lowest stiffness. All samples after the first cycle have almost equal energy absorbed.

All samples have relative axial strain values (0.72 – 0.76%) and primarily equal strain amplitude peaks for the loading and reversal curves at the mid-life cycles, as shown in **Figure 4.19c**. The stresses at the extrema degraded for all samples, and the hysteresis loops became broader and more rectangular. Both the 2.50 and 5.00 mm show similar energy loss and stiffness behaviors, while the 1.85 mm sample has higher stiffness and less energy loss as the hysteresis loop's area is spacious.

Figure 4.19d shows the hysteresis loops at the end of the test; the three tests exhibit the same behavior as the mid-life cycles, except that the samples lose more energy as the hysteresis loops areas decrease. In addition, the reversal of the 5.00 mm has a higher axial strain value than that for the loading curve. However, the 1.85 and 2.50 mm have comparable axial strain values to the mid-life cycles. The 1.85 mm still exhibited the highest stiffness and lower energy loss.

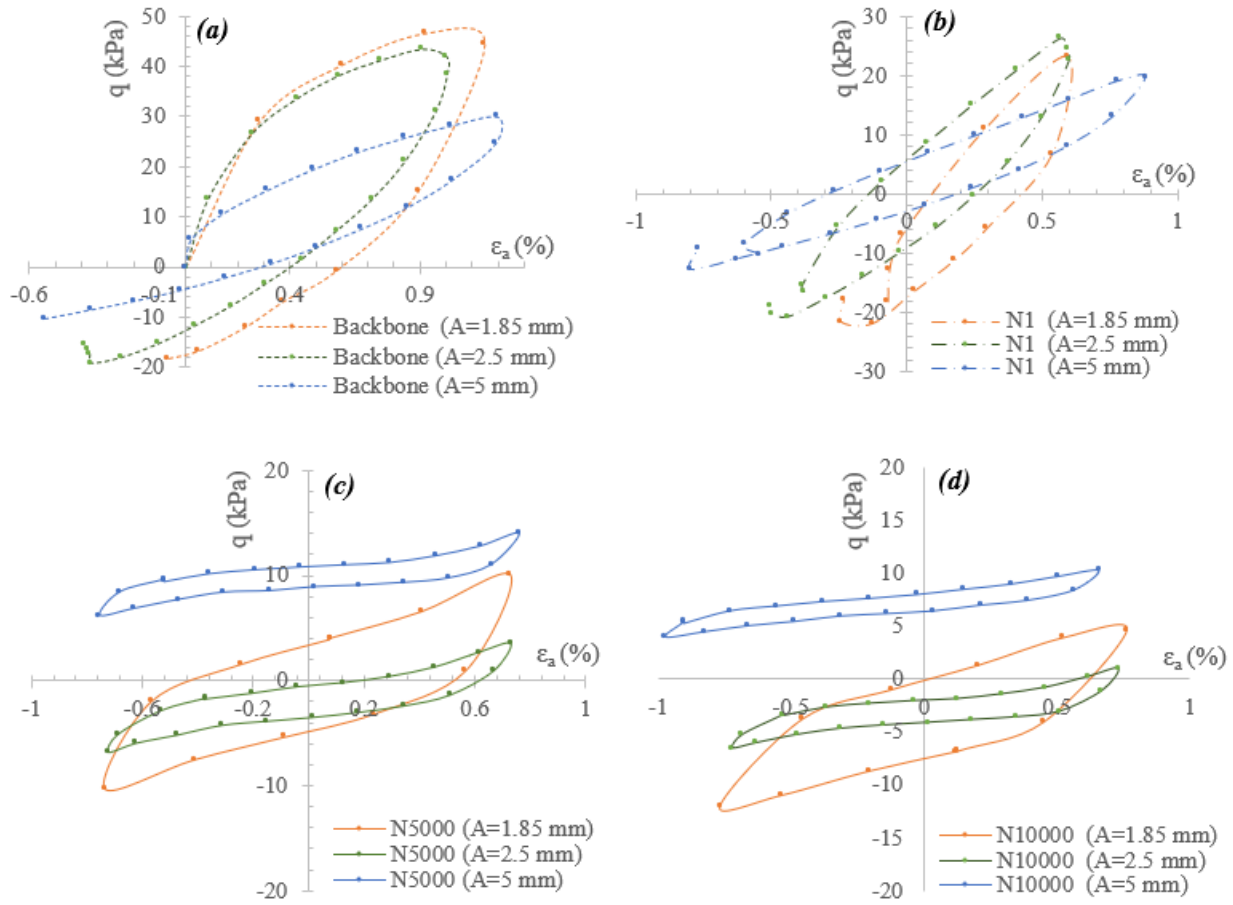


Figure 4.19: Hysteresis loops during the test (q_{cyc} vs ϵ_a) for different amplitudes: (a) First backbone, (b) First cycle, (c) At mid-life, and (d) At the end of the test.

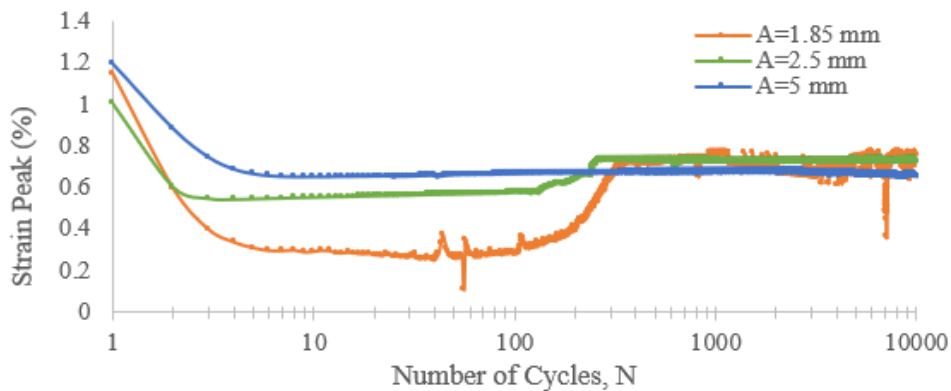


Figure 4.20: Strain-Time history profile for different amplitudes.

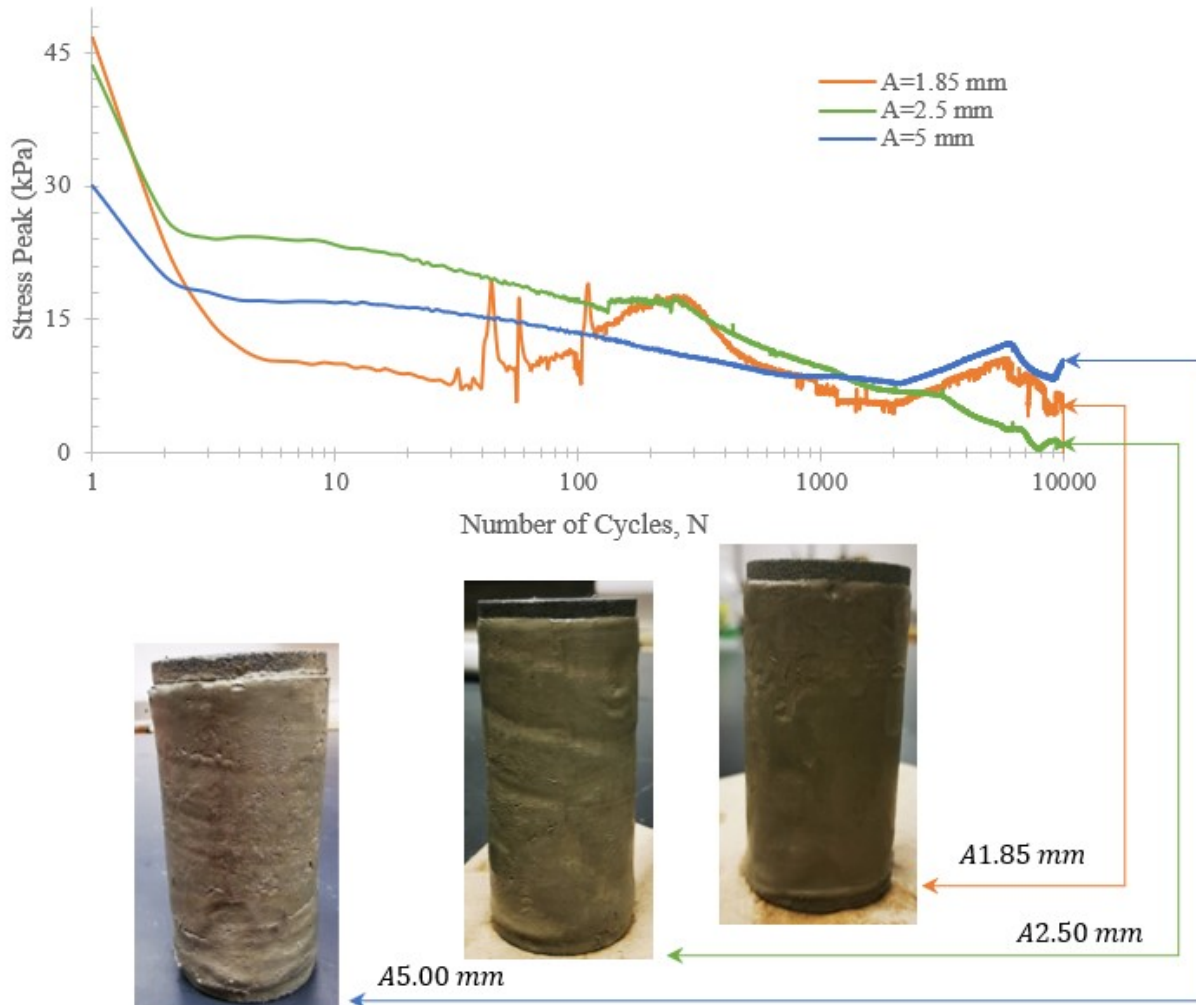


Figure 4.21: Stress-Time history profile and samples after testing for different amplitudes.

The strain-time profile in **Figure 4.20** shows that all samples followed the same form of strain amplitude progressing during the test. All turning points, increasing or decreasing strain amplitudes, were happening at almost the same number of cycles. At $200 < N < 300$ cycles, the strain amplitude for all samples becomes relatively the same and continues till the end of the test.

The stress-time profile (**Figure 4.21**) shows samples' different behavior after the first few cycles. The 2.50 and 5.00 mm tested samples degraded under cyclic loading linearly in the first few cycles, then continued degrading in a hyperbolic relationship in the semilog curve ($\sigma - \log N$). The 5.00 mm sample reached the maximum degradation at $N > 1500$ cycles followed by oscillating cycles of hardening and softening till the test end. In comparison, the 2.50 mm sample continues the degradation till $N \cong 7000$ cycles, then oscillating cycles of hardening and softening follow. The 1.85 mm sample exhibited different behavior after $N \cong 100$ cycles; hardening for 200 cycles then continued degrading to reach a maximum degradation at $N > 1500$ cycles followed by a similar behavior to the 5.00 mm tested sample. Most of the degradation occurs in the first ten cycles and gradually degrade.

At the end of the test, the 5.00 mm sample exhibited a thick, soft layer representing clay flow at the bottom side (**Figure 4.21**) and initiated multiple cracks at the middle and bottom sides with no complete propagation and failure. The 2.50 mm sample has a thin clay flow layer at the bottom side with a hair crack initiated at the middle of the sample. The 1.85 mm sample has only a thin clay flow layer at the bottom side with no apparent cracks initiation.

The generation of pore water pressure during the test is shown in **Figure 4.22**. The 1.85 mm tested sample generates a higher *pwp* ($\Delta u \cong 230 \text{ kPa}$), followed by the 5.00 mm sample where a $\Delta u \cong 180 \text{ kPa}$ was generated. Furthermore, the lowest *pwp* were recorded for the 2.50 mm sample ($\Delta u \cong 81 \text{ kPa}$). It can be seen that the *pwp* of both 2.50 and 5.00 mm tested samples increased rapidly during the first ten cycles, then tended to stabilize or increase at a slow rate. In contrast, the lower strain amplitude generates *pwp* by a slow rate for the first few cycles and then increases rapidly and reaches the maximum value after $N \geq 300$ cycles. Therefore, there is no particular relevance between the generated *pwp* and the marine clays' behavior; more tests are required to perform to understand this relationship better.

The strain amplitude is an essential variable that affects the fatigue behavior of marine clays under cyclic loading. Therefore, the marine clays' response to cyclic loading under different strain amplitudes will be studied thoroughly in the forthcoming sections. Four cyclic triaxial tests will be performed as listed in **Table 4.2**, and the samples will be cycled until failure to achieve the desired goal.

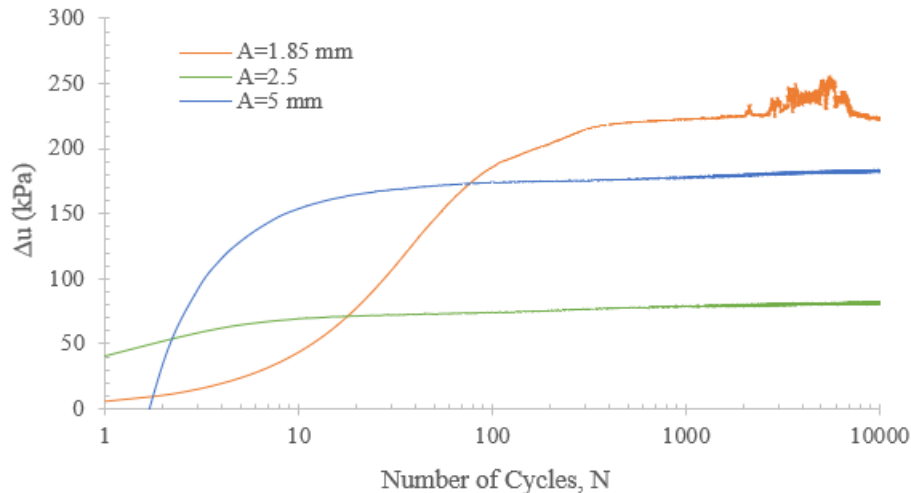


Figure 4.22: Pore water pressure generation during the tests for different amplitudes.

4.3.4 Effect of Frequency

Although in literature, the sea waves are agreed to last for 10 to 11 seconds per cycle equivalent to 0.1 Hz, two more slow cyclic triaxial tests were performed for comparison. Frequencies of 0.05 and 0.01 Hz were applied to samples from Abitibi marine clays, and equal strain amplitude and effective confining pressure were selected for the tests ($\pm\Delta\varepsilon_a = 5.00\%$, $\sigma'_3 = 50 \text{ kPa}$). The clay has an initial water content of $w\% = 58\%$ and is subjected to 4500 cycles. The stress degradation, strain profile, hysteresis loops with the number of cycles were reported for comparison.

It can be seen in **Figure 4.23a** that for slower cyclic tests, the samples had enough time to receive the 5% strain amplitude ($\varepsilon_a = 2.5\%$) at the beginning of the test. Hence, the 0.05 and 0.01 Hz tested samples behave plastically compared with the 0.1 Hz sample, which behaves elastically and reaches a maximum strain of 1.2%. From the reversals, the 0.05 and 0.01 Hz samples dissipated more energy, and the 0.1 Hz tested sample recovered energy maintaining the elastic behavior. The strength at the extrema was almost the same for 0.05 and 0.1 Hz, showing that faster cyclic loading will have a quicker reversal maintaining the sample in the elastic range and higher stiffness. In comparison, the 0.05 Hz can continue deforming under loading to achieve the applied strain amplitude, while the 0.01 Hz tested sample required less loading to achieve it.

The first cycles of the tested samples shown in **Figure 4.23b** indicate that for both 0.05 and 0.01 Hz, a stress relaxation started where the stress values at the extremes dropped and tended toward zero. The 0.1 Hz sample continues to behave elastically with stress softening. The mean strain (ε_m) for the 0.05 and 0.1 Hz tests are shifted to the positive side with a higher mean strain value ($\varepsilon_m = 0.71$) for the 0.05 Hz test, and the 0.01 Hz test maintain a mean strain $\varepsilon_m \rightarrow 0$. The high mean stress indicates that the sample could not achieve the applied strain amplitude during unloading. The 0.05 Hz recovered more energy in the first cycle and has a pointed hysteresis loop than the slowest test (0.01 Hz) which has a broader hysteresis loop. The 0.1 Hz continues to behave elastically with a pointed hysteresis loop.

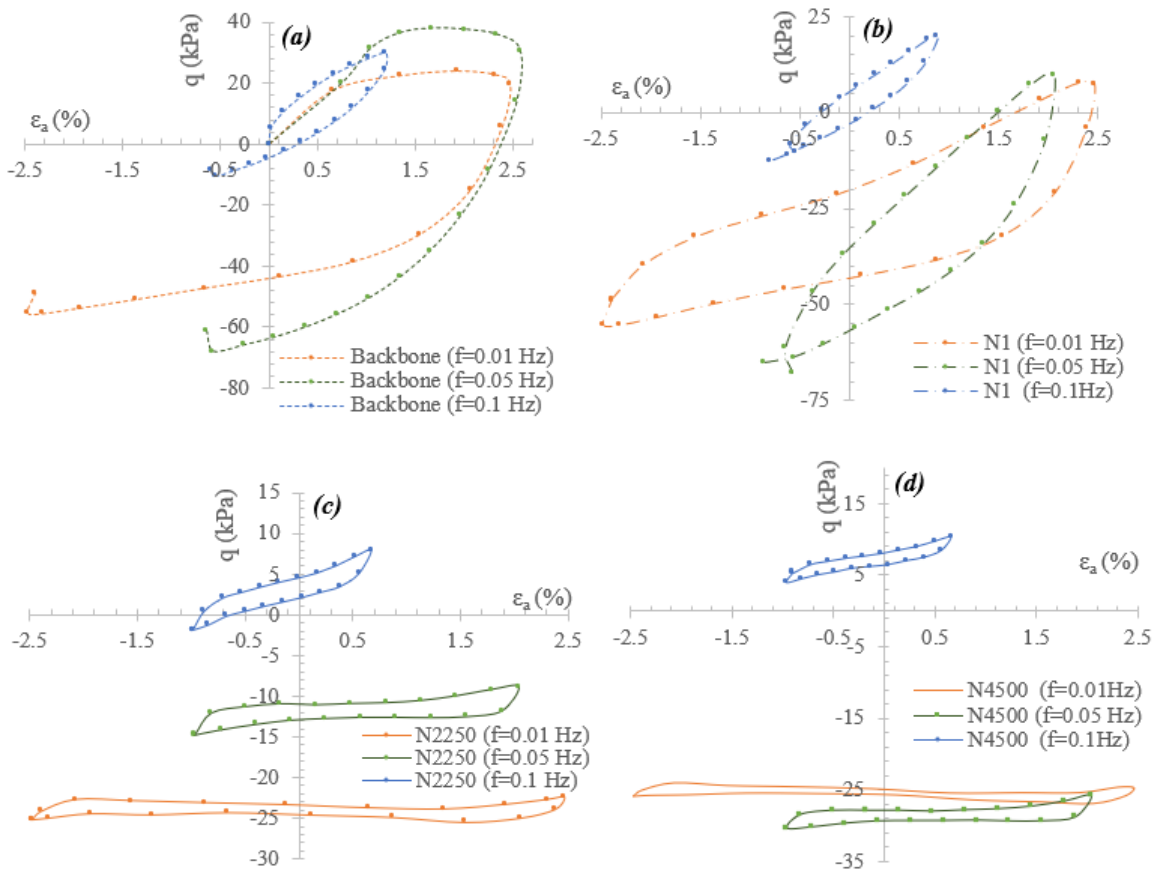


Figure 4.23: Hysteresis loops during the test (q_{cyc} vs ε_a) for different frequencies: (a) First backbone, (b) First cycle, (c) At mid-life, and (d) At the end of the test.

In the mid-life cycles (**Figure 4.23c**), the mean strain (ϵ_m) for the 0.1 Hz test become closer to zero in which the reversals are reaching higher (ϵ_{min}) compared with the first and initial cycles. There is an apparent decrease in the stiffness for all samples; the 0.1 Hz tested sample is still showing higher stiffness and recovered energy with higher elastic strain ranges $\Delta\epsilon_e$. Both 0.05 and 0.01 Hz tested samples' hysteresis loops were shifted down, and the mean stresses and strain became negative. The same behavior was recorded for all samples at the end of the test, as shown in **Figure 4.23d**. Lower stiffnesses and recovered energy were recorded for all tests, and plastic strains are dominant.

From the strain-time profile history in **Figure 4.24**, the 0.01 Hz test has the most stabilized strain amplitude where the mean strain remains constant during the test and $\epsilon_m \rightarrow 0$. The 0.05 and 0.1 Hz tests have the same behavior where the strain amplitude decreased at the first few cycles, then tended to stabilize till the end of the test. However, the slower tests showed higher strain amplitude. On the other hand, the stress-time history for 0.05 and 0.01 Hz tests exhibited a stress relaxation. The stress amplitude decreased and then tended to stabilize or decrease gradually, regardless of the hardening and softening periods recorded for the 0.01 Hz sample a. Both samples' stress amplitude was meeting or becoming close for most of the cycles during the test.

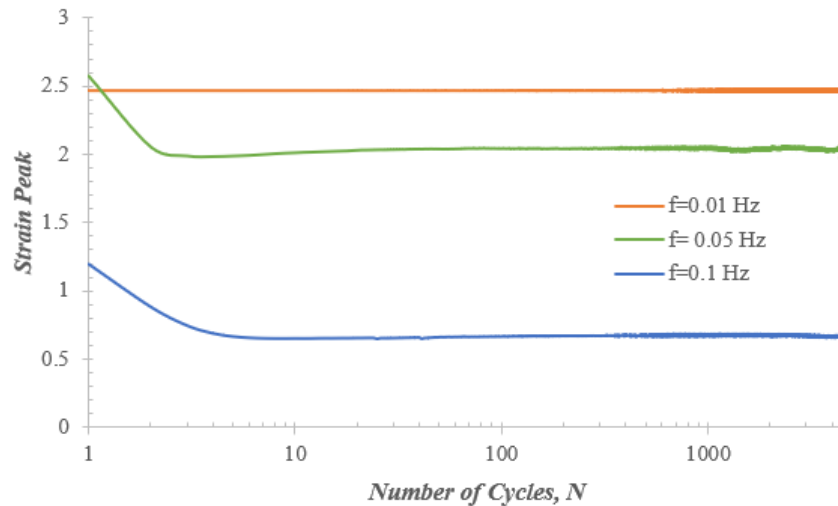


Figure 4.24: Strain-Time history profile for different frequencies.

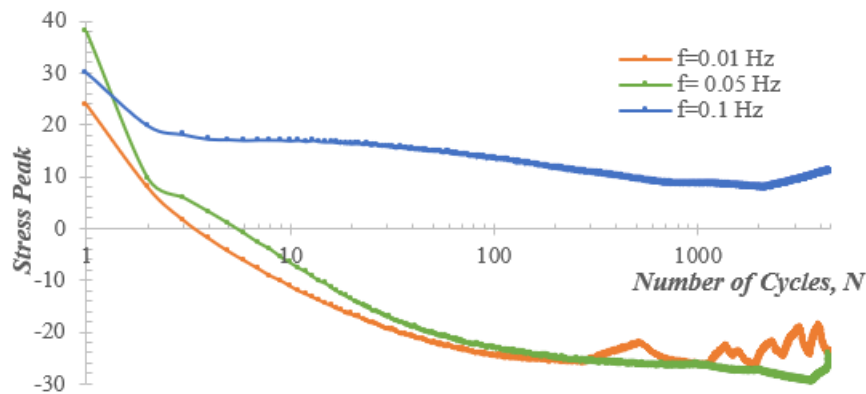


Figure 4.25: Stress-Time history profile for different frequencies.

The marine clay samples tested under slow cyclic loading exhibited larger plastic strain amplitudes than the fast loading (0.1 Hz); the period required to finish the cycle (20 – 100 seconds) might be an essential factor in this behavior. Consequently, as the stress amplitude tended to zero for the first few cycles (stress relaxation) and continued in negative until the end of the test, the marine clay can be considered cyclically stable in slow cyclic loading.

The sea waves and winds on sea surfaces produce a wave frequency of 0.1 Hz on average; this value will be applied for estimating the fatigue life of marine clays in this research to simulate the field conditions of offshore structures.

4.4 MARINE CLAYS FATIGUE LIFE ESTIMATION

Monopiles and foundations supporting offshore structures in marine clays tolerate a serviceability failure due to long-term deformations of the infrastructure elements under cyclic loading. The failure occurs as the marine clays' strength deteriorates with time, causing lateral deformations to monopiles and failure. Therefore, predicting the fatigue life of marine clays can provide the offshore structures' designers with beneficial parameters to enhance the design criteria.

The strain-controlled cyclic tests can better predict and describe the fatigue life of marine clays as it provides the actual stress and strain response during cycling. The preceding section briefly discussed the effect of confining pressure, strain amplitude, and frequency on the marine clays' fatigue behavior. The marine clays' hysteresis loops and the stress/strain-time profile can be efficient criteria to predict when a fatigue crack was initiated and how long the clay will resist before propagation and failure.

The most controversial issue in studying the fatigue life of marine clays is the definition of failure; how many cycles should be applied, and when should tests be stopped? Many tests were conducted on Abitibi clay samples to answer these questions as a preliminary investigation for lack of information in the literature. The cyclic investigative tests were performed under different strain amplitudes and number of cycles, $N \geq 10^2$. The samples' surfaces were examined for any signs of failure after being removed for each test. Then, the number of cycles needed for each amplitude to reach complete failure is determined.

A digital microscope with 1000x magnification was used to inspect the cracks on the sample surface. **Figure 4.26** shows a paradigm of a microscopy investigation before and after loading for a sample tested under 5.00 mm amplitude in a strain-controlled cyclic test to define the required cycles to reach failure. For example, in **Figure 4.26c**, cracks propagated on the clay sample's surface were detected after cycling of $N \geq 10000$ cycles. Then, for 5.00mm amplitude strain-controlled test, a minimum of 10000 cycles should be applied to reach failure. Eventually, the four strain-controlled tests in **Table 4.2** were investigated in the same way. The number of cycles until failure to predict marine clays' fatigue life and achieve the desired goal of this research was defined.

Table 4.3: Number of cycles required to reach failure for the strain-controlled tests.

σ'_3 (kPa)	Clay	Depth (m)	Target	$\pm\Delta\epsilon_a$ (%)	f	N
200	Abitibi	7.25	Life Estimation	0.75	0.1	35000
200		8.35		1.25	0.1	28000
200		16.8		2.5	0.1	20000
200		7.15		5	0.1	15000

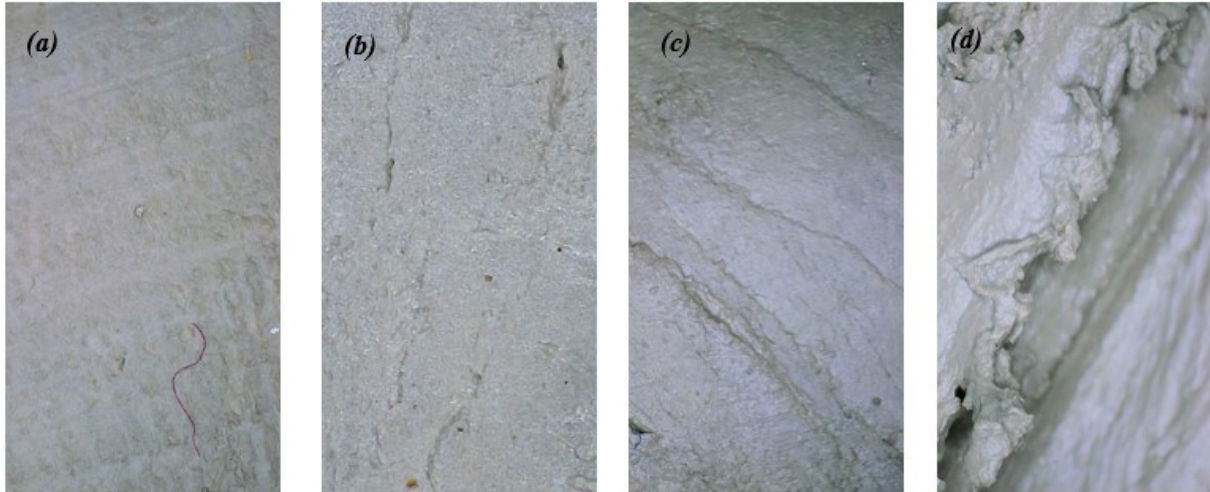


Figure 4.26: Microscopy surface investigation for 5.00mm amplitude strain-controlled test: (a) Before testing, (b) Crack initiated ($N \geq 3000$), (c) Shear bands and crack propagation ($N \geq 10^3$) and (d) 2x zoom for a propagated crack.

4.4.1 Strain-Controlled Tests Analysis

The first step in defining the number of cycles at which a crack initiated during fatigue testing is to analyze and understand the deformation and stress changes during cycling. As discussed in the preceding sections, the stress/strain-time profiles are efficient tools for understanding fatigue behavior. The strain profile should be constant as the applied strain amplitude is constant, but the strain changes during cycling in three stages and become constant on average in the last stage. On the other hand, the stress profile keeps changing during cycling until failure is reached. The stress and strain profiles can be expressed using the tip extremes values for the loading stage or the mean stress/strain values, considering the effect of the reversals (or unloading curves). The mean strain profile should be constant and close to zero for a typical constant strain amplitude. In contrast, the mean stress profile is expected to change during testing, indicating marine clays' strength softening and hardening behavior.

The stress and strain-time profiles of the selected tests are shown in **Figures 4.27 & 4.28** for the tip extrema at the end of the loading curve. It can be seen that the strain amplitude ϵ_a of the first three tests with $\Delta\epsilon = 5.00, 2.50$ and 1.25 % did not reach the targeted value during the test. For example, when applying $\Delta\epsilon = 5.00$ mm, the strain amplitude (ϵ_a) should reach a value of 2.50 %. However, it started with a value of 0.93 % and stabilized at 0.72 % to the end of the test. Similarly, both tests with $\Delta\epsilon = 2.50$ and 1.25 % show the same behavior, except that for $\Delta\epsilon = 1.25$ %, the strain amplitude (0.55 %) was closer to the targeted value (0.625 %). By decreasing the applied strain $\Delta\epsilon$, the strain amplitude (ϵ_a) during cycling become steady; for the low applied amplitude $\Delta\epsilon = 0.75$ %, the strain amplitude has a constant value ($\epsilon_a \cong 0.352$) from the beginning to the end of the test. This behavior indicates that the marine clay could not provide the required strength to reach the targeted strain amplitude at higher values within the specified time of each cycle (10 seconds).

The strain-time profiles, as indicated in **Figure 4.27**, have three stages for all tests except the low applied amplitude of $\Delta\epsilon = 0.75$ %. In the first stage, clays exhibited an abrupt decrease for a few cycles not exceeding $N \leq 10$ cycles, followed by a gradual increase as a second stage, and ended

up with a steady strain amplitude in the third stage. Once more, by decreasing the applied strain amplitude, the change in each stage becomes less. In the first stage, it is assumed that the decrease is due to clay's interparticle rearrangement when the load is first applied. The gradual increase in the second stage can support this assumption. The clay's stress amplitude slightly increased during this stage, as seen in **Figure 4.28**, showing hardening behavior that provided more strength to achieve the targeted strain amplitude. The beginning of the third stage is different for each applied strain amplitude, and a steady strain amplitude (ε_a) is reached at the end of the test. As an initial presumption, the crack initiation occurred during or at the end of this stage, discussed later in the following section.

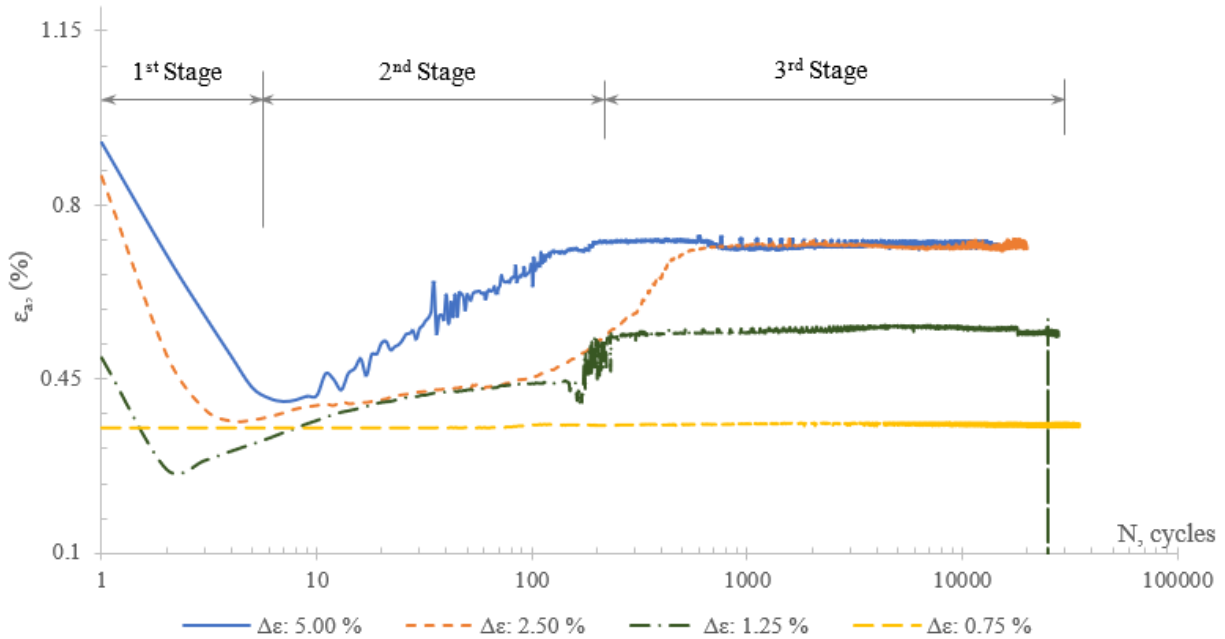


Figure 4.27: Strain-time profiles for all tests.

The stress-time profile shown in **Figure 4.28** shows that the stress amplitude changes in three different stages during the test. The first stage is similar to that for the strain-time profile, and the clay's interparticle rearrangement is considered in this stage. The second stage has a slight increase in stress amplitude (hardening) followed by a continuous decrease (softening) up to specific cycles that depends on the applied strain amplitude $\Delta\varepsilon$. The softening behavior in the 2nd stage is repeated for all tests, intervened with hardening periods. This stage's hardening and softening periods can be positive (compressive) or negative (tensile), depending on the marine clay properties and the applied strain amplitude. Finally, in the 3rd stage, the clay's behavior is disturbed with frequent hardening and softening periods in a ratcheting manner. In an initial presumption, the fatigue failure occurred during this stage. The hysteresis loops for all amplitudes at selected cycles in each test are also shown in **Figure 4.28**; the loops in gray are reference loops to compare and detect the change in the clay's behavior. Four different loops were selected from each test at different stages: the initial condition (first and second cycles), one cycle showing the hardening behavior after the first stage, one cycle during softening, and one cycle in the last stage of the test.

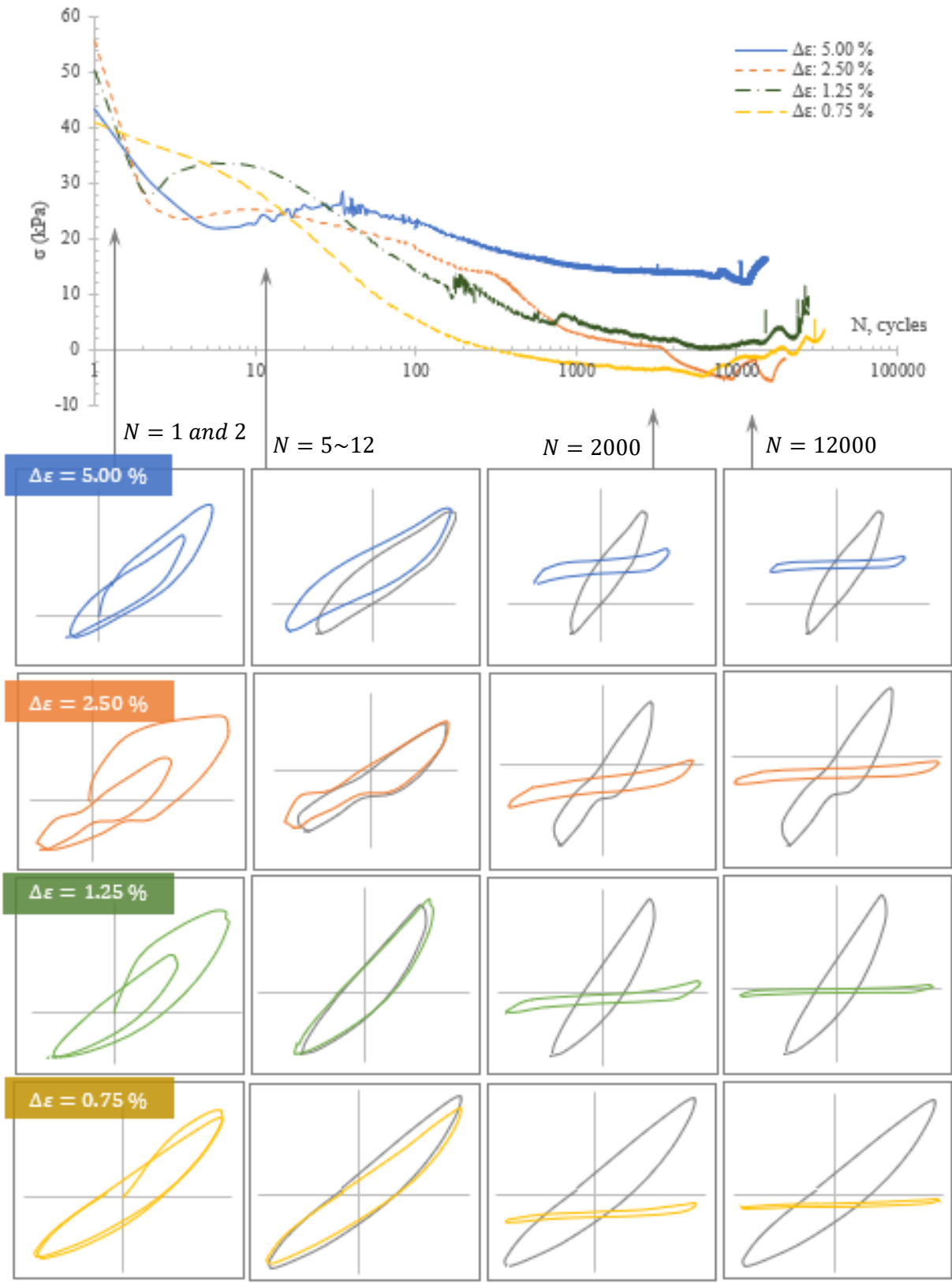


Figure 4.28: Stress-time profiles and hysteresis loops at different stages.

The marine clay properties and initial condition control the first response to cyclic loading (backbone curve). However, all samples under different applied strain amplitudes instantly show softening behavior in the second cycle, as shown in the first group of the hysteresis loops in **Figure 4.28**. The softening value depends on the initial condition and the applied strain amplitude. It can be seen that at the lowest strain amplitude $\Delta\varepsilon = 0.75\%$, the second extrema is close to the initial condition with typical and fully reversed hysteresis loops. As discussed previously, all tests exhibited some stress hardening at the beginning of the second stage except for $\Delta\varepsilon = 0.75\%$; the second group of hysteresis loops shows this behavior. Also, the hysteresis loops for lower amplitudes are approximately typical and fully reversed.

The third and fourth groups of hysteresis loops in **Figure 4.28** change the loops' shape from pointed to rectangular like loops with increasing cycling. As a result, the plastic strains become dominant and control the behavior, in addition to the significant decrease in the stress amplitude ($\Delta\sigma$). This behavior can be an indicator of fatigue crack initiation. Finally, the marine clay show more fatigue and energy dissipation at a high number of cycles for lower strain amplitudes,

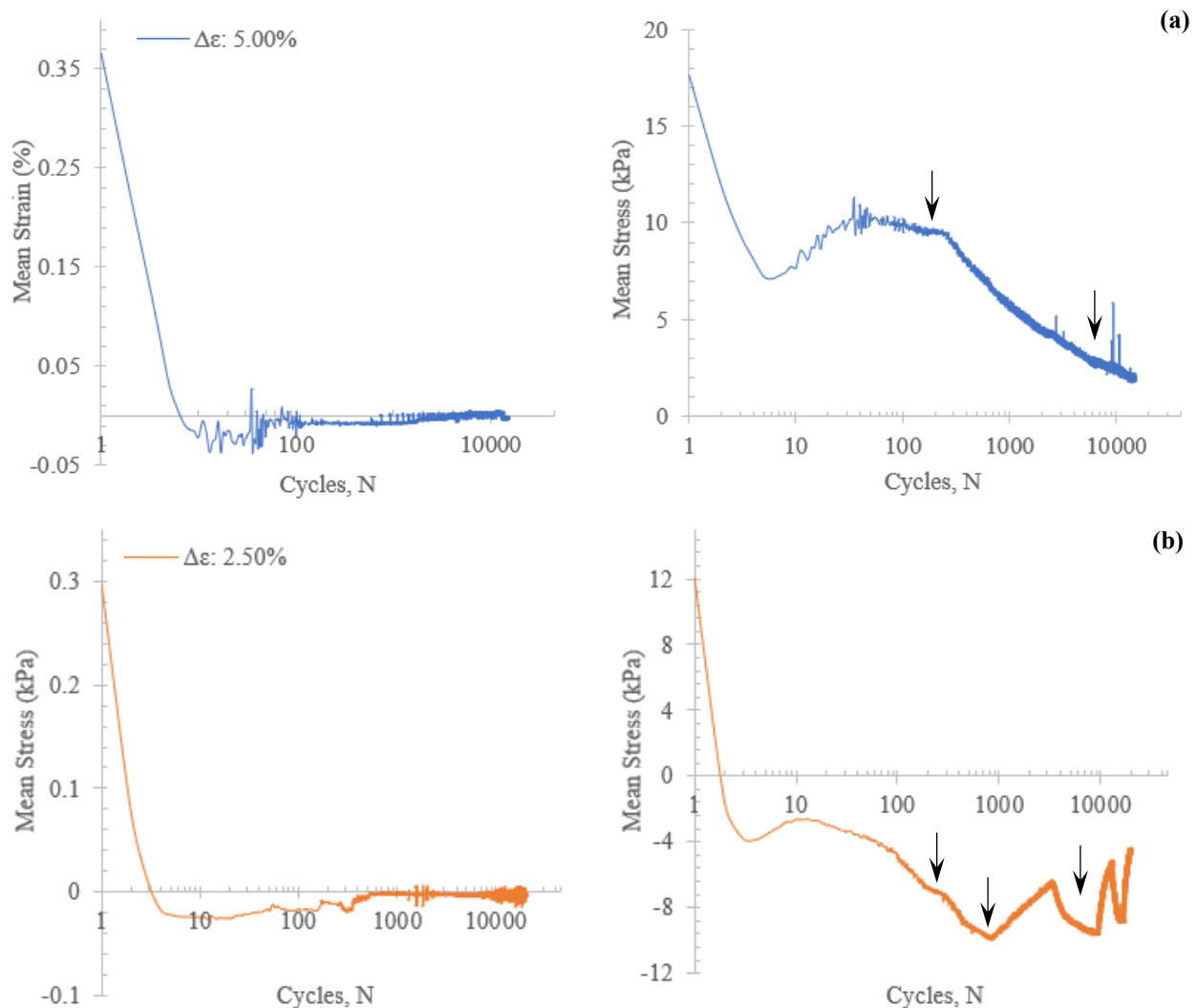


Figure 4.29: Mean stress and strain: (a) $\Delta\varepsilon = 5.00\%$, (b) $\Delta\varepsilon = 2.50\%$, (c) $\Delta\varepsilon = 1.25\%$ and (d) $\Delta\varepsilon = 0.75\%$.

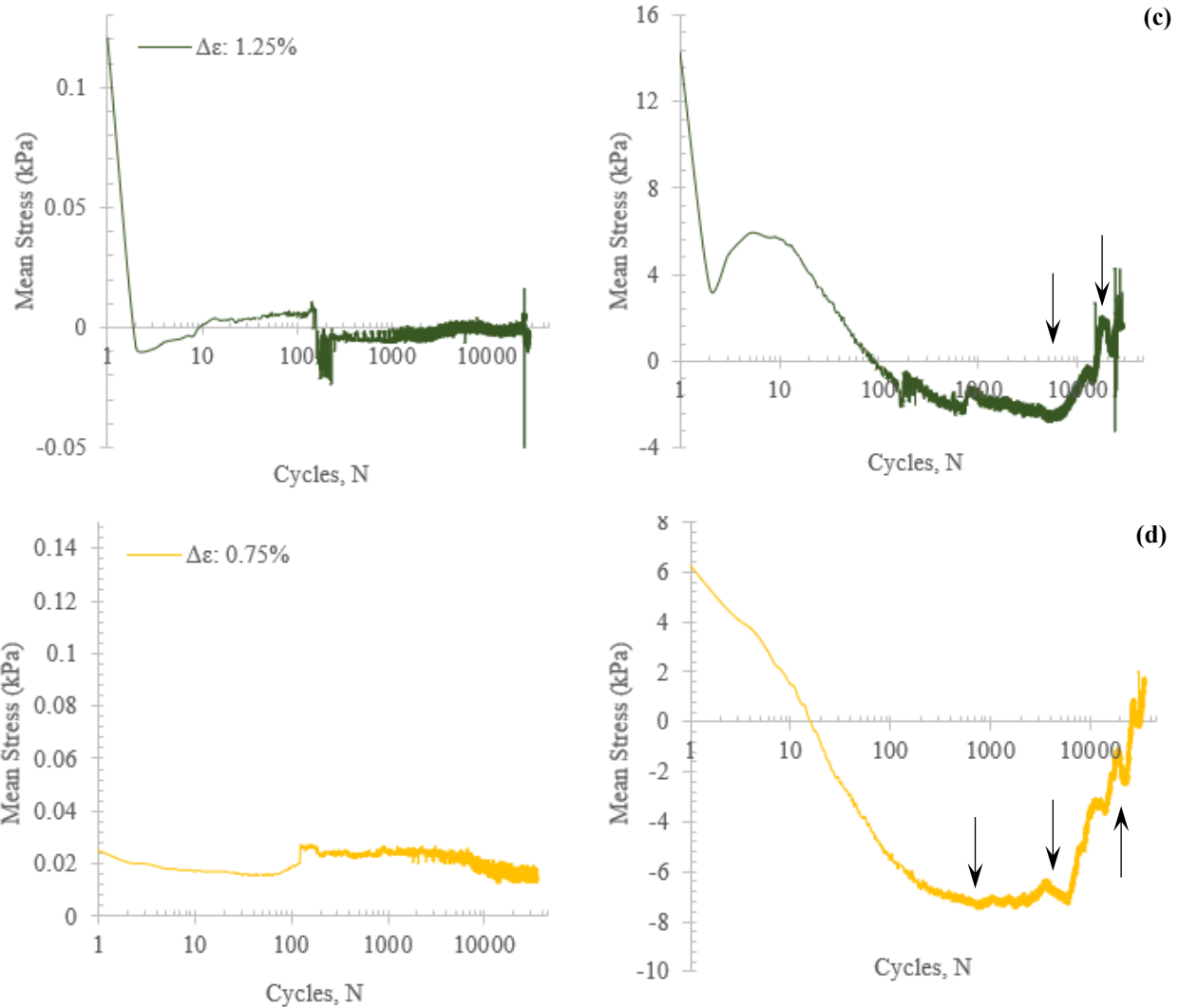


Figure 4.29 (cont.): Mean stress and strain: (a) $\Delta\varepsilon = 5.00\%$, (b) $\Delta\varepsilon = 2.50\%$, (c) $\Delta\varepsilon = 1.25\%$ and (d) $\Delta\varepsilon = 0.75\%$.

The mean stress and strain in **Figure 4.29** can be used to understand the marine clay's fatigue behavior. As seen in the figure, the mean strain for all tests tends to stabilize after the first few cycles; all values oscillated close to zero, which indicates that the applied strain amplitude remains stable during the test despite the change in the peak strain values discussed previously. The mean stress for all amplitudes changes during the test, moving up and down and indicating periods of softening/hardening. The negative mean stress (σ_m) implies that the sample is in the tensile region; still, it is softening or hardening. It can be seen that samples with negative mean stress tend to relax to a certain number of cycles, then continue oscillating until failure. Add to this, the initial condition of the clay and its origin may reflect negative mean stress; the sample tested under $\Delta\varepsilon = 2.50\%$ as an example.

It is essential to mention that most tests were performed twice with two different samples to ensure that the behavior is typical. For the $\Delta\varepsilon = 2.50\%$, the second tested sample failed within the same

range of cycles and has mostly the same behavior compared with the sample results discussed above, except that the mean stress was in compression ($+ve \sigma_m$). The sample with negative mean stress was selected to be discussed in this research to highlight that the marine clay initial condition controls some fatigue behavior parameters; the sample chosen was stiffer and collected at a deeper depth.

The black arrows in **Figure 4.29** are pointed at overturning points where constant mean stress or change in the behavior is detected. The constant mean stress represents a period of stable hysteresis loops, and in most cases, it is followed by a substantial change in behavior. A group of stabilized hysteresis loops can be defined as a fatigue limit where no change in the clay behavior is detected, followed by a group of unstable loops. Therefore, it is anticipated that the crack's initiation and failure occurred at these points. Also, most samples have an unforeseen drop or increase in the peak and mean stress at the end of the test, which indicates the disturbance occurred with crack propagation and samples' collapse. The marine clay showed more oscillated behavior before the collapse with a lower applied strain amplitude.

The oscillated behavior between softening and hardening after the mid-life of most tested samples can be explained by opening and closing cracks. When a fatigue crack is initiated, and with the increase in pore water pressure during testing, the cracks filled with new structured clay paste that works as a cementing agent lead to closing the cracks, and consequently, hardening behavior follows. Thus, the cracks filled with the cemented material become a clay cluster that behaves plastically and prevents crack propagation or failure. This behavior elucidates the delay in failure despite narrowing hysteresis loops, which reflects a reduction in the clay resistance and stiffness at constant strain values, as shown in **Figure 4.28**. On the other hand, a surface crack will propagate rapidly, leading to disturbed behavior and failure by continuing cycling and considering the significant decrease in stiffness.

A surface microscopical investigation was performed after the failure of tested samples, and **Figure 4.30** and **4.31** shows the surface investigation results. In **Figure 4.30**, the surface cracks filled with the cemented clay cluster for different samples were detected. The two photos to the left show propagated cracks filled with the cemented clay cluster, which indicates that even after the crack propagated, still the crack might be filled with the cementing cluster and continue with the oscillated behavior. On the other hand, some surface cracks initiated and do not propagate, as seen in the two photos to the right. These cracks are also filled with the cemented cluster in which the latter might help prevent the propagation.

The fatigue of marine clays can be in the form of surface notches, intrusions, or extrusions, as shown in **Figure 4.31**. Most of the detected notches were located on an uncracked surface for the tested samples, and no extended cracks were seen around the notches. Consequently, it can be concluded that only longitudinal cracks can propagate inside the sample and lead to failure, and notches are surface defects. Add to this, the extrusion notches were initiated as intrusions and then filled with cemented clay clusters to form the extrusions.

Figure 4.32 shows (left and middle photos) a microscopy investigation of surface crack at two different spots of a propagated crack associated with shear slip bands. The photo on the right (half-cut) indicates the propagation of the surface cracks inside the sample. The cavities and complete separation formed inside the sample at the propagated crack side draw attention to the volume change associated with the crack propagation and failure, which can be an efficient criterion to

define the failure. Accordingly, the volume change during testing will be considered in the subsequent section to determine the marine clay fatigue life.

The cemented clay cluster's color in most cracks and notches is different from the original sample, drawing to a new plastic material formation with different properties. **Figure 4.33** shows a microscopy investigation for a notch and crack after 24 hours of air drying; both are reduced in volume after removing water, forming surface punctures which are the main signs of marine clay fatigue when subjected to long-term cyclic loading.

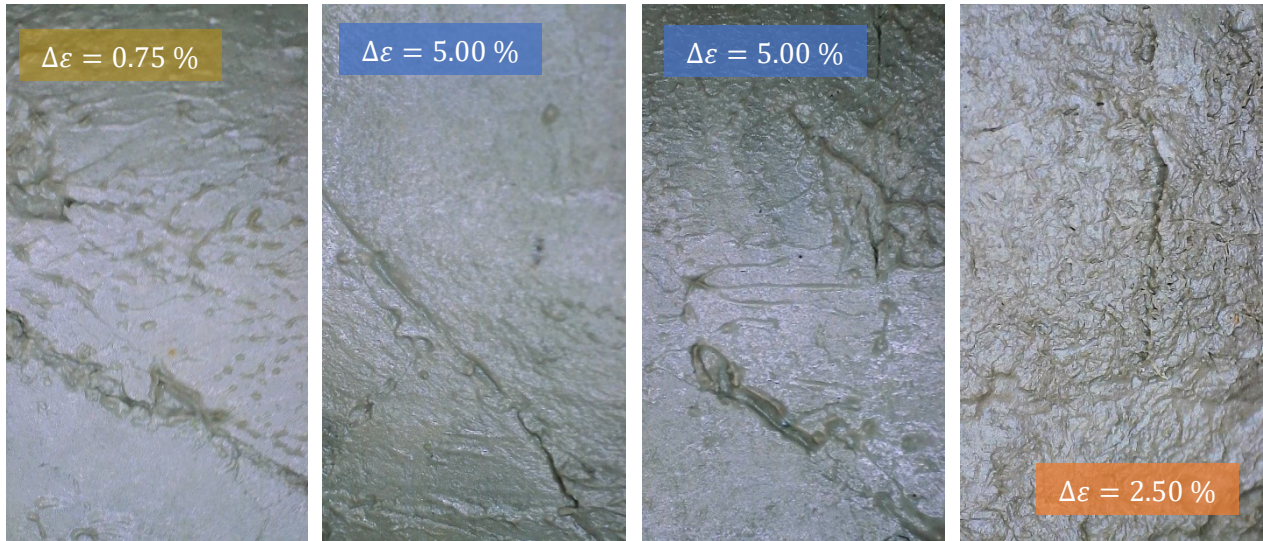


Figure 4.30: Microscopy investigation for surface fatigue cracks filled with cemented clay paste for different samples.

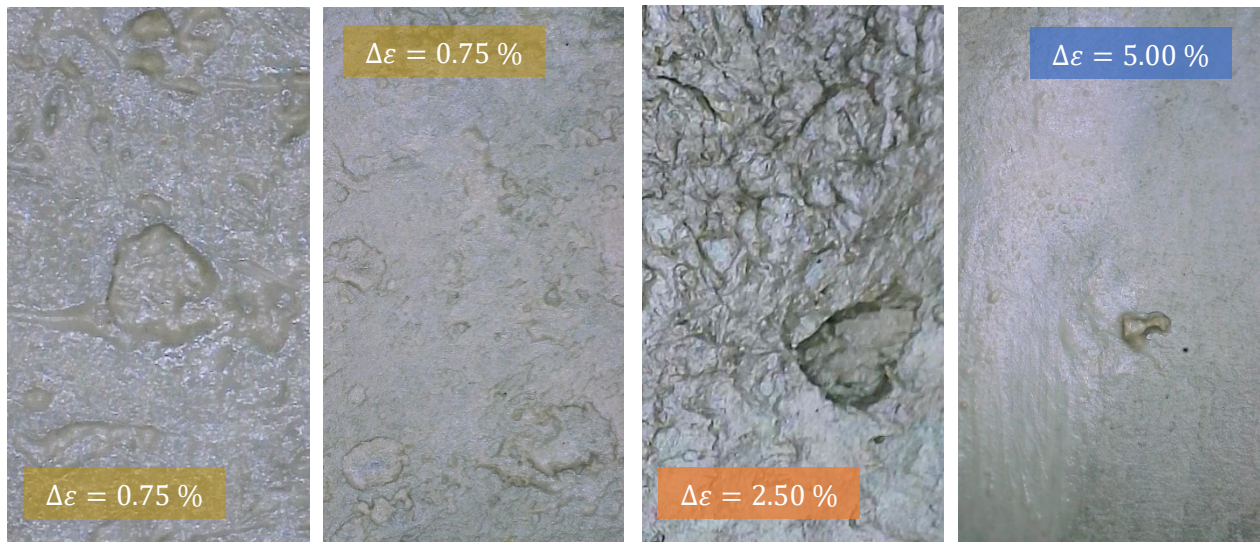


Figure 4.31: Microscopy investigation for surface fatigue notches in the form of intrusions and extrusions.

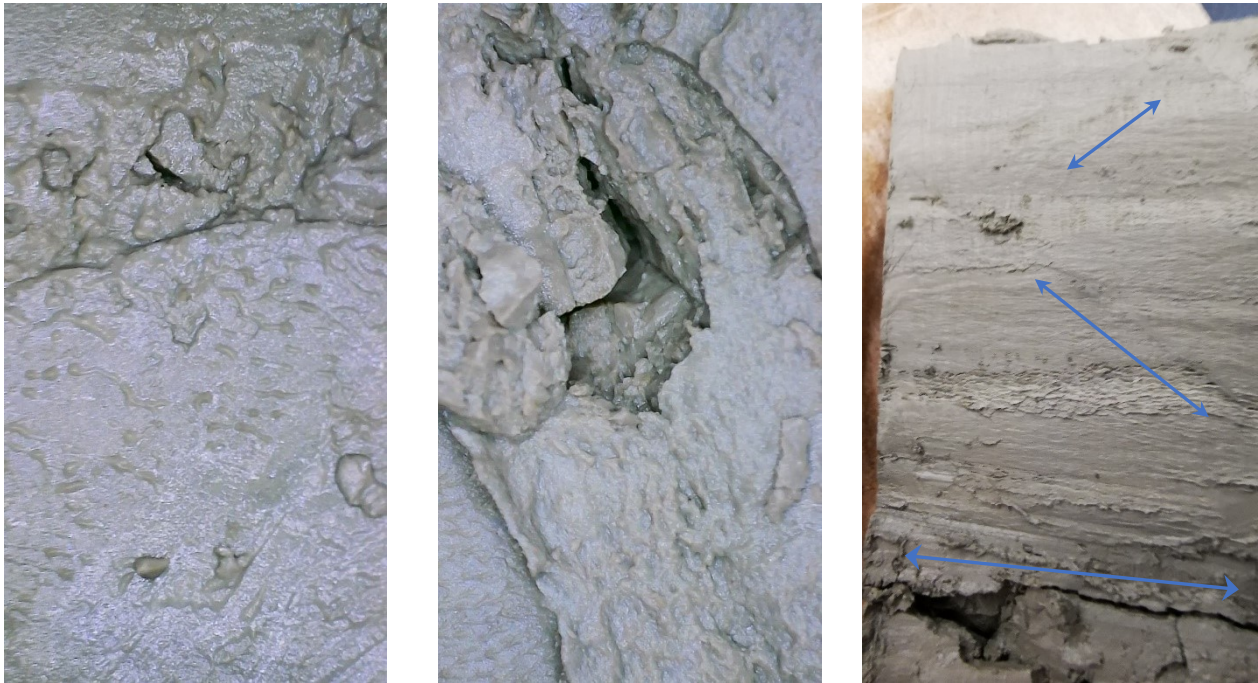


Figure 4.32: (a) Microscopy investigation for surface crack slip bands, and (b) Crack propagation in a half-cut sample.



Figure 4.33: Microscopy investigation for surface crack cementation and surface notches after 24 hours air drying.

The previous discussion highlighted the effect of pore water pressure generation during cyclic testing of marine clays. The pore water pressure is generated rapidly during the first few cycles, then tends to increase at a slow rate for a large number of cycles. Furthermore, finally, it stabilized after mid-life, in which it changed for $\leq 2.0 \text{ kPa}$ until the end of the test (**Figure 4.34**).

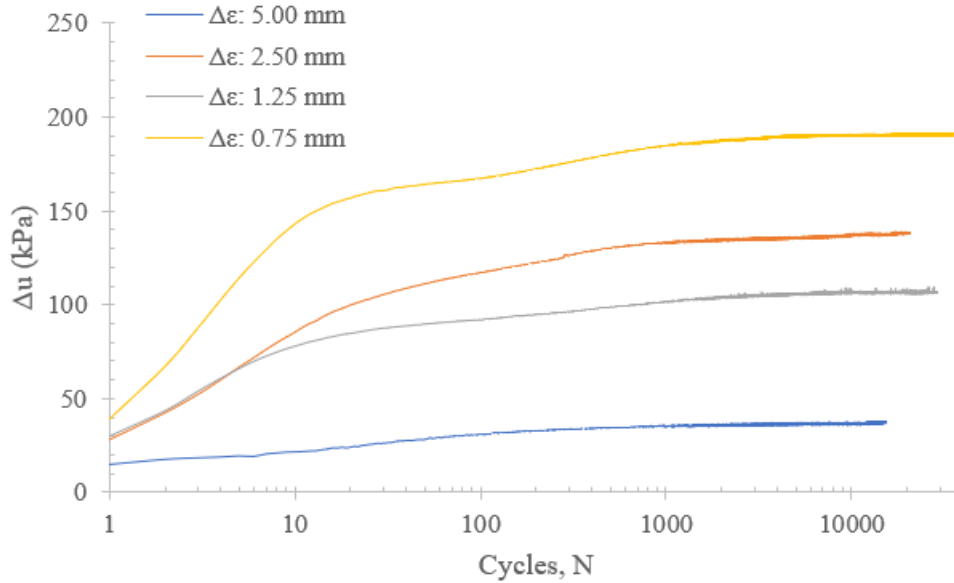


Figure 4.34: Pore water pressure generated during the performed strain-controlled tests.

4.4.2 Fatigue Initiation and Propagation -Life

Following the strain-controlled tests' analysis in the preceding section, it is found that the marine clay resistance to long-term cyclic loading deteriorates with time until failure occurs. Three stages can describe the fatigue life of marine clays: softening at the early ages of cycling, stabilized behavior (or fatigue limit), and a softening behavior at a higher rate that ends with failure.

The hysteresis loops in the stress-strain diagram of the performed strain-controlled tests form a rosette that indicates the fatigue life stages of marine clays (**Figure 4.35**). The first softening stage represented by the pointed hysteresis loops becomes longer with decreasing the applied strain amplitude $\Delta\varepsilon$. The hysteresis loops with pointed curves soften with time until a certain point, then change shape and become vast with a significant change in the total stress amplitude ($\Delta\sigma$). This behavior highlights the importance of the total stress amplitude to describe the fatigue of marine clays.

Due to the lack of information in the literature and the absence of a criterion to define marine clays' fatigue parameters, the experimental results and observations will be used to predict the fatigue crack initiation and failure. The change in stress amplitude ($\Delta\sigma$) is another efficient parameter that can measure the change in the hysteresis loop and help detect the crack initiation and failure of marine clays under cyclic loading. Also, as discussed in the previous section, the volume change that occurred due to the reported opening and closing cracks during the marine clay life can help predict when a crack is first initiated and when a crack will propagate to failure. **Figures 4.36 to 4.39** show *the changes in strain amplitude ($\Delta\sigma$) and volume change (ΔV)* for the four strain-controlled tests performed to estimate the fatigue life of marine clays.

Figures 4.36 and 4.37 show the changes in the stress amplitude and volume of the samples tested under applied strain amplitudes of $\Delta\varepsilon = 5.00\%$ and $\Delta\varepsilon = 2.50\%$, respectively; the three fatigue life stages of marine clays are apparent. Both samples soften in the first stage up to a certain number

of cycles, $N \cong 100$ Cycles for $\Delta\varepsilon = 5.00\%$ and $N \cong 200$ Cycles for $\Delta\varepsilon = 2.50\%$, then stabilize as seen in the figures. The stabilized stage extended for a few cycles in the test performed under $\Delta\varepsilon = 5.00\%$, then the total stress amplitude decreased steeply until the end of the test. From the change of volume curve, it can be seen that the volume decreased slightly at a nominal rate during the first softening stage. After that, the volume change started to increase rapidly, which reflected a severe change in the clay's structure. This point, pointed by a black arrow in the figure, can be considered the first crack initiation and the number of cycles reported, $N = 136$ Cycles.

Using the same criterion, and for $\Delta\varepsilon = 2.50\%$, the end of the stabilized stage was associated with a severe increase in the volume, as shown in **Figure 4. 37**. Therefore, the number of cycles required to initiate a crack in this test is $N = 388$ Cycles.

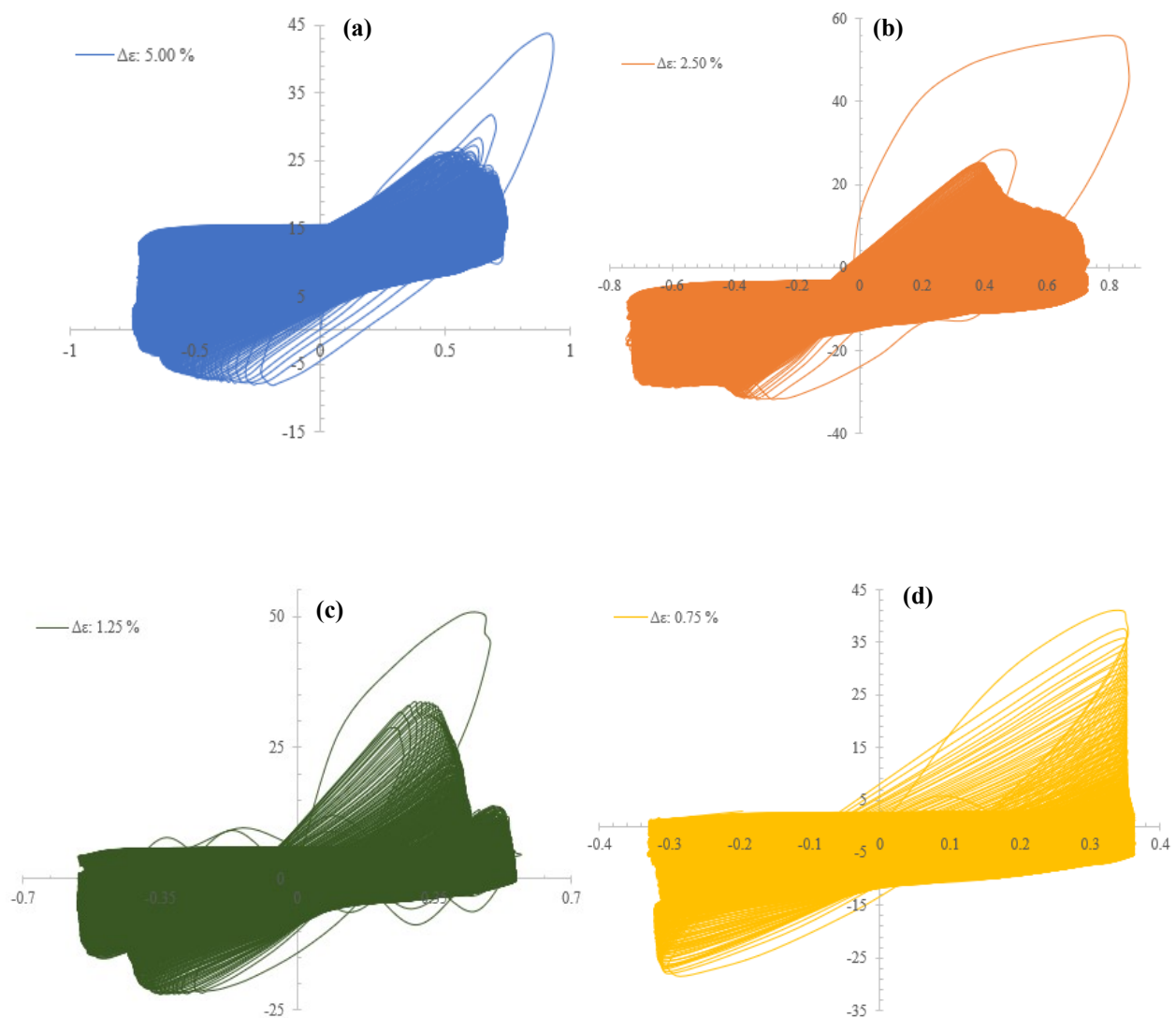


Figure 4.35: Hysteresis loops of the performed strain-controlled tests: (a) $\Delta\varepsilon = 5.00\%$, (b) $\Delta\varepsilon = 2.50\%$, (c) $\Delta\varepsilon = 1.25\%$, and (d) $\Delta\varepsilon = 0.75\%$.

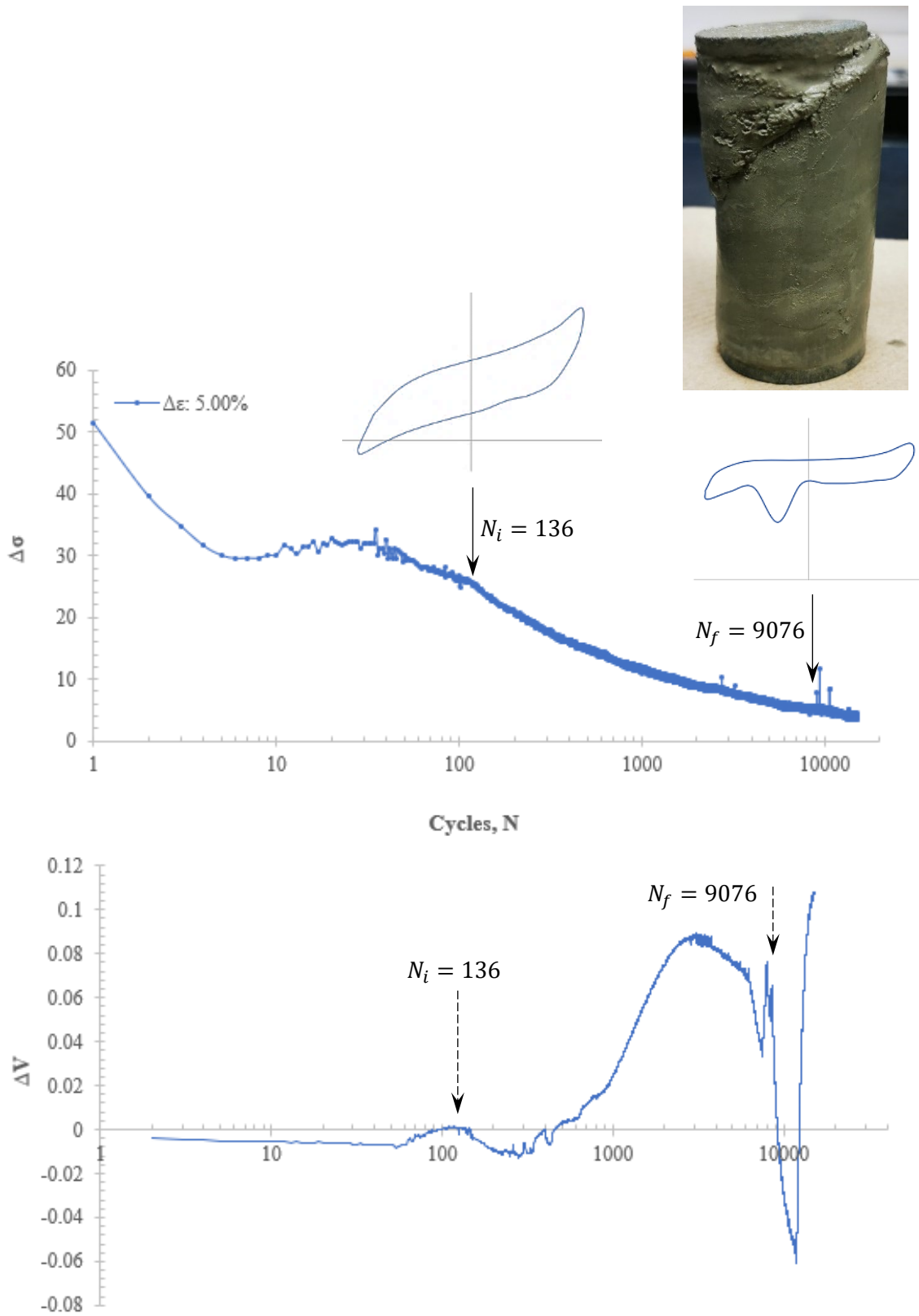


Figure 4.36: The changes in stress amplitude ($\Delta\sigma$) and volume change (ΔV) for $\Delta\epsilon = 5.00\%$.

Once a crack is initiated, the clay softens at a higher rate associated with volume changing until a sudden drop in the volume is detected. At this point, a disturbance in the stress amplitude is also detected, as seen in **Figures 4.28, 4.29, and 4.36**. The drop in sample height can explain the sudden drop in volume after a crack propagated, and the number of cycles at this point can be recorded to define the marine clays' fatigue failure. For $\Delta\varepsilon = 5.00\%$, the failure was recorded at $N = 9076$ cycles, pointed by a black arrow in **Figure 4.36**. The hysteresis loops at both crack initiation and failure were also shown in the figure; the unstable hysteresis loop is considered as a sign of failure.

Referring to **Figure 4.37** and following the same guidelines, the volume change diagram shows a continuous increase and decrease in volume, making it harder to define the failure of the $\Delta\varepsilon = 2.50\%$ sample. The volume change oscillating can explain the softening and hardening behavior detected previously in **Figure 4.28**, associated with opening and closing cracks. A closer view of the total stress amplitude for the range of cycles changes in volume is included in **Figure 4.37**. The clay sample continues softening, and a new stable region is detected, followed by softening until the end of the test. A stress disturbance occurred after $N > 15000$ cycles, but another failure sign is required to define the failure of this clay sample. Therefore, the total strain amplitude $\Delta\varepsilon$ change by increasing the cycles number can be used.

The distribution of $\Delta\varepsilon$ is shown in **Figure 4.37**, and an increase in the total strain amplitude is detected at the same range of cycles where the total stress amplitude shows some disturbance. Consequently, the failure of the $\Delta\varepsilon = 2.50\%$ sample is assumed to occur at $N = 17666$ cycles. The sample after failure and hysteresis loops for the cycles of crack initiation and failure are included in **Figure 4.37**. As mentioned before, the sample was collected from a deep depth, and the clay is stiff, which can explain the behavior at failure and that the sample did not show clear signs of failure. Also, the crack shown in the figure is propagated but still filled with clay, and therefore, no sudden drop in the clay height was recorded.

At lower applied strain amplitude $\Delta\varepsilon = 1.25\%$, it is found that the sample kept softening without any signs of crack initiation, represented by the stable stage, until $N > 700$ cycles. Also, multiple stable stages were recorded, pointed by black arrows in **Figure 4.38**, which means that multiple cracks were initiated during cycling. The stable region followed by softening and associated with significant volume change will be recorded as the first crack initiated. The primary crack initiation of the $\Delta\varepsilon = 1.25\%$ test is recorded at $N = 730$ cycles.

For detecting the failure of $\Delta\varepsilon = 1.25\%$ test, the same criterion followed for $\Delta\varepsilon = 5.00\%$ can be used as the sample show a stress amplitude disturbance associated with a volume change, as seen in **Figure 4.38**. Therefore, the failure will be assumed to start from the first total stress disturbance that occurred at $N = 23715$ cycles and is followed by a series of unstable cycles. The unstable hysteresis loop at this point is shown in the figure.

The marine clay sample tested under $\Delta\varepsilon = 1.25\%$ shows multiple cracks opening on the surface, as shown in **Figure 4.38**, which explains the volume oscillating and the multiple stable stages. Some of these cracks propagated and led to failure, while others did not reproduce but remained open. In addition, the surface investigation of the clay sample shows more fatigue signs than the samples tested under higher strain amplitude. This behavior was observed in **Figure 4.35**, where the hysteresis loops soften for an extended period before changing their shape and stabilizing. Another sign of fatigue is the clay flow detected near the propagated crack for all tested samples.

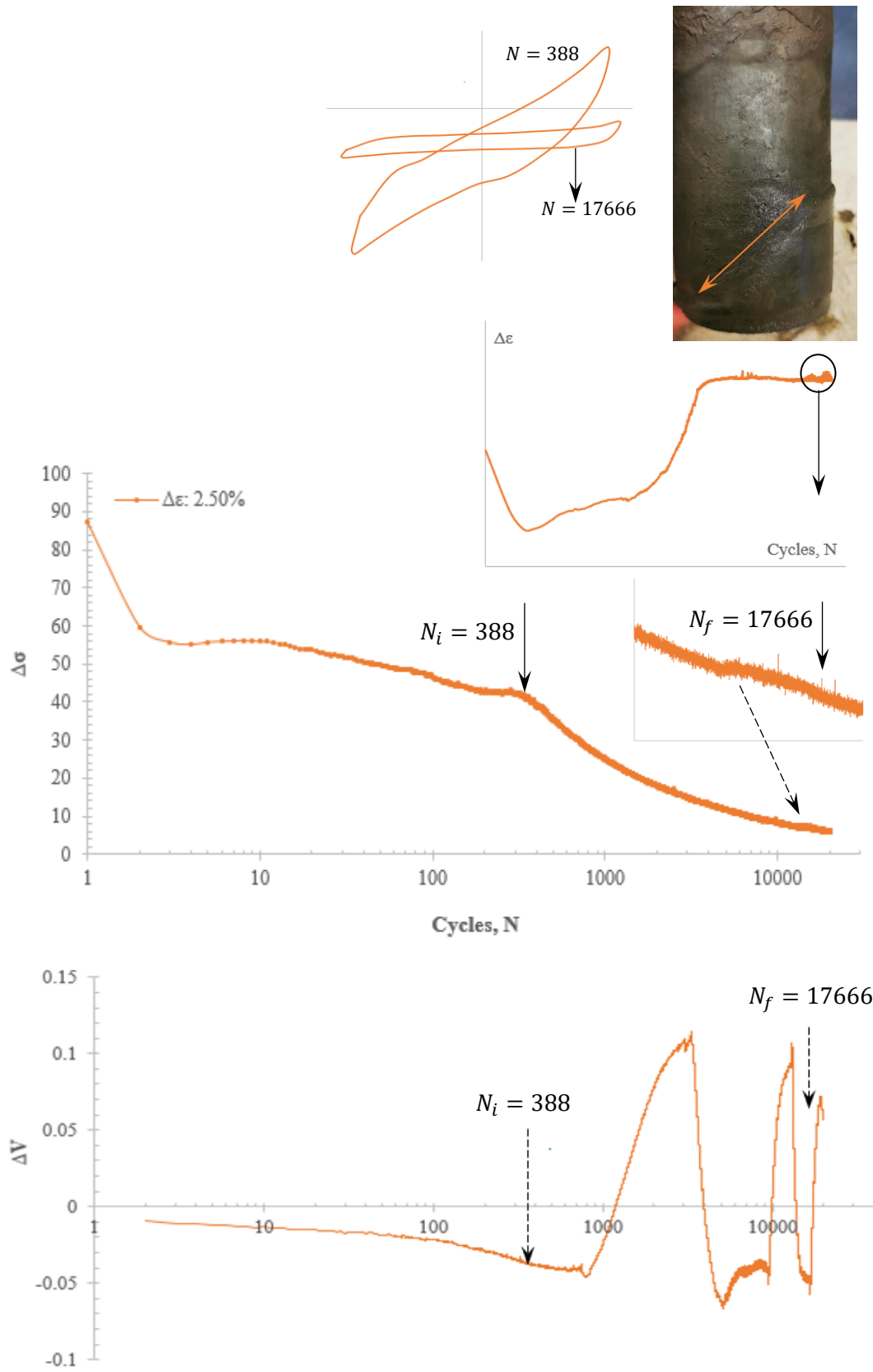


Figure 4.37: The changes in stress amplitude ($\Delta\sigma$) and volume change (ΔV) for $\Delta\varepsilon = 2.50\%$.

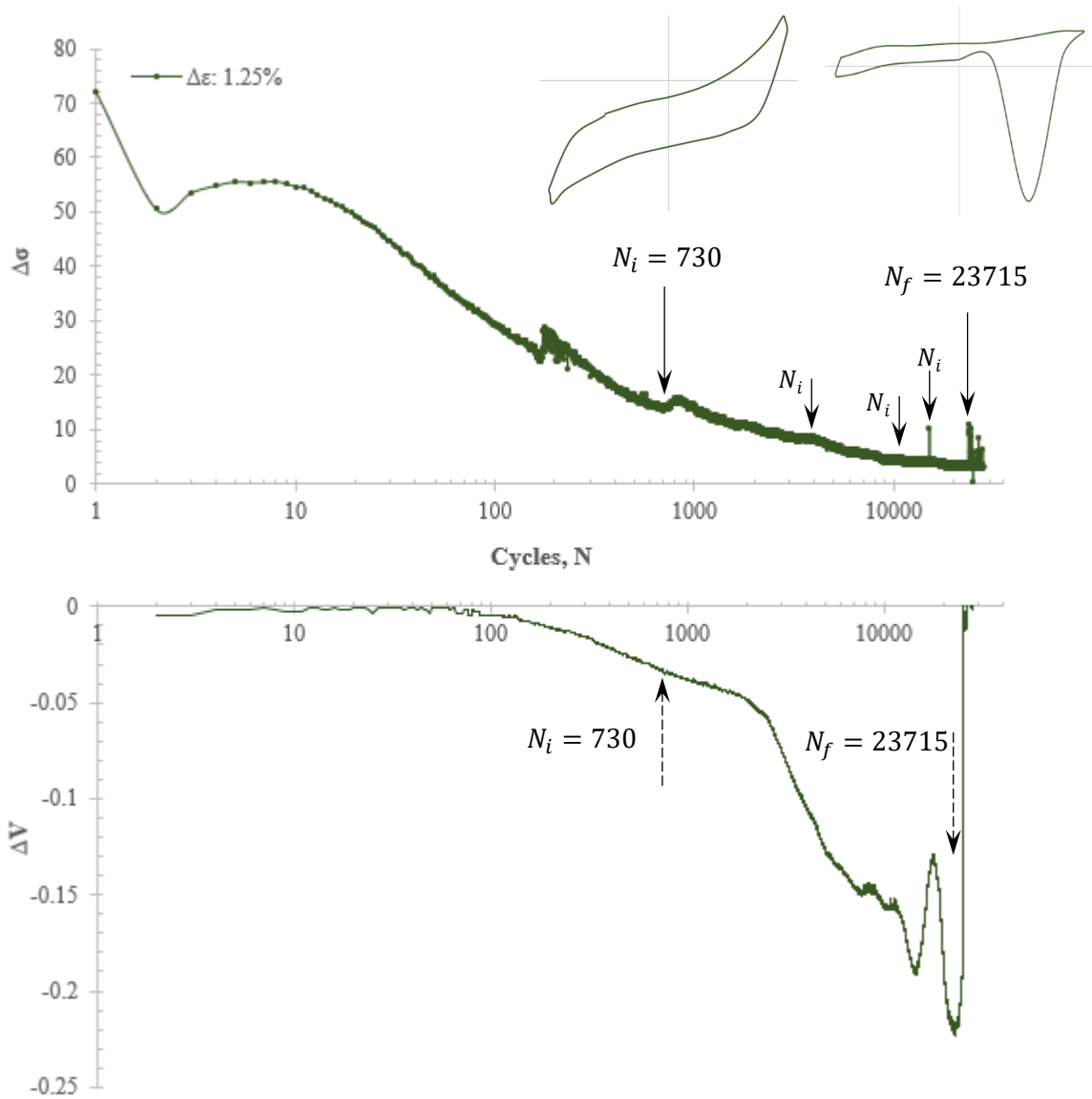
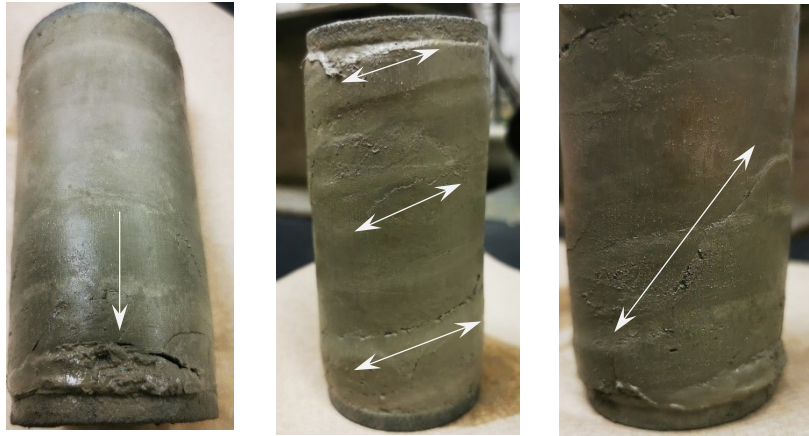


Figure 4.38: The changes in stress amplitude ($\Delta\sigma$) and volume change (ΔV) for $\Delta\varepsilon = 1.25\%$.

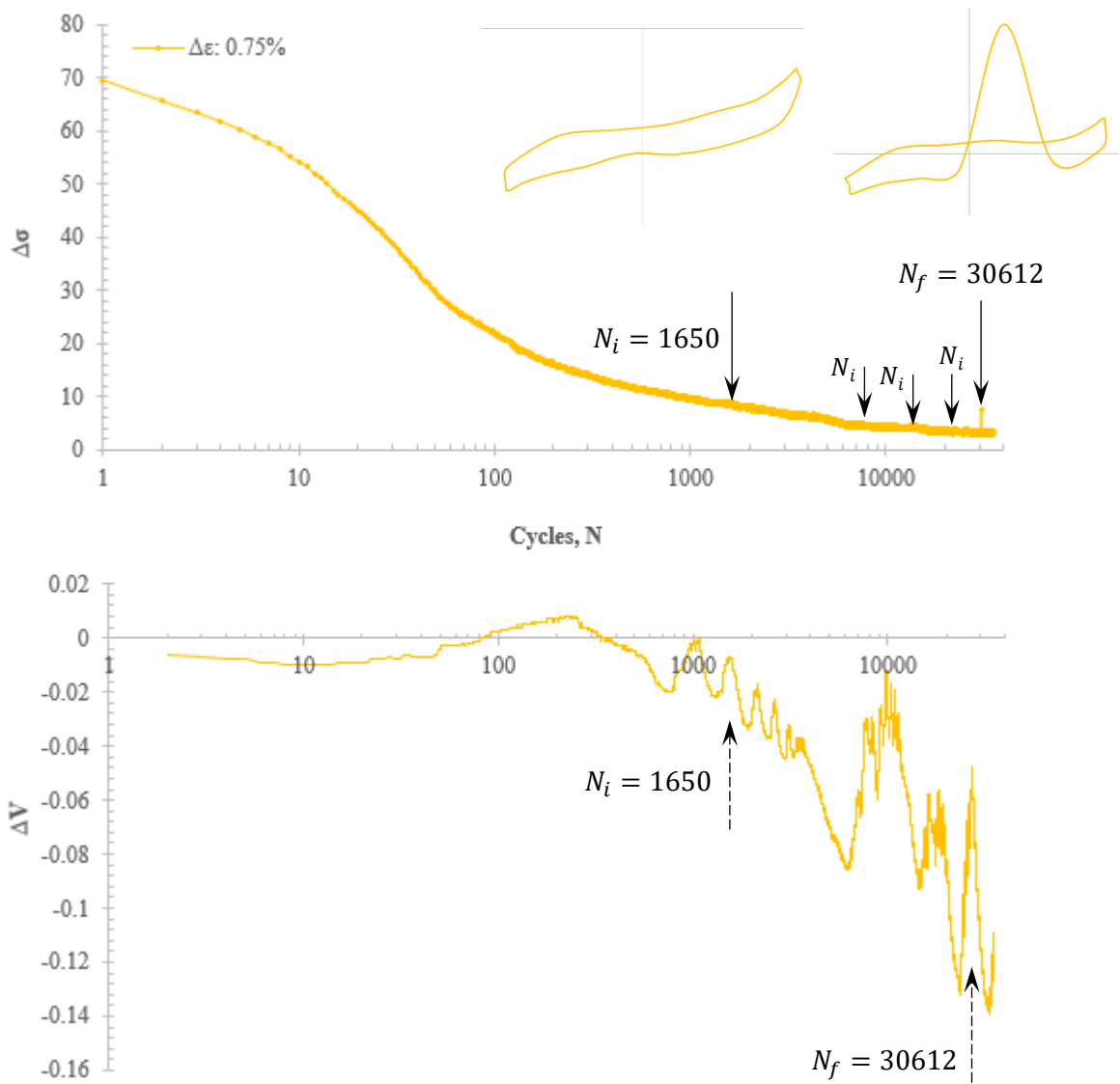


Figure 4.39: The changes in stress amplitude ($\Delta\sigma$) and volume change (ΔV) for $\Delta\varepsilon = 0.75\%$.

The change in stress amplitude and volume change for the marine clay sample tested under $\Delta\varepsilon = 0.75\%$ is shown in **Figure 4.39**. The first crack initiated is detected at $N = 1650$ cycles, where the first stable region, stress softening, and significant volume change was detected. The sample at a very low strain amplitude $\varepsilon_a = 0.375\%$ continue softening for an extended period without any significant volume change; this behavior is also considered stress relaxing as the change in stress amplitude and degradation decreases. The shape of the hysteresis loop at the crack initiation stage shows an unstable loop, although it is fully reversed with a constant strain amplitude.

The tested sample, similar to the $\Delta\varepsilon = 1.25\%$ sample, exhibited multiple fatigue surface cracks that propagate or have a limited length. In addition, a flow near the propagated crack was also detected, as seen in **Figure 4.39**. The failure of the sample, associated with a disturbance in the stress amplitude and volume change, was detected at $N = 30612$ cycles.

While for the total amplitudes $\Delta\varepsilon = 5.00$ and 2.50% , the cracks were initiated at early ages, and the crack propagation stage represented more than 90% of the estimated fatigue life, at lower amplitudes, a slight delay in the crack initiation was recorded, and multiple cracks initiated during the fatigue life. For the $\Delta\varepsilon = 0.75\%$, the sample relaxes, which delays both crack initiation and the time required to reach failure. However, the crack propagation represented more than 90% of the estimated fatigue life. **Table 4.4** is a summary of the strain-controlled tests and fatigue life estimation.

Table 4.4: Life estimation for Abitibi marine clays.

$\Delta\varepsilon$ (%)	$\pm\varepsilon_a$ (%)	N	Life estimation		Time to failure (Hrs)	$\Delta\varepsilon_{True}$ (%)	$\Delta\varepsilon_{p-True}$ (%)	$\Delta\varepsilon_{e-True}$ (%)	Transition point N_t
			Crack initiation N_i	Failure N_f					
0.75	0.375	35000	1650	30612	85.03	0.68	0.6	0.08	3500
1.25	0.626	28000	730	23715	65.88	1.1	0.95	0.15	1850
2.5	1.25	20000	388	17666	49.07	1.43	1.24	0.19	1200
5	2.5	15000	136	9067	25.19	1.45	1.2	0.25	700

The applied strain amplitudes $\Delta\varepsilon$ listed in **Table 4.4** are considered constant during testing. However, the actual strain amplitudes recorded from the strain-controlled tests were not compatible with these values, specifically for the higher strain amplitudes $\Delta\varepsilon = 5.00$ and 2.50% . Both samples reach values of 1.45 and 1.43, respectively, which may conceivably be the highest strain amplitude the Abitibi clays can withstand. On the other hand, the actual recorded values were very close to the applied strain amplitudes for the other two tests with lower amplitudes. The strain amplitude, as defined previously, is divided into two components: the elastic and plastic strain (**Equation 4.3**), which is one of the strain-controlled cyclic tests features.

$$\Delta\varepsilon_{Total} = \Delta\varepsilon_{Elastic} + \Delta\varepsilon_{Plastic} = \frac{\Delta\sigma}{E_s} + \Delta\varepsilon_{Plastic} \dots\dots\dots \mathbf{4.3}$$

The actual strain amplitude ($\Delta\varepsilon_{Total}$) and the two strain components are recorded at failure and listed in **Table 4.4**. At the beginning of the test, the elastic strain is dominant and tends to decrease by increasing the number of cycles; in contrast, the plastic strain component becomes dominant by increasing the number of cycles. While the hysteresis loops were changing during testing, and with

many cycles applied in each test, it was hard to record and calculate the strain components to study their variation with the number of cycles. The most stable cycles were recorded in the $\Delta\varepsilon = 5.00\%$ test; the strain components were approximately estimated by measuring the secant modulus in compression and tension. Their variation with the number of cycles is shown in **Figure 4.40**. The figure shows the total strain amplitude increasing for the first two stages discussed before, then stabilized until the end of the test. The elastic strain component rises at the first stage and tends to decrease until the end of the test. Finally, the plastic strain component decreased and then increased, explaining the change in the hysteresis loops from pointed to rectangular-like loops. This behavior change is expected at the transition point in **Figure 4.40**, where the elastic and plastic strains become equals. Before the transition point, elastic strains are dominant, and after the transient point, the plastic strains are dominant and control the marine clay behavior until failure occurs.

One of the limitations in this study is defining the transition point for the strain-controlled tests by calculating the strain components from the raw data. Therefore, for the three remaining tests, the transition point where defined by investigating the hysteresis loop near where it changes its shape and where pore water pressure accumulates and tends to stabilize—also, a change in the strain amplitude associated with the pore water pressure stabilization. The transition point occurs at later ages by decreasing the total strain amplitude, as listed in **Table 4.4**.

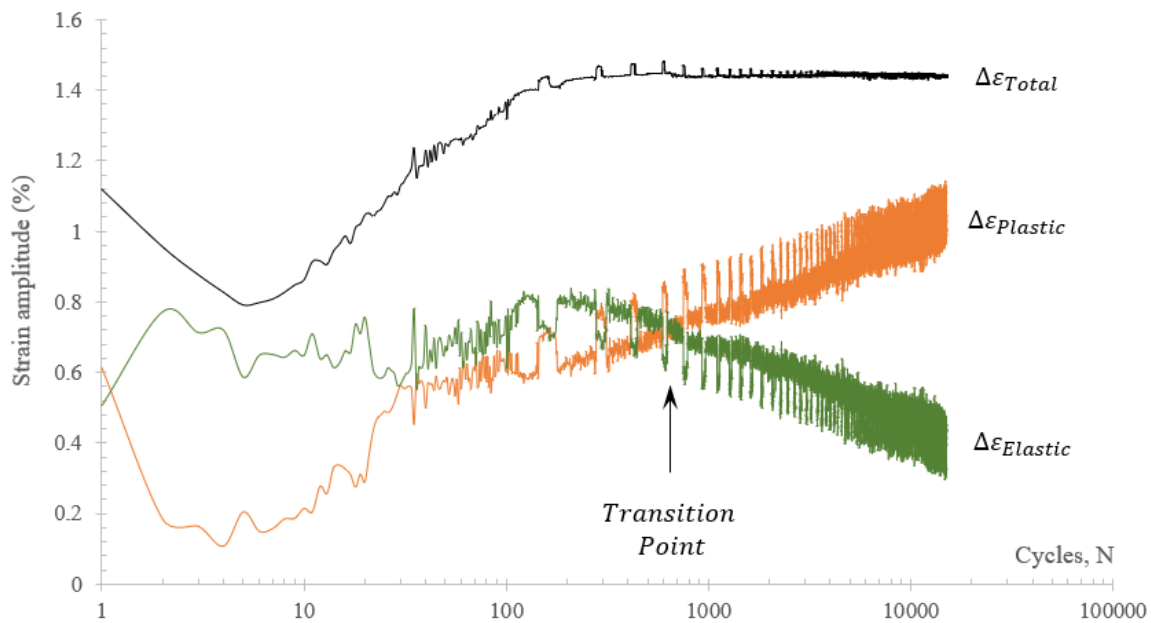


Figure 4.40: Total strain amplitude and Elastic/Plastic strain components for $\Delta\varepsilon = 5.00\%$.

It can be concluded that the strain contributes to the fatigue life of marine clays subjected to long-term cyclic loading. Therefore, by defining the marine clay fatigue life and the transition point, the serviceability of foundations supporting offshore structures might be increased by considering the plastic behavior after crack initiation and the fact that the failure takes place after a long time of the crack initiation; damage tolerant design. **Figure 4.41** shows the correlations of $\Delta\varepsilon - N$ for the crack initiation, transition, and failure of marine clays. In addition, the marine clay fatigue life and the elastic-to-plastic behavior transition can be measured given **Equations 4.4** to **4.6**.

$$N_f = a(\Delta\varepsilon)^{-b} \dots\dots\dots 4.4$$

$$N_i = a(\Delta\varepsilon)^{-b} \dots\dots\dots 4.5$$

$$N_t = a(\Delta\varepsilon)^{-b} \dots\dots\dots 4.6$$

Where:

N_f : Number of cycles (reversals) to failure.

$\Delta\varepsilon$: Total strain amplitude (%).

a and b : Constants measured in experimental tests: $a = 27085, b = 0.623$.

N_i : Number of cycles at first estimated crack initiation.

a and b : Constants measured in experimental tests: $a = 1095.6, b = 1.268$.

N_t : Number of cycles at the transition point (elastic-to-plastic).

a and b : Constants measured in experimental tests: $a = 2523.8, b = 0.816$.

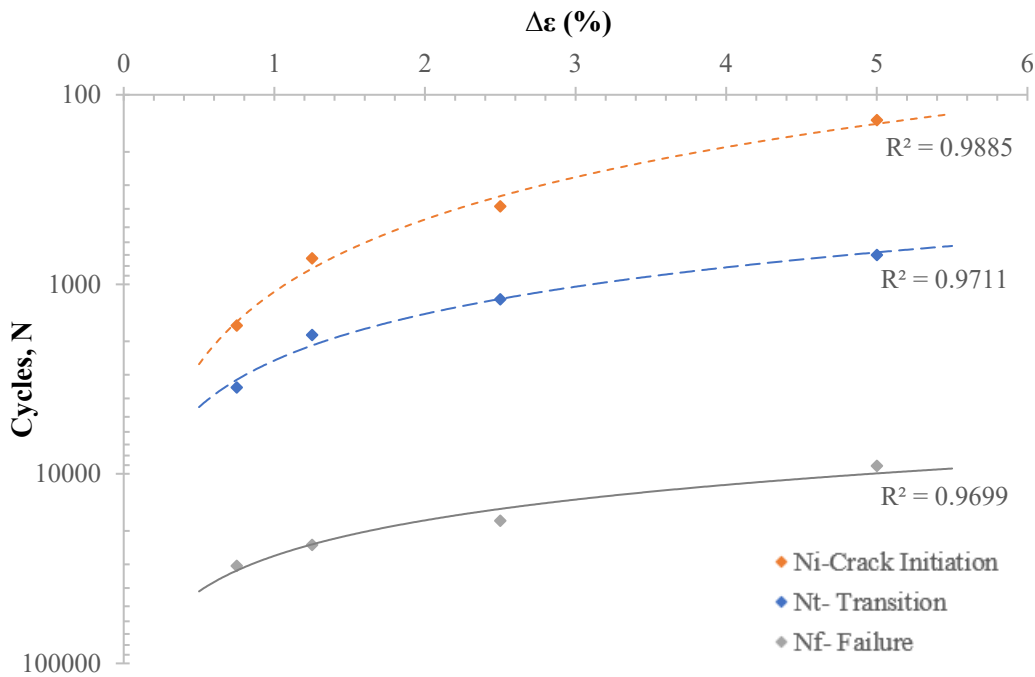


Figure 4.41: $\Delta\varepsilon - N$ curves for Abitibi marine clays' Fatigue life estimation.

It can be seen that the plastic strains control marine clay behavior and become dominant at the early stages of marine clay life, supporting the behavior presented previously of strength hardening periods after marine clays' strength degradation/softening. Moreover, the fatigue cracks filled with cemented materials behave as plastic and compressible zones, which can also explain that the failure occurs after a long time of the crack initiation. **Figure 4.42** shows some marine clay samples after testing and air drying for days; the figure shows the sample's damage after removing water.



Figure 4.42: Marine clay samples after testing and air drying for 48 Hours.

The fatigue life estimation given by **Equation 4.4** is measured based on the applied total strain curve as a generalized correlation, which can be better express the fatigue life at higher strain amplitudes. This correlation and the received strain amplitude during testing are shown in **Figure 4.43**; both curves meet at lower strain amplitudes of $\Delta\varepsilon = 1.25\%$ and 0.75% , and then the actual strain curve stabilizes at a value of $\Delta\varepsilon \cong 1.44\%$ for higher strain amplitude. The two dashed lines in the figure represent the actual elastic/plastic strain components, where the summation of these two curves can express the actual fatigue life. The true fatigue life curve can be applicable for Abitibi marine clays and other clays having the same properties.

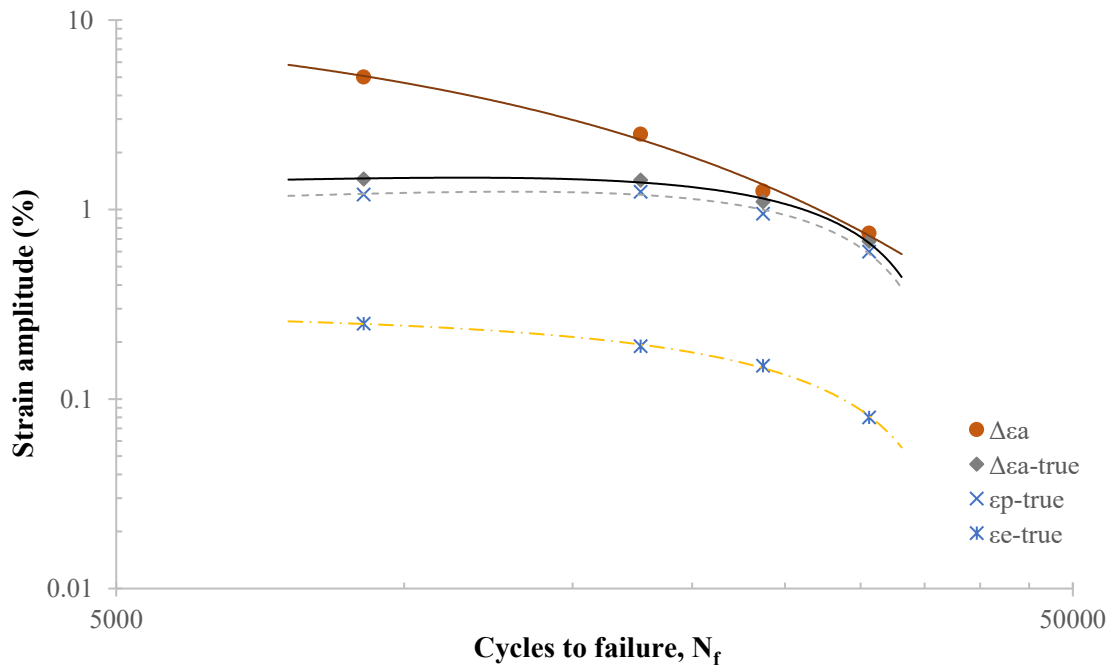


Figure 4.43: Actual $\Delta\varepsilon - N$ and strain components' curves for Abitibi marine clays.

4.4.3 Degradation Index of Marine Clays

The degradation index and degradation parameter are two significant design parameters; many researchers in the literature performed both stress and strain-controlled cyclic tests to formulate these two parameters. Most of the studies in the literature performed short-term cyclic tests, and the degradation index was measured using the correlations summarized in **Table 4.5**. Only studies performed using strain-controlled tests were included.

Most of the studies agreed on the linear relationship of the degradation index and the number of cycles ($\delta - N$) and measured δ using the equation shown in **Table 4.5**. The degradation parameter (t) measures the rate of marine clay degradation and is obtained from the slope of the linear curves of ($\delta - N$) at different strain amplitudes $\Delta\varepsilon$. All studies agreed that the degradation parameter has a nonlinear relationship with increasing the strain amplitude, and different correlations were proposed in the literature, as listed in **Table 4.5**. The maximum number of applied cycles was 100 cycles; some researchers applied transient loading where incremental strain amplitudes were applied for every 100 cycles, with a maximum of 600 cycles.

Table 4.5: Summary for the degradation index correlation in the literature (Strain-controlled).

<i>Study</i>	$\delta - N$	$t - \Delta\varepsilon$ (or γ)	Applied N	Max. amplitude
(Idriss, Dobri, & Singh, 1978)	$\delta = N^{-t}$	<i>Nonlinear</i>	100	4
(Idriss, Moriwaki, Wright, Doyle, & Ladd, 1980)	$\delta = N^{-t}$	$\frac{\gamma}{0.4 + 7.3\gamma_c^{0.61}}$	100	$\gamma_c = 0.5$
(Vucetic & Dobry, 1988)	$\delta = N^{-t}$	$\frac{\varepsilon_c}{1.5 + 1.6\varepsilon_c}$	98	5
(Lee & Sheu, 2007)	$\delta = N^{-t}$	$t = 0.0275\varepsilon_c^2 + 0.236\varepsilon_c$	100	4.2
(Mortezaie & Vucetic, 2013)	$\delta = N^{-t}$	Hyperbolic	20	$\gamma_c = 0.5$
(Xiao, Guib, & Xuc, 2018)	$\delta = N^{-t}$	Hyperbolic	100	$\gamma_c = 1$

In this study, four-strain amplitudes were used to estimate the fatigue life of the Abitibi marine clays, discussed in the preceding section. From the collected data, the secant modulus of elasticity and degradation index has been measured using **Equations 4.1** and **4.2**. The degradation index distribution with the number of cycles is shown in **Figure 4.44**; it can be seen that for the tests performed under strain amplitudes of $\Delta\varepsilon = 5.00$ and 2.50% , the degradation index has two different rates of change: (1) at $N < 100$ cycles, and (2) at $N \geq 100$ cycles. The second phase has a higher degradation rate, indicating that the clay has a more stable behavior at an early age.

Per the previous discussion and the fatigue life estimation, it was found that the first 100 cycles do not reflect the actual behavior of the marine clays subjected to long-term cyclic behavior. However, the change in degradation index for $N \geq 100$ cycles can represent the degradation parameter of the $\Delta\varepsilon = 5.00$ and 2.50% strain amplitudes; the degradation parameter was calculated for the two phases, shown in **Figure 4.44a, b**.

The tests performed under a lower strain amplitude of $\Delta\varepsilon = 1.25$ and 0.75% show a higher rate of degradation at earlier ages than the $\Delta\varepsilon = 5.00$ and 2.50% tests. The lower rate of degradation change occurred in the first 10 to 15 cycles. The life estimation discussion found that the tested clay

dropped the stress and strain amplitudes during the first few cycles. This unstable behavior decreases with decreasing the applied strain amplitude, explaining the degradation index stable rate for the $\Delta\varepsilon = 5.00$ and 2.50% strain amplitudes. Therefore, the degradation index rate was measured in one phase, as shown in **Figure 4.44c, d**.

The degradation index (δ) for all tests has the formula given by **Equation 4.7**, where (t) in the equation is the degradation index change or the degradation parameter. The degradation index equations and degradation parameters are summarized in **Table 4.6**.

$$\delta = a(N)^{-t} \dots \dots \dots \mathbf{4.7}$$

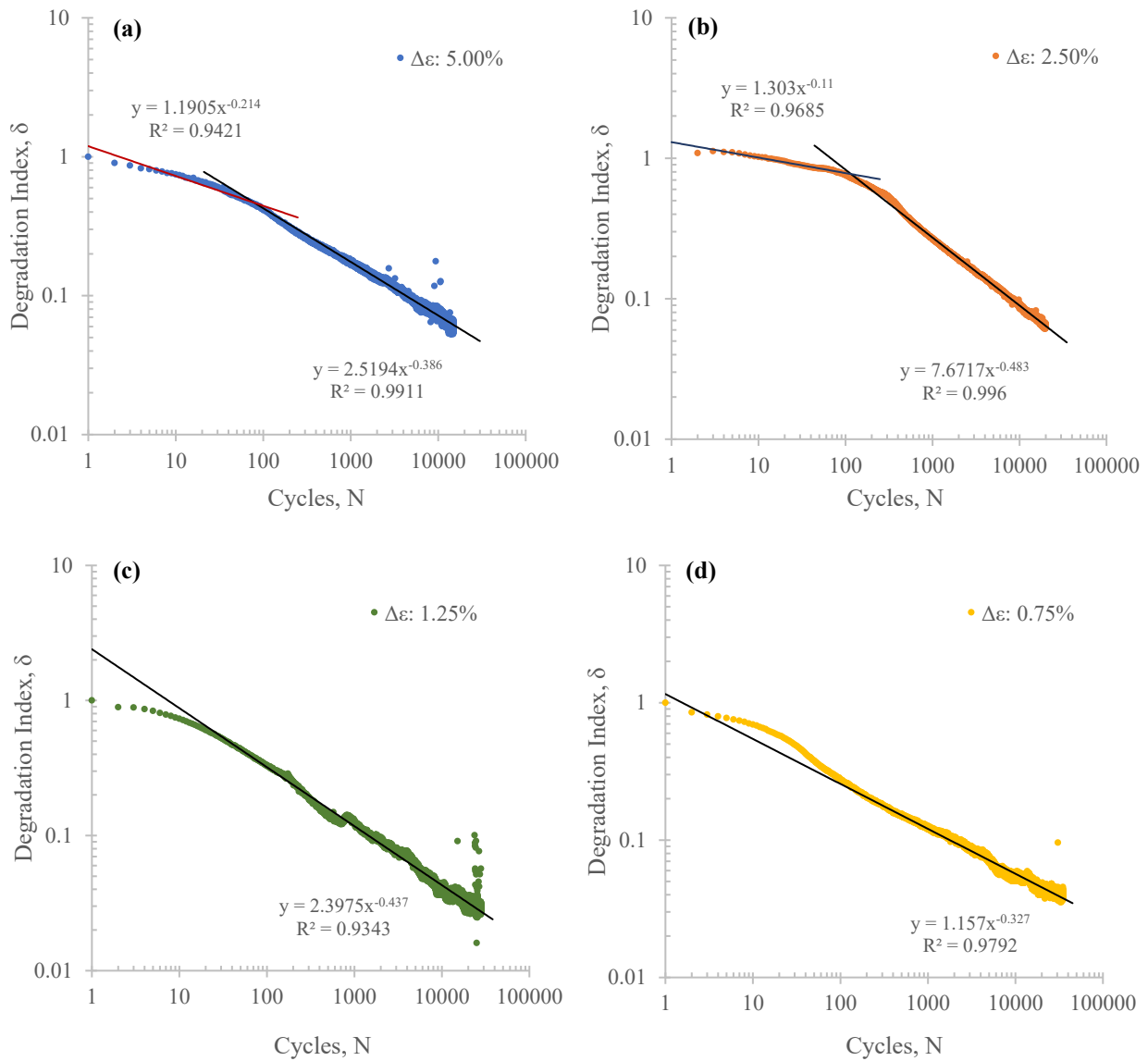


Figure 4.44: Degradation index and parameter for the tested samples.

Table 4.6: Summary for the degradation index correlations in this study.

$\Delta\varepsilon$ (%)	Applied N (Cycles)	Range (Cycles)	$\delta - N$ Formula	t
5.00	15000	$N < 100$	$\delta = 1.19N^{-0.214}$	0.214
		$N \geq 100$	$\delta = 2.52N^{-0.386}$	0.386
2.50	20000	$N < 100$	$\delta = 1.30N^{-0.110}$	0.110
		$N \geq 100$	$\delta = 7.67N^{-0.483}$	0.483
1.25	28000	28000	$\delta = 2.40N^{-0.437}$	0.437
0.75	35000	35000	$\delta = 1.16N^{-0.327}$	0.327

Figure 4.45 shows the fitting curve for the correlations between the degradation parameter (t) and the strain amplitude ($\Delta\varepsilon$), assuming that the degradation rate of the second phase is dominant for the $\Delta\varepsilon = 5.00$ and 2.50% tests. The best-fitted curve is a second-degree polynomial curve, given by **Equation 4.8**.

$$t = -0.031(\Delta\varepsilon)^2 + 0.19(\Delta\varepsilon) + 0.224 \quad \dots\dots\dots 4.7$$

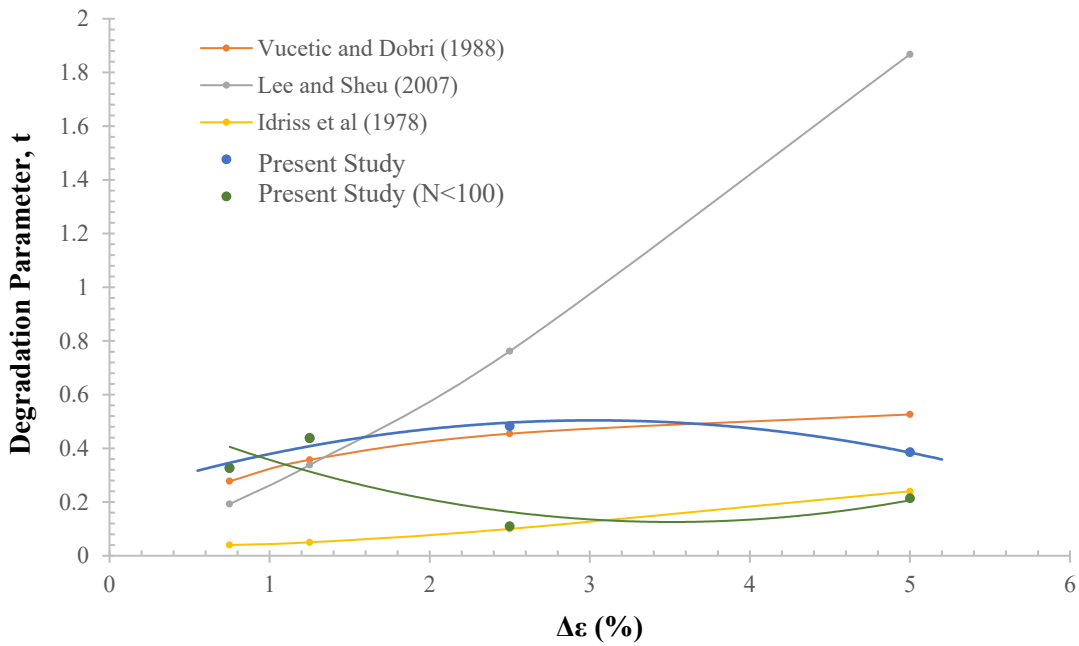


Figure 4.45: Degradation parameter for this study and studies in the literature.

The degradation parameter (t) was calculated from the available equations and curves in the literature and included in **Figure 4.45** for comparison purposes. It is important to recall that the maximum performed cycles in these studies are 100 cycles, and in this study, the samples cycled to failure. Therefore, it can be seen in the figure that the fitted curve in this study has a slightly good agreement with the one proposed by (Vucetic & Dobry, 1988). While (Idriss, Dobri, & Singh, 1978) underestimated the degradation parameter for all strain amplitudes, and (Lee & Sheu, 2007) overestimated the degradation parameter for higher strain amplitude and underestimated it at lower values.

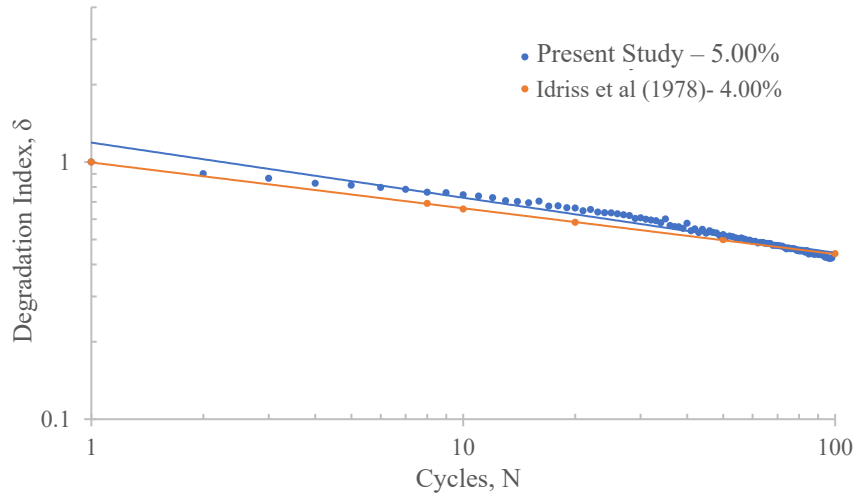


Figure 4.46: Degradation index for this study compared with (Idriss, Dobri, & Singh, 1978).

The degradation parameter for $N < 100$ cycles measured in this study is also included in **Figure 4.45**. It shows an excellent agreement at higher amplitudes with (Idriss, Dobri, & Singh, 1978), while other studies overestimated the degradation parameter at these amplitudes. On the other hand, at lower strain amplitudes, all studies underestimated the degradation parameter (t).

A test performed under strain amplitude of 4.00% in the study of (Idriss, Dobri, & Singh, 1978) was selected to compare the degradation parameter (δ) measured from the available data in the study and the measured index in this study for $\Delta\varepsilon = 5.00$ and $N < 100$ cycles. The two measured data are shown in **Figure 4.46**, and both studies exhibited a high agreement.

Most of the studies in the literature agreed that the significant marine clay degradation occurs in the early stages of loading and consequently performed their analysis on a low number of cycles that do not exceed 100 cycles. In this study, the results match this assumption for samples strained at higher amplitudes $\Delta\varepsilon = 5.00\%$. The clays' samples reach a degradation index of $\delta \cong 0.45$, showing 55% degradation and $\delta \cong 0.75$ for 25% degradation in the first 100 cycles. The clays show higher degradation for lower cyclic strain amplitude where a degradation index of 0.35 and 0.20 for $\Delta\varepsilon = 1.25$ and 0.75%, respectively. The initial conditions and marine clays' properties can affect the degradation index.

CHAPTER 5

MONOPILE-MARINE CLAY CYCLIC FATIGUE RESPONSE

Despite different researchers' efforts, methods proposed are not adopted widely in design codes where they still adopt the $p - y$ curves criteria for clayey soils proposed by (Matlock, 1970). However, the researchers are still conducting laboratory and field studies to examine the suitability of Matlock criteria to the recent offshore structures and provide new field and laboratory data trying to describe the actual behavior of the Clay-Pile system. (Matlock, 1970) His study reported that clays tolerate permanent deformations during cyclic loading, affecting the pile-clay response. Most of the deterioration occurs at $N \leq 100$ cycles, and then the system tends to stabilize except for higher loading levels. Following Matlock, many researchers performed experimental tests on the pile-clay system to define the threshold load level at which the system maintained equilibrium; in other words, it exhibited fewer pile-head deformations. Most researchers reported that the API code overestimates or underestimates the pile-clay response to lateral cyclic loading.

5.1 MONOPILE-MARINE CLAY CYCLIC RESPONSE ASSESSMENT

When applying load-controlled tests on the monopile-clay system, the main target will be measuring the pile capacity described by the pile-head lateral deformation. Consequently, studies in the literature adopted different criteria to define whether the pile-clay system will tolerate large lateral deformations that lead to failure or exhibit small lateral deformation with no possible damages. In common with marine clays' stress-controlled testing, the loading levels, or the cyclic stress ratios, are the main factors affecting the system response to lateral cyclic loading. Moreover, one of the researchers' concerns was to define the threshold load level at which the pile-clay system maintains equilibrium to help the designers safely design the offshore structures. The load level is given by the ratio between maximum cyclic stress amplitude (P_{ult}) and the ultimate static capacity (P_{us}).

Earlier, researchers measured the possibility of system failure by reporting the pile head deformation during cycling and recorded the threshold load level where a remarkable or sudden increase in lateral deformation happened during testing. Then, to correlate the marine strength deterioration adjacent to the monopile with the resulted lateral movement of the pile movement, the researchers defined

the threshold load levels concerning the pile geometry (diameter and length). Recently, the research directed toward the serviceability requirement for a monopile-clay system as it tolerates long-term deformation during its life span. Moreover, they adopted the serviceability limit state (SLS) design requirements in defining the threshold load level.

A group of datasets was collected from the literature to define a general criterion for the threshold load level and listed in **Table 5.1**. Researchers applied a different number of cycles; some researchers restricted their studies to a total of 100 *cycles*, and others adopted different criteria in defining the number of cycles required to fail or stabilize. In addition, the lateral pile-head deformation was measured to define the threshold loading level; the criteria adopted in each study are also listed in the table.

Figure 5.1 shows a regression analysis performed on the threshold load levels' data points based on the literature's dataset collation. The local polynomial regression (or moving regression) best fits the data, and a fourth-order polynomial fitted curve with a coefficient of determination $R^2 \cong 0.91$ (relatively low variance) can define the failure envelope, as seen in the figure. The proposed failure envelope that separates the datasets that exhibited large lateral head and lower deformations are shown in **Figure 5.2**. In the absence of long-term cyclic tests in the literature, the envelope shown in the figure is applicable for a maximum of $N \cong 5000$ *cycles*. Furthermore, the criteria used to define at which loading level the system will tolerate large deformations varied in the studies. Consequently, the envelope is valid for a monopile-clay system with similar conditions.

Table 5.1: List of collected data from the literature.

Study	Datasets	Criteria	Clays	Cycles
(Karlsruud & Haugen, 1985)	5	1. $y = 1.0 - 1.5 \text{ mm}$ 2. $Disp. \text{ rate} > 0.5 \text{ mm/min}$ 3. y_N increase by 0.5 or 1.0 mm relative to y_i	Marine clay	60 - 460
(Rao, Rao, & Prasad, 1992)	5	Pile head deformation at All stabilized high load levels	Marine clay	375 - 600
(Rao & Rao, 1993)	5	1. $y > 0.2D$ 2. Sudden increase for y with no signs of stabilization	Marine clay	70 - 500
(Prasad & Rao, 1994)	13	1. $y > 0.2D$ 2. Sudden increase for y with no signs of stabilization	Marine clay	40 - 500
(Kumar, Rao, & Sundar, 2007)	5	$\frac{y}{D} \times 100 < 3\%$	Marine clay	1200 - 1700
(Hong, et al., 2017)	3	Pile head rotation $< 0.5^\circ$ for wind turbines	Specwhite Kaolin	100
(Liao, Wu, Wang, Yan, & Ouyang, 2021)	9	SLS	Marine clay	Up to 5000

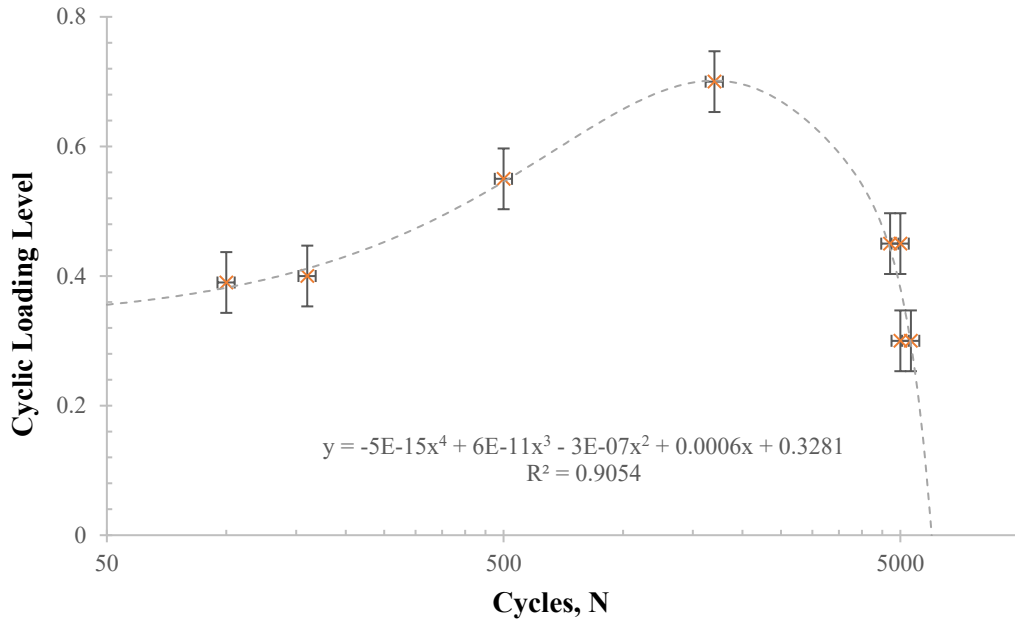


Figure 5.1: Polynomial regression model for the threshold CSR of the collected dataset.

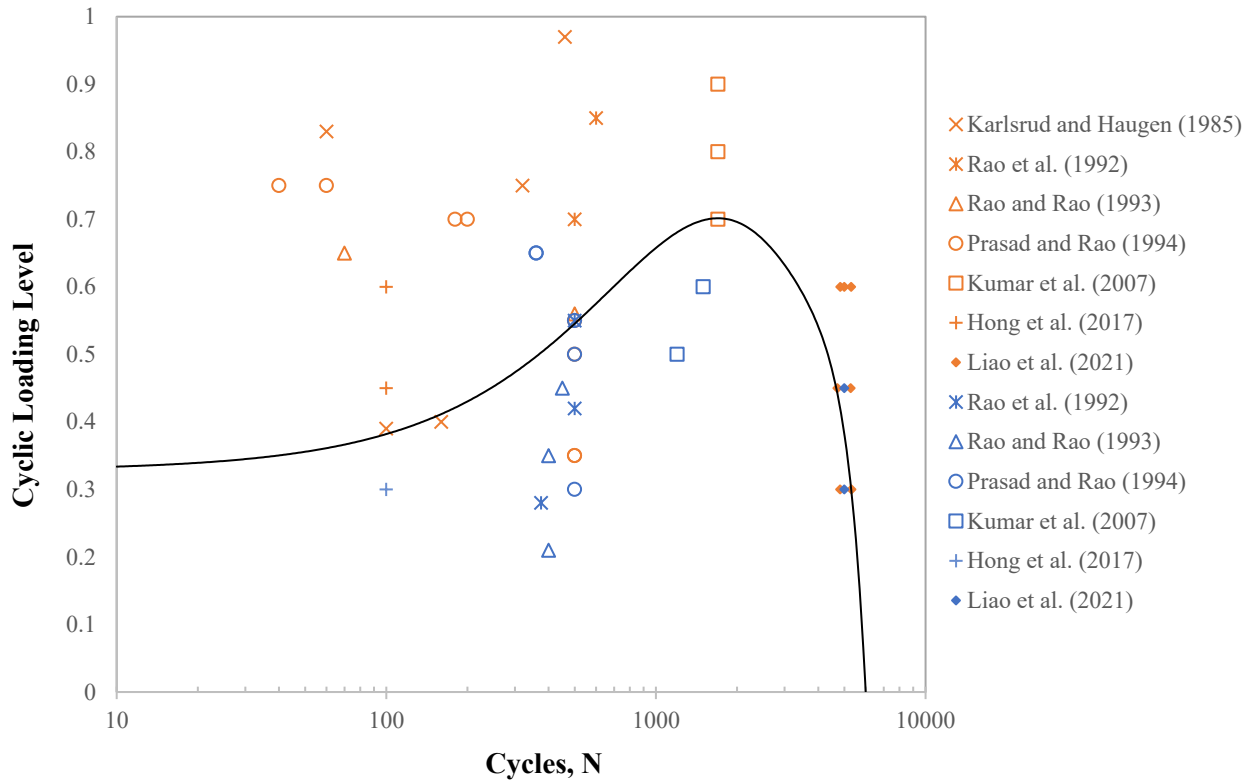


Figure 5.2: Proposed demarcation line for the collected dataset of monopile-clay system.

Most studies reported high lateral pile head deformation for higher loading levels; however, some tests considered failed at low lateral head deformations, as seen in **Figure 5.3**. It can be seen in the figure that a limit of $y \cong 4\text{mm}$ and a loading level of 60% was reported by the researchers in which higher values might cause damage to the monopile-clay system. (**Karlsrud & Haugen, 1985**) in their study, the system was considered to fail even if low pile head movement occurred at all loading levels. They defined the failure criteria by a sudden deformation increase with a high rate and the initial pile head movement. (**Rao & Rao, 1993**) and (**Prasad & Rao, 1994**) also followed the same criteria; however, they recorded higher pile head deformations. These results highlighted the importance of studying the degradation of the monopile-clay system in parallel with the system's capacity to understand this behavior better and decide whether to consider these relatively low deformations a failure or not, which was also reported by (**Karlsrud & Haugen, 1985**).

On the other hand, some of the tests performed by (**Liao, Wu, Wang, Yan, & Ouyang, 2021**) were considered failed under low loading levels and exhibited low pile head deformations. Their study performed tests under three different frequencies to measure the effect of increasing frequencies on the system's capacity. It is essential to mention that all frequencies were higher than $f \geq 0.45\text{ Hz}$ with a highest loading level of 60%. Other studies performed the tests for frequencies of $f \cong 0.1\text{ Hz}$, which simulate the surface wave frequencies. As reported earlier in this study, lower frequencies can delay the clay failure, and marine clays exhibited a relaxation behavior when studying the fatigue behavior of marine clays under low frequencies.

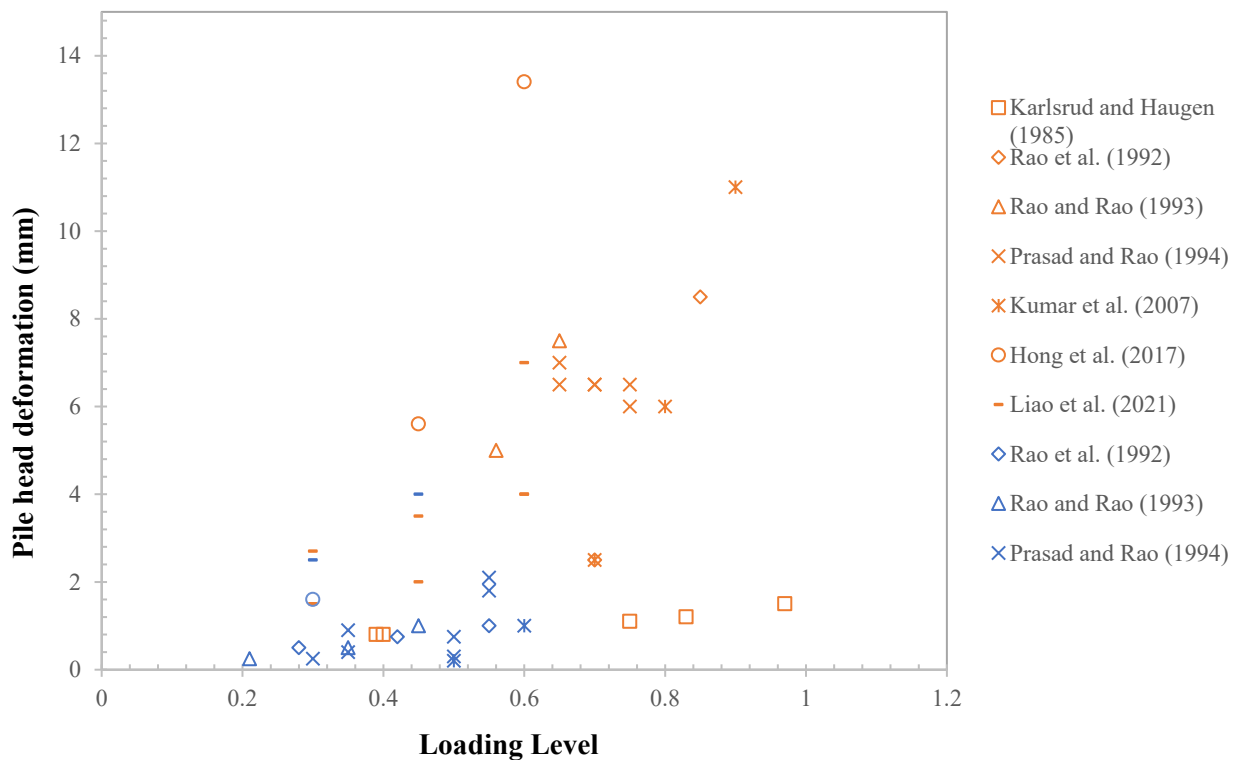


Figure 5.3: Pile head deformation with loading levels for different studies.

5.2 MONOPILE-MARINE CLAY FATIGUE BEHAVIOR

The monopile-marine clay system undergoes large deformations during its life span as it is subjected to lateral cyclic loading over time. Therefore, the design of the monopile-clay system has different criteria as summarized by (Arany, Bhattacharya, Macdonald, & Hogan, 2017); the serviceability limits state criterion (*SLS*) concerns the allowed lateral pile head deformation after long-term loading to avoid failure. The pile geometry and the soil stiffness are essential parameters in predicting the pile head movement. Moreover, the fatigue limit state criterion (*FLS*) concerns the fatigue life of the system, which can be defined by the number of cycles required to reach failure.

The maximum deformation allowance defines the failure in design codes, expressed by lateral pile head movement or rotation. However, the displacement-controlled test can better estimate the fatigue behavior, where a constant displacement amplitude is applied to measure the stress and stiffness degradation. Therefore, the fatigue life can be estimated and used in the design process. (Karlsrud & Haugen, 1985) reported that the upper part of a flexible offshore pile is more displacement-controlled than load-controlled and that studying the degradation is essential. However, very few studies in the literature conducted displacement-controlled tests (i.e. (Zhang, White, & Randolph, 2011), (Su, Wu, Du, & Yan, 2014), and (Senanayake, et al., 2015)). Their studies performed the tests for a limited number of cycles and measured the stiffness degradation by increasing the number of cycles.

In the preceding chapter, the fatigue life of marine clays was discussed in detail in which a series of strain-controlled were performed under different strain amplitudes. As a result, the marine clay fatigue behavior was defined by three equations that represent: (1) crack initiation (N_i), (2) transition (N_t), and (3) failure (N_f). The transition number of cycles occurs when the plastic deformations become dominant and control the marine clay response to cyclic loading, which is found to associate the stage where the pore water pressure stabilizes or increases slowly. Moreover, the failure occurred after reaching the transition point. The marine clay stiffness degradation was also discussed in the preceding chapter, and the degradation rate of the marine clay was determined for different amplitudes. Therefore, it is believed that the degradation parameter measured for the fatigue life of marine clays can be used efficiently in the design of the monopile-clay system.

In the absence of long-term, large-scale field or experimental tests due to the high cost and many limitations, numerical modeling was an efficient tool to inspect the long-term behavior of the monopile-clay system. However, studies in the literature performed tests for a few cycles to reduce the computational effort of the numerical models. In addition, they performed their models on scaled monopiles and clay domains. This study performed a simple 2D *FEM* numerical analysis under displacement-controlled loading in ABAQUS to study large-scale monopile-clay system fatigue behavior. The main objectives of these numerical models are to inspect the marine clay strength degradation over the embedded depth of the monopile for a large-scale problem and to inspect the plastic strain transition point.

5.3 2D FEM DISPLACEMENT- CONTROLLED MODELS

5.3.1 Model Geometry and Boundary Conditions

Increasing the monopile size to improve the monopile-clay system response to lateral cyclic loading is one of the main concerns in the industrial field. The offshore monopile's diameters can reach 8m and a length of 80 m or more. In the 2D *FEM* models, the monopile has a diameter ($D = 3\text{ m}$) and

length ($L = 40\text{ m}$) with a relative stiffness of $< 10^2$. The marine clay domain has a dimension of $30 \times 40\text{ m}$ with the monopile embedded length of (30 m), as shown in **Figure 5.4**. The monopile head is free to simulate the field conditions and subjected to lateral displacement-controlled cyclic loading. The model material properties are also shown in **Figure 5.4**, where the marine clay's properties tested in the preceding chapter are used in the numerical analysis.

The boundary conditions and loading process is shown in **Figure 5.5**. The lateral boundaries of the marine clay domain are restrained with roller supports to prevent the horizontal movement of the entire system. In addition, the bottom boundary is prevented from both lateral and vertical movements by pin supports along the boundary length. For loading, first, the marine clay domain geostatic stresses are applied by defining the gravity load, in which Abaqus calculate the gravity loads based on the material density and acceleration. Then, a cyclic displacement-controlled load is applied, as shown in **Figure 5.5**. Two *FEM* models were performed under two different amplitudes; the displacement amplitudes were calculated based on the *SLS* requirements of offshore monopiles supported wind turbines. The highest amplitude was 0.35 m which was calculated based on an allowable tilting of the monopile of (0.5°), and the other amplitude was one-third the highest magnitude ($\cong 0.12\text{ m}$).

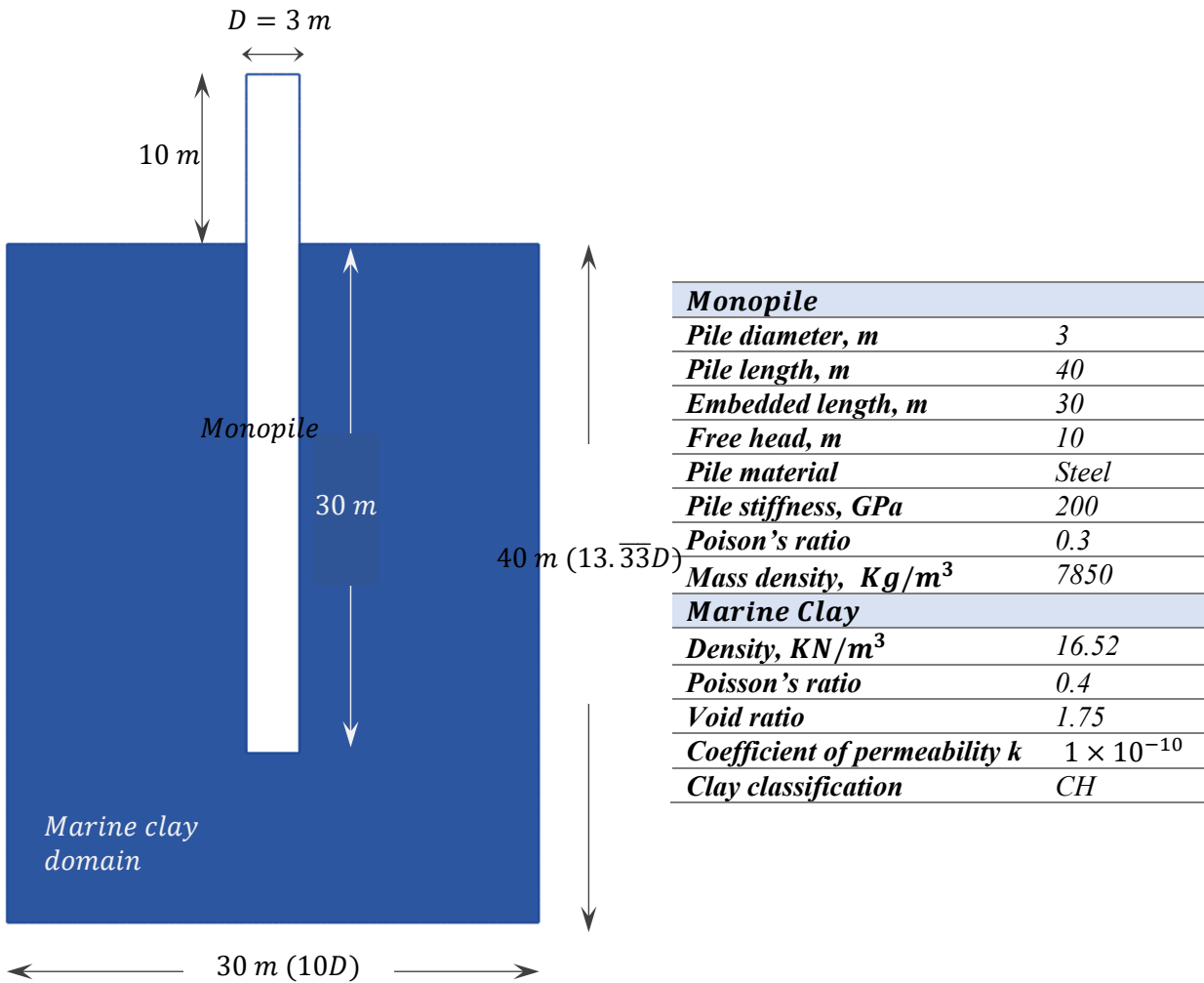


Figure 5.4: 2D FEM Model Geometry and material properties.

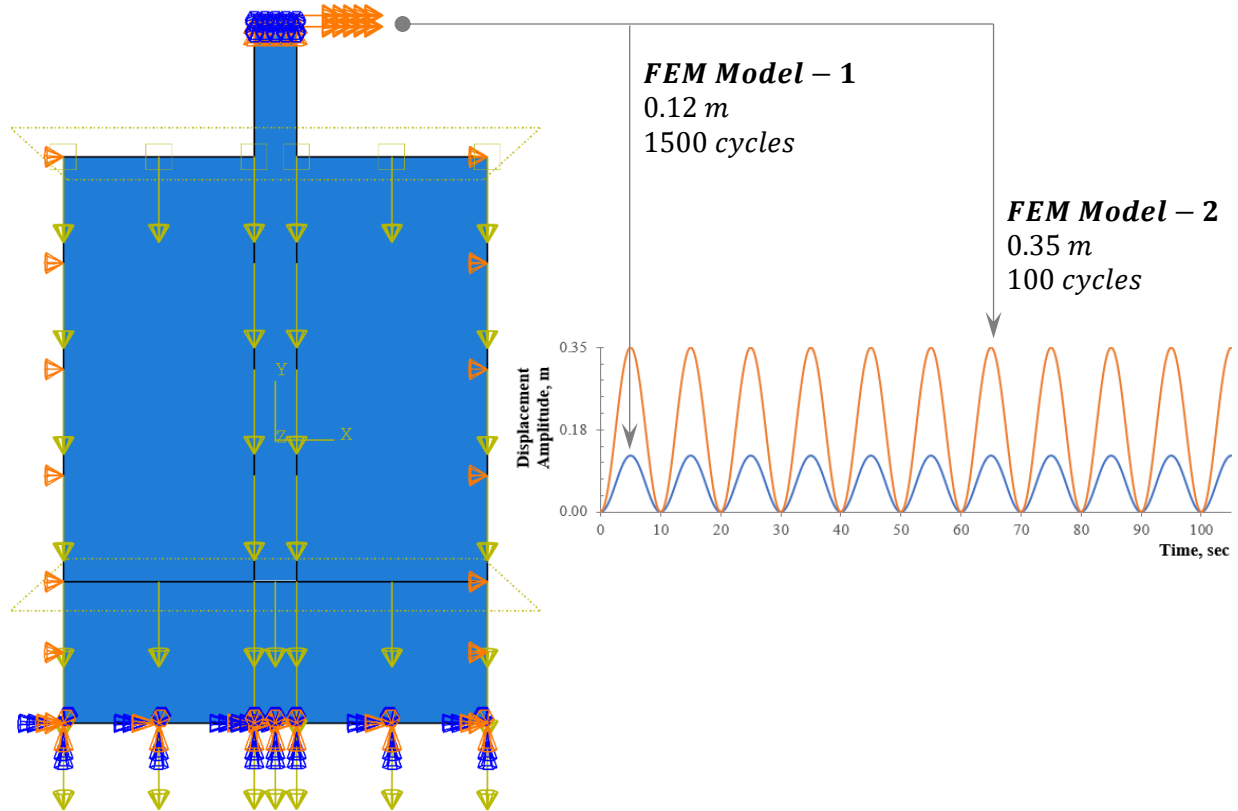


Figure 5.5: 2D *FEM* model boundary conditions, gravity, and applied loads.

5.3.2 FEM Model Meshing and Modelling Procedure

The monopile and marine clay domains were discretized to fine meshes; as shown in **Figure 5.6**, the monopile mesh has 200 *elements type CPS4R* (4-noded plane stress element in Abaqus). The marine clay domain meshing has 1786 *elements type CPE8RP* (8-noded pore pressure, plane strain element in Abaqus). The monopile-marine clay interaction is modeled using a surface-to-surface interaction with penalty friction of Mohr-Coulomb of 0.35. No gap opening or surface split was allowed while applying the cyclic load.

The marine clay response to cyclic loading is modeled using the constitutive model Drucker-Prager with shear hardening behavior available in Abaqus. The Drucker-Prager model captures the hardening or softening behavior of materials exhibiting long-term plastic deformation. The failure surface is defined in **Equations 5.1** and **5.2**, where: β , and d are the material angle of friction and cohesion, respectively. The parameter t is the deviatoric stress measure, and $K = 1$.

$$F_s = t - p \tan \beta - d = 0 \dots \dots \dots 5.1$$

$$t = \frac{1}{2} q \left[1 + \frac{1}{K} - \left(1 - \frac{1}{K} \right) \left(\frac{\tau}{q} \right)^3 \right] \dots \dots \dots 5.2$$

$$\tau = s \cos \phi, s = 1/2 (\sigma_1 - \sigma_3), d = \sqrt{3}/2 \tau (1 + 1/K)$$

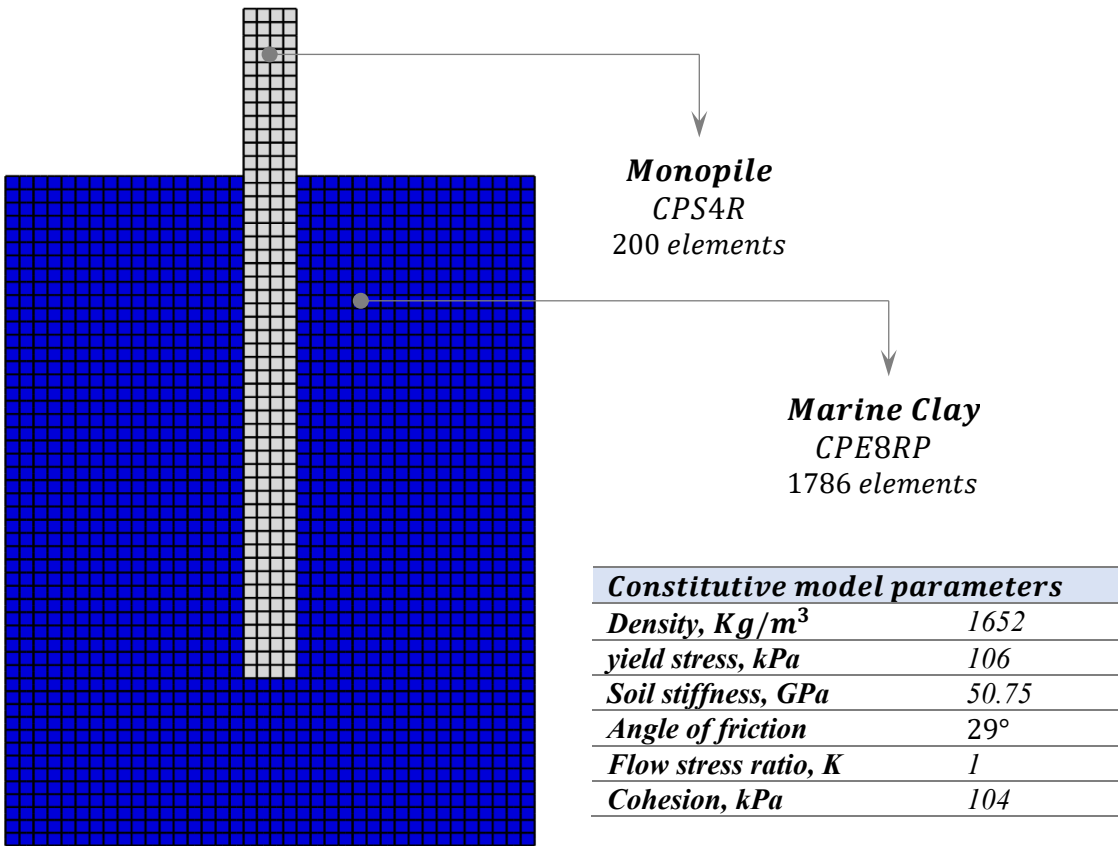


Figure 5.6: 2D *FEM* model domain discretization and constitutive model parameters.

The first step in the numerical analysis for 2D *FEM* models is to apply the geostatic loads to the soil domain. Then the cyclic displacement-controlled loading is applied following the executed cyclic loading table and maintaining the undrained condition by imposing the pore water pressure values at the surface and the bottom. The model allows for pore water pressure progression during cyclic loading.

5.4 ANALYSIS OF THE 2D FEM MODELS

5.4.1 *P – N* Profiles

The displacement-controlled tests efficiently measure the actual clay response to long-term loading. The *P – N* profiles over the embedded length of the monopile in the *FEM* model are shown in **Figures 5.7** and **5.8**. The *P – N* represents the development of soil resistance with increasing the number of cycles. In addition, an inspection for both the right and left sides was performed to measure the clay response to lateral cyclic loading when a 0.12 *m* displacement was applied to the top of the monopile. The results in the figures are presented in two forms: the *FEM* model results and the *P – N* profile at different depths. It can be seen in the figures that three main areas around the pile exhibited high load accumulation: at shallow depths left and right and at the pile tip.

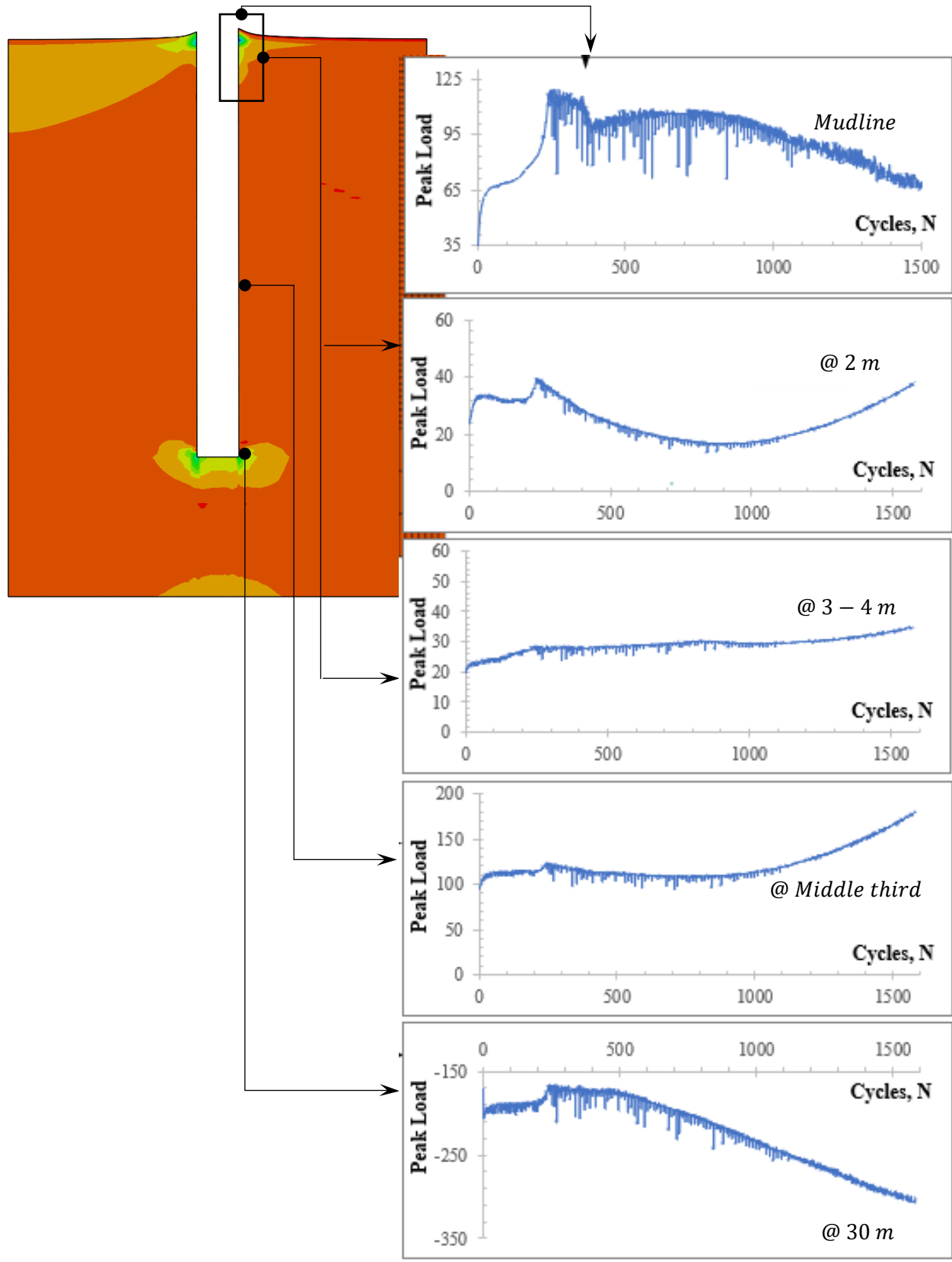


Figure 5.7: 2D FEM model ($y = 0.12m$) peak load profile: right-side.

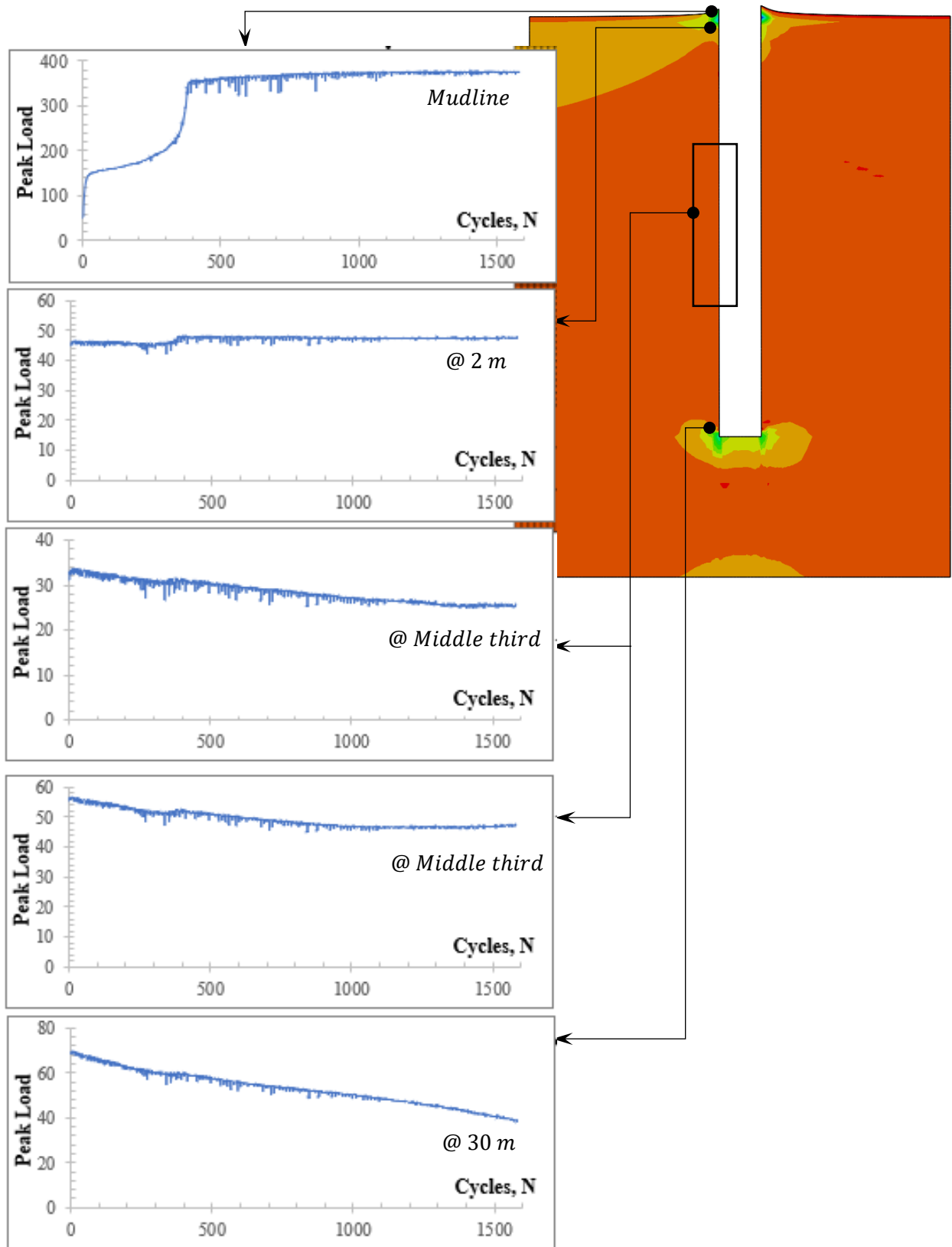


Figure 5.8: 2D FEM model ($y = 0.12m$) peak load profile: left-side.

The clay at shallow depths was deformed and showed degradation in its resistance, where a deformed shape is detected at the mudline from the right side. The $P - N$ profiles for three depths starting from the mudline are shown in **Figure 5.7**; at the mudline, the clay increases resistance at the first few cycles, followed by a steep degradation until the end of the test. The clay reached an ultimate load of $P_{ult} \cong 118$ kN after about 300 cycles, then degraded, showing softening behavior followed by slight hardening and continuing to soften until it reaches a $\cong 45\%$ degradation by the end of the loading cycles.

At lower depth $d \cong 2m$, the clay exhibited periods of softening and hardening without any signs of failure, and maximum degradation of $\cong 43\%$ was recorded during cycling. Moving down and at depth $d \cong 3 - 4m$, the clay tends to stabilize with slight periods of softening and hardening. The clay at shallow depths was remolded by cycling with pore water pressure generation, which can explain the clay's behavior near the mudline to a certain depth. The pore water pressure generation and plastic strain distribution are shown in **Figure 5.9**. Moreover, the clay behavior shows more hardening with no degradation at the middle part of the embedded length. It continues with the stabilized behavior till a certain point near the pile tip, where the clay shows softening and high deformations. This behavior was also recorded by (Byrne, et al., 2015). The researchers proposed new design components to account for the remolding behavior and the potential rotation of the monopile at the tip side.

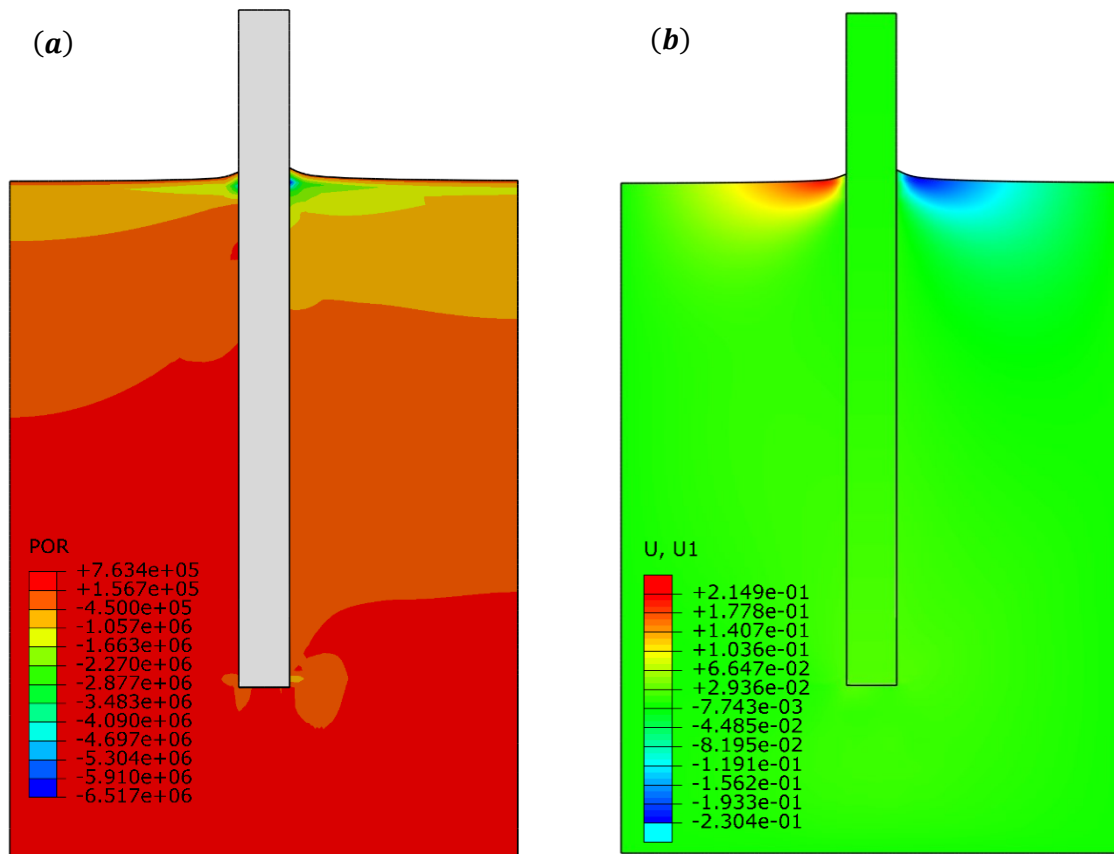


Figure 5.9: 2D *FEM* model ($y = 0.12m$): (a) pore water pressure distribution and (b) Displacement in x .

Figure 5.8 shows the $P - N$ profiles at the left side of the pile. The clay at the mudline level shows a stabilized behavior with an accumulation of pore water pressure and deformations. At a depth of $d \cong 2m$, the clay also shows a stabilized behavior with a slight increase in the peak amplitude. The reported increase in the peak amplitude in the right and left sides is referred to as the increase of plastic strains, which will be discussed in the subsequent sections. The clay at the middle third of the embedded length (left side) has the same behavior, where a slight degradation is reported till the mid-life and then stabilized until the end of cycling. Then, again, the clay softens at the pile's tip, and maximum degradation of $\cong 45\%$ is recorded.

The pore water pressure profile in **Figure 5.9** shows an accumulation at shallow depth at the loading side and behind the pile top side. In addition, there is a high negative pore water pressure accumulation at the pile tip corners from both sides, reflecting that the clay started to behave plastically at these points. As a result, the clay will continue degrading until it reaches failure by increasing the number of cycles. This behavior was reported when studying the fatigue behavior of marine clays in the preceding chapter, where the clay failed after the plastic strains became dominant and controls the behavior under cyclic loading. Furthermore, to check the effect of the applied displacement amplitude, the *FEM* model was also tested under $0.35 m$ amplitude, the maximum allowed amplitude per the SLS requirements of wind turbines.

For the higher displacement amplitude ($0.35 m$), a total of 100 cycles was performed for comparison. The pore water pressure and lateral displacement profiles are shown in **Figure 5.10**, in which higher values were recorded compared with the $0.12 m$ displacement amplitude. It can be seen that a higher pore water pressure is generated in a less applied number of cycles; however, the *pwp* profiles were almost the same for both models.

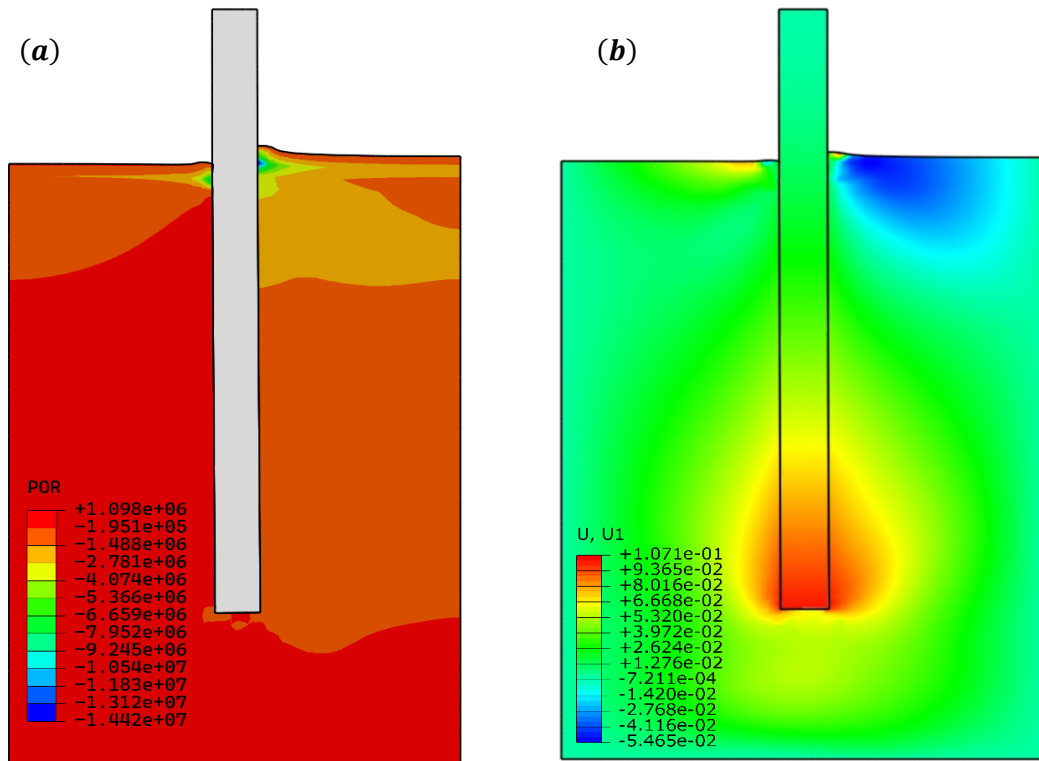


Figure 5.10: 2D *FEM* model ($y = 0.35 m$): (a) pore water pressure distribution and (b) Displacement in x .

The lateral displacement profile, in addition to the high deformations at shallow depths, shows high lateral displacements at the pile end tip, as shown in **Figure 5.10b**. This behavior is because the pile was extensively displaced laterally at the pile-head, which led to a rotation of the pile at a certain depth from the pile tip, explaining the lateral displacement accumulation. Moreover, the deformations at the mudline differ from those reported under lower displacement amplitude (0.12 m). The deformed shape at the left side can indicate the possibility of a gap opening, while at the lower amplitude, and after a higher number of cycles, the clay was showing remolding with no signs of gap opening.

Figure 5.11 shows the $P - N$ profiles at the mudline and monopile's tip for the 0.35 m displacement amplitude model. Again, a degradation in clay resistance is reported at both levels, with no signs of failure. However, the monopile-clay system is expected to fail if more cycles are applied. The clay reaches the ultimate resistance after 20 cycles compared with 300 cycles in the lower amplitude model (0.12 m). This behavior highlighted the effect of the displacement amplitude that the monopile can carry. It is essential to mention here that the strain amplitude represents the total displacement that the system can carry. This displacement might have resulted from wind, surface loads, or a combination of lateral forces. In other words, applying displacement waves as lateral loading can represent different loading types.

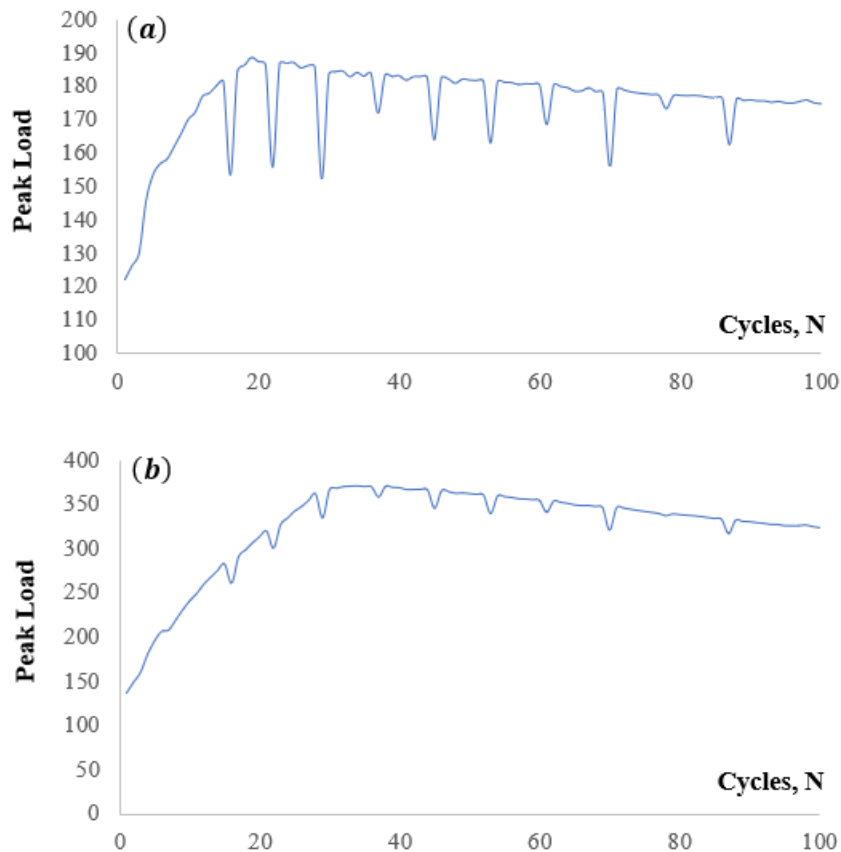


Figure 5.11: 2D *FEM* model ($y = 0.35\text{ m}$) peak load profile: (a) Mudline level and (b) At the pile tip.

5.4.2 $\delta - N$ Profiles

The displacement-controlled loading applied in the 2D FEM models was based on moving the pile head laterally for a particular displacement δ , and then measuring the clay's response and load degradation through the monopile embedded length. Therefore, the displacement amplitude is expected to remain constant through the analysis. Nevertheless, similar to the behavior detected in the preceding chapter, the clay response could not reach the targeted displacement value, as shown in Figures 5.12 and 13.

Figure 5.12 shows the $\delta - N$ profile at the mudline and tip of the monopile, where the displacement amplitude decreased during the first few cycles then continued to increase till the end of the test. The marine clay tested in the preceding chapter exhibited the same behavior, and it was reported that the change in the displacement amplitude is a sign of changing behavior. A deformation of $\delta \cong 0.11 \text{ m}$ was detected at the pile head when applying a displacement of $\delta \cong 0.12 \text{ m}$ at the pile head. For the same loading conditions, a displacement of $\delta \cong -0.055 \text{ m}$ was reported at the pile tip, explaining the clay degradation at this area as discussed in the preceding section. In addition, the monopile exhibited a rotation at the bottom side, leading to remolding and softening of the clay.

Similarly, Figure 5.13 shows the same behavior for the FEM analysis performed under $\delta \cong 0.35 \text{ m}$, where a displacement of $\delta \cong 0.33 \text{ m}$ was detected at the mudline, and $\delta \cong 0.17 \text{ m}$ at the monopile tip.

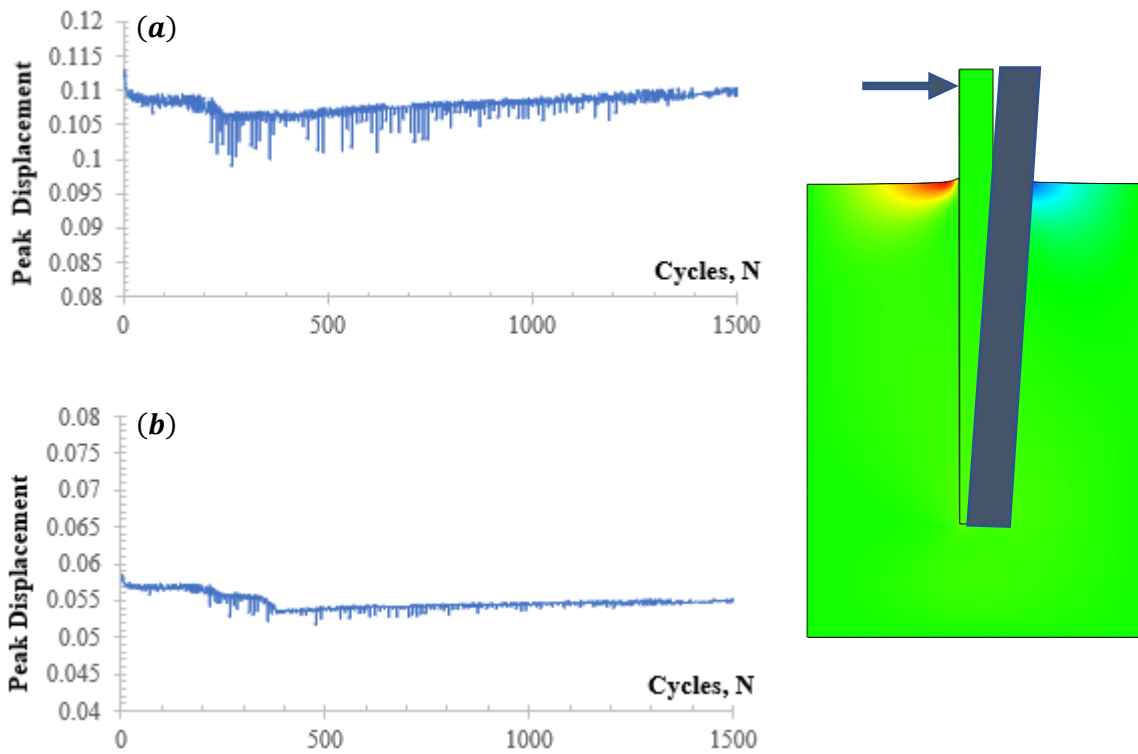


Figure 5.12: 2D FEM model ($y = 0.12 \text{ m}$) peak displacement profile: (a) Mudline level and (b) At the pile tip.

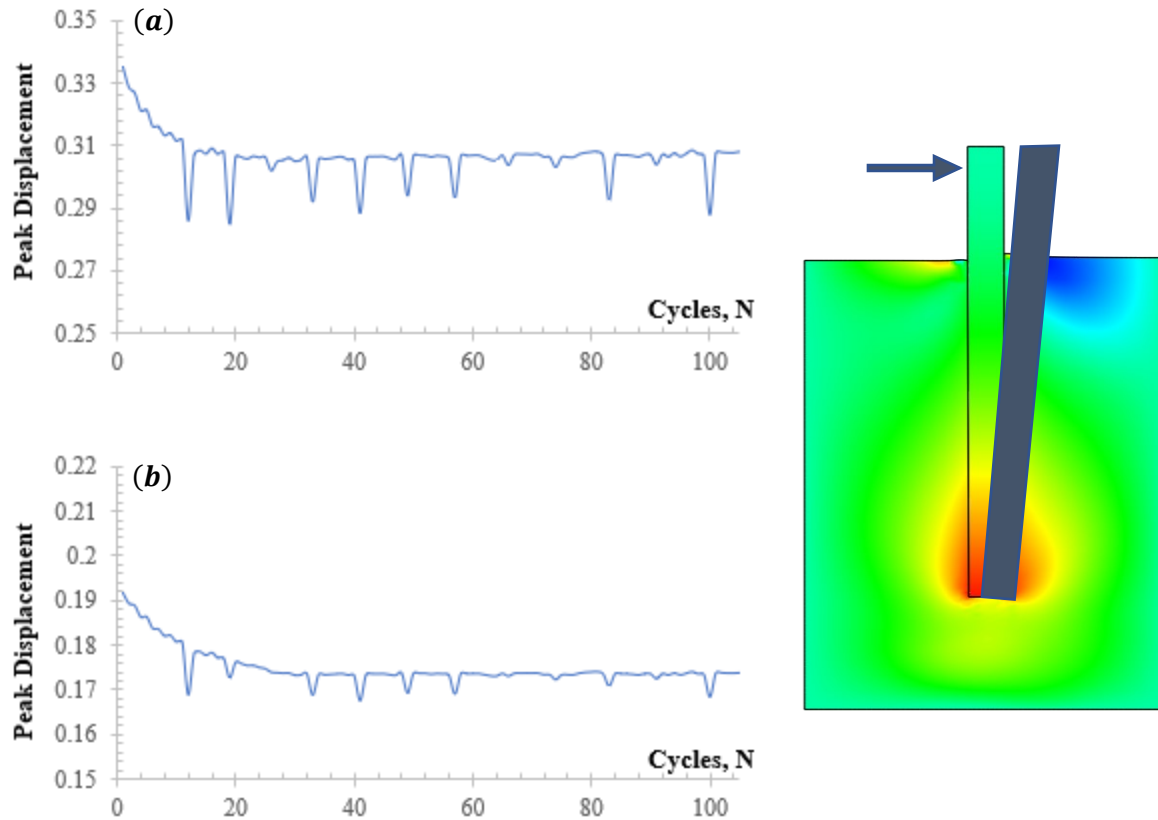


Figure 5.13: 2D *FEM* model ($y = 0.35 \text{ m}$) peak displacement profile: (a) Mudline level and (b) At the pile tip.

5.4.3 Strain Development

When studying the fatigue behavior of marine clays in Chapter 4, it was found that through the fatigue life of clays, there is a transition point at which clay changes behavior when the plastic strains become dominant. The hysteresis loops became rectangular-like in shape where the plastic strains increased and controlled the clay's behavior. Moreover, it was found that the transition occurred when the pore water pressure tended to stabilize. In the 2D *FEM* numerical analysis, the development of the plastic strain was detected to check if it would exhibit the same behavior. **Figure 5.14** and **Figure 5.15** show the development of elastic and plastic strains during cycling and pore water pressure generation at the mudline level.

The pore water pressure in the *FEM* analysis with high amplitude stabilized at early ages and after 20 *cycles*, as shown in **Figure 5.14**. Consequently, the plastic strains control the behavior earlier. Therefore, the failure is expected to occur if more cycles are applied as the plastic strains tend to stabilize, not to increase when it becomes dominant. This behavior is expected when a high amplitude is applied due to excessive deformations and is identical to the results obtained in the experimental investigation of marine clays, where the higher amplitude, the earlier transition point occurs.

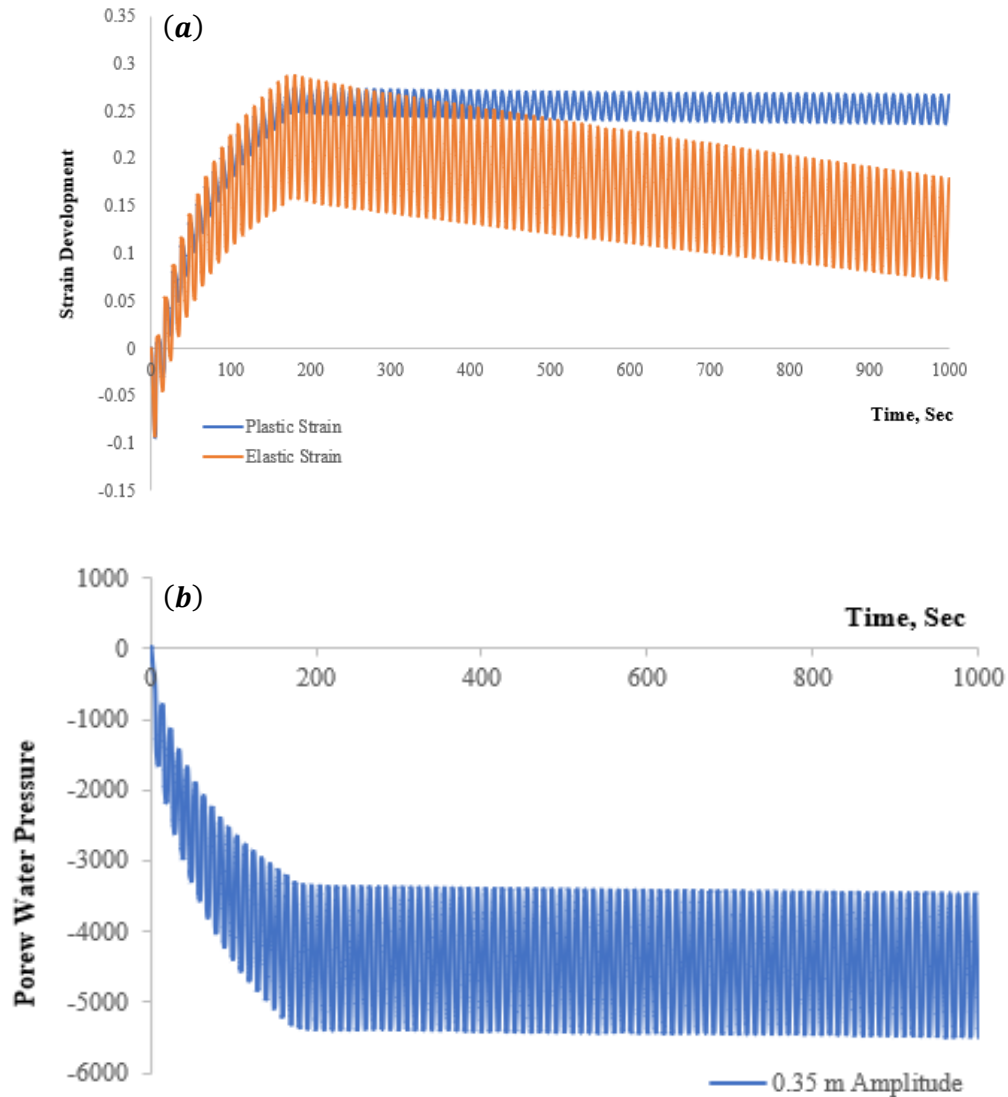


Figure 5.14: 2D *FEM* model ($y = 0.35$ m): (a) Strain development and (b) Pore water pressure generation.

The plastic strains for the lower applied amplitude (**Figure 5.15**) have a sudden increase after about 200 cycles, then tend to decrease slightly and continue increasing until the end of the analysis. It is expected that the plastic strains will continue increasing until failure; the plastic strain initiation can be seen in **Figure 5.16** around the pile head and is expected to extend to more expansive areas if more cycles were applied. The plastic strain profiles for the entire clay domain in **Figure 5.16** show that the accumulation of high stresses, pore water pressures, and lateral deformations is associated with high plastic strains. This fact highlighted the importance of defining the transition point as a critical design factor indicates that cracks have already been initiated, and failure will occur sometime after this point.

The plastic and elastic strain are mainly accumulated at the mudline level near the monopile head and the corners of the monopile tip. As seen in **Figure 5.16**, the nominal strains can indicate the location of the critical depth from the top and bottom. These areas are the primary concern as they exhibit a change in behavior and load degradation, which should be considered in the design process. Add the effect of increasing lateral head displacement, where the clay distorted more at the mudline for the 0.35 m analysis. It is believed that the clay's parameters will change in these areas, and water becomes part of the clay structure. This behavior was observed in the experimental investigation of the fatigue of marine clays.

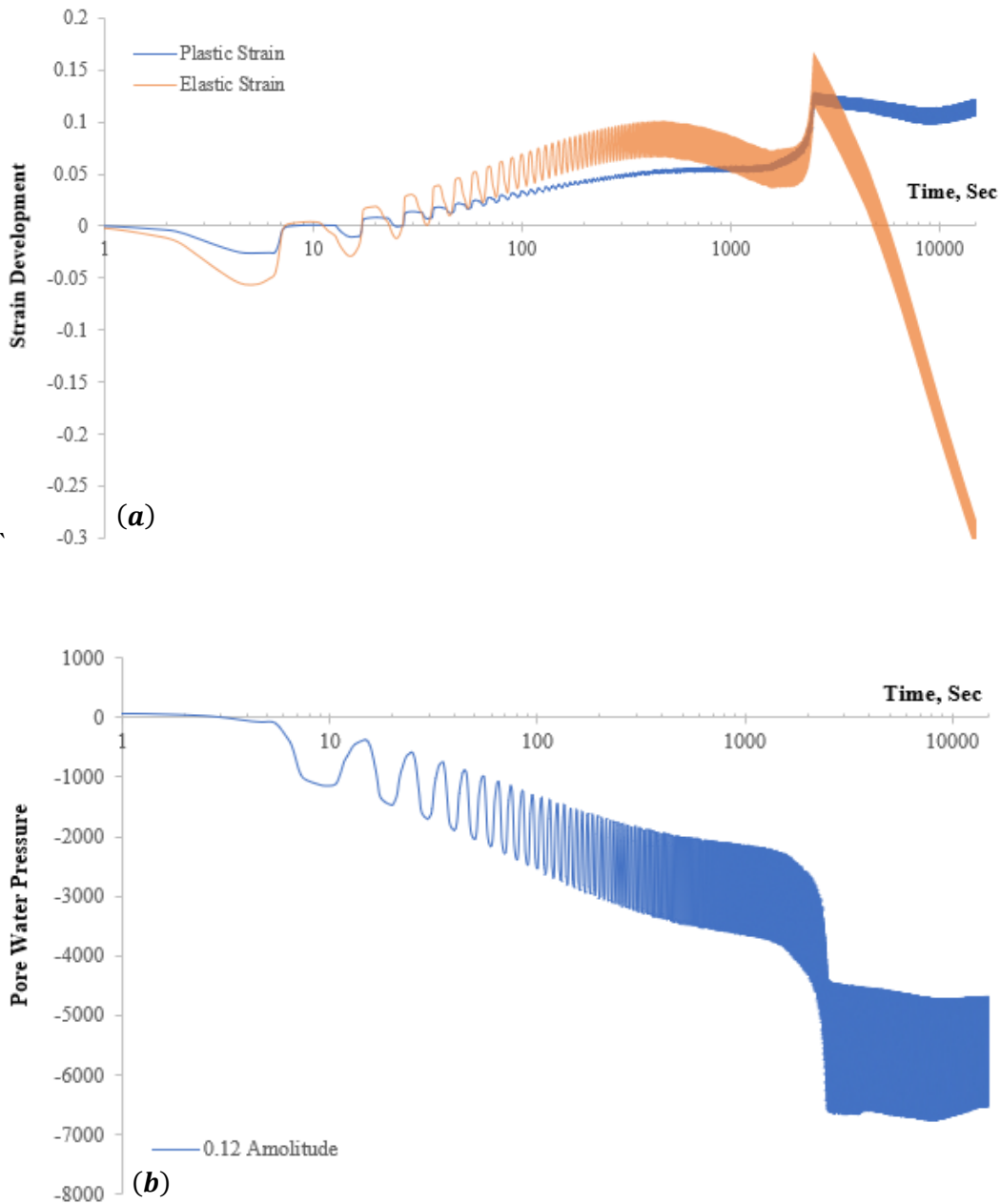


Figure 5.15: 2D *FEM* model ($y = 0.12$ m): (a) Strain development and (b) Pore water pressure generation.

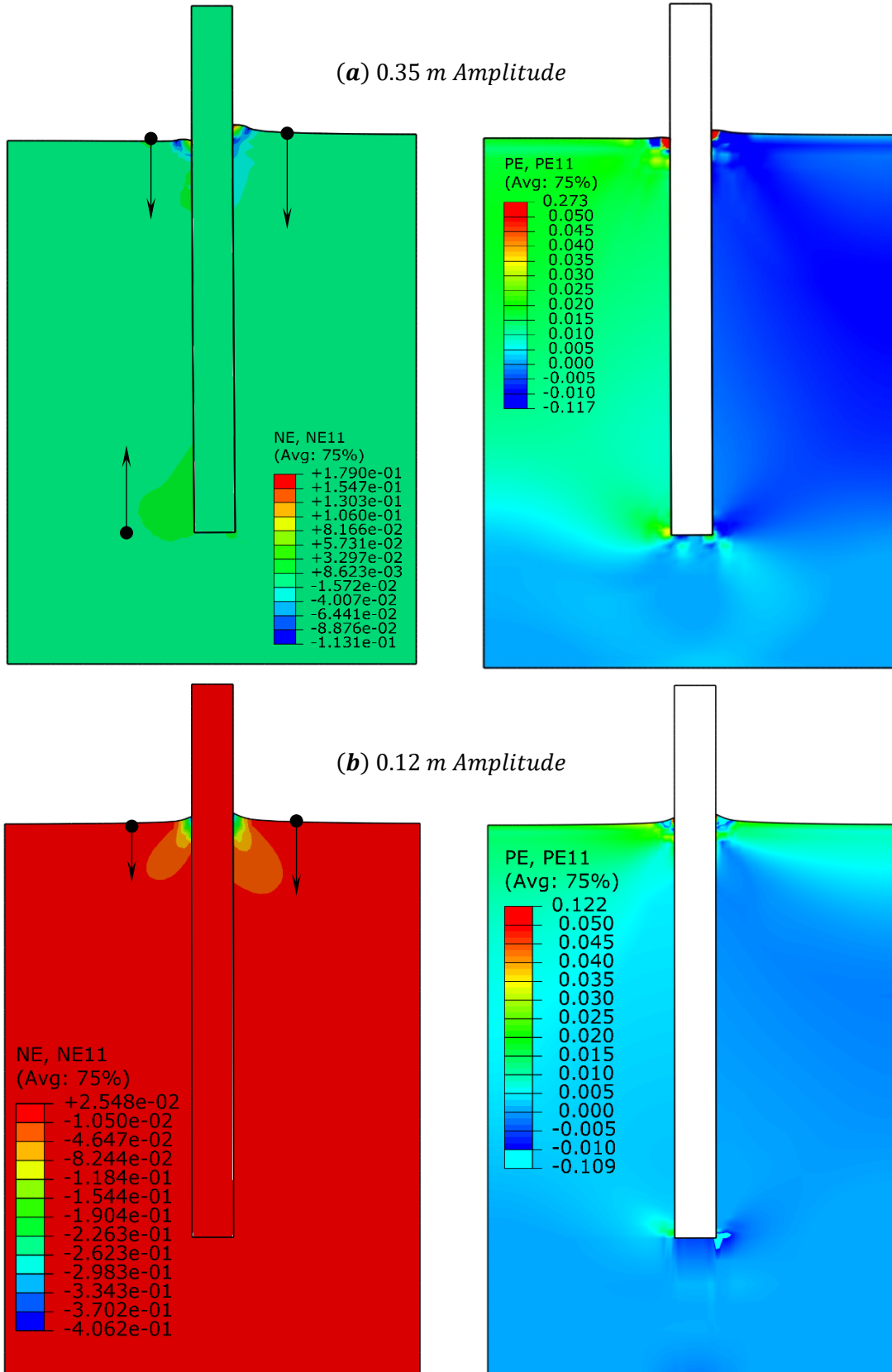


Figure 5.16: 2D *FEM* models strain profiles: (a) $y = 0.35\text{ m}$ and (b) $y = 0.12\text{ m}$.

5.4.4 Stiffness Profiles

The clay stiffness is expected to degrade at the mudline to a certain depth (critical depth, x_r) as proposed by (Matlock, 1970), and for depths greater than x_r till the pile tip, the clay strength stabilized after reaching a peak value. In the displacement-controlled numerical investigation performed in the present study, this behavior was detected at the left side of the monopile but only in the middle third of the embedded length. Different lateral load capacities were detected at the right side, i.e., the loading side. In addition, most researchers reported that the Matlock method overestimates or underestimates the initial load stiffness and the lateral pile head movement.

The present study investigated the stiffness degradation by applying a predefined lateral movement and measuring the monopile-clay response with increasing cycles. The clay stiffness was measured based on the secant modulus (E_s) that was defined in the preceding chapter, which can be modified by Equation 5.3.

$$E_s = \frac{\Delta P}{\Delta y} \dots\dots\dots 5.3$$

The clay stiffness profiles through the critical depth and at the bottom left side (0.12 m) of the monopile embedded length are shown in Figure 5.17 for the selected depths. At the mudline level, clay strengthened at the early ages and up to about 200 cycles, then tended to stabilize up to $N \cong 1100$ cycles and continue to degrade until the analysis's end slightly. Similar behavior was detected for the stiffness profiles at the critical depth below the mudline. However, after degrading to a certain number of cycles, the clay shows a hardening behavior as the stiffness increases until the analysis's end.

The periods of softening and hardening were detected when studying the fatigue behavior of marine clays in the preceding chapter; it was concluded that this behavior is due to opening and closing the fatigue crack initiated before reaching the transition point. Moreover, water becomes part of the clay structure by forming a clay paste with new parameters. For the 0.12 m displacement amplitude, the transition point was at $N = 200$ cycles, and the degradation or hardening/softening periods started after this point. The clay at this stage behave plastically, and the new clay's parameters can define the clay fatigue life and when the clay will degrade and reach failure, which might extend to $10^4 - 10^7$ cycles.

The secant stiffness degraded from the first applied cycle for the bottom left side of the monopile embedded length. An increase in stiffness was detected at the transition point, followed by a steep degradation till $N \cong 1100$ cycles. Then tends to stabilize till the end of the analysis showing an endurance limit of 850 kN/m.

(Matlock, 1970) proposed that the clay lateral capacity tends to stabilize after 100 cycles. From the performed FEM analysis, it can be concluded that this hypothesis can be approved at high displacement amplitude (or large lateral head deformation), as seen in Figure 5.17. The secant stiffness of the clay subjected to 0.35 m displacement amplitude decreases during the first 20 cycles, then tends to stabilize or degrade at a slow rate. However, still, the behavior could be changed after the 100 cycles. Furthermore, it is essential to recall that the transition point of this analysis was detected earlier at $N = 20$ cycles, which explain the endurance limit achieved at this level of loading. Which again highlighted the importance of defining the transition point.

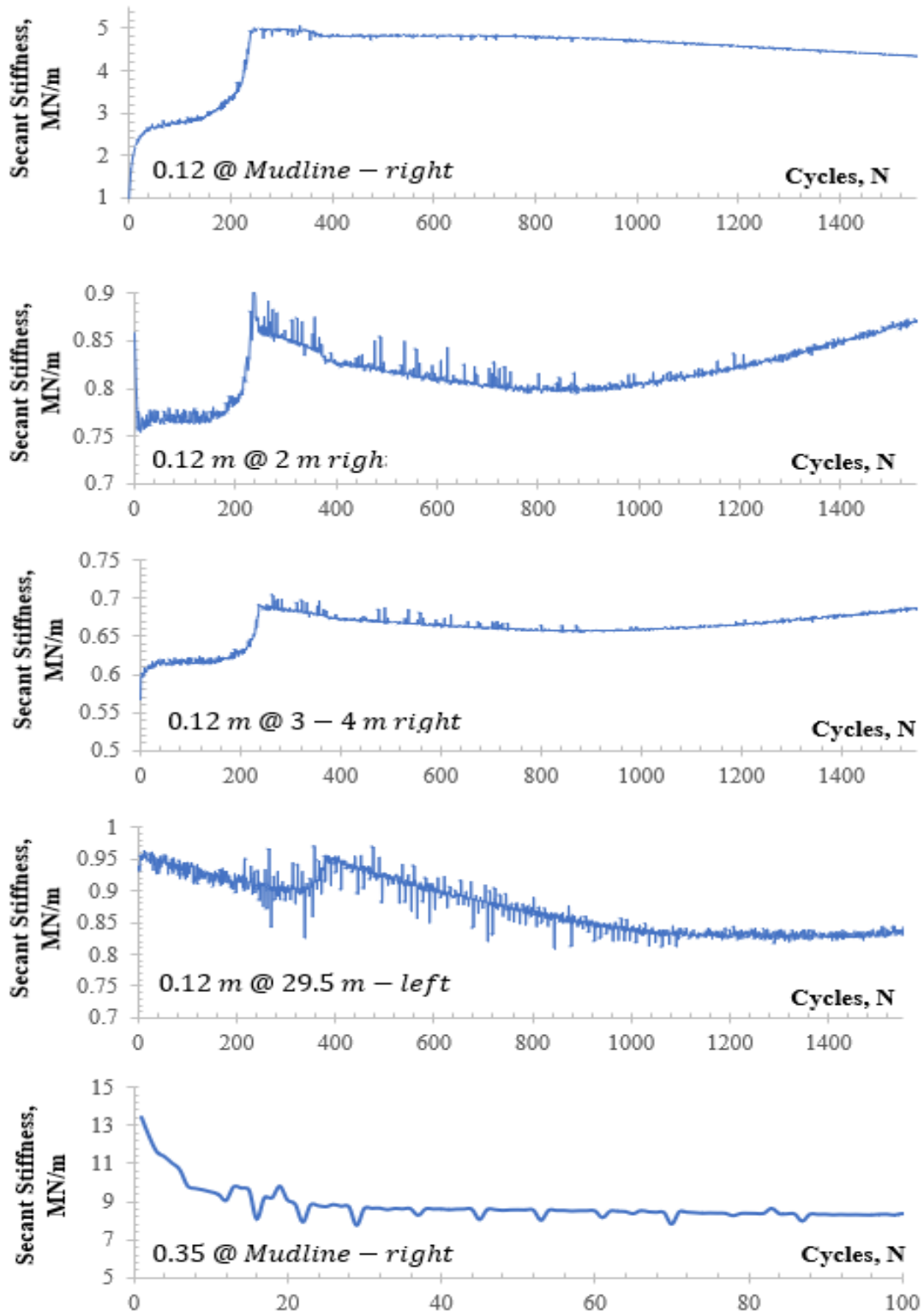


Figure 5.17: Secant stiffness profiles for the 2D FEM analysis at different depths.

CHAPTER 6

CONCLUSIONS AND FUTURE WORK

The response of the Monopile-Clay system to lateral cyclic loading drew the attention of researchers over the years; they conducted experimental, field, and numerical studies to examine the suitability of the methods adopted in the design codes, which is still a controversial issue. This research aims to study the cyclic performance of marine clays and the monopile-clay system and measure the marine clay fatigue life and how it interferes with the system's failure. The research has three main phases: (1) A parametric sensitivity analysis using the Artificial Intelligence technique to allocate the clay parameter(s) that primarily affect its behavior when subjected to cyclic loading. Moreover, predictive models were proposed to predict whether the marine clay will fail or maintain equilibrium. (2) The fatigue life estimation of marine clays was measured by performing a series of strain-controlled tests under different strain amplitudes. In addition, a new correlation of the degradation parameter (t) was proposed based on cycling the marine clays until failure, (3) 2D numerical investigation was performed under the same tested parameters of the strain-controlled tests to measure the monopile-clays system fatigue life.

6.1 CONCLUDED REMARKS

Three types of analysis were performed to assess whether the marine clay under cyclic loading will fail or maintain equilibrium: regression, classification, and Machine learning. As a result, the following remarks can be concluded:

1. The regression analysis was an efficient tool to predict the threshold cyclic stress ratio that can safely apply to marine clay without failing. The proposed failure envelop defined by the fifth-order polynomial fitted curve with a coefficient of determination $R^2 \cong 0.92$ was based on a dataset of 227 points collected from the literature. The curve fitting can successfully and efficiently find the threshold CSR for a given number of cycles in short-term loading. For long-term conditions or when $N \cong 3000$ cycle, the proposed failure envelope, and equation should

be conservatively used. Long-term behavior is still controversial, and few researchers performed long-term stress-controlled cyclic loading.

2. The classification analysis using machine learning techniques is another efficient tool to assess the marine clay behavior under cyclic loading. However, only clay response can be assessed in classification analysis, i.e., whether it will fail or maintain equilibrium. The classifiers in machine learning use algorithms that measure the probability of the occurrence of the dependent variable given two independent variables (CSR, N). Moreover, by providing confidence scores and contour lines, deciding whether the clay will fail or not become more flexible and efficient.
3. The machine learning classifiers also efficiently select the marine clay parameter or parameters that primarily affect the clay behavior. Eleven parameters were selected out of 23 physical and mechanical properties. The selected parameters had high probability confidence scores in which the model accuracy decreases in their absence. All classifiers approved that the loading level CSR and number of cycles are the most parameters that control the marine clay response to cyclic loading and the cyclic strain, which came in the 3rd level of importance. These three properties are cyclic parameters, and the other selected features were physical and mechanical properties.
4. The cyclic strain has a complicated interrelationship with other parameters, which cannot be predicted and assumed to be an independent parameter that should be tested separately to measure its effect on the cyclic response of marine clays.
5. The selected parameters, excluding the cyclic strain, efficiently predict whether the marine clay will fail or maintain equilibrium in the predictive artificial neural network model (ANN), which is also an efficient tool for this purpose. Furthermore, the artificial neural network technique has the advantage that the inputs are marine clay's parameters that can be measured in experimental investigation. Consequently, the assessment is based on several clay properties, making the prediction more efficient than the regression and classification techniques requiring only two parameters.

Marine clay fatigue behavior and life estimation are crucial factors in fulfilling the design criteria, the fatigue and serviceability limit state. Strain-controlled tests were performed in the present study under four different strain amplitudes. The following remarks can be concluded:

1. It was found that confining pressure does not affect the fatigue behavior of marine clays in terms of degradation, softening, and hardening. Different initial stiffnesses and peak stress amplitudes were recorded, but the clay shows the same fatigue behavior when subjected to two different confining pressures ($\sigma_3 = 50 \text{ kPa}$ and $\sigma_3 = 250 \text{ kPa}$).
2. The loading frequency has a significant effect on fatigue behavior. Very low frequencies lead to stress relaxation and delay the failure as the clay degraded in the first few cycles and reached an endurance limit. Higher frequencies lead to progressive degradation with time until the clay fails. The frequency that simulated the field condition for wind and surface wave loads was used in the strain-controlled experimental investigation ($f = 0.1 \text{ Hz}$).

3. It was found that marine clay degraded with increasing cycles to a specific limit. During its fatigue life, fatigue cracks initiated and propagated then went through cycles of hardening and softening until failure occurred. The hardening and softening behavior is referred to as opening cracks that weaken the clay. However, cracks in the existence of water in an undrained condition will be filled with clay paste with new parameters. A microscopy investigation detected this behavior for clay samples after failure.
4. When cracks are filled with a clay paste, the clay behaves plastically, and the hysteresis loops become rectangular-like in shape. This observation continued until failure occurred; only the areas of hysteresis loops decreased as the energy dissipated. The failure was detected when hysteresis loops had a disturbing shape.
5. Three major turning points in the marine clay's fatigue life were defined: (1) the crack initiation, (2) the crack propagation fatigue life, and (3) the transition point where the plastic strains become dominant and control the clay's behavior. The transition point is a crucial key in the fatigue behavior as the failure will be expected at any time after this point, depending on the applied strain amplitude. Therefore, three correlations were proposed in the present study to estimate the fatigue life of marine clays, given the strain amplitude.
6. The strain amplitude can represent any loading condition in which the cyclic loading in the field is transferred to clay and can be represented in two forms: load amplitude and displacement amplitude. The load amplitude has a complicated form, where waves, winds, and other environmental loads, have different distributions over the superstructure. Therefore, when applying a displacement amplitude, this amplitude can reflect a combination of load amplitudes. Moreover, strain-controlled tests are more efficient in detecting long-term behavior.
7. The degradation index δ and parameter t were also measured based on the fatigue behavior analysis. Most of the studies in the literature measured the degradation parameter for 100 *loading cycles* or less. However, the results obtained in the present study were found that clay changes behavior through its fatigue life and that 100 *cycles* cannot precisely reflect the marine clay degradation behavior. Therefore, a new correlation for the fatigue degradation parameter was proposed and can be used to develop new load-deformation curves that account for the actual load degradation during long-term cyclic loading.

A 2D FEM large-scale numerical analysis was performed to investigate the monopile-system response to cyclic loading:

1. A failure envelope was proposed in the present study using the available data in the literature to predict the threshold loading level at which the monopile-clay system can maintain equilibrium. However, the proposed failure envelope is not recommended for sensitive field conditions as the collected datasets have different failure criteria in the absence of definitive failure criteria.
2. Numerical analysis is an efficient tool in modeling large-scale geotechnical problems. In the present study, a 2D displacement-controlled FEM analysis was proposed for inspection

purposes, in which the performance of large diameter monopile embedded in marine clays was investigated. The clay load profiles show the same behavior detected when studying the clay fatigue behavior under strain-controlled tests.

3. Transition points were also investigated in the numerical analysis, and it was concluded that the clay changed behavior after this point. The clay degrades to a certain point, then stabilizes, softens, and hardens. The clay response after the transition point changes with depth, showing degradation at the mudline level and the monopile's tip, and inconsistent behavior at the middle third of embedded length at the loading side, while stabilizing on the other side. However, the system lateral response tends to stabilize at the middle of the embedded length.
4. The system performance changes when the plastic strain becomes dominant and pore water pressure stabilizes.
5. (**Matlock, 1970**) proposed that the clay lateral capacity tends to stabilize after 100 cycles. Other researchers also performed their studies adopting Matlock's theory. However, from the performed *FEM* analysis, it can be concluded that this hypothesis can be approved at high displacement amplitude (or large lateral head deformation) when the system is subjected to extensive lateral movement. The secant stiffness of the clay subjected to high displacement amplitude decreases during the first few cycles then tends to stabilize or degrade at a slow rate. However, still, the behavior could be changed after the 100 cycles.

6.2 RESEARCH LIMITATIONS

1. The lack of data in the literature was the primary concern in performing machine learning analysis. The models' accuracy can be improved if more extensive dataset ranges were used in the analysis.
2. The triaxial machine used to perform the strain-controlled tests in the experimental investigation limits the frequencies applied in cyclic tests. A maximum frequency of 0.1 Hz can be used, whereas it is vital to measure the fatigue behavior of marine clays at higher frequencies.
3. There was no way to monitor the sample during cyclic strain-controlled tests; the membrane is opaque, and the machine setup does not allow for the installation of an inner camera with high resolution to detect the surface crack initiation and propagation. Digital microscopy was used to detect the sample's surface after failure.
4. The cyclic tests' plastic and elastic strain components cannot be calculated using the triaxial machine software. Therefore, manual calculations and investigations were performed to measure the transition life.
5. Performing a 3D large-scale numerical analysis with an adequate constitutive model requires high-performance desktops to overcome the high computational efforts of such problems.

6.3 FUTURE WORK

However, in the present study, and for strain-controlled tests, the depth at which the sample collected effect was studied through one of the check tests; further studies are recommended. Three equations were proposed to estimate the fatigue life of marine clays, in addition to a new correlation for the degradation parameter. More strain-controlled tests can be performed on different marine clays with different parameters to modify the proposed equations and become applicable for a broader range of marine clays. In addition, further studies on the microstructure of marine clays under cyclic loading are required to understand better the formation of new clay paste that filled the fatigue cracks initiated during cyclic loading. Inspecting the properties of the new clay paste can help in developing new design criteria that consider changing clay properties during its fatigue life. Finally, large-scale 3D numerical displacement-controlled analysis can be performed to inspect the clay degradation profile at different depths and with varying properties. The effect of pile geometry and varying the clay parameters can also be studied. New load-transfer curves can be proposed to replace the current method adopted in the design codes, which is still controversial.

REFERENCES

- API. (2005). Recommended Practice for Planning, Designing and Constructing Fixed Offshore Platforms—Working Stress Design. American Petroleum Institute. Washington, D.C.: API Publishing Services.
- API, A. P. (2000). Recommended Practice for Planning, Designing and Constructing Fixed Offshore Platforms. API Publishing Services.
- Arany, L., Bhattacharya, S., Macdonald, J., & Hogan, S. J. (2017). Design of monopiles for offshore wind turbines in 10 steps. *Soil Dynamics and Earthquake Engineering*, 92, 126-152.
- Baturynska, I., & Martinsen, K. (2021). Prediction of geometry deviations in additive manufactured parts: comparison of linear regression with machine learning algorithms. *Journal of Intelligent Manufacturing*, 32, 179–200.
- Bouزيد, D. A., Bhattacharya, S., & Dash, S. R. (2013). Winkler springs (p-y curves) for pile design from stress-strain of soils: FE assessment of scaling coefficients using the mobilized strength design concept. *Geomechanics and Engineering*, 5(5), 379-399.
- Budkowska, B. B., & Priyanto, D. G. (2003a). Nonlinear Behaviour of Laterally Loaded Long Piles Penetrating Soft Clay Below Water Table Subjected to Cyclic Loading—Sensitivity Analysis Part I: Theoretical Formulation. *International Journal of Offshore and Polar Engineering*, 13(3), 169-174.
- Budkowska, B. B., & Priyanto, D. G. (2003b). Nonlinear Behaviour of Laterally Loaded Long Piles Penetrating Soft Clay Below Water Table Subjected to Cyclic Loading—Sensitivity Analysis Part II: Numerical Investigation. *International Journal of Offshore and Polar Engineering*, 13(3), 293-300.
- Byrne, B., McAdam, R., Burd, H., Houlsby, G., Martin, C., Gavin, K., . . . Skov Gretlund, J. (2015). Field testing of large diameter piles under lateral loading for offshore wind applications. 1255 Proceedings of the XVI ECSMGE 2015 (pp. 1255-1260). Edinburgh: ICE Publishing.
- Byrne, B., McAdam, R., Burd, H., Houlsby, G., Martin, C., Zdravkovic, L., . . . Skov Gretlund, J. (2015). New design methods for large diameter piles under lateral loading for offshore wind applications. 3rd International Symposium on Frontiers in Offshore Geotechnics (ISFOG 2015) (pp. 10-12). Oslo: ICE Publishing.
- Canadian Geotechnical Society. (2006). Canadian Foundation Engineering Manual. Vancouver, B.C.: Canadian Geotechnical Society.
- Chakrabarty, N., & Biswas, S. (2020). Navo Minority Over-sampling Technique (NMOTe): A Consistent Performance Booster on Imbalanced Datasets. *Journal of Electronics and Informatics*, 2(2), 96-136.
- Dewaikar, D. M., Padmavathi, S. V., & Salimath, R. S. (2008). Ultimate lateral load of a pile in soft clay under cyclic loading. The 12th International Conference of International Association for Computer Methods and Advances in Geomechanics (pp. 3498-3507). Goa: IACMAG.

- DING, J., LIU, H., & HU, L. (2007). Response of Marine Clay to Cyclic Loading. Proceedings of the Sixteenth (2007) International Offshore and Polar Engineering Conference (pp. 1188-1192). Lisbon, Portugal: The International Society of Offshore and Polar Engineers (ISOPE).
- Dunnivant, T. W., & O'Neill, M. W. (1989). Experimental p-y Model for Submerged Stiff Clay. *Journal of Geotechnical Engineering*, 115(1), 95-114.
- Fakharian, K., Ahmari, S., & Amiri, A. (2008). 3-D Numerical Investigation of Piles under Monotonic and Cyclic Lateral Loads in Clay. The Eighteenth International Offshore and Polar Engineering Conference (pp. 670-675). Vancouver: International Society of Offshore and Polar Engineers.
- Guo, L., Wang, J., Cai, Y., Liu, H., Gao, Y., & Sun, H. (2013). Undrained deformation behavior of saturated soft clay under long-term cyclic loading. *Soil Dynamics and Earthquake Engineering*, 50, 28-37.
- Haiderali, A. E., Nakashima, M., & Madabhushi, S. P. (2015). Cyclic lateral loading of monopiles for offshore wind turbines. *Frontiers in Offshore Geotechnics III* (pp. 711-716). London: Taylor & Francis Group.
- Hanna, A., & Javed, K. (2014). Experimental investigation of foundations on sensitive clay subjected to cyclic loading. *Journal of Geotechnical and Geoenvironmental Engineering*, 140(11), 04014065.
- Hastie, T., Tibshirani, R., & Friedman, J. (2017). *The Elements of Statistical Learning: Data Mining, Inference, and Prediction* (Second Edition ed.). New York, NY: Springer Science+Business Media.
- Hong, Y., He, B., Wang, L., Wang, Z., Ng, C., & Masin, D. (2017). Cyclic lateral response and failure mechanisms of semi-rigid pile in soft clay: centrifuge tests and numerical modelling. *Canadian Geotechnical Journal*, 54(6), 806-824.
- Hu, L., Ding, J., & Liu, H. (2010). Mechanical Behavior of Marine Clay Under Wave Loading. *International Journal of Offshore and Polar Engineering*, 20(1), 72-79.
- Hyde, A. F., Yasuhara, K., & Hirao, K. (1993). Stability Criteria for Marine Clay Under One-Way Cyclic Loading. *Journal of Geotechnical Engineering*, 119(11), 1771-1789.
- Hyodo, M., Yasuhara, K., & Hirao, K. (1992). Prediction of Clay Behaviour in Undrained and Partially Drained Cyclic Triaxial Tests. *Soils and Foundations*, 32(4), 117-127.
- Idriss, I. M., Dobry, R. M., Doyle, E. H., & Singh, R. D. (1976). Behavior of soft clays under earthquake loading conditions. Offshore Technology Conference. Texas: OnePetro.
- Idriss, I. M., Dobry, R., & Singh, R. D. (1978). Nonlinear behavior of soft clays during cyclic loading. *Journal of the Geotechnical Engineering Division*, 104(12), 1427-1447.
- Idriss, I., Moriwaki, I., Wright, S. G., Doyle, E. H., & Ladd, R. S. (1980). Behavior of Normally Consolidated Clay Under Simulated Earthquake and Ocean Wave Loading Conditions. International symposium on soils under cyclic and transient loading, (pp. 437-445).

- Javed, K. (2011, February). Behavior of Sensitive Clay Subjected to Static and Cyclic Loading. Doctoral dissertation. Montreal, QC, Canada: Concordia University.
- Jeong, S., Kim, Y., Kim, J., & Shin, S. (2007). Cyclic lateral load tests of offshore large diameter piles of Incheon Bridge in marine clay. The Seventeenth International Offshore and Polar Engineering Conference (pp. 1353-1360). Lisbon: International Society of Offshore and Polar Engineers.
- Karlsruud, K., & Haugen, T. (1985). Behaviour of piles in clay under cyclic axial loading-results of field model tests. Behaviour of Offshore Structures (pp. 589-600). Netherlands: ELSEVIER SCIENCE PUBLISHERS B.V.
- Kerr, A. D. (1964). A Study of a new Foundation Model. *Acta Mechanica*, 1(2), 135-147.
- Khemakhem, M., Chenaf, N., Garnier, J., Rault, G., Thorel, L., & Dano, C. (2010). Static and cyclic lateral pile behavior in clay. *Physical Modelling in Geotechnics* (pp. 953-958). London: Taylor & Francis Group.
- Kumar, N. D., Rao, S. N., & Sundar, V. (2007). Performance of Caisson in Soft Clay Under Cyclic Lateral Loading. *Geotechnical Engineering*, 38(1), 16-23.
- Lee, C.-J., & Sheu, S.-F. (2007). The stiffness degradation and damping ratio evolution of Taipei Silty Clay under cyclic straining. *Soil Dynamics and Earthquake Engineering*, 27, 730-740.
- Lei, H., Xu, Y., Jiang, M., & Jiang, Y. (2020). Deformation and fabric of soft marine clay at various cyclic load stages. *Ocean Engineering*, 195, 106757.
- Li, D., Zhou, N., Wu, X., & Yin, J. (2017, October). The Quasi-static Properties of Natural Marine Clay under Tidal Low Frequency Cyclic Loading in Yangtze Estuary, China. In *IOP Conference Series: Materials Science and Engineering* (Vol. 250, No. 1, p. 012042). IOP Publishing.
- Li, L. L., Dan, H. B., & Wang, L. (2011). Undrained behavior of natural marine clay under cyclic loading. *Ocean Engineering*, 38(16), 1792–1805.
- Liao, W., Wu, J., Wang, Z., Yan, K., & Ouyang, F. (2021). Experimental investigation of monopile in overconsolidated marine clay subjected to multiple cyclic lateral loading events. *Marine Georesources & Geotechnology*, 1-14.
- Lombardi, D., Bhattacharya, S., & Wood, M. D. (2013). Dynamic soil–structure interaction of monopile supported wind turbines in cohesive soil. *Soil Dynamics and Earthquake Engineering*, 49, 165-180.
- Matasović, N., & Vucetic, M. (1995). Generalized cyclic-degradation-pore-pressure generation model for clays. *Journal of geotechnical engineering*, 121(1), 33-42.
- Matlock, H. (1970). Correlations for design of laterally loaded piles in soft clay. *Offshore Technology in Civil Engineering's Hall of Fame Papers from the Early Years*, (pp. 77-94).
- Mortezaie, A. R., & Vucetic, M. (2013). Effect of Frequency and Vertical Stress on Cyclic Degradation and Pore Water Pressure in Clay in the NGI Simple Shear Device. *JOURNAL OF GEOTECHNICAL AND GEOENVIRONMENTAL ENGINEERING*, 139(10), 1727-1737.

- Moses, G. G., & Rao, S. N. (2007). Behavior of Marine Clay Subjected to Cyclic Loading with Sustained Shear Stress. *Marine Georesources and Geotechnology*, 25, 81-96.
- Negnevitsky, M. (2002). *Artificial Intelligence, A Guide to* (1st ed.). Addison- Wesley.
- Prasad, Y. V., & Rao, S. N. (1994). Pullout behaviour of model pile and helical pile anchors subjected to lateral cyclic loading. *Canadian geotechnical journal*, 31(1), 110-119.
- Rajashree, S. S., & Sundaravadivelu, R. (1996). Degradation model for one-way cyclic lateral load on piles in soft clay. *Computers and Geotechnics*, 19(4), 289-300.
- Rao, S. N., & Moses, G. (2003). Behaviour of Marine Clay Under Wave Type of Cyclic Loading. *The 22ND International Conference on Offshore Mechanics and Arctic Engineering* (pp. 495-503). Mexico: American Society of Mechanical Engineers.
- Rao, S. N., & Rao, K. M. (1993). Behaviour of rigid piles in marine clays under lateral cyclic loading. *Ocean Engineering*, 20(2), 281-293.
- Rao, S., Rao, K., & Prasad, Y. (1992). Behavior of Vertical Piles Under Static and Cyclic Lateral Load in Marine clays. *International Offshore and Polar Engineering Conference* (pp. 475-482). San Francisco: The International Society of offshore and Polar Engineers.
- Reese, L., & Welch, R. C. (1975). Lateral Loading of Deep Foundation in Stiff Clay. *Journal of the Geotechnical Engineering Division*, 633-649.
- Ren, X. W., Xu, Q., Xu, C. B., Teng, J. D., & Lv, S. H. (2018). Undrained pore pressure behavior of soft marine clay under long-term low cyclic loads. *Ocean Engineering*, 150, 60-68.
- Sa'don, N. M., Pender, M. J., Abdul Karim, A. R., & Orense, R. (2014). Pile Head Cyclic Lateral Loading of Single Pile. *Geotechnical and Geological Engineering*, 32(4), 1053-1064.
- Senanayake, A., Rendon, E., Wang, S. T., Gerkus, H., Stevens, R. F., & Gilbert, R. B. (2015). Design of large diameter monopiles under lateral loads in normally to moderately overconsolidated clay. *Offshore Technology Conference*. Texas, USA: OnePetro.
- Shahin, M. A., Jaksa, M. B., & Maier, H. R. (2008). State of the Art of Artificial Neural Networks in Geotechnical Engineering (Vol. 8). *Electronic Journal of Geotechnical Engineering*.
- Su, D., Wu, W. L., Du, Z. Y., & Yan, W. M. (2014). Cyclic degradation of a multidirectionally laterally loaded rigid single pile model in compacted clay. *Journal of Geotechnical and Geoenvironmental Engineering*, 140(5), 06014002.
- Vucetic, M., & Dobry, R. (1988). DEGRADATION OF MARINE CLAYS UNDER CYCLIC LOADING. *Journal of Geotechnical Engineering*, 114(2), 133-149.
- Wang, J., Guo, L., Cai, Y., Xu, C., & Gu, C. (2013). Strain and pore pressure development on soft marine clay in triaxial tests with a large number of cycles. *Ocean Engineering*, 74, 125-132.
- Wichtmann, T., Anderson, K., Sjursen, M., & Berre, T. (2013). Cyclic tests on high-quality undisturbed block samples of soft marine Norwegian clay. *Canadian Geotechnical Journal*, 50, 400-412.

- Xiao, W., Guib, Y., & Xu, G.-Z. (2018). Effect of organic content and frequency on degradation and pore pressure in marine organic soils. *MARINE GEORESOURCES & GEOTECHNOLOGY*, 36(1), 108–122.
- Xiaoa, W., Guib, Y., & Xuc, G.-Z. (2018). Effect of organic content and frequency on degradation and pore pressure in marine organic soils. *MARINE GEORESOURCES & GEOTECHNOLOGY*, 36(1), 108–122.
- Yao, M., & Anandarajah, A. (2003). Three-dimensional discrete element method of analysis of clays. *Journal of Engineering Mechanics*, 129(6), 585-596.
- Zdravković, L., Taborda, D., Potts, D., Jardine, R., Sideri, M., Schroeder, F., Skov Gretlund, J. (2015). Numerical modelling of large diameter piles under lateral loading for offshore wind application. *Third International Symposium on Frontiers in Offshore Geotechnics (ISFOG 2015)*. Oslo.
- Zhang, C., White, D., & Randolph, M. (2011). Centrifuge modeling of the cyclic lateral response of a rigid pile in soft clay. *Journal of Geotechnical and Geoenvironmental Engineering*, 137(7), 717-729.
- Zhang, J., Sun, Y., & Cao, J. (2020). Experimental Study on the Deformation and Strength Characteristics of Saturated Clay under Cyclic Loading. *Advances in Civil Engineering*.
- Zhang, L. &. (2013). Nonlinear analysis of laterally loaded rigid piles in cohesive soil. *International Journal for Numerical and Analytical Methods in Geomechanics*, 37(2), 201-220.
- Zhou, J., & Gong, X. (2001). Strain degradation of saturated clay under cyclic loading. *Canadian Geotechnical Journal*, 38(1), 208-212
- Zhu, B., Zhu, Z.-j., Li, T., Liu, J.-c., & Liu, Y.-f. (2017). Field Tests of Offshore Driven Piles Subjected to Lateral Monotonic and Cyclic Loads in Soft Clay. *Journal of Waterway, Port, Coastal, and Ocean Engineering* , 143(5), 05017003-1/11.

APPENDIX A

MACHINE LEARNING PYTHON SAMPLE CODES AND RESULTS

A.1 CLASSIFIERS FOR SAFE ZONE

```
#-----  
# Logistic Regression Model  
#-----  
from sklearn.linear_model import LogisticRegression  
classifier = LogisticRegression(random_state = 0)  
classifier.fit(X_train, y_train)  
  
y_pred = classifier.predict(X_test)  
print(np.concatenate((y_pred.reshape(len(y_pred),1), y_test.reshape(len(y_test),1)),1))  
  
from sklearn.metrics import confusion_matrix, accuracy_score  
cm = confusion_matrix(y_test, y_pred)  
print(cm)  
accuracy_score(y_test, y_pred)  
  
#-----  
# Naive Bayes Model  
#-----  
  
from sklearn.naive_bayes import GaussianNB  
classifier = GaussianNB()  
classifier.fit(X_train, y_train)  
  
#-----  
# Kernel SVM model  
#-----  
  
from sklearn.svm import SVC  
classifier = SVC(kernel = 'rbf', random_state = 0)  
classifier.fit(X_train, y_train)  
  
#-----  
# Decision Tree model  
#-----  
  
from sklearn.tree import DecisionTreeClassifier  
classifier = DecisionTreeClassifier(criterion = 'entropy', random_state = 0)  
classifier.fit(X_train, y_train)
```

```
#-----  
# Random Forest model  
#-----  
  
from sklearn.ensemble import RandomForestClassifier  
classifier = RandomForestClassifier(n_estimators = 10, criterion = 'entropy', random_state = 0)  
classifier.fit(X_train, y_train)  
  
#-----  
# SVM model  
#-----  
  
from sklearn.svm import SVC  
classifier = SVC(kernel = 'linear', random_state = 0)  
classifier.fit(X_train, y_train)  
  
#-----  
# K-NN Model  
#-----  
  
from sklearn.neighbors import KNeighborsClassifier  
classifier = KNeighborsClassifier(n_neighbors = 4, metric = 'minkowski', p = 2)  
classifier.fit(X_train, y_train)
```

A.2 ANN MODELS TEST RESULTS-F/E PREDICTION

Depth	w%	wL%	Ip%	Yo	St	qs	CSR	N	S%	F/E	y-predict
1.55	0.56	0.25	0.10	-0.94	-0.23	0.52	-1.47	-0.24	0.76	0	0
1.55	0.56	0.25	0.10	-0.94	-0.23	0.52	-0.25	-0.33	0.76	0	0
1.64	0.56	0.21	-0.40	-0.53	-0.72	-0.67	0.09	-0.34	0.76	0	0
-0.41	-0.42	-0.60	-0.15	0.31	1.05	0.53	1.28	-0.33	-1.25	0	0
-0.45	0.09	0.13	0.03	0.25	-0.10	0.53	-0.47	-0.33	-2.30	1	1
1.55	0.56	0.25	0.10	-0.94	-0.23	0.52	-0.81	0.40	0.76	0	0
-1.37	2.10	2.24	2.33	-1.52	-1.26	0.85	-0.47	0.16	0.76	1	1
-0.53	-0.83	-0.35	-0.89	0.81	-0.89	-0.92	-1.17	-0.32	-1.61	1	1
-1.37	1.84	2.24	2.33	-1.52	-1.26	0.85	-1.52	-0.08	0.76	1	1
-1.37	1.84	2.24	2.33	-1.52	-1.26	0.85	-1.17	0.06	0.76	1	1
1.64	0.57	0.21	-0.40	-0.53	-0.72	-0.67	1.98	-0.34	0.76	0	0
-1.37	1.84	2.24	2.33	-1.52	-1.26	0.85	0.86	0.54	0.76	1	1
-0.53	-0.83	-0.35	-0.89	1.68	-0.89	-0.82	0.23	-0.32	0.76	0	0
1.64	0.49	0.21	-0.40	-0.53	-0.72	-0.67	-1.03	-0.30	0.76	0	0
1.46	0.33	0.21	-0.09	-0.56	-0.74	-0.77	0.37	-0.34	0.76	0	0
-0.33	-1.97	-1.57	-1.44	1.98	1.68	0.33	-0.82	-0.33	0.36	1	1
-0.41	-0.42	-0.60	-0.15	0.13	1.05	0.53	-0.61	-0.33	-1.80	1	1
-1.37	1.84	2.24	2.33	-1.52	-1.26	3.33	1.70	1.05	0.76	1	1
1.46	0.11	0.21	-0.09	-0.56	-0.74	-0.64	-0.61	-0.19	0.76	0	0
-1.37	1.84	2.24	2.33	-1.52	-1.26	0.85	0.23	0.29	0.76	1	1
-0.45	0.09	0.13	0.03	0.91	-0.10	0.53	-0.68	-0.33	-0.47	1	1
-0.41	-0.42	-0.60	-0.15	0.07	1.05	0.60	-0.82	-0.33	-1.96	1	1
-0.41	-0.42	-0.60	-0.15	0.12	1.05	-0.21	-0.19	-0.33	-1.81	1	1
-0.41	-0.42	-0.60	-0.15	0.23	1.05	0.67	1.63	-0.34	-1.50	0	0
-0.33	-1.97	-1.57	-1.44	2.14	1.68	-1.36	0.23	-0.33	0.76	0	0
-0.41	-0.42	-0.60	-0.15	0.79	1.05	-1.19	-0.47	-0.33	0.12	0	0
1.64	0.51	0.21	-0.40	-0.53	-0.72	-0.67	0.09	-0.34	0.76	0	0
-0.33	-1.97	-1.57	-1.44	1.88	1.68	0.33	-0.47	-0.34	0.09	1	1
1.55	0.56	0.25	0.10	-0.94	-0.23	0.52	-1.62	0.69	0.76	0	0
-1.37	2.10	2.24	2.33	-1.52	-1.26	0.85	-0.82	0.14	0.76	1	1
1.46	0.02	0.21	-0.09	-0.56	-0.74	-0.64	-0.12	-0.32	0.76	0	0
-0.53	-0.83	-0.35	-0.89	1.32	-0.89	-0.95	1.63	-0.33	-0.21	0	0
-0.41	-0.42	-0.60	-0.15	0.18	1.05	0.60	-0.47	-0.33	-1.65	1	1
-0.41	-0.42	-0.60	-0.15	0.82	1.05	-1.19	-0.61	-0.33	0.21	1	1
-0.33	-1.97	-1.57	-1.44	1.48	1.68	0.16	0.93	-0.34	-0.96	0	0
-0.41	-0.42	-0.60	-0.15	0.38	1.05	-1.19	-0.61	-0.33	-1.07	1	1
1.46	0.09	0.21	-0.09	-0.56	-0.74	-0.65	0.86	-0.34	0.76	0	0
-0.41	-0.42	-0.60	-0.15	0.59	1.05	-0.08	0.23	-0.33	-0.44	0	0
-0.41	-0.42	-0.60	-0.15	0.49	1.05	-0.01	-0.12	-0.34	-0.72	1	0
-1.37	2.10	2.24	2.33	-1.52	-1.26	0.85	-1.52	-0.08	0.76	1	1
-0.53	-0.83	-0.35	-0.89	0.08	-0.89	1.62	-0.82	-0.33	-3.63	1	1

A.3 CYCLIC STRAIN PREDICTION- ANN MODELS RESULTS

Training set	ANN-1			ANN-2		
	$\varepsilon_a\%$	Predicted $\varepsilon_a\%$	APE	$\varepsilon_a\%$	Predicted $\varepsilon_a\%$	APE
0	0.97	1.18	21.67	0.97	8.37	762.49
1	16.11	14.75	8.47	16.11	15.52	3.67
2	-20.19	19.14	-194.84	-20.19	22.22	-210.08
3	2.66	2.04	23.34	2.66	3.02	13.57
4	1.89	2.31	22.15	1.89	1.45	23.09
5	1.75	3.39	93.45	1.75	-3.34	290.61
6	15.28	12.90	15.60	15.28	14.28	6.52
7	5.53	4.46	19.43	5.53	4.37	21.03
8	15.68	16.27	3.78	15.68	56.15	258.08
9	22.62	9.51	57.94	22.62	8.53	62.30
10	6.18	5.87	5.09	6.18	5.05	18.34
11	0.73	0.42	42.20	0.73	0.26	64.06
12	6.99	5.64	19.30	6.99	3.15	54.90
13	1.43	0.19	86.37	1.43	2.58	80.60
14	3.50	4.18	19.48	3.50	-93.50	2771.38
15	2.00	3.36	68.00	2.00	-0.37	118.34
16	0.22	-0.63	386.08	0.22	-0.85	487.43
17	-16.88	27.17	-260.90	-16.88	22.48	-233.16
18	0.24	1.50	523.09	0.24	7.33	2953.46
19	4.23	5.87	38.77	4.23	0.27	93.61
20	1.13	1.02	9.72	1.13	1.14	0.82
21	4.98	4.14	16.82	4.98	5.73	14.98
22	6.72	7.74	15.13	6.72	12.63	88.00
23	6.23	7.35	17.92	6.23	6.01	3.55
24	1.39	3.41	145.65	1.39	-13.92	1101.41
25	26.66	-14.59	154.74	26.66	-15.38	157.71
26	8.00	4.24	47.05	8.00	3.71	53.58
27	3.83	4.25	10.88	3.83	3.59	6.38
28	13.46	16.55	22.93	13.46	19.02	41.26
29	11.44	26.82	134.40	11.44	97.62	753.31
30	-1.54	17.26	-1219.20	-1.54	20.64	-1438.01
31	0.78	1.55	98.23	0.78	1.99	154.99
32	2.08	4.83	132.31	2.08	2.91	39.74
33	10.97	13.92	26.93	10.97	14.81	34.97
34	5.88	-2.96	150.42	5.88	2.25	61.82
35	1.33	1.58	18.82	1.33	1.77	33.44
36	2.01	6.43	219.97	2.01	-0.90	144.92
37	1.76	2.32	31.83	1.76	2.28	29.60
38	1.16	0.96	17.50	1.16	4.89	321.39
39	3.46	3.54	2.45	3.46	3.56	2.93
40	2.77	4.06	46.45	2.77	3.15	13.81
APE Mean			22.93			53.58
ANN model parameters	<i>2 hidden layers 20 neurons each Batch size: 20 Epochs: 15000 77.07%</i>			<i>3 hidden layers 20-25-25 neurons Batch size: 20 Epochs: 15000 46.42%</i>		

Training set	ANN-3			ANN-4		
	$\varepsilon_a\%$	Predicted $\varepsilon_a\%$	APE	$\varepsilon_a\%$	Predicted $\varepsilon_a\%$	APE
0	0.97	3.25	234.56	0.97	-0.14	114.63
1	16.11	16.75	4.00	16.11	16.60	3.04
2	-20.19	21.68	-207.38	-20.19	20.73	-202.71
3	2.66	3.04	14.10	2.66	4.27	60.63
4	1.89	2.35	24.47	1.89	2.89	52.72
5	1.75	4.33	147.67	1.75	0.41	76.33
6	15.28	17.44	14.11	15.28	16.95	10.95
7	5.53	4.98	9.97	5.53	4.84	12.41
8	15.68	17.34	10.57	15.68	9.21	41.27
9	22.62	22.30	1.44	22.62	16.00	29.28
10	6.18	5.82	5.77	6.18	5.96	3.61
11	0.73	1.12	52.93	0.73	-0.04	105.21
12	6.99	8.05	15.10	6.99	8.04	15.06
13	1.43	1.44	0.69	1.43	1.13	21.01
14	3.50	7.38	110.85	3.50	-14.05	501.30
15	2.00	4.31	115.42	2.00	0.82	58.81
16	0.22	0.42	92.08	0.22	-0.62	379.82
17	-16.88	23.03	-236.40	-16.88	22.68	-234.36
18	0.24	3.27	1264.18	0.24	-1.95	911.11
19	4.23	3.07	27.34	4.23	6.34	50.00
20	1.13	1.26	11.75	1.13	0.76	32.99
21	4.98	4.60	7.65	4.98	1.65	66.86
22	6.72	5.98	11.02	6.72	7.60	13.08
23	6.23	8.72	39.91	6.23	-0.72	111.63
24	1.39	5.08	265.19	1.39	0.83	40.23
25	26.66	-13.41	150.31	26.66	-11.63	143.64
26	8.00	6.82	14.70	8.00	5.25	34.41
27	3.83	3.76	1.94	3.83	4.03	5.29
28	13.46	18.18	35.03	13.46	13.59	0.98
29	11.44	20.10	75.66	11.44	15.99	39.75
30	-1.54	18.00	-1266.60	-1.54	14.29	-1026.44
31	0.78	1.82	132.97	0.78	2.05	163.30
32	2.08	4.71	126.23	2.08	6.86	229.87
33	10.97	15.58	42.07	10.97	14.13	28.83
34	5.88	-4.93	183.86	5.88	15.31	160.30
35	1.33	1.52	14.46	1.33	1.63	22.19
36	2.01	10.37	415.69	2.01	5.81	188.88
37	1.76	4.50	155.74	1.76	3.41	93.49
38	1.16	2.06	77.18	1.16	1.13	2.32
39	3.46	3.73	7.69	3.46	3.34	3.51
40	2.77	3.26	17.80	2.77	3.89	40.49
APE Mean			24.47			40.23
ANN model parameters	<i>3 hidden layers 20-25-25 neurons Batch size: 11 Epochs: 25000 75.53%</i>			<i>3 hidden layers 25-20-20 neurons Batch size: 7 Epochs: 25000 59.77%</i>		

```
# Computing the absolute percent error  
APE=100*(abs(TestingData['εa%']-TestingData['Predictedεa%'])/TestingData['εa%'])  
TestingData['APE']=APE
```

```
print('The Accuracy of ANN model is:', 100-np.mean(APE))
```

APPENDIX B

STRAIN-CONTROLLED CYCLIC CHECK TEST RESULTS FOR $\Delta\varepsilon = 2.50\%$ AT $D = 7.25m$

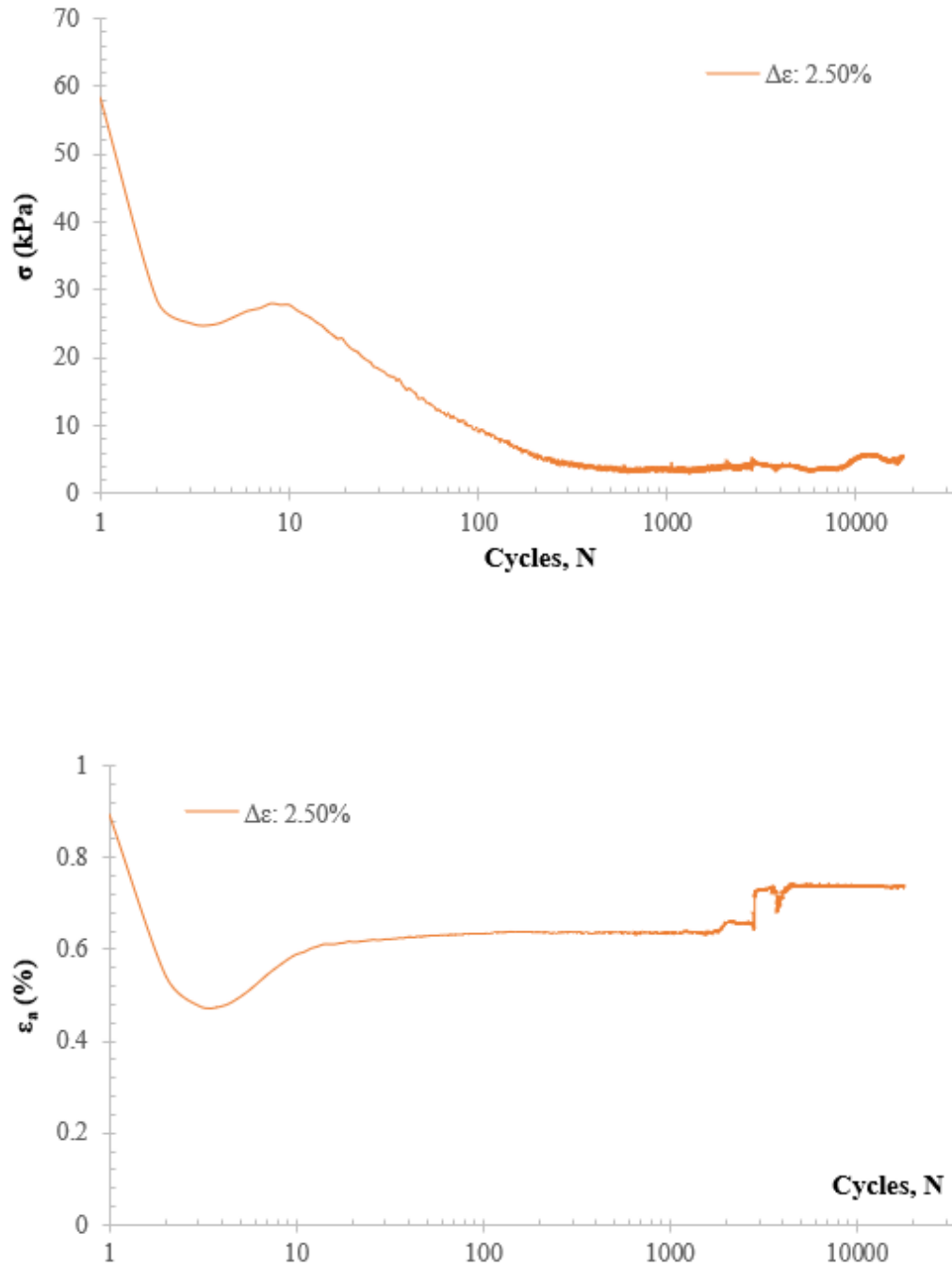


Figure A.1: Peak stress and strain amplitudes for $\Delta\varepsilon = 2.50\%$ check test.

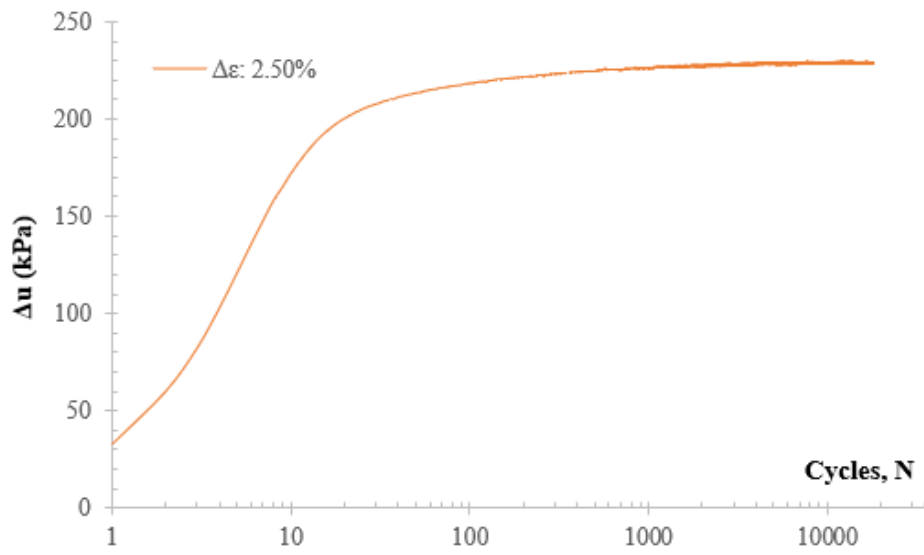


Figure A.2: Pore water pressure generation for $\Delta\epsilon = 2.50\%$ check test.

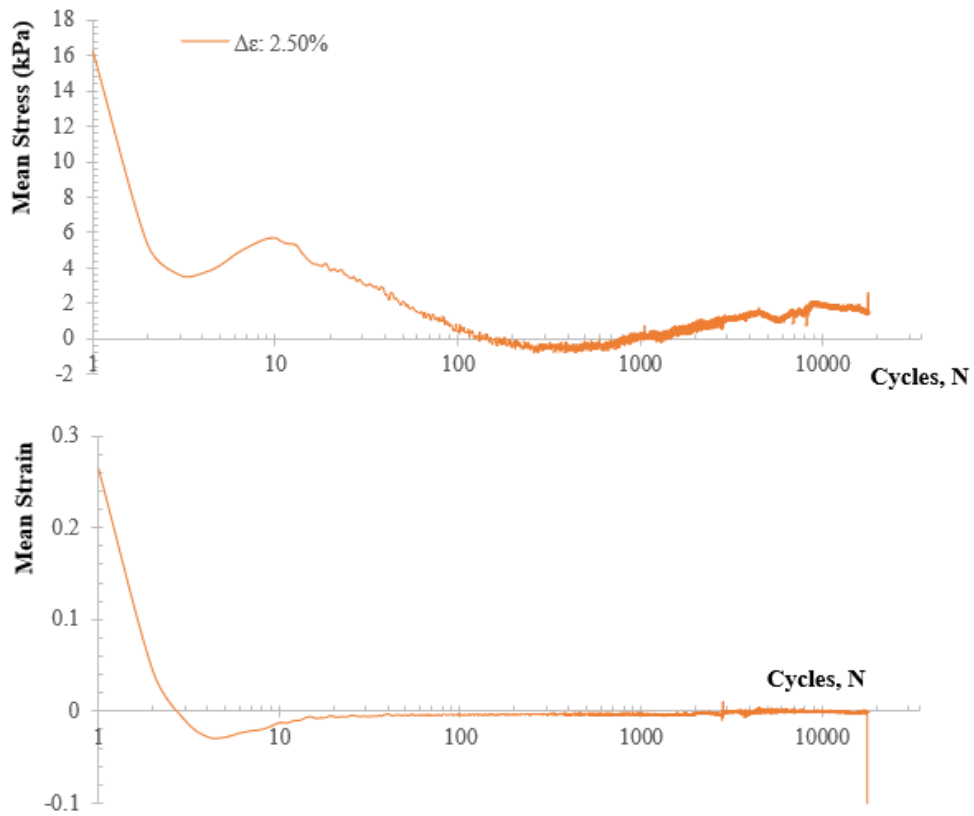


Figure A.3: Mean stress and strain amplitudes for $\Delta\epsilon = 2.50\%$ check test.

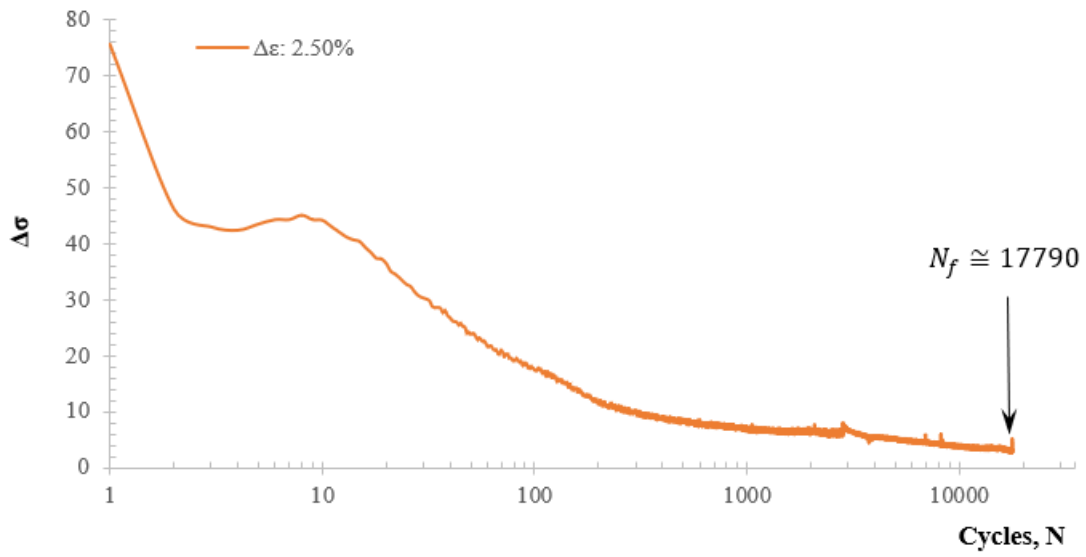


Figure A.4: The changes in stress amplitude ($\Delta\sigma$) for $\Delta\varepsilon = 2.50\%$ check test.

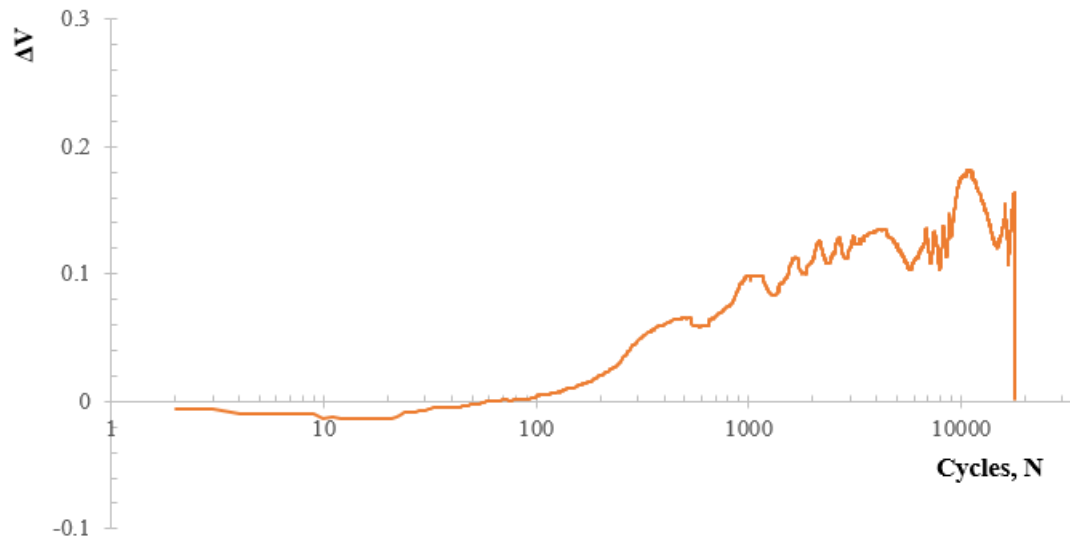


Figure A.5: Volume change for $\Delta\varepsilon = 2.50\%$ check test.

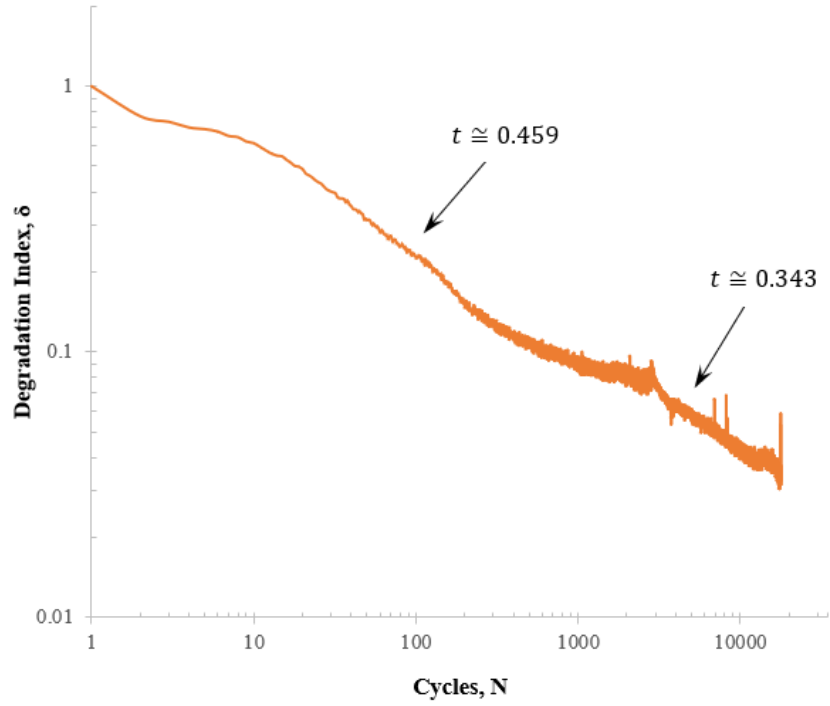


Figure A.6: Degradation index and parameter for $\Delta\varepsilon = 2.50\%$ check test.

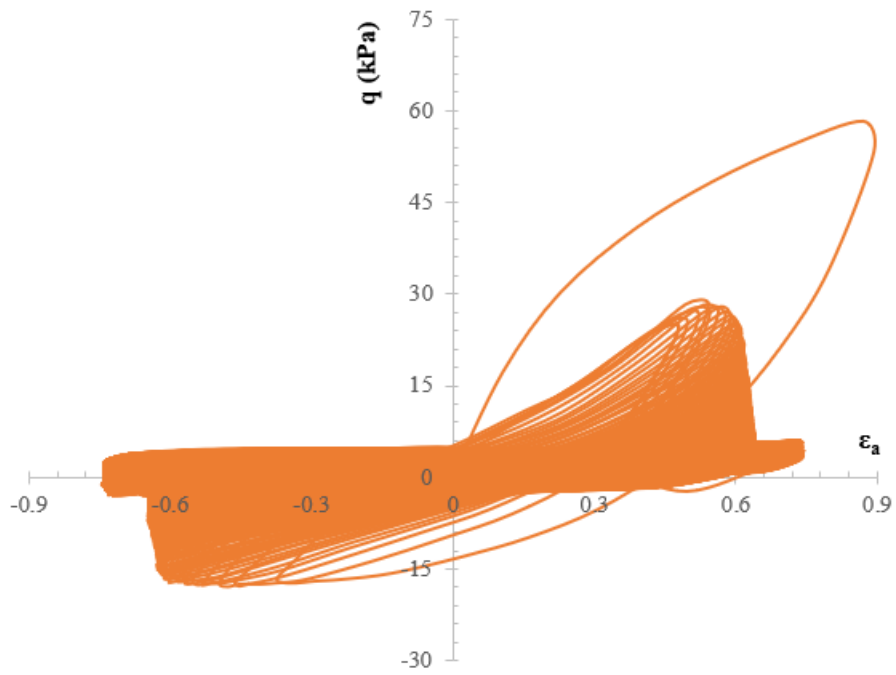


Figure A.7: Hysteresis loops for $\Delta\varepsilon = 2.50\%$ check test.